

General Disclaimer

One or more of the Following Statements may affect this Document

- This document has been reproduced from the best copy furnished by the organizational source. It is being released in the interest of making available as much information as possible.
- This document may contain data, which exceeds the sheet parameters. It was furnished in this condition by the organizational source and is the best copy available.
- This document may contain tone-on-tone or color graphs, charts and/or pictures, which have been reproduced in black and white.
- This document is paginated as submitted by the original source.
- Portions of this document are not fully legible due to the historical nature of some of the material. However, it is the best reproduction available from the original submission.

NASA CR- 86284

DEVELOPMENT OF OPTIMUM CLAMP COMBINATIONS
FOR
STRAP-DOWN INERTIAL MEASURING UNITS WITH
FIELD REPLACEABLE SENSORS

By

John S. Howland,
Seth R. Goldstein,
and
Dikrun Der Marderosian

September 1968

Prepared under Contract No. NAS 12-591 by
FOSTER-MILLER ASSOCIATES, INC.
Waltham, Massachusetts

Electronics Research Center
NATIONAL AERONAUTICS AND SPACE ADMINISTRATION

FACILITY FORM 502

N70-14211 (ACCESSION NUMBER)	(THRU)
218 (PAGES)	(CODE)
CR-86284 (NASA CR OR TMX OR AD NUMBER)	14 (CATEGORY)



Mr. Walter Messcher
Technical Monitor
NAS 12-591
Electronics Research Center
575 Technology Square
Cambridge, Massachusetts 02139

Requests for copies of this report should be referred to:

NASA Scientific and Technical Information Facility
P.O. Box 33, College Park, Maryland 20740

NASA CR-

DEVELOPMENT OF OPTIMUM CLAMP COMBINATIONS
FOR
STRAP-DOWN INERTIAL MEASURING UNITS WITH
FIELD REPLACEABLE SENSORS

By

John S. Howland,
Seth R. Goldstein,
and
Dikrun Der Marderosian

September 1968

Distribution of this report is provided in the interest of information exchange and should not be construed as endorsement by NASA of the material presented. Responsibility for the contents resides with the organization that prepared it.

Prepared under Contract No. NAS 12-591 by

Foster-Miller Associates, Inc.

Waltham, Massachusetts

Electronics Research Center

NATIONAL AERONAUTICS AND SPACE ADMINISTRATION

TABLE OF CONTENTS

Summary	1
Introduction	2
Background	2
Objective	3
Philosophy of Approach	3
Description of the System	4
Review of the State-of-the-Art	8
Sensor Testing and Mounting	8
Precision Machining	12
Metrology	13
Clean Room Technology	14
Material Considerations in Clamp Design	15
Material Instability	16
Interface Considerations	38
Wear of the Locating Surfaces	38
Effects of Fluid Films	45
Dirt and Foreign Particles	46
Thermal Contact Resistance	55
Summary and Conclusions	57
Preliminary Design of the Fixed Clamp	59
Concept Generation	59
Concept Evaluation	64
Summary and Conclusions	74
Preliminary Design of the Adjustable Clamp	76
Concept Generation	76
Concept Evaluation	80
Summary and Conclusions	85
Configurational Design	86
Zero-Moment Configuration	86
Symmetry Considerations	87
Conclusions	94
State-of-the-Art	94
Material Considerations	95
Interface Considerations	96
Preliminary Design of the Fixed Clamp	97
Preliminary Design of the Adjustable Clamp	98
Configurational Design	99
Recommendations	101
References	102

REPRODUCING PAGE BLANK NOT FILMED.

APPENDICES

A	Feasibility of a Dirt-Absorbent Coating on the Fixed Clamp Interface	105
B	Fixed Clamp Concepts	114
C	Distributed Parameter Load-Deflection Analysis of the Plane-on-Plane Clamp Geometry	128
D	Load-Deflection Analysis of the Plane-on-Plane Clamp Geometry with Discrete Mounting Pads	138
E	Analysis of Point and Line Contact Fixed Clamp Geometries	143
F	Load-Deflection Analysis of the Cylinder-in-Hole Fixed Clamp Concept	149
G	Analysis of Cylinder-in-Hole Clamping Techniques	154
H	Analysis of Misalignment Due to Thermal Expansion	170
I	Schematic Diagrams of Adjusting Clamp Concepts	182
J	Design Goals for the Clamp System	197
K	Deformation of the Cylindrical Shell Element of a Cylinder-In-Hole Clamp	200

LIST OF ILLUSTRATIONS

Figure

- 1 Schematic of Strapdown Inertial Measuring Unit (I.M.U.) Showing Clamps
- 2 Schematic of Four Combinations of Adjustable and Rigid Internal and Mutual Clamps
- 3 Schematic Diagram of Sensor Showing the Input and Output Axes
- 4 Gyro Input Axis Orientation Using a Locating Pin
- 5 Gyro Clamping Using a Belly Band
- 6 Gyro Clamping Using Mounting Pads
- 7 Schematic Diagram Showing Exaggerated Misalignment Due to Wear of the Mounting Pad
- 8 Misalignment Due to a Rigid Particle Between Rigid Surfaces
- 9 Soft Particle Trapped Between Rigid Flat Surfaces of Sensor Clamp and Mounting Block
- 10 Hard Particle Embedded in Soft Surface of Mounting Block
- 11 Model of Rigid Spherical Particle Pressed into a Soft Surface
- 12 Interaction of Foreign Particles and Rough Mating Surfaces
- 13 Schematic Diagram of Contact Between Real Surfaces
- 14 Typical Force-Deflection Characteristics for a Belleville Washer
- 15 Schematic Diagram of the Assumed Clamp Configuration Illustrating the Major Overall Dimensions used for Concept Evaluation
- 16 Zero-Moment Clamp Configuration
- 17 Optimum Moment Configuration with Minimum Interface Piece Size
- 18 Various Configurational Symmetries About the I. A.
- 19 Various Configurations Providing I. A. Axi-Symmetry and Symmetry about the x-y Plane Containing the Center of Mass
- 20 Schematic Diagram of Configurationally Symmetric Designs

LIST OF ILLUSTRATIONS (Continued)

Figure

- A-1 Geometry for the Analysis of a Dirt-Absorbent Coating
- A-2 Indentation of a Particle into the Coating
- A-3 Indentation into a Medium of Finite Thickness
- A-4 Simplified Analysis of Thin Coating Deflection in the Presence of Nonuniform Clamping Forces and Accelerations
- B-1 Series of Point Contacts Maintaining Alignment in the Presence of Dirt
- B-2 Clamping the Sensor with Hydraulic Pressure
- B-3 Controlled Force Clamp
- B-4 Clamping the Sensor Fixture Using Dowel Potting Techniques
- B-5 Cylinder Placed in Fluted Hole
(Looking Down onto Mounting Block)
- B-6 Clamping the Sensor by Means of Hydraulic Cylindrical Contraction
- B-7 Fixed Clamp Using Cone-in-Tapered Hole Geometry
- B-8 Self-Tapping Sensor Fixture
- B-9 Clamping the Sensor with Expandable Plugs
- B-10 Clamping the Sensor with Collet-Type Clamps
- B-11 Split Cylindrical Clamp
- B-12 Precision Jig Maintaining Alignment During Solidification of Joint
- B-13 Center Mounting Jig for Aligning Input Axis Parallel to Hole Axis
- B-14 Cylindrical Jig for Aligning Input Axis Parallel to Hole Axis
- B-15 Air Bearing Jig for Aligning Input Axis Parallel to Hole Axis
- B-16 Repeatability Verification Using Miniature Autocollimators
- B-17 Optical Flat Belly Band Clamping and Verification Technique
- C-1 Rigid Block Clamped to an Elastic Foundation
- C-2 Elastic Foundation Deflections

LIST OF ILLUSTRATIONS (Continued)

Figure

- C-3 Elastic Block Clamped to a Rigid Foundation
- C-4 Dimensionless Acceleration Force, $\frac{F_a}{2lbE} \times 10^6$
Limiting Unbalanced Clamping Load versus Acceleration
- D-1 Lumped Parameter Idealization of the Plane-on-Plane
Geometry with Mounting Pads
- E-1 Three Point Contact Clamping Geometry
- E-2 Cylinder in a V-Block Locating Geometry
- F-1 Schematic Diagram Showing the Lumped Parameter Model for
the Cylinder-in-Hole
- F-2 Allowable Asymmetry in Interference versus Asymmetry in
Structure Stiffness for Various Values of Nominal Interference
- G-1 Transient Temperature Response of a Cylinder, Initially
at T_0 , After Being Subjected to a Step Change in
External Surface Temperature
- G-2 Two Piece Split Clamp
- H-1 Plane-on-Plane Fixed Clamp and Lumped-Parameter Thermal Resistance
- H-2 Lumped-Parameter Thermal Network Representing Plane-on-Plane Clamp
- H-3 Dimensions of Plane-on-Plane Clamp Selected for Thermal Calculations
- H-4 Angular Distortion of the Plane-on-Plane Clamp Due to Asymmetric
Thermal Contact Resistances
- H-5 Cylinder-in-Hole Fixed Clamp, and Lumped-Parameter Thermal Network
- H-6 Dimensions of Idealized Cylinder-in-Hole Configuration
- H-7 Angular Distortion of Cylinder-in-Hole Clamp Due to Asymmetric
Thermal Gradients

LIST OF ILLUSTRATIONS (Continued)

Figure

- I-1 Adjustable Internal Clamp, Three-Point Sensor Support
Differential Beam Adjustment Concept
- I-2 Adjustable Internal Clamp, Three-Point Sensor Support
Differential Beam and Spring Adjustment Concept
- I-3 Adjustable Internal Clamp, Three-Point Sensor Support
Catenary Action Adjustment Concept
- I-4 Adjustable Internal Clamp, Three-Point Sensor Support
Interchangeable, Compressible Column Concept
- I-5 Adjustable Internal Clamp, Three-Point Sensor Support
Selected Fit Adjustment Using Precision Gage Elements
- I-6 Adjustable Internal Clamp, Three-Point Sensor Support
Direct Screw Adjustment Concept
- I-7 Adjustable Internal Clamp, Three-Point Sensor Support
Direct Differential Screw Adjustment Concept
- I-8 Adjustable Internal Clamp, Three-Point Sensor Support
Transverse Wedge Adjustment Concept
- I-9 Adjustable Internal Clamp, Spherical Seal Sensor Support
Combination Adjusting and Locking Screws Concept
- I-10 Adjustable Internal Clamp, Pin and Radial Clamp Adjusting Concept
- I-11 Adjustable Internal Clamp, Perpendicular Flexure Adjustment Concept
- I-12 Adjustable Internal Clamp, Four-Point Spherical Sensor Support
Perpendicular Traverse Adjustment Concept
- I-13 Adjustable Internal Clamp, Ring End Sensor Support
Double Offset Eccentric Adjustment Concept
- I-14 Adjustable Internal Clamp, Perpendicular Trunion Adjustment Concept

LIST OF TABLES

- I Recommended Heat Treatment for Obtaining High Dimensional Stability in Selected Alloys
- II Summary of Stability Characteristics of Gage Blocks, in Order of Merit
- III Micro Yield Stress and Microcreep Data for Various Alloys
- IV Dimensional Stability Under Stress for Beryllium
- V Precision Mechanical Properties of Various Materials
- VI Microcreep Data for Some Materials
- VII Summary of Micro Yield Stresses for Ceramics
- VIII Micro Yield Stress and Dimensional Stability Limit of Beryllium and Beryllia
- IX Comparison of Microcreep Characteristics of Various Materials Arranged in Order of Decreasing Micro Yield Stress
- X Effect of Temperature Cycling (-50 to +100°F) on Specimen Length
- XI Misalignment of a Plane-on-Plane Fixed Clamp Due to Adhesive Wear
- XII Relaxation Time for Various Squeeze Films
- XIII Methods for Orienting a Straight Line in Space
- XIV Potential Clamping Forces
- XV Classification of Fixed Clamp Concepts
- XVI Classification of Adjustable Clamp Concepts

DEVELOPMENT OF OPTIMUM CLAMP COMBINATIONS
FOR
STRAP-DOWN INERTIAL MEASURING UNITS WITH
FIELD REPLACEABLE SENSORS

By

John S. Howland, Seth R. Goldstein, and Dikrun Der Marderosian

Foster-Miller Associates, Inc.
Waltham, Massachusetts

SUMMARY

The economics of strapdown inertial guidance systems would be improved if the sensor elements could be individually replaced in the field without subsequent adjustment and verification of alignment.

The objective of the study has been to investigate the factors affecting the feasibility of such a system and to develop methods for establishing and maintaining sensor alignment. The preliminary design goal was sensor input axis alignment within ± 5 arc-seconds.

The key element in this system is the provision of an extremely accurate and stable clamping system to hold the sensor. This clamping system must include an adjustable internal clamp to allow prealignment of the sensor assembly in the laboratory, and a fixed clamp to allow field replacement without adjustment or verification.

This study included the analysis of a number of fundamental factors affecting the feasibility of the clamp system, and the preliminary conceptual design tasks for the fixed and adjustable clamps. The fundamental factors investigated included the state-of-the-art of precision machining, the stability of material, wear, the effects of fluid films, the effects of dirt and foreign particles, the response to thermal loading, and the deflections due to mechanical loading.

The results of the fixed clamp design study provided two promising fixed clamp concepts. Both of these concepts employ plane-on-plane locating geometry. Because dirt which can cause potential misalignment cannot be eliminated, it must be accommodated by the clamp. The two fixed clamp concepts provide two methods for accomplishing this. The first method involves assembly with a wiping motion under light load to sweep the dirt into the "valleys" in the surface roughness. This was found promising from preliminary experiments. The second method provides a vacuum-deposited coating of a soft material with an extremely accurately controlled thickness. This coating (which must be thicker than the largest dirt particle) absorbs particles which can potentially cause misalignment. The best method for providing the clamping force for each of these concepts was found to be spring-loaded retainers.

The preliminary design of the adjustable clamp provided three promising concepts. Each of these utilizes tripod adjustment and support, resulting in the minimum size and complexity of structure. The concepts differ in their method of providing adjustment. The first, the Compressible Column Concept, provides adjustment by the material deformation in compressing a column. The second, the Selected Fit Concept, provides adjustment by means of a range of gage block spacer elements. The third, the Transverse Wedge Concept, provides direct mechanical motion between the sensor and mounting block.

In order to span the required adjustment range of 25 arc-minutes while adjusting to within 2 arc-seconds, it was found necessary to combine a coarse and fine adjustment for each concept. The coarse adjustment in each case is by means of a family of spacer elements. The three concepts selected provide varying degrees of fine adjustment range.

The verification means in the laboratory must be capable of resolving alignment of the axis to of the order of 1 arc-second. The readout, however, must also be accurate enough to make the proper selection of gage block elements. The three concepts selected provide a range of required accuracies, the Selected Fit Concept being the most stringent with a readout requirement of 1.5 arc-secs. The Column Compression and Transverse Wedge Concepts follow with readout requirements of 5 arc-secs and 37 arc-secs, respectively.

It is recommended that these fixed and adjustable clamp concepts be implemented with test prototype hardware, and be tested to determine their basic performance capabilities. General recommendations for the factors to be tested are provided.

INTRODUCTION

This report presents the results of an analytical design study of the factors involved in mounting normalized inertial gyroscopes and accelerometers to an inertial sensing unit so that alignment is ensured without field adjustment. Factors studied include interface conditions such as surface roughness, dirt, films, wear, foreign material, dimensional stability, mechanical and thermal loads, and clamp configurations.

Background

Strapdown inertial navigation systems offer several potential advantages over gimballed systems. These include reduced complexity, smaller size and weight, lower power, and minimum configurational restraint. The advantages, however, are offset by the major disadvantage that with the present state-of-the-art in mounting and clamping techniques, the entire inertial measuring unit must be removed to an assembly and gaging facility in order to replace a

sensor and to ensure that it be aligned with sufficient accuracy. This economic disadvantage would be eliminated if the sensor elements could be individually replaced in the field without subsequent adjustment and verification of alignment.

Objective

The objective of this study has been to investigate the factors affecting the feasibility of a strapdown system with field replaceable sensors, and to develop methods for establishing and maintaining sensor alignment. The key element in this system is the provision of an extremely accurate and stable clamp to hold the sensor. The design goal for this program has been a maximum angular error of ± 5 arc seconds between the sensor input axis and the reference axis.

Philosophy of Approach

The philosophy of approach has been to investigate general classes of design concepts, and to identify one or more offering the best probability for success before engaging in detailed design. This is accomplished by a process of concept generation, classification, design evaluation, and analysis. This approach provides economy in the analysis of the concepts since advantage is taken of the unifying characteristics within the classes. It also assures that detailed design work is done only on those concepts with the best chance of success, since each class represents a number of different, but basically similar, designs. Furthermore, the systematic procedure tends to counter prejudice against concepts in the early stage of the design process, and helps ensure that no important concept categories are overlooked.

DESCRIPTION OF THE SYSTEM

To define the terminology needed for subsequent discussion, consider the Inertial Measuring Unit (IMU) shown schematically in Figure 1. It consists of a basic mounting block to which are attached several sensors (rate gyros and accelerometers) by means of "mutual" clamps. The sensor unit itself consists of a sensor body mounted to an interface piece by means of an "internal" clamp. The internal and mutual clamps can be either adjustable or fixed, thus giving four general combinations as illustrated in Figure 2.

The bulk of the effort in this study has been concentrated on the Adjustable-Fixed combination of Figure 2(b) for the following reasons:

- (a) Preliminary study showed that a sensor cannot be aligned by a fixed clamp to sufficient accuracy with respect to the interface piece so that subsequent adjustment is not necessary. Thus, the Fixed-Fixed clamp of Figure (a) is not feasible within the present state-of-the-art of sensor fabrication.
- (b) The Fixed-Adjustable combination of Figure 2(c) requires adjustment and verification of alignment in the field. The prime objective of this study was to identify techniques to avoid this necessity. Thus, since the Adjustable-Fixed combination appears to provide a feasible means for accomplishing this objective, no further work was devoted to the Fixed-Adjustable concept.
- (c) The Adjustable-Adjustable combination of Figure 2(d) appears to provide an unnecessary redundancy of adjustment as well as requiring the field adjustment and verification discussed in (b) above.

A schematic diagram of the sensor itself is shown in Figure 3. It can be seen that in addition to the Sensor Input Axis mentioned in the previous section, there is a Sensor Output Axis which must be located with respect to a reference or nominal direction by the clamping system. The accuracy required for the output axis, however, is much less stringent, the allowable error being of the order of 10 times that for the input axis or approximately 50 arc-seconds. Preliminary study indicated that this accuracy is consistent with the conventional machining, assembly, and locating procedures followed with precision assemblies of this type. For example, in an assembly of the type shown in Figure 3, it is expected that the output axis can be located about the Input Axis repeatably and with sufficient accuracy by means of a locating pin. Consequently, no further work was devoted to the location of the output axis.

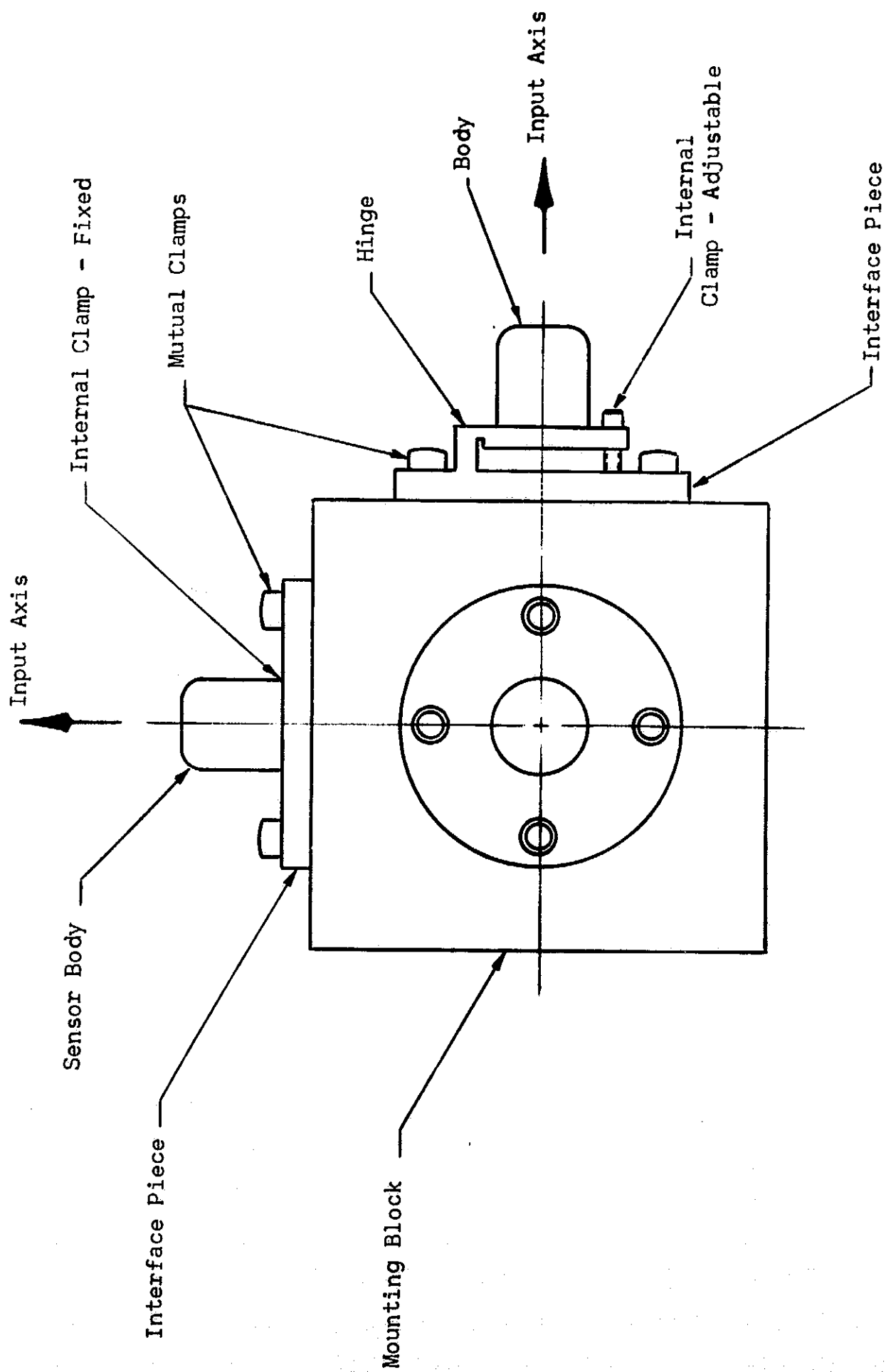
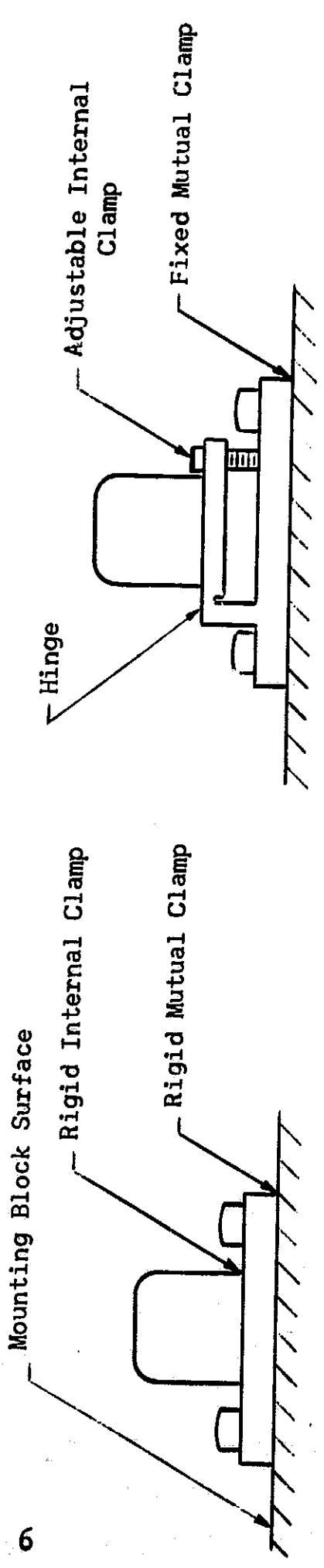
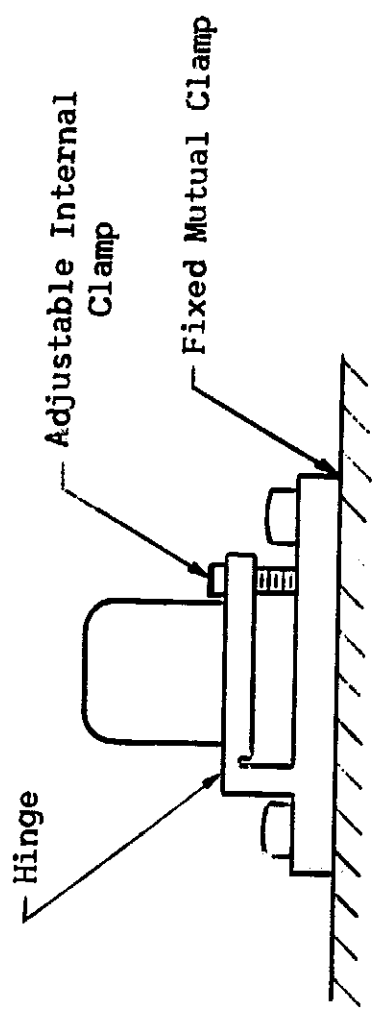


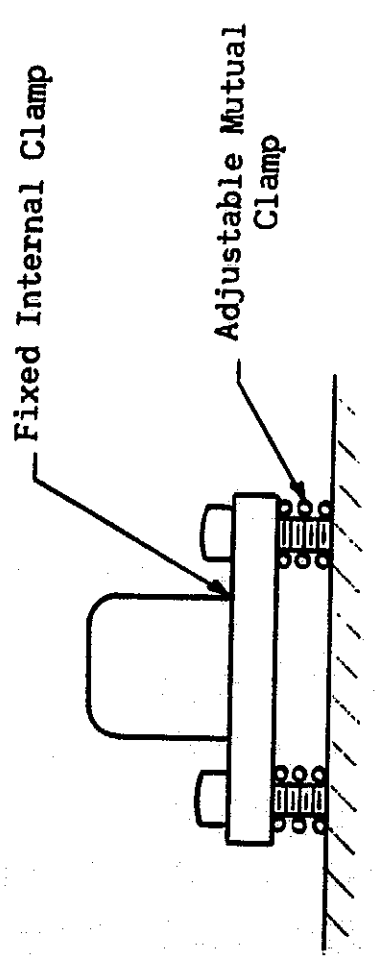
Figure 1. Schematic of Strapdown Inertial Measuring Unit (I.M.U.) Showing Clamps



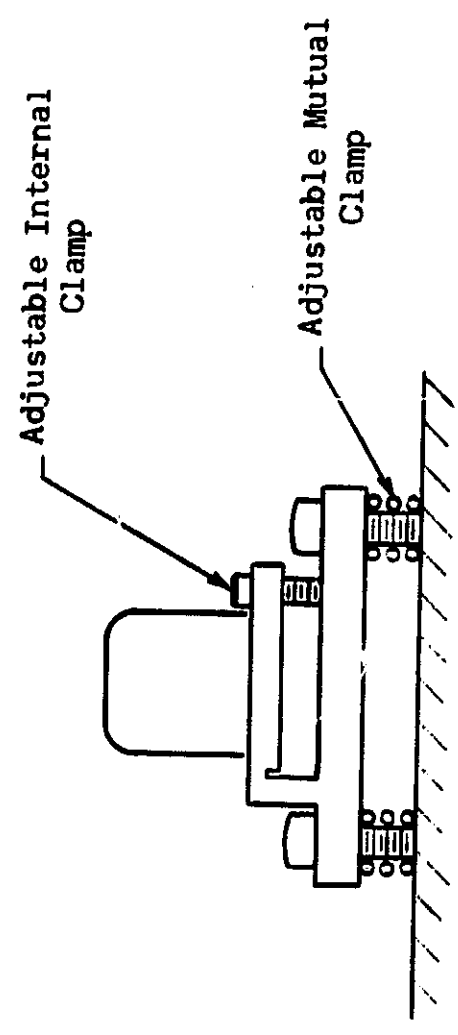
(a) Fixed-Fixed



(b) Adjustable-Fixed



(c) Fixed-Adjustable



(d) Adjustable-Adjustable

Figure 2. Schematic of Four Combinations of Adjustable and Rigid Internal and Mutual Clamps

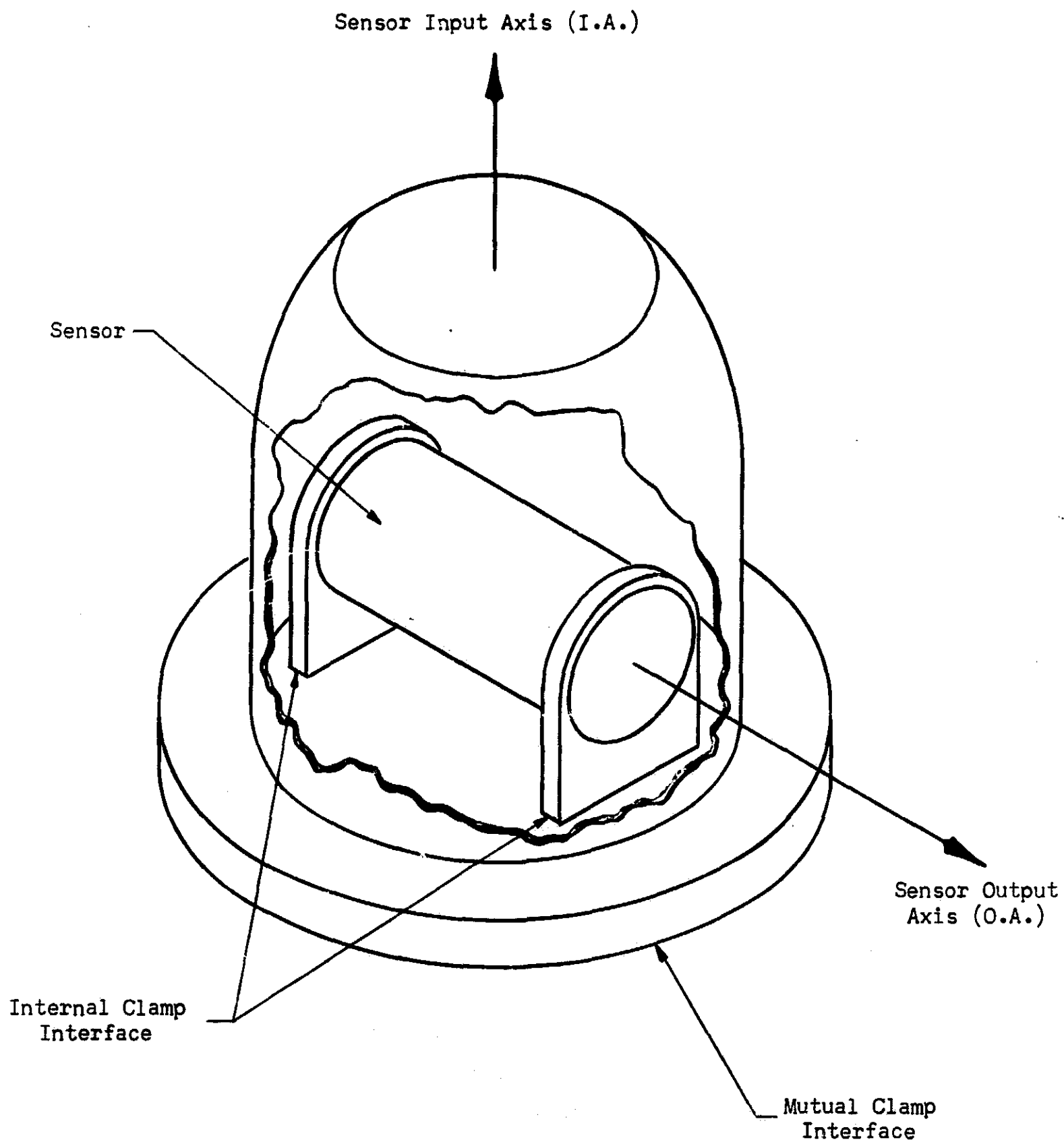


Figure 3. Schematic Diagram of Sensor Showing
The Input and Output Axes

REVIEW OF THE STATE-OF-THE-ART

A review was conducted of the present state-of-the-art in a number of areas critical to the development of an improved clamping system. These areas included existing techniques for testing and mounting gyros and other sensors, precision machining, metrology, and clean-room technology.

Information was obtained by means of a search of relevant technical journals, trade periodicals, and by contacting manufacturers and research institutions. In addition, a computer literature search covering the NASA, IAA, and DDC literature was conducted through NASA, ERC. In most instances, the only method by which a realistic (rather than an overly conservative) estimate of the state-of-the-art could be obtained was to rely upon verbal communication with persons directly involved in the various areas. In the following discussion, the sources for these verbal references are cited in accompanying footnotes.

Sensor Testing and Mounting

The Massachusetts Institute of Technology Instrumentation Laboratory and several gyro manufacturers* were consulted to obtain information on testing, transferring, and clamping inertial gyros. The pertinent areas of interest are discussed below.

Transfer of the gyro fixture.- The gyro input axis is located while the gyro is on a spin table. The gyro is either attached directly to the table or it is held in a test fixture which is attached to the table. The gyro must then be transferred to the mounting fixture in which it will be used. This transfer presently results in a large angular error as compared to the ± 5 arc-second goal for this program. For example, contacts with the previously cited sources indicate that this error is of the order of 30 to 60 arc-seconds.

This leads to the conclusion that an adjustable internal clamp will be required and that the adjustment of the gyro input axis, relative to the nominal axis on the mutual clamp, must be performed after assembly.

Location of the gyro input axis.- The gyro input axis is most often located with respect to a reference in one of two ways:

- (a) along a radius of a cylinder relative to a point on the periphery of the cylindrical case; or
- (b) perpendicular to a mounting surface on the gyro or gyro fixture.

*Nortronics, Kearfott, Honeywell, NASA Huntsville

The Massachusetts Institute of Technology Instrumentation Laboratory uses the first technique with gyros for the Apollo program. The angular orientation of the cylindrical gyro can inside the gyro fixture is initially effected to within approximately 60 arc-seconds by a locating pin near the periphery at one end of the gyro can as shown by Figure 4. Then from the other end, the can is rotated for fine adjustment so that the input axis orientation is accurate to within ± 10 arc seconds. The actual location of the input axis can be determined to within about 2 arc-seconds. Deviations of the input axis out of a plane that is perpendicular to the axis of the can are not very important for the mission, and are estimated to be on the order of several minutes of arc.

The Nortronics Precision Products Division in Norwood, Massachusetts adjusts a gyro in its fixture so that the input axis is within ± 10 arc-seconds of being perpendicular to a reference surface on the fixture. Contact with Kearfott and Honeywell also indicated that this figure is representative of the state-of-the-art. The NASA, Huntsville facility can locate the input axis on a strapdown gyro to within approximately ± 4 arc-seconds. The axis may deviate from perpendicularity to the mounting surface by 20 arc-seconds.

Thus, it appears that an improved adjustable clamp is required if the overall alignment is to be within the ± 5 arc-second goal. Also, to take advantage of the improved clamping techniques, an improvement will likely be required in the techniques for measuring the deviations of the input axis from its expected location relative to the gyro fixture. With the present location accuracy in the 2 to 4 arc-second range, a substantial portion of the ± 5 arc-second error budget is used up in the internal adjustment even with an improved adjustable clamp capable of adjustment to this accuracy. This probably will not leave enough error margin for the subsequent mating of the external fixed clamp in the field.

Methods of clamping gyros.- The Massachusetts Institute of Technology Instrumentation Laboratory's Apollo gyros are fixed in position by tightening threaded rings around the ends of the can. With this arrangement, it has been found difficult not to slightly alter any fine adjustment that was made before the rings are tightened.

Another technique uses a "belly band" around the middle of the gyro can. This ring is then attached to a mounting block as shown in Figure 5. This technique utilizes symmetry to reduce thermal strains.

Figure 6 shows a different clamping arrangement that is used by NASA, Huntsville. It is important that the three mounting pads lie in a plane, and that the toe clamps be tightened uniformly.

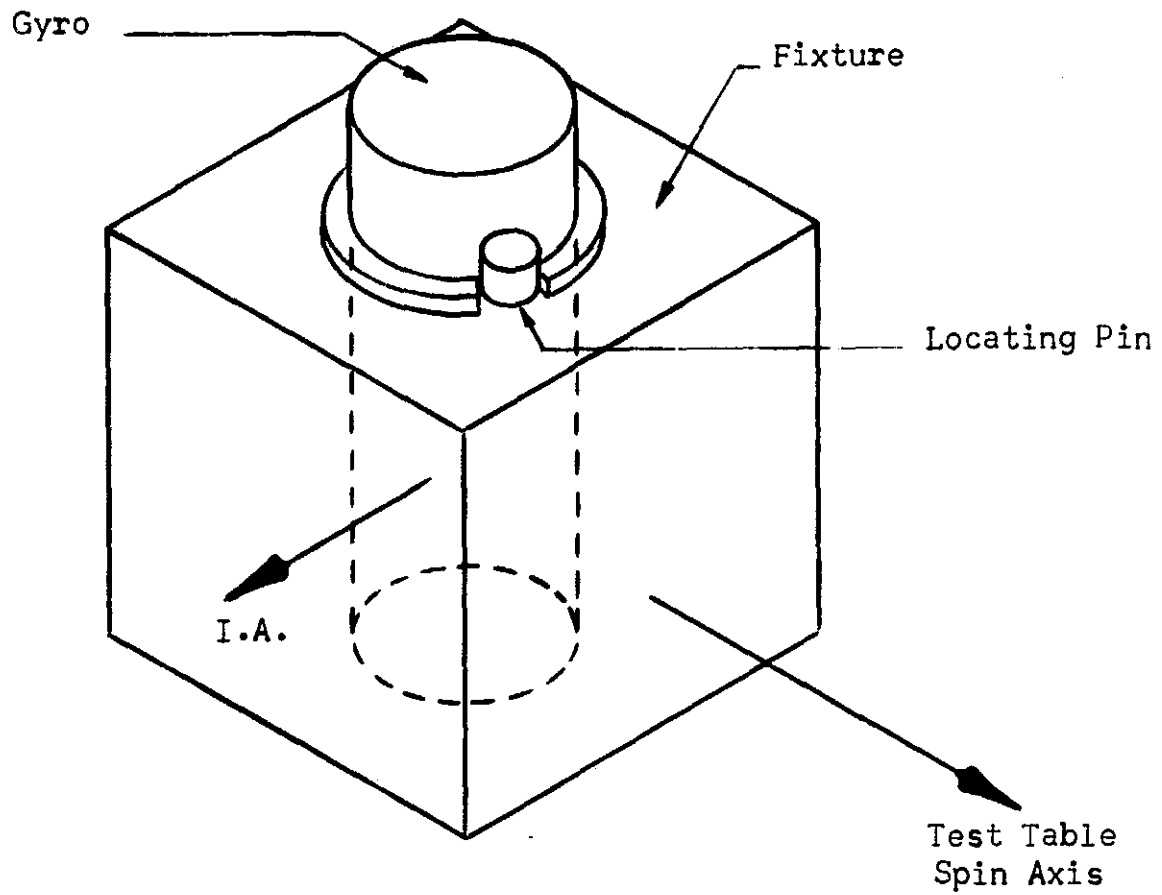


Figure 4. Gyro Input Axis Orientation Using a Locating Pin

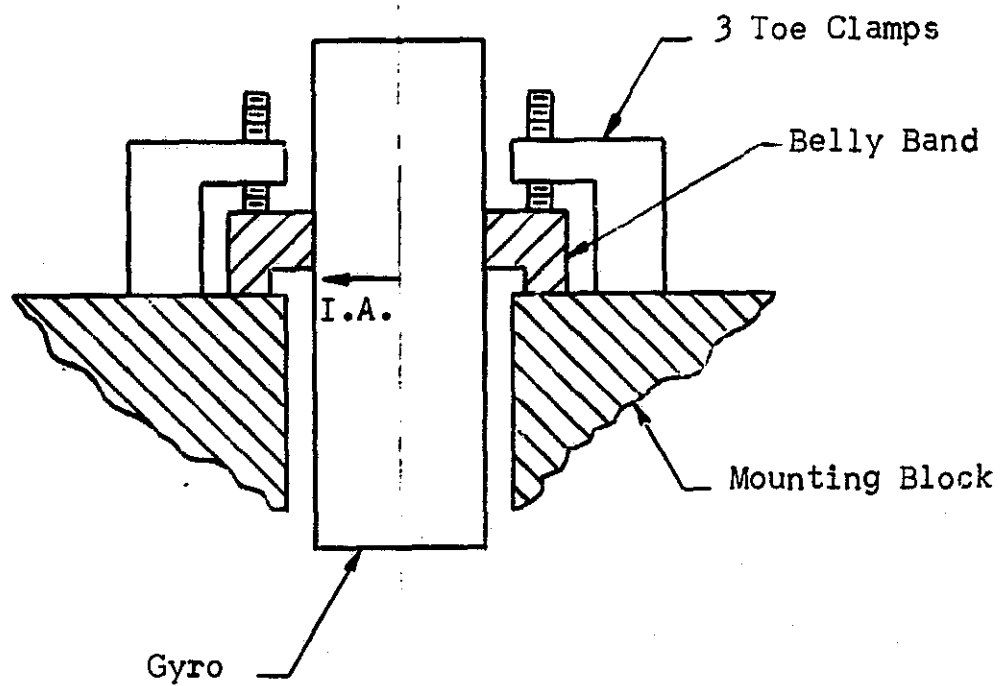


Figure 5. Gyro Clamping Using a Belly Band

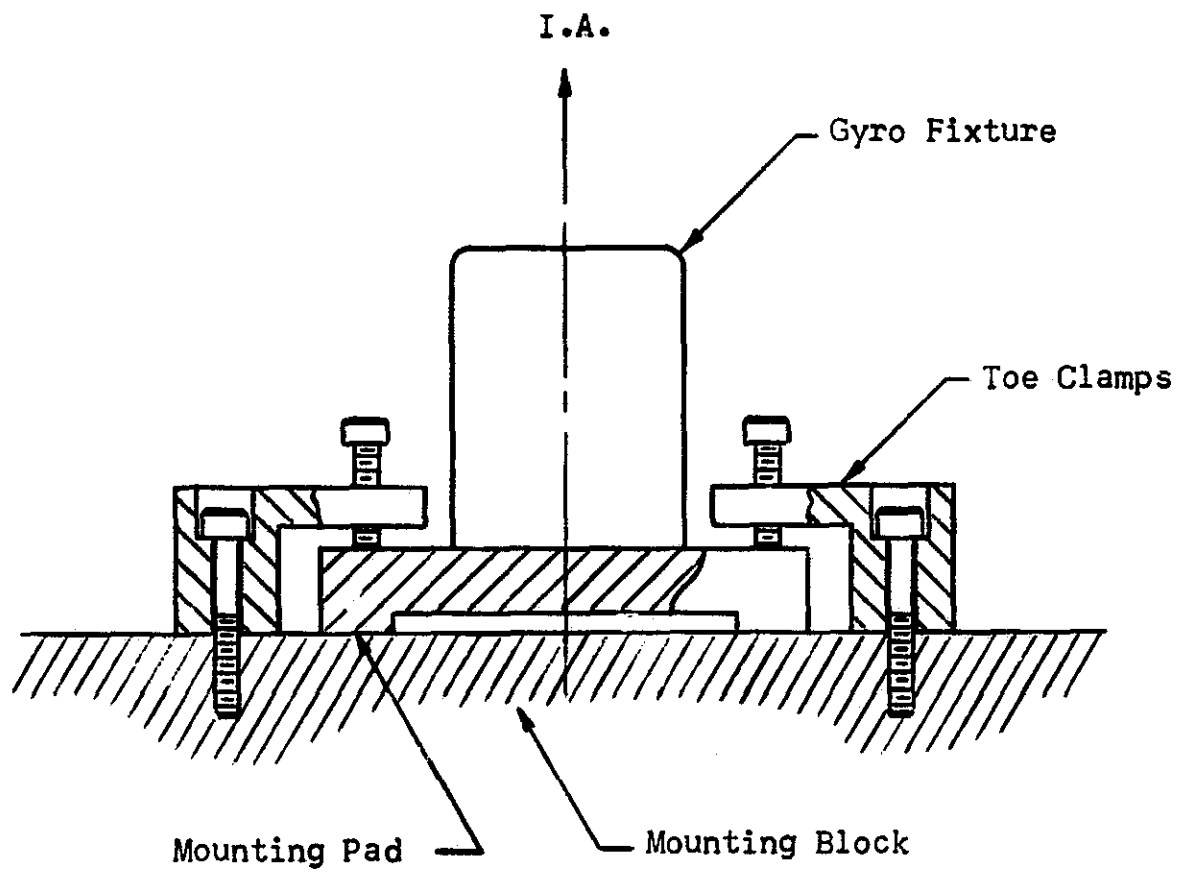


Figure 6. Gyro Clamping Using Mounting Pads

Precision Machining

To evaluate the feasibility of different clamping concepts, it is necessary to know how accurately various types of machining can be done. Machining considerations may govern whether or not it is necessary to use adjustable clamps with verification to hold the gyro to the mounting block with the desired precision. Precision machining capabilities will also influence the overall system geometry. The following companies were contacted and are referenced in the discussion below.

- (1) Starret Company
Athol, Massachusetts
- (2) Athbro Precision Engineering Company
Sturbridge, Massachusetts
- (3) Speedring Engineering Company
Detroit, Michigan
- (4) Van Keuren Company
Watertown, Massachusetts
- (5) National Bureau of Standards
Washington, D.C.
- (6) Moore Special Tool Company
Bridgeport, Connecticut
- (7) Pratt & Whitney Machine Tool - Gage Division
West Hartford, Connecticut

One of the simplest means of establishing three orthogonal axes is to make them perpendicular to three mutually perpendicular surfaces of a precision cube. Consequently, the accuracy with which three mutually perpendicular surfaces can be produced is of paramount interest. Laboratory master gage blocks are accurate to $\pm 1 \mu$ in, and master angle gage blocks to $\pm 1/4$ second of arc^{(1)*}. Flatness and parallelism of 1 to 2 μ in/in are attained in these blocks. The accuracy to which a 10-inch cube could be made has been estimated at 1 sec of arc, with flatness and parallelism as above⁽²⁾.

One way to orient the gyros is to put a cylinder into a hole. Therefore the accuracy with which a hole can be machined perpendicular (or at some other angle) to a surface is of interest. If the hole and the surface can be machined simultaneously, the axis of the hole can be held to within 1 arc-second of perpendicularity to the surface. This is not possible if three holes are to be orthogonal to each other and to three orthogonal surfaces. In this latter case, it is estimated that the axis of the hole can be held to within 2 arc-seconds of perpendicularity to the surface^(2,3).

*Superscripts refer to sources of information given in the preceding list.

Other important considerations in producing holes are their roundness and location. It has been estimated that a 3-inch diameter hole that is 4 inches long can be machined within $\pm 2 \frac{1}{2} \mu$ in of being perfectly round⁽²⁾. It is estimated that holes can be located to approximately 10μ in accuracy⁽³⁾.

The accuracy with which cylinders and spheres can be produced is also of interest. Cylinders can be machined accurately to 5μ in with a surface roughness of 0.5μ in⁽⁴⁾. Spheres can be machined to diametral accuracies of less than 3μ in⁽⁵⁾.

On the basis of this information, it appears that the art of ultra precision machining is sufficiently advanced so that it will not be the limiting factor in achieving clamping accuracies of 5 arc-seconds. However, for 2 arc-seconds accuracy to be achieved, the geometry will have to be restricted to two parallel mating planes so that machining errors do not use up the entire error budget.

Metrology

If adjustable clamps are used, the ultimate precision of the mounting process is limited by the ability to measure the orientation of the gyro relative to the IMU, rather than by the ability to accurately machine the clamps. Consequently, the state-of-the-art of precision measurement of distances and angles is of interest. Sources of information in this area were as follows:

- (1) Moore Special Tool Co.
Bridgeport, Connecticut
- (2) Engis Equipment Co.
North Grove, Illinois
- (3) Perkin-Elmer Corp.
Norwalk, Connecticut
- (4) Van Keuren Company
Watertown, Massachusetts

By using precision rotary indexes, it is possible to achieve angular displacements in fractions of a degree that are accurate to 0.1 seconds or arc^{(1)*}. Using precision autocollimators, it is possible to measure deviations from perpendicularity as small as 0.05 seconds of arc⁽²⁾. Pentaprisms are available that turn a beam of light 90° to within 0.5 seconds of arc⁽²⁾. With these instruments, parallelism and perpendicularity can be measured to within fractions of an arc-second.

*Superscripts refer to the sources of information given in the preceding list.

With laser interferometers, it is possible to measure distances to 10 μ in over many feet⁽³⁾. The National Bureau of Standards measures gage blocks to within $\pm 1 \mu$ in, and optical flats under ideal conditions can be used to measure flatness to within 1 μ in⁽⁴⁾.

It thus appears that the art of angular measurement is about an order of magnitude more advanced than the art of angular machining. Consequently, if sufficiently high adjustment resolution can be achieved, adjustable clamps can yield greater mounting precision than nonadjustable clamps by utilizing this measurement capability.

Clean Room Technology

The amount and size of dirt and other foreign particles that are present usually affect the accuracy of precision mounting. This problem can be approached either by devising a technique that minimizes the sensitivity to these particles, or by elimination of the objectionable particles. Consequently, the state-of-the-art of clean room technology is of interest.

At the present time, the most stringent clean room standards are those established by Federal Standard 209A. A Class 100 clean room can have a maximum of 100 particles/cu ft larger than 0.5 microns, and 1 particle/cu ft larger than 5 microns. (1 micron is approximately 40 μ in.) The filters that are available to meet these requirements will also filter 0.3 micron particles with an efficiency of 99.97%. It appears that this represents the state-of-the-art for some time to come, because the present mechanism of filtering particles less than 0.3 microns changes from an interference process to a diffusion process which is less suited to continuous-flow clean rooms. The best way to minimize these small particles is to use a portable ultra-clean work station inside an ultra-clean workroom. Nevertheless, it is still highly probable that there will be some 0.3 micron particles left in the environment.

Since 0.3 micron particles can cause fixed clamp misalignment beyond the ± 5 arc-second goal for this program, the main effect of the clean room is to decrease rather than eliminate the probability of misalignment. Thus, a desirable design goal for the clamping system is to provide the capability of dealing with the dirt in the normal atmosphere, thereby eliminating the need of a clean room environment for field installation of the sensors.

MATERIAL CONSIDERATIONS IN CLAMP DESIGN

The ability of the clamping system to maintain the alignment of the sensor will be influenced considerably by the properties of the materials selected for each of the system components.

It is convenient to consider a material to be characterized by: (a) a set of nominal properties which govern its behavior under normal short time loads; and (b) a set of material stability properties which describe the ability of the material to resist dimensional changes over relatively long periods of time.

In general, it may be stated that the following qualitative characteristics are desirable for the nominal properties of the clamping elements:

- (a) high stiffness (Young's Modulus of Elasticity);
- (b) high elastic-yield strength and micro-yield strength;
- (c) low density;
- (d) high thermal conductivity to minimize thermal gradients (unless selective conductivities are desired as a specific design feature);
- (e) low coefficient of thermal expansion for minimum thermal strain;
- (f) high degree of isotropy for both mechanical and thermal properties (unless anisotropy is to be used as a specific design concept);
- (g) high wear resistance;
- (h) failure characteristics which minimize the formation of burrs or nicks on the surface from wear particles;
- (i) corrosion resistance in the normal environment to which the clamp is exposed;
- (j) good machinability;
- (k) minimization of residual stress from machining; and
- (l) low cost.

For most engineering materials, values for the nominal mechanical and thermal properties can be obtained by reference to the various materials handbooks. Thus, it will not be attempted to present a compilation of properties in this report. Certain specific properties and desirable materials will be discussed in later sections with reference to clamp designs and their response to external loading.

The technology dealing with material instability, however, and the availability of quantitative information concerning this behavior is fragmentary with most of the work to date being aimed at rather limited and specific applications. Since information on this subject is scattered in various sources of literature and is not presented in a readily usable fashion, the remainder of this section of the report will be devoted to a critical literature review of the subject, with emphasis on the clamp design problem.

It may be generally stated that the final choice of material for a clamp element will be a compromise one. That is, those critical properties, such as listed above, whose effects cannot be overcome by proper design will be identified and will be used to choose the material. Choice of the design configuration or the incorporation of special design features will then be used to mitigate any deleterious effects of the remaining characteristics.

Material Instability

A fundamental limitation of the ability of any clamp to maintain alignment over a long period of time is that provided by instability of the material from which the clamp elements are made.

It is possible to define two general categories of material instability:

- (a) Dimensional Instability where a change in dimension over a period of time occurs in the absence of applied loading.
- (b) Microcreep where a change in dimension over a period of time occurs under an applied stress. It is distinguished from normal creep by the very small strains involved; in the microinches/inch range.

Stability of metals.- The state of available knowledge on the stability of metals has been well summarized in the two publications of the Defense Metals Information Center of the Battelle Memorial Institute (1, 2).^{*} Further work in this area continues at Battelle under the direction of R.E. Maringer (3, 4, 5, 6). A review of References (1, 2) shows very clearly that most of the work up to 1966 was concerned with measuring the dimensional stability of materials in the free, unloaded condition. This work was influenced by the desire to obtain "ultrastability" with precision gage blocks. A very limited amount of information is available on the long-term, time-dependent microcreep of metals under a state of constant applied stress. Weihrauch and Hordon's (7) work provides some of the earliest available data on long-duration, time-dependent microcreep. It was unfortunate that this work was not carried through to the next stage of measurement of configuration distortion arising from microcreep as proposed in that report.

Maringer (3, 4, 5, 6) is presently one of the prime sources for data on microcreep under constant applied stress. Lyons** at the NASA Electronics Research Center has initiated a program to obtain similar data on the lighter weight aerospace structural materials.

^{*} Numbers in parentheses refer to the List of References.

^{**} Verbal communication.

It is obvious that making measurements of changes in dimension of the order of 1×10^{-6} inches/inch over a period of months is an extremely difficult and time-consuming effort requiring measuring accuracies of the order of 1×10^{-7} inches. Short-time plastic strain measurements can be conducted rapidly, yielding a measure of plastic microstrain at various values of applied stress. A new property, Precision Elastic Limit (PEL) or Micro Yield Stress (MYS) has been defined to designate the stress at which time-independent and dependent plastic flow occur. It has arbitrarily been defined as that stress which will produce in a specimen a detectable positive residual strain of 1 micro/inch. The MYS can be significantly lower than the elastic yield stress, (0.2% plastic strain). The MYS is used as an upper limit of stress beyond which the probability of dimensional instability or time-dependent microcreep occurring is high. This does not eliminate the possibility of microcreep occurring at stress levels below the MYS. Based on measurements of microcreep, a rule of thumb has been proposed by Maringer (4) which limits the maximum stress for long-term dimensional stability to half the MYS for most metals.

Basic mechanisms leading to dimensional instability in metals.- Holden (1) and Maringer (2) have isolated two primary mechanisms leading to dimensional instability in the free unloaded condition. These are:

- (a) metallurgical instability; and
- (b) relaxation of residual stresses.

Metallurgical changes can take various forms involving ordering, precipitation and an allotropic transformation. Generally speaking, alloys having a relatively low melting point, such as those containing aluminum or magnesium, will show significant dimensional changes due to aging (precipitation) at room temperature, and must be carefully over-aged to achieve stability. Many steels are unstable due to the precipitation of carbides or the incompleteness of the austenite-martensite reaction. Because of its relative inability to alloy, its lack of a ferromagnetic domain structure, and its lack of an allotropic transformation, beryllium is comparatively free from the danger of instabilities introduced by physical changes.

Metals or alloys that do not undergo a phase change form one of the simplest classes of stable materials. The only apparent microstructural changes are in grain size, shape, and orientation. One metallurgical change which can cause small dimensional changes is ordering. Individual solute atoms often will tend to occupy specific positions in the solvent lattice relative to like or unlike atoms. Because these reactions are controlled by the diffusivity of the solute in question, the reaction rates are distinguished by a relatively strong temperature dependence. Small dimensional changes will follow changes in stress, magnetization, or possibly temperature. Such reactions can be responsible

for required warm-up times for oscillating devices, hysteresis behavior during the stress cycle, or time dependence after reaching some fixed new temperature.

An alloy that rejects a second phase from solid solutions (typical of the age-hardening alloy systems) will usually undergo a gradual change in volume. The rate of the reaction is dependent upon time and temperature, and upon the degree of departure from phase equilibrium. The reaction also may be sensitive to applied stress, the application of vibrational energy, and the level of impurities in the alloy.

A metal or alloy that undergoes a transformation from one allotropic form to another will change in volume. The change may be positive or negative, depending upon the relative specific volumes of the two phases. In steel, for example, the transformation from austenite to martensite results in a volume increase, the magnitude of which is dependent upon alloy composition.

Combinations of the several mechanisms described above may occur concurrently. For example, a steel may exhibit simultaneously a positive volume change from the transformation of retained austenite and a negative volume change from the tempering of martensite. Thus, the net volume change may be positive, negative, or zero; it also may change from one to the other over a period of time as one mechanism becomes dominant over another.

Shape distortions introduced by the relaxation of residual stresses are considerably more difficult to analyze. These stresses are most frequently introduced in the process of fabrication or heat treatment, and are characteristically nonuniform. In particular, any sort of deformation process such as extruding, rolling or forging will set up high residual stress levels. In addition, these processes tend to introduce anisotropy into the structure. Residual stresses can also be introduced by the process of joining parts together in some sort of permanent fashion. Welding, brazing, soldering or even the use of adhesives can be extremely troublesome because of the structural and material inhomogeneities introduced.

Residual stresses resulting from machining can at times be extremely high and can contribute significantly to dimensional instability if they are sufficiently high to cause microcreep. It is often difficult to reduce these stresses even after annealing at a high temperature. Another form of residual stress can be set up, as a result of changes in temperature, if the material in question is anisotropic in its thermal expansion. In most noncubic materials, the thermal expansion coefficient differs appreciably in different lattice directions. Consequently, when the temperature of a polycrystalline aggregate changes, an appreciable stress can be built up between adjacent grains. Avoiding this situation can become complex, for the thermal expansion coefficient, itself, is apparently influenced by both heat treatment and by the method of fabrication.

The problem is further complicated by the fact that distortions in the microinch-per-inch range can result from residual stress changes well below the present limits of experimental stress measurement. Further, present methods for the measurement of residual stresses are quantitatively useful only for sections of simple geometry. The stress distribution and consequent distortion of parts with more complex shapes can be predicted only qualitatively.

To summarize, it is extremely difficult to make generalizations about the configurational stability of components made from different materials. It may be possible to identify the general degree of metallurgical stability of the metal, but the induced residual stresses and their effect on dimensional stability of the specific component would be a function of the process of fabrication of that particular component and the type of heat treatment prescribed. Under very special conditions, it may be possible to balance the metallurgical instability with the plastic deformations induced by residual stresses to achieve satisfactory dimensional stability. This has been done by the National Bureau of Standards (8) in the development of precision gage blocks having ultra-stability. However, it will usually be necessary to reduce both the metallurgical instability and the residual stress levels to attain the necessary degree of dimensional stability. At this stage of the art, it is only possible to take a conservative stand and try to minimize both metallurgical instability and residual stresses. The problem may not prove to be as severe as anticipated when the effect of such changes on the functional performance of the component is considered. Dimensional changes arising from such instabilities could result in uniform changes in dimensions which would not affect performance.

The paragraphs to follow discuss some of the results of dimensional stability and micro yield stress measurements reported in the literature to date, as well as some of the limited data available on residual machining stresses. It is hoped that these values can be used as a guide to the selection of possible materials based on a stability consideration.

The dimensional stability of metals with no external load.- Two prime sources of data exist on the long term dimensional stability of metals.

Lement and Averback (9) have made an extensive series of measurements on the dimensional behavior of different types of steels and alloys. Data are reported for three types of exposure

- (1) 70°F;
- (2) 160°F; and
- (3) after cycling 10 times between 70°F and -95°F, with a 30-minute holding period at -95°F.

Tests were made under various types of heat treatment.

These are early measurements and their accuracy is poor when compared with present techniques. For example, length change is reported to a precision of ± 3 microinches. As such this data is considered to lack the accuracy required for this study and has not been included here. However, as a result of their extensive study of various metals and alloys under different types of heat treatment, it has been possible to select the best heat treatment for maximum stability. Table I is adapted from Reference (1) and represents those heat treatments resulting in minimum dimensional change. This table is recommended as a first-step guide for the selection of heat treatments to be used with a variety of materials.

By far the most useful work on long-term dimensional stability was reported by Meyerson (8) at the National Bureau of Standards on the development of ultrastable gage blocks. Measurements were made to an accuracy of 1×10^{-7} inches. Table II provides a list of the degree of stability attained with different metals using the heat treatment procedure described. Material selection was limited by use to those capable of yielding hard surfaces, i.e., either hardenable metals or cermets. The degree of stability obtained is extremely high, in all cases less than 1μ in/in/year, with two of the materials tested having a change in length less than 0.1μ in/in/year. Four different categories of materials were tested. The most stable materials and treatments in each of these categories were as follows:

- (1) Fully Hardened Steels - 52100 steel; hardened, stabilized, ground, stress-relieved, and lapped.
- (2) Steels with Annealed Core and Hardened Surface -
 - (a) 41J Stainless; annealed core, nitrided, with white layers removed from nongaging faces, stress-relieved, and lapped.
 - (b) 1010 Steel; pack carburized, case-hardened, stabilized, case partially removed from nongaging surfaces, stress-relieved, and lapped.
- (3) Steels with Partially Hardened Core and Hardened Surface -
 - (a) 17-4 PH Stainless; hardened, aged, nitrided, nitride removed from nongaging surfaces, stress-relieved, and lapped.
 - (b) Nitralloy 135; hardened, tempered, nitrided, white layer removed from nongaging surfaces, stress-relieved, and lapped.
- (4) Ceramics or Cermets -
 - (a) Titanium Carbide with Steel Binder; hardened, tempered, ground, stress-relieved, and lapped.
 - (b) Titanium Carbide with 25% Nickel Matrix; stress-relieved.

Table 1
Recommended Heat Treatments for Obtaining High Dimensional Stability in Selected Alloys
 (Adapted from Reference 1)

Alloy	Initial Condition	Desired Condition	Heat Treatment	Rockwell Hardness	Thermal Expansion Coefficient 10^{-6} / °C	Elastic Modulus 10^6 psi	Elastic Limit 10^3 psi
1112 steel	cold drawn	stress relieved	800F, 1 hr, A. C. or 1200F, 1 hr, A. C.	B95 B77	11.8 11.8	28.5 28.4	71.0 43.0
1045 Steel	cold drawn	stress relieved annealed	1200F, 1 hr, F. C. (a) 1550F, 1/2 hr, F. C. (b) 300F, 1 hr, A. C.	B93 B90	- 11.2	- -	- -
1144 steel	hot rolled	annealed hardened and tempered	1550F, 1/2 hr, F. C. (a) 1550F, 1/2 hr, O. Q. (b) 1100F, 1 hr, W. Q.	B85 C23	- 11.1	- -	- -
4140 steel	hot rolled	annealed hardened and tempered	1550F, 1/2 hr, F. C. (a) 1550F, 1/2 hr, O. Q. (b) 1000F, 2 hrs, A. C.	B95 C38	11.4 -	- -	- -
10100 steel	annealed	hardened and tempered*	(a) 1450F, 1/2 hr, W. Q. (b) 350F, 1 hr, A. C.	C64	11.8	-	-
Manganese Die Steel	annealed	hardened and tempered*	(a) 1450F, 1/2 hr, O. Q. (b) 300F, 1 hr, A. C.	C65	11.9	-	-
Tungsten Die Steel	annealed	hardened and tempered*	(a) 1600F, 1/2 hr, O. Q. (b) 300F, 1 hr, A. C.	C65	11.6	-	-
52100 steel	annealed	hardened and tempered*	(a) 1550F, 1/2 hr, O. Q. (b) 250F, 10 hrs, A. C. or 400F, 1 hr, A. C.	C65 C62	11.9	-	-
High C High Cr Die Steel	annealed	hardened and tempered* hardened and tempered*	(a) 1850F, 1/2 hr, A. C. (b) 300F, 2 hrs, A. C. or 500F, 2 hrs, A. C. (a) 1900F, 1/2 hr, A. C. (b) 320F, 1 hr, A. H. (c) 950F, 1 hr, O. Q. (d) Repeat (b) and (c) four times (e) 450F, 1 hr, A. C.	C63 C61 C60	10.3 -	- -	- -
M-2 High Speed steel	annealed	hardened and tempered*	(a) 2220F, 3 min, O. Q. (b) 1050F, 2 1/2 hrs, O. Q. (c) Repeat (b) three times (d) 900F, 1 hr, A. C.	C65	-	-	-
303 Stainless steel	cold drawn	quench-annealed and stress relieved	(a) 1950F, 1/2 hr, W. Q. (b) 600F, 1 hr, A. C. (c) 200F, 20 hrs, A. C.	B82	16.1	27.9	10.0
310 Stainless steel		quench-annealed and stress relieved	(a) 1950F, 1/2 hr, W. Q. (b) 750F, 1 hr, A. C.	B84	14.6	-	-
410 Stainless steel		hardened and tempered	(a) 1800F, 1/2 hr, O. Q. (b) 450F, 1 hr, A. C. or 600F, 1 hr, A. C.	C46 C41	- 10.2	- 31.4	- 10.8
440C Stainless steel	annealed	hardened and tempered	(a) 1900F, 1/2 hr, O. Q. (b) 500F, 1 hr, A. C.	C61	10.2	-	-
2-Nickel	cold drawn	age hardened	1000F, 9 hrs, F. C. to 900F, A. C.	C40	12.4	32.1	11.4
Inconel	cold drawn	annealed	(a) 1700F, 1 hr, F. C. (b) 200F, 24 hrs, A. C.	B71-75	12.7	30.1	15.0
K-Monel	cold drawn	age hardened	1000F, 9 hrs, F. C. to 900F, A. C.	C37	13.4	28.2	11.0
Hastalloy B	cast	quench-annealed and stress relieved	(a) 2100F, 1 hr, W. Q. (b) 1950F, 1 hr, W. Q. (c) 600F, 1 hr, A. C.	B95	10.4	-	-
Regular Invar	cold drawn	stress relieved	(a) 1200F, 1 hr, A. C. (b) 200F, 48 hrs, A. C.	-	-	-	-
Free Cut Invar	cold drawn	stress relieved	(a) 1200F, 1 hr, F. C. (b) 200F, 20 hrs, A. C.	B90-95	1.5	22.0	47.5
	cold drawn	quench-annealed	(a) 1525F, 1/2 hr, W. Q. (b) 1200F, 1 hr, A. C. (c) 200F, 48 hrs, A. C.	B79	-	-	-
Ni-Span-HI	cold drawn	solutionized and aged	(a) 1800F, 1 1/4 hrs, W. Q. (b) 1250F, 20 hrs, A. C.	C30	15.5	-	-
Beryllium-Copper	cold drawn	solutionized and aged	(a) 1450F, 7 hrs, W. Q. (b) 600F, 2 hrs, A. C.	C37	15.9	19.0	58.5
2017 (17 S) Aluminum alloy	solutionized	solutionized and aged	(a) 940F, 1/2 hr, W. Q. (b) 350F, 11 hrs, A. C.	B67	21.5	-	-
2024 (24 S) Aluminum alloy	solutionized	solutionized and aged	(a) 930F, 1/2 hr, W. Q. (b) 375F, 12 hrs, A. C. or 400F, 2 hrs, A. C.	B71 B72	21.4	10.8	32.0
356 Aluminum alloy	cast	solutionized and aged	(a) 1000F, 2 hrs, W. Q. (b) 310F, 4 hrs, A. C.	B58	20.8	10.5	12.0
Low M Magnesium alloy	extruded	stress relieved	500F, 1/4 hr, A. C.	E36	24.2	-	-
150A Titanium alloy	hot rolled	normalized hardened and stress relieved	1550F, 1/2 hr, A. C. (a) 1550F, 1/2 hr, O. Q. (b) 600F, 1 hr, A. C.	C38 C53	- 8.2	- -	- -
9271-5Cr-3Al Titanium alloy	cold drawn	annealed and stress relieved	(a) 1380F, 3 hrs, F. C. (b) 600F, 1 hr, A. C.	C34	8.6	-	-
Nitrelloy 135 mod.	nitrided	stress relieved	1000F, 1 hr, A. C.	15H54	12.1	-	-

*Treatment recommended if service temperature is maintained at about 70F.

A. C. - air cool
F. C. - furnace cool
O. Q. - oil quench

W. Q. - water quench
A. H. - air heat
B. W. Q. - boiling water quench

Table II

Summary of Stability Characteristics of Gage Blocks, in Order of Merit

(Adapted from Reference 8)

Material and Identifying Treatment	Surface Hardness, R _C	Maximum Period Observed Months	Condition of Case Hardening on Non-Gaging Faces			Average Change in Length pin/in/yr
			Intact	Partially Removed	Completely Removed	
17-4PH, hardened, aged, nitrided	> 70	22			X	+0.05
Titanium carbide, 25% Ni, stress relieved	72	20				-0.07
410, annealed core, nitrided	68	45		X		+0.10
Titanium carbide, steel binder, hardened and tempered	65	19				-0.10
1010, pack carburized, case hardened	66	30		X		+0.11
52100, directly quenched or martempered, stabilized, R _C 62	62	49				-0.13
Nitralloy 135 mod, hardened, tempered, nitrided	68	34		X		+0.17
1010, carbonitrided, case hardened	65	20			X	+0.17
Nitralloy 135 mod, hardened, tempered, nitrided	68	34			X	+0.19
52100, directly quenched or martempered, stabilized, R _C 60	60	50			X	+0.20
410, annealed core, nitrided 2-step	67	45	X			+0.20
Nitralloy 135 mod, hardened, tempered, liquid nitrided	57-69	17			X	+0.21
52100, annealed, chromium plated	68	48		X		+0.21
1010, annealed core, thermal sprayed	62	17			X	+0.25
T15, hardened, tempered to R _C 62	62	19				+0.27
8620, carbonitrided, case hardened	66	36			X	+0.29
52100, directly quenched or martempered, stabilized, R _C 65	65	49				-0.30
Chromium carbide, Ni binder, as received	> 68	20				-0.34
1010, annealed core, chromium plated	68	25		X		+0.35
Aluminum oxide, no binder	> 70	29				+0.38
8620, liquid carburized, case hardened	65	32			X	+0.38
Nitralloy 135 mod, annealed core, nitrided	68	17			X	+0.40
52100, annealed, flame plated	72	30			X	+0.41
8620, gas carburized, case hardened	64	20			X	+0.42
410, annealed core, nitrided	68	30			X	+0.44
T15, hardened, tempered to R _C 65	65	20				+0.49
1010, annealed core, chromium plated	68	36			X	+0.58
W4, hardened, stabilized	65	16				+0.59
Commercial through-hardened steel gage blocks, AA grade	65	25				-0.67
Titanium carbide, 40% Ni, stress relieved	68	19				-0.78
420, hardened, tempered, nitrided	65	16			X	+0.80
D2, annealed core, nitrided	65	16		X		+0.81
410, annealed, chromium plated	68	24			X	+0.85
D2, hardened, stabilized	58	16				+0.86
D2, annealed, flame plated	72	24			X	+0.89
410, annealed, flame plated	72	23			X	+0.96
52100, hardened, deliberately unstable	66	7				-25.0

Micro-yield stress and microcreep in metals.- Precision measurements of Micro-Yield Stress or the Precision Elastic Limit have been made by Maringer (3), Weihrauch and Hordon (7), Mikus, et al., (10), Jennings (11), Heuget (12), and Rockower (13). There is limited data on the long-time microcreep of materials under constant values of stress.

Table III is a compilation of results by Hordon (7) and Mikus (1). The table shows the MYS at three temperatures, 75F, 150F and 200F. There is a drop-off in the value of the MYS between 75F and 150F, with a small change occurring beyond 150F to 200F.

Dimensional stability has been reported for both the unstressed and stressed conditions. However, the minimum stress at which measurements were made usually exceeded 50% of the MYS so that no data is available on the effect of very low stresses on the long-time dimensional stability.

Hordon's results show that even for metals which have relatively high values of dimensional stability under no stress, the dimensional changes measured under stress are quite high, greater than 40 μ in/in. This indicates that the materials would have to be worked at much lower values of stress, if better stability were to be maintained.

The same comments can be made for the 52100 tool steel used by Mikus (10). Stress can cause an appreciable increase in the dimensional change over the unstressed conditions.

Table IV shows the results of Hughel (12) on the average MYS and microcreep data on various forms of commercial beryllium. The results show that when the stress level is 50% or less than the MYS, strains resulting from microcreep are low, approximately 2 to 3 μ in/in. As the stress level approaches the MYS, the resulting microcreep strains increase rapidly to 10 to 20 μ in/in.

As a result of a program investigating the stability of structural materials for spacecraft applications being conducted at Battelle Memorial Institute under the direction of Maringer (3, 6), data on the precision mechanical properties of various materials, as well as microcreep behavior, has been obtained. Table V provides a compilation of the micro-yield stress behavior. MYS values at 1 μ in/in and 5 μ in/in have been included to indicate the effect of strain hardening. Microcreep data on some of the metals listed in Table V, as reported in Reference (4), are shown in Table VI. The table also includes the total strain recovery after unloading, indicating that hysteresis type of effect may be present.

A comparison of Tables III and VI shows the apparent difference between the resulting magnitudes of microstrain. The aluminum 6061 was tested by both Hordon (Table III) and

Table III
Micro Yield Stress and Microcreep Data for Various Alloys
 (Adapted from References 7 and 10)

No.	Material	Alloy	Treatment	Hardness Rockwell	Stress Level psi	Microinch per inch Length Change in Time												Micro Yield Stress psi		
						75F			150F			200F			75F	150F	200F			
						100 hrs	500 hrs	1000 hrs	100 hrs	500 hrs	1000 hrs	100 hrs	500 hrs	1000 hrs						
1	Stainless Steel	310	(1) Quench Anneal 1950°F in H ₂ , 1/2 hr, W. Q. (2) Rough Machine (3) S. R. 750°F in Air 1 hr, A.C. (4) Final Machine (5) Stabilize 200°F, 20 hrs, A.C.	B83	0	-0.8	-2.5	-1.5	-3	-5	-5	-5	22,700	20,400	20,000					
						80	100	130	100	150										
						210	360	200	330	220										
						320	580	330	>600	400										
2	Ni-Alloy	Invar 36	(1) H.T. 1525°F in H ₂ , 1/2 hr, W.Q. (2) Rough Machine (3) H.T. 1200°F in H ₂ , A.C. (4) Final Machine (5) Stabilize 48 hrs, 200°F, A.C.	B85	0	-1	-2.2	-2	-4	-3.5	-5	26,400	25,000	24,700						
						50	70	70	120	130										
						140	200	140	230	240										
						280	360	350	430											
3	Aluminum Alloy	356-T6	(1) Solution anneal, 2 hrs, 1000°F Air (2) Boiling Water Quench (3) Rough Machine (4) Temper 4 hrs 310°F, A.C. (5) Final Machine	F77	0	-2.5	-3.5	-3.5	-4.2	-4.5	-5	8,100	7,350	7,150						
						40	50	50	80	50										
						100	170	100	220	160										
						180	330	170	370	280										
4	Aluminum Alloy	6061	(1) Solution anneal, 2 hrs, 970°F Air (2) Water Quench (3) Rough Machine (4) Age Harden, 6 hrs 350°F, A.C. (5) Final Machine	B55	0	+10	+20	+5	-5	-25	-35	12,400	11,700	10,430						
						40	60	80	160	80										
						140	180	130	260	150										
						210	280	230	380	260										
5	Magnesium Alloy	AZ92A	(1) Solution anneal, 20 hrs, 750°F SO ₂ Atmosphere (2) Air Blast Cool (3) Rough Machine (4) Age Harden, 4 hrs, 500°F, A.C. (5) Final Machine		0	+35	+70	+60	+90	+100	110	5,280	5,040	4,780						
						40	50	40	60	60										
						75	90	75	110	130										
						130	230	120	230	200										
6	Tool Steel (Ref. 10)	S2100 Structure D Austempered S2100 Structure A S3100 Structure B	Austenitize 1/2 hr at 1550F, Austemper 1 hr, 500F, A.C. Austenitize 1/2 hr at 1550F, O. Q. 90F and Temper 10 hrs, 250F Austenitize 1/2 hr at 1550F, O. Q. 90°F, Temper 1 hr, 550F		0	-	-	1	0	-	-	-	-	-						
						-	-	5.5	3.5	-	-	-	-							
						-	-	8	6	-	-	-	-							
						0	0	2	5	-	-	-	-							
						-	-	35	55	-	-	-	-							
		70	90	-	-	-	-													
		2	1	-	-	-	-													
		3	15	-	-	-	-													

Data for 400 hrs and 1,000 hrs instead of 100 hrs and 500 hrs

Notes:
 A. C. - Air Cool
 W. Q. - Water Quench
 H. T. - Heat Treat
 O. Q. - Oil Quench
 S. R. - Stress Relieve

Table IV

Dimensional Stability Under Stress for Beryllium

(Adapted from Reference 12)

Beryllium, Mesh Size & Grade	Average Precision Limit psi	Test Stress psi	Total Test Time hrs	Total Strain $\mu\text{in/in}$
-200, 100% Virgin	2,200	3,800	803	+41.4
		1,700	347	+ 7.2
		1,665	420	- 2.9
-200, Standard Production Grade	2,663	500	384	+ 2
		1,900	384	+ 3.7
		4,500	829	+ 9.9
-200, 60% Recycle +40% Virgin	4,100	2,400	560	+ 6.8
		2,800	556.5	+ 3
		3,940	97	+20.6
-200, 100% Recycle	4,300	3,600	508	+ 6.9
		5,200	469	+ 6.6
-325, 100% Virgin	6,500	4,800	555	+10.8
		6,200	137	+14.6
		6,400	489	+10.1
Subsieve, 100% Virgin	4,333	3,090	359	+ 0.3
		4,040	359	+13.8
		5,340	431.5	+10.3
Subsieve, 100% Recycle	11,167	9,260	420	+ 2.9
		10,450	418	+ 4.7

Table V

Precision Mechanical Properties of Various Materials

(Adapted from References 3 and 6)

Material	Alloy	Heat Treatment	MYS, 1 μ in/in psi	MYS, 5 μ in/in psi
Aluminum	2024-T4	As Received	38,000	45,000
		1 hr at 400F	29,000	39,500
		1 hr at 450F	28,800	37,000
		1 hr at 500F	20,200	28,200
	5456-H34	As Received	17,500	19,400
		1 hr at 400F	19,500	21,000
		1 hr at 450F	19,800	21,000
		1 hr at 500F	18,600	20,000
	6061-T6	As Received	18,400	26,800
1 hr at 400F		25,400	29,900	
1 hr at 450F		20,800	25,000	
1 hr at 500F		10,200	16,200	
Magnesium	AZ31	As Received	3,200	4,200
		1 hr at 450F	3,340	3,880
Nickel	Ni-Span-C	1 1/4 hr, 1800F; W.Q.; 21 hr, 1250F, A. C.	39,000	50,000
Stainless Steel	440C	1/2 hr, 1900F, O.Q, Hold 2 min; Immerse in Liquid Nitrogen 30 mins; 1 hr, 520F, A. C.	69,780	96,700
Aluminum	A356 Cast	16 hr, 1000F, B.W.Q.; 4 hr 310F, A. C.	7,550	10,500
Molybdenum	TZM	As Received	24,000	52,000
		1 hr at 2200F in H ₂	52,200	60,500
		1 hr at 2600F in H ₂	49,000	52,000
Beryllium	I-400	As Received	5,000	10,400
		1 hr at 1100F in vacuum	6,800	17,000
		1 hr at 1500F in vacuum	5,200	12,100
Note:		W.Q. - Water Quench O.Q. - Oil Quench	B.W.Q. - Boiling Water Quench A. C. - Air Cooled	

Table VI

Microcreep Data for Some Materials

(Adapted from Reference 4)

Material	Alloy	Stress Relief Heat Treatment	Approximate Level of		Total Creep Strain (at about 1400 hrs) μ in/in	Total Strain Recovery (1400 hrs after Unloading) μ in/in
			Stress psi	Percent MYS		
Aluminum	2024	400F, 1 hr, Furnace Cooled, Air	18,000	50	5	< 1
			24,000	70	8.5	~ 1
	5456	Same	11,000	50	38.5	21
			15,000	70	44.5	31
			18,000	90	64.5	49
	6061	Same	15,000	50	1	1
			18,000	70	5	2
			24,000	90	10.5	3.5
Magnesium	AZ31	450F, 1 hr, F.C., Air	1,700	50	3.5	< 1
			2,500	70	7	< 1
			3,000	90	10.5	3
Molybdenum	TZM	2200F, 1 hr; F. C., H ₂	27,000	50	1.8	0
			30,000	60	-1.3	0
			38,000	70	0.6	0
Beryllium	I-400	1100F, 1 hr; F.C., Vacuum	4,500	50	< 10	(-6)*
			5,900	70	5	(-3)
			7,000	90	7	(-4)

*Recovery strain was in the same direction as creep strain.

Maringer (Table VI). Maringer's results of microcreep were practically an order of magnitude smaller than those measured by Hordon. An explanation for this discrepancy is not obvious. It may partly be due to an improvement in the loading methods and greater stability in the control of environmental conditions. The above results show that all materials tested above would creep at stresses as low as 50 percent of the MYS with the exception of TZM Molybdenum. Microcreep of TZM at stresses less than 90 percent of the MYS is essentially zero. In this respect it is a desirable material.

Of the aluminum alloys, 5456-T34 is the most susceptible to microcreep, having creep strains an order of magnitude higher than either 6061-T6 or 2024-T4 which are roughly comparable. The AZ-31 magnesium exhibits appreciable microcreep at loads greater than 2000 psi.

The microcreep recovery experiments indicate that considerable hysteresis behavior in some materials such as 5456-T34 aluminum can occur. This would make it completely unsuitable for a precision load-unload type of application. 2024-T4 Aluminum with its very low recovery, would function reasonably well in such an application, with TZM molybdenum being the best in this respect.

Data on the microcreep of beryllium are not as consistent as the other metals and may be a result of the nonuniformity of the starting material (4).

Residual stresses due to machining.- The various forms of machining required to produce a specimen of the required dimensions can involve considerable deformation and consequently can develop considerable residual stresses. A measure of the severity of these residual stresses can be obtained from measurements made by Bonfield et.al. (14) on beryllium. Maximum residual compressive stresses of 38,000, 22,000, and 13,000 psi were induced by the processes of turning, grinding or sawing. With these high residual stresses in beryllium, having a MYS of 4000 psi, microcreep can be confidently predicted and dimensional instability must be expected.

As a result of the research work conducted at Battelle, under Maringer, it is postulated that the majority of dimensional instability observed in beryllium, and many other materials as well, is the direct result of residual stresses introduced by machining.

An attempt (6) was made to measure machining residual stresses in the specimens of Ni-Span-C and 440C stainless steel machined by common shop practice. These stresses were computed from the change in length of the specimen accompanying chemical etching of the surface. In this fashion maximum residual stresses have been found of 15,000 psi in compression in Ni-Span-C, and of 8000 psi in tension in 440C stainless steel. It is planned to extend these measurements to other metals. This information

will then be used as baseline data to assess the magnitude of the residual stresses introduced by various machining operations. From this, various sequences of cuts amenable to a final machining operation could be set up and an optimum final machining sequence selected for each material. Ultimately, other machining parameters would be examined, such as rpm, tool feed, lathe turning versus grinding and lapping. The program outlined above is quite ambitious and if completed should yield invaluable data to aid in both material selection and clamp design.

Dimensional stability of ceramic materials.- From the standpoint of dimensional stability, ceramic materials have the advantage of virtually no phase transformations in the environmental ranges encountered in gyro practice (13, 15). Also, stress-induced instability is minimized due to greater elastic strength. In addition, they provide a number of the generally desirable properties listed in a previous paragraph including:

- (a) High stiffness
- (b) High elastic strength
- (c) Low coefficient of thermal expansion
- (d) High wear resistance
- (e) Corrosion resistance.

These are offset by the difficulty in fabricating complex configurations, by low ductility, and by relatively high cost. As the need for ceramic parts increases, however, the state-of-the-art in ceramic fabrication is improving, making the cost comparable to that of beryllium (13).

Table VII gives a summary of the micro-yield stress for a number of ceramic materials. Of the various ceramics tested, beryllia has the advantage of an extremely high thermal conductivity, making it desirable from the standpoint of thermal dissipation and minimum temperature gradient.

Table VIII shows some recent data obtained on the MYS and the "Dimensional Stability Limit" of beryllia. This data was obtained by the Southwest Research Institute under contract to the M.I.T. Instrumentation Laboratory (13), as part of a program to investigate the physical properties of beryllia as a material for integrating gyros. The dimensional stability limit in this case was defined as the maximum stress below which the plastic strain was less than or equal to $\pm 2.7 \mu$ in/in over a period of 200 hours. The strain limit was determined by the maximum sensitivity of the optical strain gage used for measurement of strain.

Long-term dimensional stability data on ceramic gage blocks was obtained by Meyerson (8) and the results are included in Table II. The materials tested included aluminum oxide, titanium carbide and chromium carbide. All of these had high dimensional stability, less than 0.4μ in/in/year.

Table VIISummary of Micro Yield Stresses for Ceramics

(Adapted from Reference 15)

Ceramic Material	Number of Specimens	Micro Yield Stress (psi)		Ultimate Strength (psi)	
		Average	Standard Deviation	Average	Standard Deviation
Alumina	4	23,000	3,000	23,000	3,000
Beryllia	4	20,000	2,000	20,000	2,000
Grade A Glass-Bonded Mica	6	4,000	500	9,000	1,000
Grade B Glass-Bonded Mica	6	3,500	1,000	11,000	1,000

Table VIII

Micro Yield Stress and Dimensional Stability Limit of
Beryllium and Beryllia

(Adapted from Reference 13)

Material	MYS psi	Dimensional Stability Limit* psi
Beryllium	8,710	8,710
Beryllia "A"	12,300	6,150
Beryllia 'B'	20,700	11,680
Beryllia C	11,900	9,500

*Note: Microcreep strain $< \pm 2.7 \mu$ in/in after 200 hrs.

A comparative chart of the microyield stress of various metals and ceramics is provided in Table IX. It is seen that the MYS of beryllia compares favorably with that of most metals.

Ceramic materials have an added advantage over ductile metals from a wear standpoint. Being brittle in nature, scratches formed on the surface result in loose wear particles which could be dusted off without leaving a burr or nick on the surface. Scratches produced on the surface of most ductile metals are due to plastic flow and result in a burr being formed on the surface. As discussed under "Interface Considerations" a burr of this type on a locating surface can result in misalignment.

Configurational instability.- The only report on configurational instability available at the present time is a study by Gross (16) on the configurational stability of various beryllium gyro components. The stability of parts made from hot-pressed, forged beryllium was compared with that of parts made from hot-pressed and stress-relieved beryllium; the stress relief being performed prior to finish machining of the pieces.

Configurational instability or distortion was defined in terms of the change in flatness of optical-quality flat reference surfaces on two typical gyro components, i.e., gyro and housings and rotor halves. These components were stored for 90 days at various temperatures.

Typical changes in measured flatness ranged between 0 to 16 microinches for the rotor half. The presence of holes in the parts had very little effect on the overall change in flatness. The end housings made of hot-pressed, forged beryllium exhibited a flatness change of 10 microinches as compared to 20 to 32 microinches for end housings made of hot-pressed and stress-relieved beryllium.

Since the linear dimensions of the reference flats were not reported, it is not possible to make an estimate of the distortion in microinches/inch.

Another series of tests was designed to specifically study the effect of drilling holes on flatness distortion. The rotor halves were lapped flat, and then holes were drilled with the hole axes normal to the lapped surface. The drilling operation resulted in an average change in flatness of 74 microinches for the hot-pressed, stress-relieved beryllium; and 21 microinches for the hot-pressed beryllium. Gross (16) has attributed this distortion to the stress imposed by the drilling operation rather than a result of redistribution of residual stresses in the material. On this basis, it is concluded that in any such manufacturing process lapping should follow a drilling operation.

This study shows that parts made of hot-pressed beryllium are configurationally more stable than hot-pressed and stress-relieved beryllium.

Table IX

Comparison of Microcreep Characteristics of Various Materials
Arranged in Order of Decreasing Micro Yield Stress

Number	Material	Micro Yield Stress* psi
1	6Al-4V Titanium Rod	70,000
2	440 C Stainless Steel	69,780
3	Inconel X	65,000
4	TZM - Molybdenum	52,200
5	High Speed Tool Steel	50,000
6	Ni-Span-C	39,000
7	2024 - TA Aluminum	38,000
8	6061 - T6 Aluminum	25,400
9	High Purity Alumina	23,000
10	High Purity Beryllia	20,000
11	5456 - H34 Aluminum	19,500
12	CRES 310 Steel Rod	12,000
13	A356 Cast Aluminum	7,550
14	Beryllium I-400	6,800
15	Glass Bonded Mica	4,000
16	AZ-31 Magnesium	3,340
17	Hot Pressed Beryllium	2,000

*For each material the highest value of MYS, has been reported corresponding to the best heat treatment for the material.

The investigation, however, is specifically devoted to beryllium gyro components, and is therefore limited in its usefulness. Neither adequate part dimensions, nor sequence of machining operations has been provided to permit any definite conclusions. It is nevertheless useful in providing the only data available at this time on the configurational instability of an aerospace guidance component. It shows conclusively that dimensional instability can lead to configurational distortion. More tests of this type with different shapes, materials, machining, and heat treatments should be carried out to determine the magnitude of such distortions to be anticipated. The work of Maringer at Battelle on dimensional instability and the effect of residual machining stresses, as reported in previous paragraphs, may well form the guide lines for further investigation in this area.

At this time, it is possible to make the general statement that a symmetrical design configuration will minimize possible distortions.

Dimensional instability due to thermal cycling.- The effect of thermal cycling on dimensional instability of typical aerospace materials has been reported by Maringer (5, 17). The two studies utilized different types of test specimens, and different types of sample preparation and test techniques. These differences may account for some of the significant variation in results obtained between the two studies. Consequently, the results reported herein are to be taken as preliminary values requiring further confirmation. This study is presently continuing at Battelle (17) and the results reported herein should be reviewed when further data become available.

Table X shows the effect of temperature cycling, from -50°F to 100°F (5). The total time for one cycle was about 90 minutes. The magnitude of the dimensional change for all the metals studied is extremely high. However, there is a possibility that these large values may be a result of experimental inaccuracies associated with bending of the thin specimens used.

Nevertheless, it is interesting to note that most of the dimensional change occurs in the first three cycles. Thus it may be desirable to subject the component to thermal cycling before final machining to eliminate such changes. The final machining process should preferably be one such as chemical etching, which induces a minimum of residual machining stresses.

In the subsequent study (17), using cylindrical specimens, dimensional changes accompanying thermal cycling are significantly smaller than those reported in Table X. The materials tested are Ni-Span-C, 440C stainless steel, A356 cast aluminum, Berylco "Super PEL" beryllium, and Ti-5Al-2.5 Sn. With the exception of the titanium alloy, these materials are different from those reported

Table X

Effect of Temperature Cycling (-50 to +100°F) on Specimen Length

(Adapted from Reference 5)

Material	Specimen Number	Average MYS, 10 ³ psi	Change in Length, Δε, μin/in		
			3 Cycles	9 Cycles	30 Cycles
2024-T4	A12	33	63.5	62.0	65.0
	A22		31.7	31.7	36.0
6061	C32	26	2.8	7.2	21.6
	C33		10.1	23.1	43.3
TZM	1	53	13.0	11.5	13.0
	2		10.1	8.6	27.2
Ti-6Al-4V	E13	93	90.7	69.7	98.5
	E22		58.0	49.4	50.7
Ti-5Al-2.5 Sn	D3	78	55.0	58.0	72.5
	D14		20.3	15.9	27.5
AZ 31 Mg	F24	3.6	58.0	80.0	-
	F34		-14.6	-11.6	-
I 400 Be	6	7.9	- 2.5 (5 cycles)	- 6.0 (10 cycles)	-10.0 (20 cycles)

in Table X. The thermal cycle is also different, and consists of the following steps:

- (1) 10 minutes at 212°F;
- (2) 10 minutes at room temperature;
- (3) 10 minutes at -100°F; and
- (4) 10 minutes at room temperature.

Dimensional stability of the specimens was measured immediately after thermal cycling and also after long periods of time, up to 6 months. Initial data obtained for Ni-Span-C, A356 cast aluminum and Ti-5Al-2.5 Sn are summarized below:

Ni-Span-C

Thermal cycling did not cause an immediate change in length nor a significant instability for a period of 720 hours.

A356 Cast Aluminum

An immediate contraction of 4 to 5 microinches/inch was noted upon thermal cycling, but no trend toward instability was observed thereafter for a period of 1440 hours.

Ti-5Al-2.5 Sn

No immediate change in length on thermal cycling nor any indication of instability was observed for a period of 720 hours after cycling.

For the same material, Reference (5) reported dimensional changes of 55 and 20.3 microinches/inch after 3 cycles.

Thermal cycling of hot-pressed, forged beryllium resulted in configurational distortion (16). A cube of this material when thermally cycled from +75°F to +165°F to -65°F to +75°F showed an anisotropic permanent set of 19.4 ± 3.8 microinches/inch/cycle. This could possibly be a result of the anisotropic thermal expansion coefficient exhibited by forged beryllium. The difference between thermal expansion coefficients in the forging direction and in the plane of forging is -1.14 ± 0.16 microinches/inch/°F. The hot-pressed beryllium showed no anisotropic permanent set on thermal cycling.

In general, it may be stated that forging operations which induce anisotropic properties in materials should be avoided for clamp elements.

Summary and conclusions.- The state-of-the-art on the stability characteristics of materials both under stress and in the free state is still in its infancy. Considerable work needs to be done before an optimum material can be picked to provide maximum dimensional stability. Some understanding is available of the possible metallurgical phase changes inducing instability in metals and desirable heat treatments to minimize these changes.

Successful hardening and heat treating processes have been developed for hardenable steels used for precision gage block

materials to provide ultrastability. However these materials are heavy and may prove to be undesirable for aerospace applications. Also MYS and microcreep data on these materials is not available.

Limited data on microcreep characteristics of the lighter weight, lower strength alloys is available. But corresponding data on dimensional stability is lacking. The early work of Lement and Averbach (9) is the only source of data on types of heat treatment to provide maximum dimensional stability.

Residual machining stresses have been shown to have a considerable effect on dimensional stability. Very little, however, is known about the stress level resulting from different types of machining operations on various materials.

Microcreep values obtained for the lower strength alloys tested indicate that the MYS appears to be a useful indication of the stress value where significant dimensional changes will occur with time.

Ceramics, in particular beryllia, appear quite attractive from a dimensional stability point of view, having both good mechanical and thermal properties as well as a high dimensional stability.

On the basis of the information summarized in the preceding paragraphs, the following general conclusions may be drawn concerning the design of clamp elements:

- (1) A metal or ceramic material should be selected which is known to be metallurgically stable, on the basis of past data.
- (2) A symmetrical geometrical configuration should be used wherever possible relative to the critical axes. Symmetrical mechanical and thermal loading should also be provided.
- (3) Machining, chemical etching, and heat treatment techniques should be chosen to minimize residual stresses. The sequence of heat treatment operations should be one which has proven in the past to provide good dimensional stability for the chosen material. Fabrication by forging should be avoided.
- (4) Operating stresses in all critical elements of the clamp should be kept below 50% of the MYS.
- (5) The fabrication process should include a number of cycles of the expected thermal operating history before the final finishing operations in order to "shake out" dimensional changes due to thermal cycling.

INTERFACE CONSIDERATIONS

A number of phenomena occurring at the various clamping interfaces are critical in determining the alignment capability of the clamping system. These phenomena, which will be discussed in this section, include wear of the surface and the formation of wear particles; the effects of dirt and foreign particles; the effects of films; and the thermal contact resistance at the interface.

Wear of the Locating Surfaces

Damage to the locating surfaces of the fixed clamp during the installation process can cause angular misalignment. Surface damage can occur due to adhesive wear between the surfaces. The type of misalignment is shown schematically in exaggerated form by Figure 7.

Another potentially deleterious effect of wear between the mating surfaces is the production of a few large wear particles which can cause misalignment greater than the specified value of 5 arc-seconds.

These factors are discussed in the following paragraphs.

Adhesive wear.- The depth of material removed due to the relative motion of unlubricated bodies loaded against each other is given by (18)

$$h = \frac{k Nx}{3 pA} \quad (1)$$

where

h = depth of material that is removed, inches

N = normal load holding the wearing surfaces together, lbs

x = distance of relative tangential motion, inches

A = contact area of the surfaces that support load N, inches²

p = hardness of material being removed, psi

k = wear coefficient, dimensionless

The wear coefficient, k, is a function of the two materials in contact. The hardness, p, is related to the material's Brinell hardness as

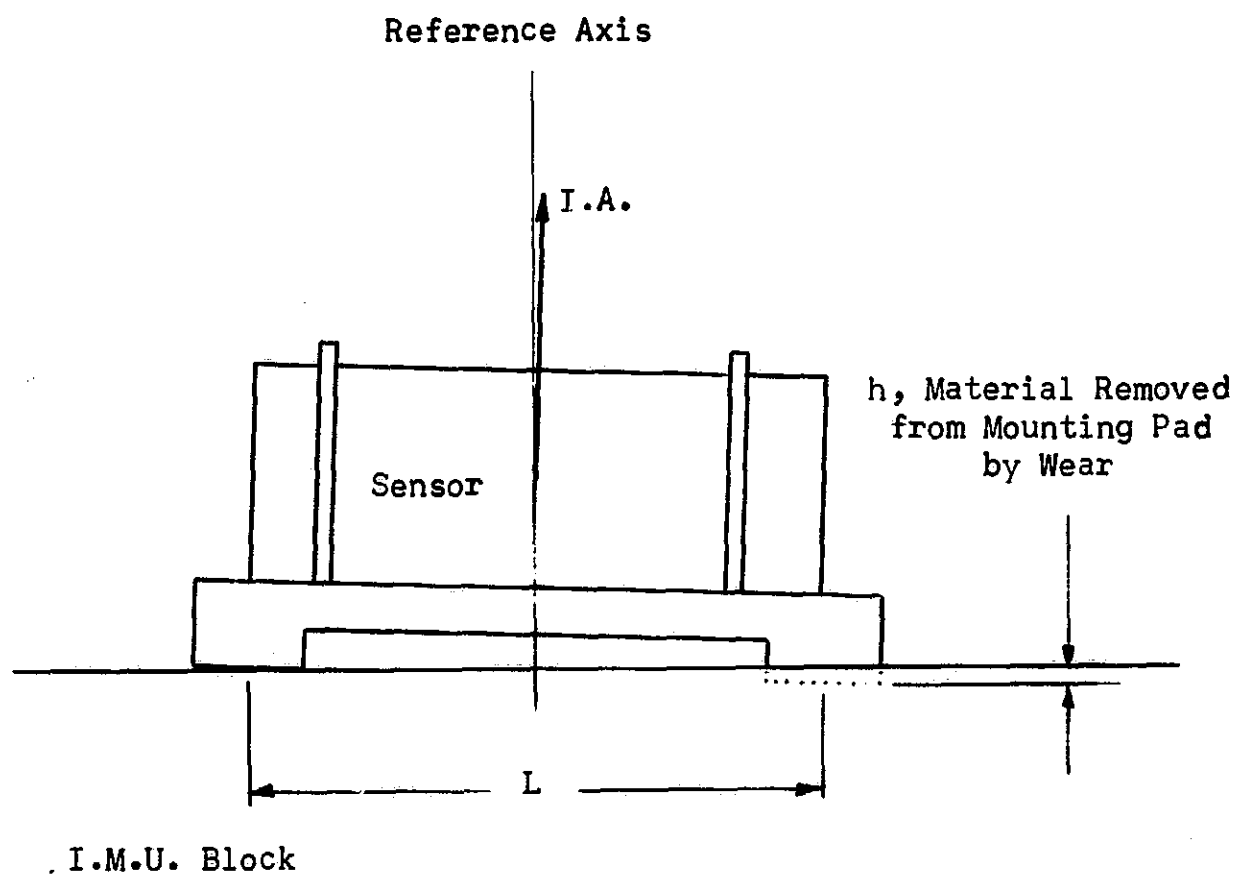


Figure 7. Schematic Diagram Showing Exaggerated Misalignment Due to Wear of the Mounting Pad

$$p = 1500 B \text{ psi}$$

where $B = \text{Brinell hardness} - \text{kg/mm}^2$

For illustration, it is convenient to assume a plane-on-plane fixed clamp as shown in Figure 7. One method for accommodating dirt particles initially on the locating surfaces is by assembly with a wiping or "wringing" motion. Using this procedure, typical values for wiping distance, x , and load, N , in Equation (1) might be

$$x = 2 \text{ inches}$$

$$N = \frac{10}{m} \text{ lbs}$$

where $m = \text{number of mounting pads.}$

The area, A , of the mounting pads is determined by the allowable limit on the contact stress for microcreep stability and would typically be 0.1 inches. Substituting these values into Equation (1) yields

$$h = 10^{-2} \frac{k}{B} \text{ inches} \quad (2)$$

Table XI gives values of B and k for several different combinations of materials. Values of h that are predicted from Equation (2) are also presented. It can be seen that the depth of material removal is very small unless soft materials such as pure aluminum are used.

If different mounting pads have unequal depths of material removal, an angular misalignment, $\Delta\theta$, can occur. The misalignment is given by

$$\Delta\theta = \frac{\Delta h}{L} \quad (3)$$

where $L = \text{distance between mounting pads having different wear depths}$

$\Delta h = \text{difference in wear depth between two mounting pads that are separated by a distance } L.$

A typical value for L is 4 inches. If it is assumed that Δh is equal to its maximum possible value, h , the misalignment, $\Delta\theta$, may be expressed by

$$\Delta\theta = \frac{h}{4} \text{ in/in} \quad (4)$$

Table XI also gives values of $\Delta\theta$ that are predicted from Equation (4). It is clearly seen that wear occurring during sensor installation causes a negligible misalignment error provided that soft mating surfaces are avoided.

Table XI

Misalignment of a Plane-on-Plane Fixed Clamp Due to Adhesive Wear

Materials	k	Brinell Hardness Kg/mm ²	h μ inches	Maximum Misalignment $\Delta \theta$ arc-seconds
Stainless Steel on Stainless Steel	20×10^{-3} (1)	200	1	1/20
Mild Steel on Mild Steel	45×10^{-3} (1)	100	4	1/5
Beryllia on Beryllia	20×10^{-3} *	600	1/3	1/60
Pure Aluminum on Pure Aluminum	50×10^{-3} *	15	27	4/3

*Estimated value

Material wear can also be caused by the relative tangential motion that occurs between the clamp and the mounting plane when the system is thermally cycled. Since each piece rises to a different temperature when the sensor is turned on, the two will expand by unequal amounts. The relative motion, x , is exceedingly small for each cycle. However, this amplitude of motion must be multiplied by the number of thermal cycles, moreover, load, N , is now the clamping load, which is considerably larger than the normal load that is used during the clamp installation.

An upper bound for the relative displacement, x , that occurs during each complete thermal cycle is given by

$$x = 2 (\alpha \Delta T L) \quad (5)$$

where L = length of the clamp, inches

α = thermal expansion coefficient, $(^{\circ}\text{F})^{-1}$

ΔT = temperature difference between the block and the plane, $^{\circ}\text{F}$

If the following typical values are assumed:

$L = 4$ inches

$N = 400$ lb

$\alpha = 10 \times 10^{-6} (^{\circ}\text{F})^{-1}$

$\Delta T = 10^{\circ}\text{F}$

$m = 4$

$A = 0.1$ inches²

Substitution into Equation (5) gives

$$x = 8 \times 10^{-4} \text{ inches}$$

The value of k for this small displacement amplitude is nearly always below 10^{-5} *. This k value is approximately a thousand times less than the previously used k values. Using the above values, Equation (1) gives

$$\begin{aligned} h &= \frac{(400 \text{ lb}) (8 \times 10^{-4} \text{ inches})}{3 (1500 \frac{\text{psi}}{\text{Kg/mm}^2})} \left(\frac{k}{B}\right) \\ &= 0.007 \times 10^{-2} \left(\frac{k}{B}\right) \text{ n } \left(\frac{\text{Kg}}{\text{mm}^2}\right) \text{ in} \quad (6) \end{aligned}$$

* Verbal communication with Prof. E. Rabinowicz, M.I.T.

If Equation (6) is compared with Equation (2) and allowance is made for the decreased value of k , it can be seen that at least 140,000 thermal cycles are necessary before thermal wear is comparable to the wear that occurs during sensor installation. Since the sensor will likely be replaced before it has been turned on and off this number of times, it is clear that the misalignment errors caused by thermal cycling wear are negligible.

The above discussion has assumed plane-on-plane clamp geometry. It is anticipated that a cylinder-in-hole clamp of similar material to the plane-on-plane type will have a comparable amount of adhesive wear due to thermal cycling. Installation wear due to wiping of the cylinder in the hole will be dependent on the contact pressure which may be difficult to control. If this pressure is maintained at the same value as is used for the plane-on-plane clamp, the installation wear for the two types of clamp will be comparable.

In conclusion, it appears that if soft surfaces are avoided, the overall wear is not sufficient to cause significant misalignment due to bulk changes in the surface geometry.

Formation of wear particles.- In the previous paragraphs, it has been shown that the magnitude of wear on typical fixed clamp elements is not sufficient to produce intolerable changes in dimension. Another potentially critical aspect of wear, however, is the production of individual wear particles large enough to produce relatively large misalignment (18).

The volume, V , of material produced by sliding wear can be computed from the relation (18)

$$V = \frac{kNx}{3p} \quad (7)$$

where k = dimensionless wear coefficient

N = Normal load, lbs

x = sliding distance, inches

p = 1500B, psi

B = Brinell hardness, $\frac{Kg}{mm^2}$

Assuming again the values used in the preceding paragraphs for a typical plane-on-plane clamp, and using the material properties given in Table XI for stainless steel on stainless steel gives

$$V = 110 \times 10^{-9} \text{ in}^3 \quad (8)$$

The diameter of individual wear particles is given by (18)

$$d = 60,000 \frac{W_{ab}}{p'} \quad (9)$$

where W_{ab} = surface energy of adhesion, $\frac{\text{ergs}}{\text{cm}^2}$

p' = the surface hardness, $\frac{\text{dynes}}{\text{cm}^2}$

For stainless steel on stainless steel, these properties are

$$W_{ab} = 2000 \frac{\text{ergs}}{\text{cm}^2} = 1.14 \times 10^{-2} \frac{\text{lb}}{\text{in}^2}$$

$$p' = 200 \times 10^8 \frac{\text{dynes}}{\text{cm}^2} = 2.9 \times 10^5 \frac{\text{lb}}{\text{in}^2}$$

Substituting into Equation (9) gives

$$d = 2.4 \times 10^{-3} \text{ inches} \quad (10)$$

With the volume removed given by Equation (8), there will be approximately 10 of these large wear particles formed. It can easily be seen that if one of these relatively large particles becomes trapped at the interface, an intolerable misalignment would result. Even if all of the particles were removed from the interface, it is likely that the surface irregularities left in the surface would be too large to achieve the desired alignment.

Because of the very small values of k which apply to the small motions resulting from thermal sliding, particle formation as a result of this motion is not significant.

From the above discussion, it may be concluded that sliding conditions consistent with the assumed example will likely produce intolerable wear particles, using conventional unlubricated materials for the clamp elements. If a sliding fixed clamp is employed and film lubrication is not possible during installation, it may be necessary to resort to the use of special combinations of materials, the surfaces of which are known to minimize the formation of these wear particles. These include cobalt on cobalt, tungsten carbide on tungsten carbide, and steel on bearing bronze.

Effects of Fluid Films

Fluid films between the mating surfaces of a clamp are a potential source of misalignment. If these films have a long relaxation time, they may cause sensor alignment to change during use, or between the time when verification is accomplished and final use, or during the verification process.

Fluids such as skin oils or water may be inadvertently introduced after cleaning the mating surfaces. Air, of course, is unavoidable during installation. In addition, it may be desirable to introduce lubrication for a fixed clamp that requires sliding in order to minimize the formation of wear particles. Also, the provision of a fluid at the mating surface is one method for mitigating the undesirable high variability of thermal contact resistance at the interface.

It is possible to ensure that after a sufficient length of time, a fluid film will flow out of the interface region between two surfaces loaded against each other to the point where the surfaces are in contact on the peaks of their asperities. The time required for the initial film to flow out of the region, however, is of interest. This relaxation time is estimated by the following analysis for typical fluids that might be present at the interface. Evaporation of the fluid is neglected since its effect would be to decrease the estimated relaxation time.

Assuming a mounting pad which is approximately square with area, A , and which is loaded against a mating surface with load, W , the relaxation time, t , for a film may be computed from the relationship

$$t = \frac{\mu A^2}{Wh} \quad (11)$$

originally developed for gas bearings (19), where

μ = viscosity of the fluid film

h = minimum film thickness given by the height of the surface asperities.

Equation (11) assumes that the initial film thickness is large compared with the final or minimum film thickness. Typical values for a clamp pad are as follows:

$A = 0.1$ inches²

$W = 100$ lbs

$h = 5 \times 10^{-6}$ inches for a lapped surface

These values substituted into Equation (11) give

$$t = 2.77 \times 10^4 \mu \frac{ft^2}{lb} \quad (12)$$

Table XII gives the viscosity for several typical fluids and the relaxation time predicted by Equation (12). It can be seen that the relaxation times for air, water, and alcohol are very short and will likely not have any practical effect on sensor alignment. If higher viscosity oils are present, however, the relaxation time may be of the order of several minutes and it should be taken into account during the assembly process.

For a cylinder-in-hole clamp operating with a similar contact stress, the relaxation time would be comparable provided the ratio of hole circumference to length is approximately unity. If a longer cylinder were employed, it would be expected that a correspondingly longer relaxation time would be required.

In conclusion, it appears that fluid film relaxation effects will be completed before a sensor is operated. However, after installation, it is advisable to wait several minutes before proceeding with verification if it is to be conducted.

Dirt and Foreign Particles

One of the major potential contributions to the misalignment of a fixed clamp is the presence of dirt or foreign particles on the locating interface when the clamp is assembled. For a typical clamp span of 4 inches, a 1 arc-second angular error can result from a single 1/2 micron particle on a hard surface. As discussed previously under "Clean Room Technology", the present state-of-the-art in clean rooms is such that many particles in this size range are not removed from the air.

Moreover, although the sensor can be conveniently mounted to the interface piece with an adjustable clamp in a clean room, mounting at the fixed clamp interface is ideally accomplished in the field where a clean area is not conveniently available. Thus, if possible, the fixed clamp should be capable of accommodating the presence of dirt particles of reasonable size.

Some of the factors which mitigate the misaligning effects of foreign particles are the averaging effects of many particles; deformation of particles and surfaces; and the roughness of the interface surfaces.

The possibility of providing a soft coating on the mating surfaces to absorb dirt particles also became apparent early in the program and was analyzed for feasibility.

Studies of these effects are described in the following paragraphs.

Table XII

Relaxation Time for Various Squeeze Films

Fluid	Viscosity, μ lb sec/ft ²	t
Air	4×10^{-7}	1/100 sec
Water	2×10^{-5}	1/3 sec
Ethyl Alcohol	3×10^{-5}	1/2 sec
SAE 30 White Mineral Oil	7×10^{-3}	2 min
Castor Oil	2×10^{-2}	5 min

Rigid particles between rigid surfaces.- The magnitude of the potential effect of foreign particles on misalignment is estimated by considering the idealized two-dimensional situation of Figure 8. The angular misalignment, $\Delta\theta$, is given by

$$\Delta\theta = \frac{d}{L} \quad (13)$$

where d = diameter of the particle

L = spacing of the mounting pads

The magnitude of this misalignment is plotted in Figure 8 for the span assumed. It can be seen that misalignment of the order of 1 arc-second is produced by a 20 microinch or 0.5 micron particle. This represents the current state-of-the-art in clean room technology. Furthermore, if the sensor is to be installed in the field, considerably larger particles could be expected to be present.

The misalignment could be reduced, of course, if there were many particles present under both mounting pads. By assuming probable size distributions for the particles present, the probability of various degrees of misalignment could be predicted by means of statistical analysis. For purposes of fixed clamp design, however, the conclusion is obvious. The design of the clamp must be capable of removing or absorbing the dirt particles present in such a way that they will not cause misalignment.

The maximum size of the particles which can be tolerated increases if deformation of the particles and surfaces occurs as in the limiting cases discussed in the following paragraphs.

Soft particles trapped between hard surfaces.- Figure 9 shows a soft particle trapped between a mounting pad on a sensor fixture and the reference plane. The pad is loaded against the plane by two forces, F_c . The force with which the sensor fixture compresses the particle, F_p , causes it to deform plastically without a significant change in its volume. The bearing area of the particle, A_p , is equal to

$$A_p = \frac{F_p}{P_p} \quad (14)$$

where P_p = flow stress of the particle

F_p = force which compresses the particle

The deformed height, h , of the particle is given by

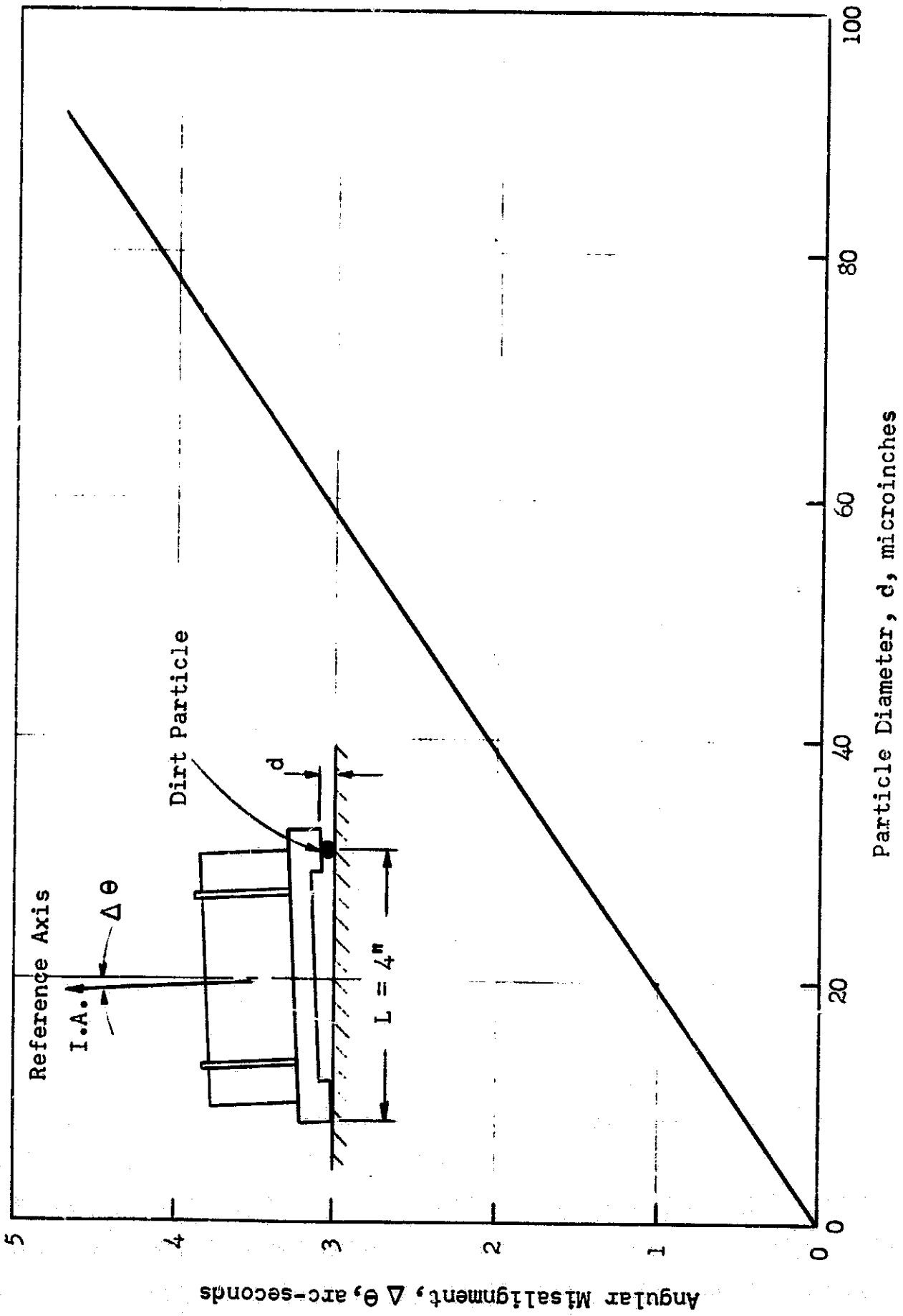


Figure 8. Misalignment Due to a Rigid Particle Between Rigid Surfaces

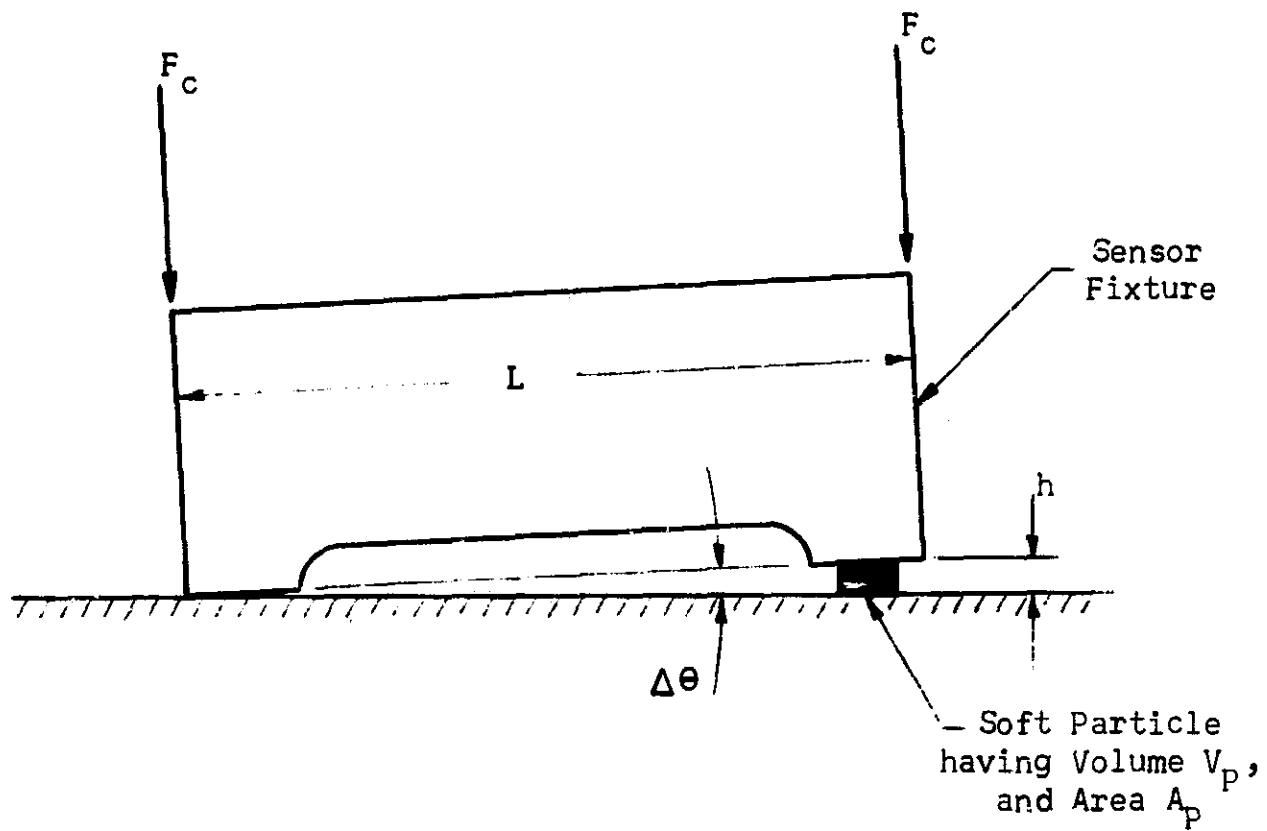


Figure 9. Soft Particle Trapped Between Rigid Flat Surfaces of Sensor Clamp and Mounting Block

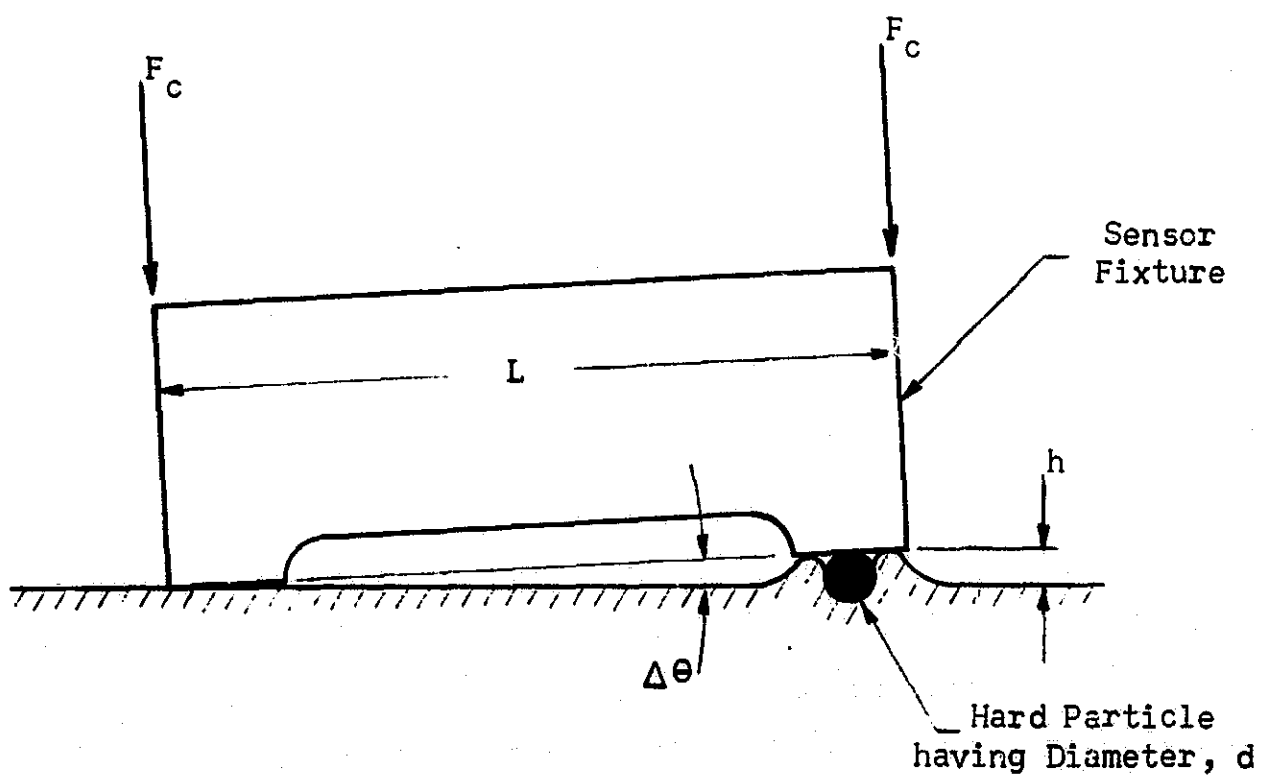


Figure 10. Hard Particle Embedded in Soft Surface of Mounting Block

$$h = \frac{V_p}{A_p} = \frac{V_p P_p}{F_p} \quad (15)$$

where V_p = original volume of the particle

If a single particle is present directly underneath one of the clamping forces, then

$$F_p = F_c \quad (16)$$

The misalignment, $\Delta\theta$, can then be written as

$$\Delta\theta = \frac{h}{L} = \frac{V_p P_p}{L F_c} \quad (17)$$

As an example, assume that the soft particle is a nylon fiber that has a diameter and length of 20 microns (800 μ inches). Then,

$$V_p = 0.4 \times 10^{-9} \text{ in}^3$$

$$P_p = 18 \text{ Kg/mm}^2 = 2.8 \times 10^4 \text{ psi}$$

Typical clamp parameters are

$$F_c = 100 \text{ lb}$$

$$L = 4 \text{ inches}$$

If the above values are substituted into Equations (15) and (17), then

$$\Delta\theta = 0.005 \text{ arc seconds}$$

Thus, it can be seen that small soft particles cause negligible misalignment in this typical case.

Large dust particles are of the order of 100 microns in diameter. If a single spherical particle of this size having the above hardness is squashed by a 100-lb force, a 0.5 arc-second error will result. If many such particles are present so that F_p is significantly less than F_c , an unacceptable misalignment error could conceivably result. However, averaging effects due to many points of contact will tend to reduce the error from the

value that is predicted when Equation (17) is evaluated for the largest particle.

Another factor that will reduce the misalignment error is particle deformation due to smearing that will occur if there is relative tangential motion between the mating surfaces. This effect was graphically demonstrated with two optical flats. Initially, when a soft particle was trapped between the flats, no fringes were seen. When flats were rubbed back and forth, smearing of the particle was observed, and fringes appeared. Further rubbing reduced the number of fringes, indicating that the flats were approaching parallelism.

Hard particles trapped between soft surfaces.- Figure 10 shows the situation that exists if a force F_p , presses a hard particle of diameter, d , into a soft mounting plane. This will occur if

$$F_p > \left(\frac{\pi}{4} d^2\right) P_s \quad (18)$$

where P_s is the hardness of the surface

Similarly, the particle can be embedded in the clamp surface.

When a particle (assumed spherical) is pressed into a surface, a ridge is generally raised on the surface as shown in Figure 11. The outside diameter of the ridge is D , and the height of the ridge is h . It is found experimentally, (18) that

$$3d < D < 5d \quad (19)$$

The volume of the ridge is given approximately by

$$V = \frac{h}{2} \times \frac{\pi}{4} (D^2 - d^2) \quad (20)$$

This must equal the volume of the particle, $\frac{\pi d^3}{6}$. Hence we have

$$h = \frac{4}{3} \frac{d^3}{D^2 - d^2} \quad (21)$$

Taking the two limits for the range given by Equation (19),

for $D = 3d$, $h = 0.16 d$

for $D = 5d$, $h = 0.06 d$

Thus, it seems reasonable to assume that h is approximately one-tenth of d .

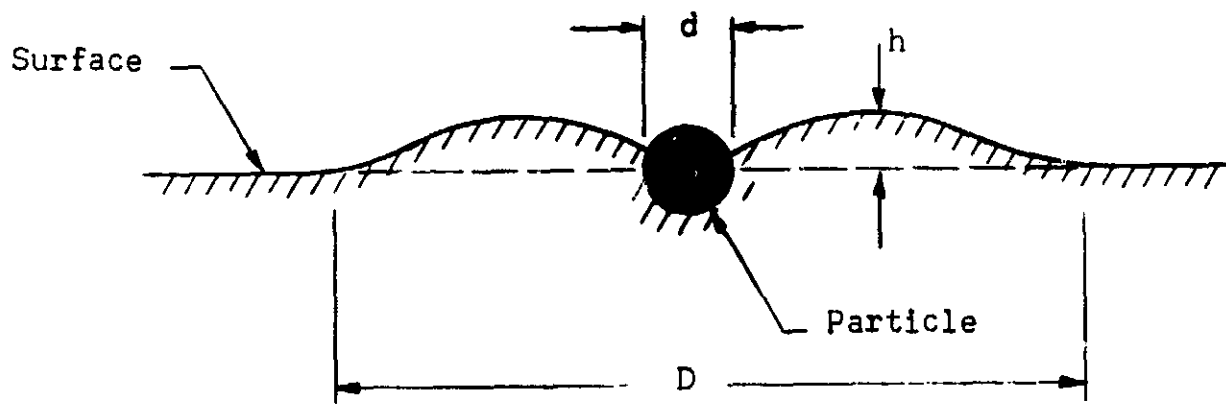


Figure 11. Model of Rigid Spherical Particle Pressed into a Soft Surface

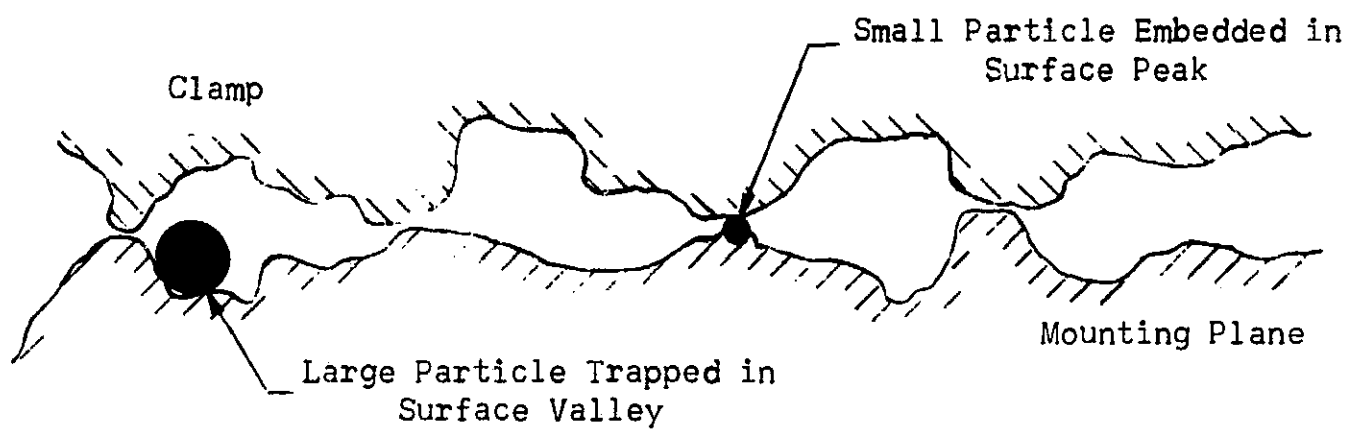


Figure 12. Interaction of Foreign Particles and Rough Mating Surfaces

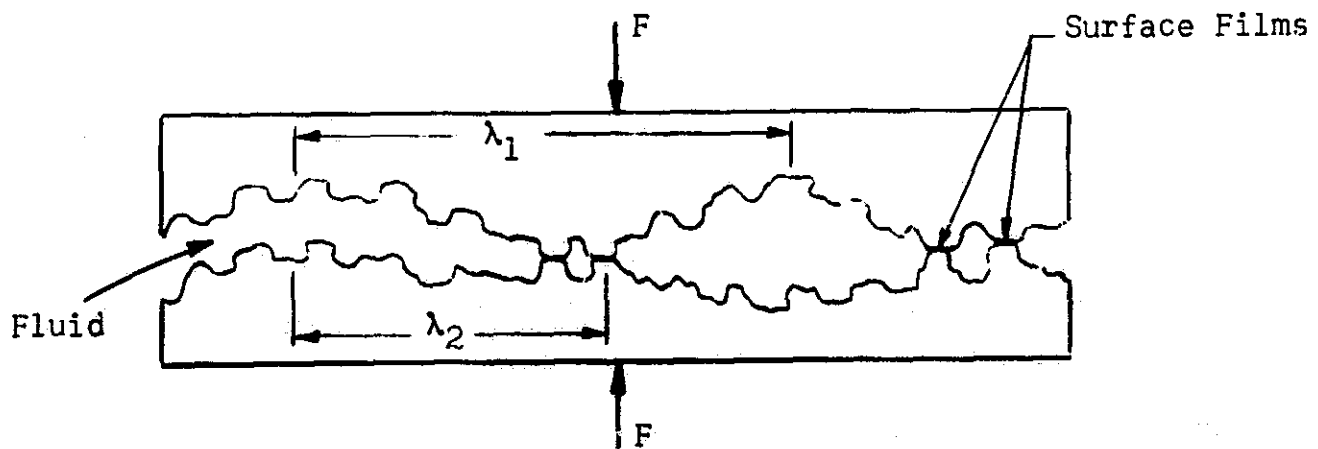


Figure 13. Schematic Diagram of Contact Between Real Surfaces

The resulting misalignment, $\Delta\theta$, is then given by

$$\Delta\theta = \left(\frac{1}{10}\right) \frac{d}{L} \quad (22)$$

As an example, the following typical values are assumed:

$$F_p = F_c = 100 \text{ lb}$$

$$P_s = 5 \times 10^5 \text{ psi (hardened steel)}$$

$$L = 4 \text{ inches}$$

If Equation (21) is solved for d , it is found that particles smaller than 0.013 inches will become embedded. Even if F_p is reduced to 1 lb, particles smaller than 0.0013 in will be embedded. Thus, hard particles that are too small to be seen and cleaned off the surface will be embedded. If Equation (22) is solved for d , it is seen that particles larger than 0.0002 in, or 5 microns, can cause misalignment errors that are larger than 1 arc-second. Therefore, it appears that embedded hard particles can cause significant misalignment errors.

Dirt particles trapped between rough surfaces.- Misalignment errors due to dirt particles can be decreased if the mating surfaces are not perfectly smooth, as shown in Figure 12. In order to be effective, the valleys must have a width and depth that is comparable to the largest expected particles. However, if the peaks have the same width as the valleys, particles that are much smaller than the peaks could become embedded in them. In many instances, these "small" particles are large enough to cause significant errors.

As an example, if the width and depth of the peaks and valleys are 0.004 inches, then large dust particles (100 microns diameter) can be accommodated. However, this scale of surface roughness is twenty times larger than hard particles of 5 microns in diameter which can cause 1 arc-second errors. Consequently, if rough surfaces are placed together without any relative tangential motion, misalignment errors can occur due to small hard particles becoming embedded in the peaks.

If a tangential motion is used after the surfaces are in light contact, it appears plausible that any particles that might have been on the peaks will be swept into the valleys, where they will no longer affect the alignment of the mating surfaces.

The above phenomenon was verified by experiments conducted during this program. A steel block having three ground mounting

pads 6 inches apart was repeatedly placed with light pressure on a granite surface plate. The alignment between the block and the plate was measured with an autocollimator. If no wiping action was used, misalignments of up to 8 arc-seconds were caused by dust and cigarette ashes placed on the mating surfaces. If the block was subsequently rubbed back and forth several times with light pressure, the misalignment was repeatedly reduced to less than 1/2 arc-second.

Dirt-absorbent coatings.- In the previous paragraphs, it was shown that wiping or rubbing two surfaces together was one means for removing the misaligning effects of dirt particles. Another method was investigated - the depositing of a thin compliant coating on the mating surface.

The relationships which govern the behavior of such a dirt-absorbent coating are developed in Appendix A. A numerical example, using lead for the coating indicated that the concept is feasible. The thickness of the coating must be at least as large as the largest hard particle to be absorbed. Taking this as 10^{-3} inches, a reasonable range of clamping load results. The angular misalignment due to a side load was found to be acceptably small for typical clamp dimensions. This is due to the fact that the small thickness of the coating compensates for its lower elastic modulus and the overall angular stiffness of the clamp is not significantly reduced.

A survey of manufacturers indicated that this concept is also feasible from a fabrication point of view. For example, a 1 mil thick coating of lead, gold, silver, aluminum, or copper can be vacuum-deposited on stainless steel with an accuracy of 1 microinch.*

The possibility of nonuniform or asymmetric long-term creep of the coating exists if there is sufficient unbalance in the clamping force. This will require experimental evaluation. However, there are design features, such as trapping the coating around the circumference of the mounting pad, which could largely eliminate such creep.

Thus, it is concluded that the use of a dirt-absorbent coating is a promising concept for avoiding the misaligning effects of dirt on the fixed clamp interface.

Thermal Contact Resistance

Another surface phenomenon which can markedly affect the alignment capability of a clamp is the thermal contact resistance across the interface between the mating parts. A simple conduction

*Verbal communication with Spectrum Systems Inc., Waltham, Massachusetts.

model was analyzed in which all of the heat generated by a sensor flows to the IMU block through mounting legs and lightly-loaded contact pads. Details are presented in Appendix II. The results show that a 10% variation in contact resistance between two opposing pads can lead to angular distortion of the order of 2 arc-seconds.

To identify the basic factors affecting the contact resistance between two elements and to obtain an estimate of the values which can occur, the literature on past work in this area was reviewed (22 through 27).

In general, it may be stated that the thermal contact resistance can vary over a wide range of values for two similar tests, especially in a vacuum. Some of the factors which contribute to this variation are illustrated schematically in Figure 13.

When real surfaces with finite roughness and waviness are loaded together, they are in physical contact over only a relatively small part of their apparent surface area. If the pad is operating in a vacuum such that all of the region surrounding these contact areas is evacuated of fluid, then virtually all of the heat flowing across the interface must flow through the limited region in actual contact. In general, the actual surface area in contact, A_c , can be predicted from a relation of the form

$$A_c = \frac{F}{\sigma_y} \quad (23)$$

where F = contact force

σ_y = local yield strength of the material.

From this relationship the thermal resistance, which is proportional to area A_c in a vacuum, would be expected to vary linearly with contact load F . This has been found to be true experimentally (22 through 27).

One factor leading to the variability in experimental results among similar experiments arises from the uncertainty of the effective value for σ_y in the microscopic layers at the two surfaces. Also, in addition to the surface area, the resistance of the contact points is a function of the local thermal conductivity of the materials which can vary due to local metallurgical anomalies, the presence of oxide films, and the temperature. Thus, the use of a metallurgically stable and homogeneous material which is not subject to surface oxidation might be expected to minimize variability from these effects.

Variation of the actual details of the heat flow field near the contact points, thereby changing the effective thermal resistance of this part of the total flow path, can also contribute to the measured variability in contact resistance. This is largely geometry-dependent and can vary with the nature of the surface roughness, the surface waviness (as shown by wavelengths λ_1 and λ_2 in Figure 13), and the machining orientation. The use of lapped, highly polished, and very flat surfaces to provide the maximum number of contact points distributed homogeneously over the interface might be expected to minimize variability from these effects.

In any event, the above factors have been found to cause variations in thermal contact resistance of up to an order of magnitude for similar tests in a vacuum (22 through 27). This degree of variation is clearly far too great to maintain the necessary thermal symmetry if the contact pads are to be located in main heat flow paths between the sensor and the IMU.

One method for improving this variability is to provide a fluid at the interface. This fluid can be either air or a liquid film. In addition to increasing the attainable conductance by an order of magnitude (from of the order of 1000 to 10,000 Btu/ft² hr °F), the conducting fluid has the effect of removing many of the factors contributing to the variability since most of the heat is conducted across the fluid film instead of the local contact points. The contact resistance also becomes much less sensitive to load variation. In the presence of a fluid, the apparent contact resistance has been found experimentally to be fairly constant with load changes.

The advantages of the fluid film can be provided by a separate thermal shunt path if it is not possible to provide a fluid film at the locating interfaces. This design feature will be discussed under "PRELIMINARY DESIGN OF THE FIXED CLAMP".

Summary and Conclusions

Phenomena occurring at the various contacting interfaces in the clamping system can have a critical effect in determining the alignment capability of the system. In summary, the major conclusions which can be drawn from studies of these phenomena are as follows:

- (a) The amount of material removed during the adhesive wear process does not appear to be sufficient to cause significant misalignment provided soft materials are not used. The formation of relatively large wear particles, however, may be important for a sliding type of fixed clamp. This will likely require the use of special combinations of surface materials or film lubrication during installation.

- (b) If fluid films are present on the locating surfaces of a fixed clamp, either unavoidably or intentionally to provide lubrication or thermal conductance, the film will likely have ample time to relax between installation and operation. However, after installation, it is advisable to wait several minutes before proceeding with verification of alignment.
- (c) Excessive misalignment of a fixed clamp can be caused by soft particles of the order of 100 microns in diameter and larger, and hard particles of the order of 5 microns and larger. Hard particles in this size range are small enough so that they can lodge in the peaks of the surface roughness of an actual surface, still causing critical misalignment.
- (d) Although, particles in the above size ranges may be largely excluded in the clean-room assembly of air adjustable clamp, it is not practical to eliminate them for the field assembly of fixed clamps. Two means for overcoming their misaligning effects seem promising at this time:
 - (1) the assembly of the clamp interfaces with a light wiping or sliding motion to sweep any particles present on the peaks of the surface roughness into the valleys; and
 - (2) the use of a vacuum-deposited, dirt-absorbent coating on the interface.
- (e) Thermal contact resistance in a vacuum has been found to vary by an order of magnitude for similar tests, while a 10% variation from one locating pad to another appears critical from an alignment point of view. Although various steps may be taken to minimize such variation, the only reliable one appears to be the removal of the contact points from the main heat flow path between the sensor and the mounting block. This may be done by providing a fluid film at the interface or through the use of a separate thermal shunt path for heat flow.

PRELIMINARY DESIGN OF THE FIXED CLAMP

As discussed under "Description of the System", an integral part of the clamping system is the fixed clamp which embodies the interface at which field installation of the sensor is effected.

The preliminary design of the fixed clamp involved both concept generation and concept evaluation as summarized in this section of the report. Chronologically, this work was accomplished in parallel with the basic studies described in preceding sections in order that the developing configurations could be taken into account for the various analyses. The initial concept generation tasks were accomplished at the outset of the study in order that the analytical studies would not prejudice the range of concepts considered.

The main design criteria used as a basis for the fixed clamp design were as follows:

- (a) The clamp should be capable of establishing the desired orientation of the input axis within an error of less than 5 arc-seconds.
- (b) The clamp should be capable of maintaining this orientation for long periods of time under the influences of thermal cycling, clamping loads, dirt, and fluid films; and should return to this orientation after subjection to 50 "g" accelerations.
- (c) The clamp design should allow the interchanging of preadjusted sensors in the field without the benefit of verification or a clean air facility, if possible.

The methods of attack used to generate design concepts included several "brainstorming" sessions involving a number of technical specialists with a range of disciplines and areas of interest. The ideas generated as a result of these sessions were then classified and evaluated by means of engineering analysis.

While it is not practically possible to report the details of verbal brainstorming sessions, the following sections summarize the framework within which the discussions were conducted, the major concepts identified, and the results of the critical analyses performed.

Concept Generation

The generation of concepts for a fixed clamp may be considered to be aimed at two main factors:

- (a) Selection of the means for locating the sensor input axis, primarily a matter of determining the most promising geometry.
- (b) Selection of the best means for supplying the clamping force.

Locating geometry.- The prime function of the fixed clamp is to establish the desired orientation of the sensor input axis relative to the reference axis on the mounting block. Consequently, it is of interest to consider the various means by which a straight line can be established in space as summarized in Table XIII.

The simplest means for orienting the sensor input axis are those of category 1 of Table XIII, and the majority of the concepts generated used methods of these types. Location of an axis perpendicular to a plane on the sensor unit can be effected by mating the plane with a like surface on the IMU block which is known to be perpendicular to the reference axis. Either or both of these planes may be continuous or determined by discrete plane mounting pads. An alternative means for defining one of the planes is by means of three contact points. In the location technique using an axis of general cylindrical surface, a right circular cylinder was considered most often. For this method, a cylinder or hole on the sensor unit, having the input axis as its centerline is mated with its inverse member on the IMU block with the reference axis as the centerline.

The remaining geometrical methods of Table XIII were used as a stimulus for concept generation, but only the concepts of a cylinder in a V-block, corresponding to method 2(b), and mounting the sensor unit on centers, corresponding to method 4, were identified as potential clamps. No promising concepts or potential advantages were identified with the rest of the geometrical methods.

Clamping force.- The second main factor distinguishing various potential fixed clamp concepts is the means for providing the clamping force to hold the sensor element and the IMU block together.

Table XIV, which was used as a concept stimulus, lists the major types of clamping forces which conceivably could be used for this purpose.

In general, it was felt desirable to avoid the use of an active force-generating system such as an electromagnet or an external pressure source in view of the possibility of failure of the source in operation. The same type of forces, however, can usually be employed in combination with an interference fit to keep the system passive. For example, electric or magnetic force could be applied during installation in such a way that an

Table XIII

Methods for Orienting a Straight Line in Space

1. Relative to a Surface
 - (a) perpendicular to a plane
 - (b) as the axis of a generalized cylinder

2. Relative to Two or More Surfaces
 - (a) parallel to two nonparallel planes
 - (1) the intersection of two planes
 - (2) parallel to the sides of a prism
 - (b) the intersection of a cylinder and a plane parallel to its axis

3. Parallel to Another Line and Passing Through a Point

4. Passing Through Two Points

Table XIV

Potential Clamping Forces

- (1) Mechanical Contact
 - (a) screws with deformable spacers or flanges
 - (b) toe clamps
 - (c) springs
 - (d) elastic deformation - bayonet type mounting - interference fit
 - (e) thermal deformation
 - (f) friction - wedges, swash plates

- (2) Fluid Pressure
 - (a) pneumatic
 - (b) hydraulic

- (3) Bonding Matrix
 - (a) adhesive
 - (b) solder
 - (c) other metallic bonds

- (4) Surface Tension

surfaces "wrung" together with a fluid film

- (5) Magnetic
 - (a) electromagnetic
 - (b) permanent magnet with switch (keeper) in magnetic circuit
 - (c) magnetostrictive

- (6) Electric
 - (a) electrostatic
 - (b) electrostrictive

interference fit, providing a mechanical clamping force, is produced upon removal of the external source. Sealed, pressurized volumes can be used to generate passive fluid pressure clamping force with suitable mechanical constraint.

Quasi-verification.- Although, as described in previous sections, it is not desirable to perform accurate measurements for the verification of alignment in the field, it was felt during the concept generation process that some advantage might be gained by integrating a less-demanding verification technique into the fixed clamp concept. This clamping strategy was termed quasi-verification. Quasi-verification was envisioned to include two basic types of systems:

- (a) Provision of a simple go, no-go type of measurement which, although not measuring the error accurately would give some indication that the degree of alignment inherent to the clamp concept has been attained. This quasi-verification would be implemented by providing for a repeatability measurement for successive assembly operations of the clamp.
- (b) Provision of a mounting jig to which the sensor is attached with verified alignment in the laboratory. The design of the jig is then such that its alignment relative to the IMU block is relatively insensitive to the presence of dirt, although it does not provide a locating means stable for long periods of time. The jig, however, is capable of maintaining alignment while, for example, a bonding matrix is formed between the members.

Fixed clamp concepts.- A range of design concepts for fixed clamps resulted from the concept generation process. This range included concepts with and without quasi-verification, and embodying the basic locating geometries and means for providing clamping forces outlined in the previous sections. Table XV shows a list of these concepts after classifying them and combining similar ideas.

Although several methods of supplying the clamping force for them are possible, the Cylinder in V-block and Mounting on Centers concepts were evaluated only as means of orientation; the locating means only, the evaluation of the other concepts included consideration of the means for providing clamping force.

For the interested reader, descriptions and schematic diagrams of most of these concepts are included as Appendix B to this report.

These concepts were evaluated both analytically and from a design standpoint to determine the conditions necessary to achieve the desired degree of axis alignment and their relative

merits and feasibilities. The results of this evaluation are described in the following sections.

Concept Evaluation

A number of fixed clamp concepts were generated as a result of the studies summarized in the previous section. This section, together with appendices, describes the evaluation of these concepts. This evaluation included a number of specific analyses to determine the effects of force and thermal loading on the clamp structure, as well as a practical design evaluation of the various methods for providing the clamping force.

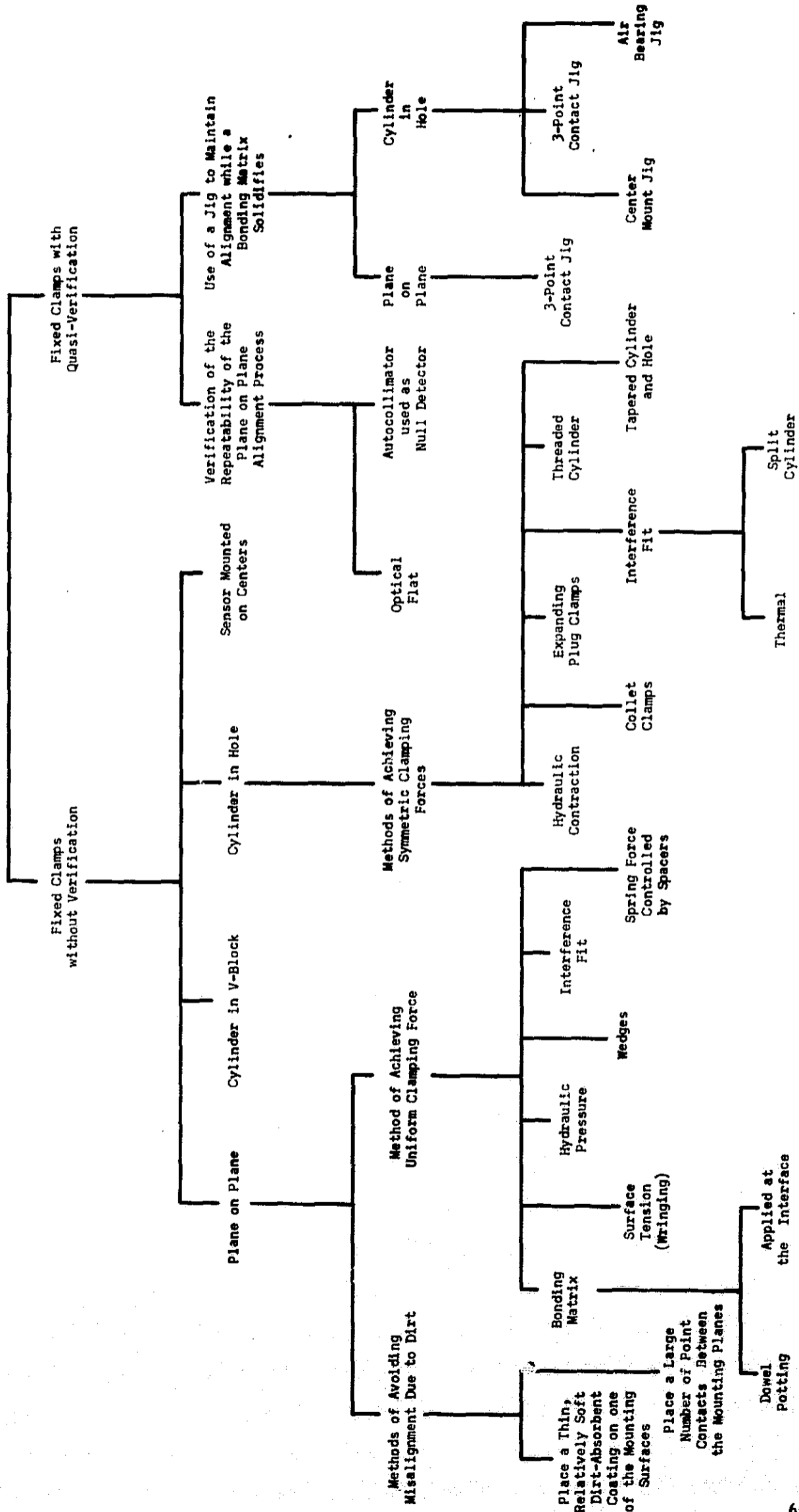
Plane-on-plane fixed clamp concepts.- A number of the concepts generated and summarized in Table XV use the plane-on-plane geometry to orient the sensor input axis. Evaluation of this class of concepts centered on general analyses of the force-deflection behavior of typical configurations, a thermal analysis of a typical contact pad concept, and preliminary design consideration of various methods of providing the clamping force in the light of these analyses. This work is summarized in the following discussion with reference to pertinent appendices.

(a) Force-deflection analyses - One method of implementing the plane-on-plane concept is to form the locating plane on the sensor element as one side of a block which is then mated and clamped with a plane on the IMU block. Appendix C presents an analysis of this situation where the IMU block is assumed to be a much larger element. The analysis combines the angular deflection of the interface block and the foundation element under the influence of an unbalanced clamping force and lateral acceleration. The results are presented in Figure C-4 of Appendix C in fairly general form, using typical ratios between the geometrical quantities and assuming that the angular deflection should be maintained less than 2 arc-seconds. A typical numerical example computed from these results shows that with a 50-g lateral acceleration, clamping force unbalance of 185 lbs is allowable with a total clamping force of 382 lbs. The clamp contact pressure is very low for this type of configuration.

An obvious design variation for the plane-on-plane clamp is the use of several discrete contact pads on one or both of the elements. This approach minimizes the surface area upon which dirt control measures must be taken, but at the expense of higher contact stress for the same clamping force. A separate lumped-parameter analysis was formulated for this geometry as described in Appendix D. The results of the analysis as applied to a typical case indicate that if four mounting pads are used, a typical pad area must be approximately 0.1 in² to avoid significant contact stresses; and that the clamping load should be of the order of 200 lbs to resist the lifting-off effects of 50-g sidewise accelerations.

Table XV

Classification of Fixed Clamp Concepts



If the misalignment due to force unbalance or asymmetry in pad spring rate is to be maintained less than 2 arc-seconds, the force or spring rate variation must be kept within 6% of the nominal values. For the dimensions assumed, the transient misalignment under a 50-g sidewise acceleration would be 3 arc-seconds. It can be seen that the main effects of limiting the pad contact area have been increased contact stress and a more stringent requirement on the degree to which the clamping force must be controlled.

The final major design variation possible for the clamping geometry of the plane-on-plane concept is the use of a three-point contact on one of the elements to define its plane. Although this was originally conceived as a possible method for minimizing the dirt problem, it was noted in the discussion of "Interface Considerations" that the critical particle size for hard particles is so small that this is not likely to be effective. The analysis of this concept is based upon the Hertz contact stresses and is described in Appendix E. The results indicate that very high stresses may be expected with typical clamping loads, even though a relatively large diameter "point" contact is used. Thus, although the asymmetry in clamping load for a 2 arc-second misalignment is not critical assuming elastic deflections only (approximately 20%), the effect of the high stresses and likelihood of plastic deformation under the contact points could lead to long-term misalignment. On this basis, the three-point contact concept was ruled out in favor of flat pads with a finite contact area.

(b) Thermal analysis - Asymmetric thermal gradients can lead to thermal distortion of the plane-on-plane clamp which cause a misalignment of the sensor input axis. The major potential sources for thermal asymmetry are variations in the thermal contact resistance across the mating surfaces of the clamp, and variations in the location of the effective source for the heat output of the sensor. These effects were predicted for a typical case in the lumped parameter analysis of Appendix H. The results, shown in Figure H-4, indicate that serious misalignments, compared to the goal for this program, can result if the thermal contact resistance of the mounting pad varies $\pm 10\%$ from the nominal value. Variations of this magnitude are felt to be quite probable, in view of the order of magnitude variations discussed under "Interface Considerations", if the clamp is to operate in a vacuum.

A design technique to avoid the effects of contact resistance variation is the provision of a relatively highly-conductive shunt path for the heat flow from the sensor to the IHU block. This concept was also analyzed as described in Appendix H and appears capable of reducing the thermal misalignment to acceptable levels. The thermal shunt may be implemented either by providing a fluid film (air or a liquid) at the clamp interface or by providing a separate symmetric shunt path.

The results of the thermal analysis were also used to indicate the effects of heat source fluctuations for an asymmetrically-located heat source. The results indicate that relatively large changes in heat output can be tolerated for an extreme location of the apparent heat source. Thus, this does not appear to be as critical as nonuniformities in contact resistance.

(c) Plane-on-plane clamping concepts - The fixed clamp concepts listed in Table XVI include a number of methods for obtaining the clamping force. The results of the preliminary design evaluation of these methods are described in the following paragraphs.

(1) The Use of Bolts to Provide the Clamping Force

The sensor fixture block can be clamped to the mounting block with bolts which are tightened with a known amount of torque, M_T . However, variations in the coefficient of friction at the threads, will cause a large uncertainty in the clamping force, F_C . By action and reaction, F_C is equal and opposite to the bolt tensile force. The bolt tensile force, T , is given by (35)

$$T = \frac{2\pi M_T}{\ell} \left[\frac{1}{1 + 2\mu'} \right] \quad (24)$$

where ℓ = thread lead

μ' = effective thread friction coefficient.

For a 10-32 thread, the value of μ' may be expected to vary in the range

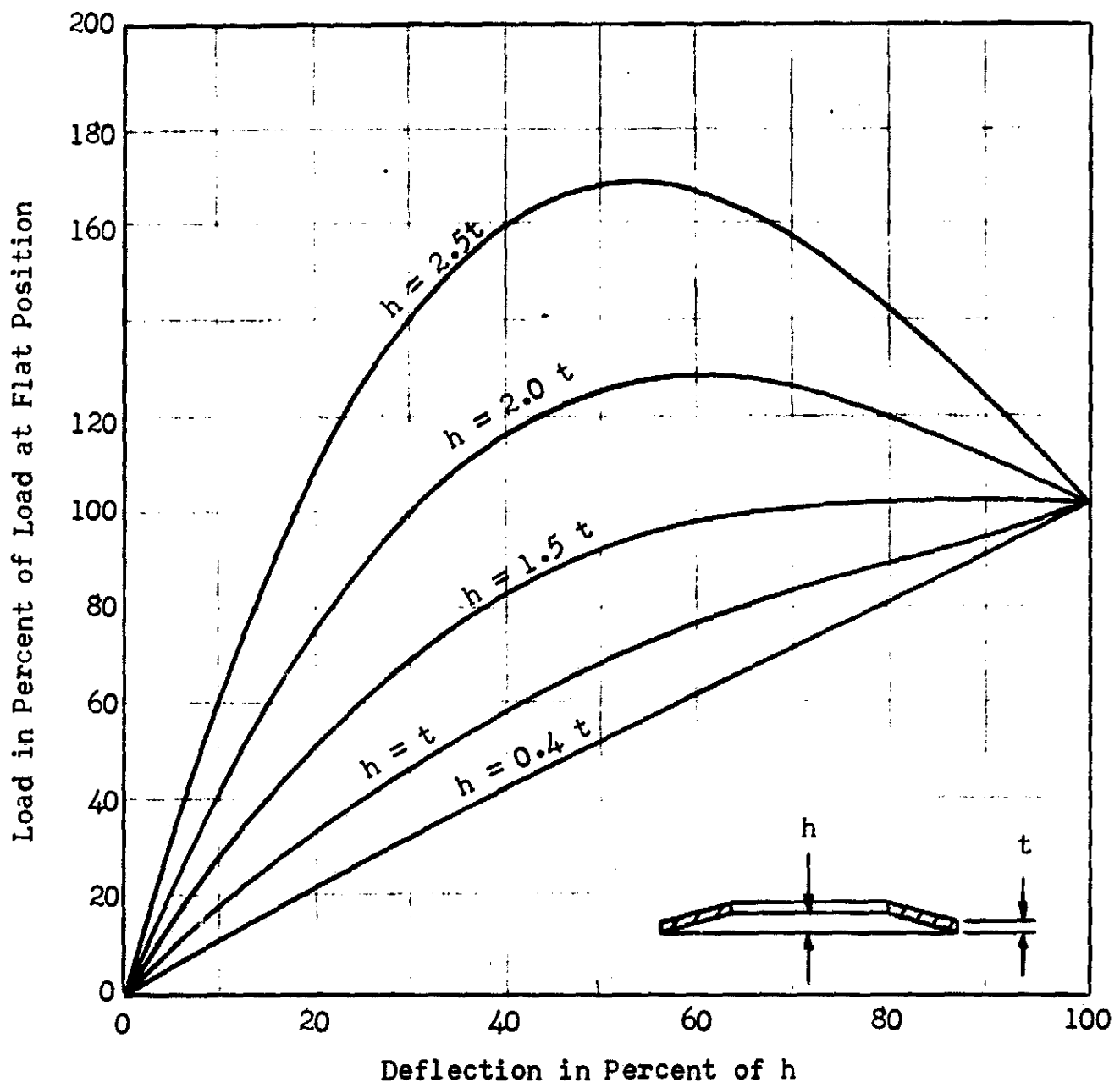
$$0.5 < \mu' < 1.5$$

Such a range could cause a variation in bolt load or clamping force by a factor of two which is too great to reliably maintain the clamping force symmetry required for this application.

(2) The Use of Springs to Provide Clamping Forces

Precisely controlled clamping forces can be obtained with springs, if spacers are used to limit the spring deflections. A typical configuration is shown in Figure B-3 of Appendix B. It is clear that if the spacer and the mounting block are not deformed significantly by overtightening the bolt, the clamping force will be as predictable as the spring constant. Spring loads at working length can be held to within one-half of one percent (36).

A different type of spring that could be used is a Belleville washer, shown in Figure 14. The force versus displacement characteristics of a Belleville washer are also shown in Figure 14 (37). If a washer with $(h/t) = 1.5$ is used, the force does not



Adapted from Reference (37)

Figure 14. Typical Force-Deflection Characteristics for a Belleville Washer

vary by more than one percent as the deflection, x , ranges between

$$0.75 < \frac{x}{h} < 0.9$$

It is therefore apparent that springs can provide clamping forces that can be controlled to a sufficient accuracy to permit acceptable sensor alignment.

(3) The Use of Hydraulic Pressure to Provide the Clamping Force

Clamping forces can be obtained by pressurizing a flexible bladder that is in contact with the gyro fixture as shown in Figure B-2 of Appendix B. In order to avoid clamping unbalance moments, it is important that:

- a. the bladder have negligible bending stiffness; and
- b. the bladder only contact the gyro fixture along a surface that is parallel to the mounting plane.

From the theory of plates and shells, it is well known that the bending stiffness is only important for deflections, δ , that are on the order of the shell thickness, t . If the deformation is such that $\delta \gg t$, bending stresses will be insignificant with respect to membrane stresses and the material will effectively have negligible bending stiffness. Clearly, a flexible bladder would fulfill this condition. Requirement b. above is easily fulfilled since surfaces can be machined to one arc-second orientation accuracy.

The pressurized bladder, however, suffers from a number of practical disadvantages compared to the simpler spring clamps as follows:

- a. an extra fixture is required to contain the bladder;
- b. pressure regulation of the bladder would be required, such as spring-loading the volume in order to avoid variation in clamping force with ambient temperature variation; and
- c. the clamp is liable to catastrophic failure due to a leak in the system.

For these reasons, using hydraulic pressure to get clamping force is not felt to be competitive with mechanical methods such as springs.

(4) Clamping with a Bonding Matrix

Two basic configurations for clamping with a bonding matrix arose from the concept generation phase of the study. These were the application of an adhesive bond at the interface

and the dowel-potting concept of Figure B-4 of Appendix B.

The use of an adhesive at the locating interface requires a prohibitive tolerance on the thickness of the bonding material, of the order of 10 to 20 μ inches.

The dowel-potting concept does not seem to offer any advantages over a controlled spring-force clamp. Furthermore, it introduces difficulty in installation and removal, and there is no straightforward method for controlling the clamping force.

For these reasons, a bonding matrix clamp was not considered further.

(5) Clamping with Surface Tension Forces

Ultrasooth surfaces that are separated by an extremely thin oil film can be joined together by surface tension effects. A common example of this is gage blocks that are "wrung" together. One disadvantage of this technique is that it is not reliable. For example, the gage blocks may stick together in spite of the fact that the film has a significant thickness. In this situation, a significant misalignment can occur if the film thickness is not uniform. Another disadvantage of this method is that it could not be used in a high-vacuum environment since the oil film would not remain on the mating surfaces. Finally, it would be difficult to produce a known clamping force. Due to these difficulties, this method of clamping was eliminated from further consideration.

(6) Producing a Uniform Contact Pressure with Wedges

The fixed clamp clamping force can be provided by forcing a wedge between two surfaces. Theoretically, with proper geometry, the resulting clamping force could be distributed uniformly over the surfaces. However, unpredictable friction effects and unavoidable cocking moments will cause the contact pressure to vary over the wedge area, making possible a high local stress with attendant yielding or microcreep. It should be noted, on the other hand, that the wedge concept is an attractive one as an adjustable clamp. In this case, which is discussed under "Preliminary Design of the Adjustable Clamp," the elements are free to move as the wedge is engaged and good wedge contact is ensured through the use of spherical joints.

(7) Generating a Clamping Force with an Interference Fit

In principle, an interference fit could be used to generate a uniform clamping force that holds a block against a plane. However, an elaborate fixture having many additional precise machining tolerances would be necessary. Moreover, means would have to be provided for regulating the interference so that the block could be inserted, and removed, thereby introducing many of the complexities inherent in the cylinder-in-hole clamp (see next section). These complexities are not felt to be warranted in comparison with the simple spring-force type of clamp.

Cylinder-in-hole fixed clamp concepts.- A number of cylinder-in-hole concepts are summarized in Table XV. Evaluation of this class of concepts included a force-deflection analysis, a thermal analysis, and analysis and consideration of a number of clamping designs.

(a) Force deflection analysis.- In general, the alignment between the mating elements of the cylinder-in-hole class of fixed clamps is obtained by producing an interference fit between the members. In addition, the interference force can be used to provide the clamping action.

An idealized lumped-parameter model was used to predict the misalignment of the axes that might be expected due to asymmetries in the interference between the members. The results of this analysis, presented in Appendix F, show conservatively that the combined stiffness of the mating cylinder and shell members will have to be held constant on the order of 1% to ensure angular error of less than 2 arc-seconds. This is well within attainable machining accuracies for typical configurations of this type.

Appendix K presents an analysis of the misaligning effects of deformation of a cylindrical shell due to a local anomaly or bump on the locating cylinder. The results show that, for dimensions consistent with precision-machined elements, the angular error from this source is not likely to be a problem.

Thus, it appears that the cylinder-in-hole class of clamps is basically feasible from the standpoint of maintaining alignment accuracy under the clamping load.

(b) Thermal analysis.- The cylinder-in-hole class of concepts was analyzed for the misaligning effects of thermal gradients using a lumped-parameter model similar to that employed for the plane-on-plane clamp. The results of this analysis, described in Appendix H, show that although serious misalignment can occur if large variation in thermal contact resistance exists around the cylinder, this concept is much less sensitive to this effect than the plane-on-plane concept when no thermal shunt path is used. If the expedient of providing a fluid film at the interface as a thermal shunt path were adopted, it is likely that there would be no significant misaligning effects from thermal gradients.

(c) Cylinder-in-hole clamping concepts.- Several methods for producing the interference between cylinder and hole are analyzed in Appendix G of this report.

It was first determined that to provide clamping against 50-g axial accelerations but not yield the hole walls, a typical cylinder-in-hole configuration requires that the radial interference lie between 0.37 and 1.6 mils. This is well within the range of attainable machining tolerances.

The following methods of producing this interference were analyzed:

- a. thermal shrink fit;
- b. external hydraulic pressure; and
- c. use of a split cylinder.

The thermal shrink fit was found to be feasible from basic considerations. The stresses produced are not excessive and are high for only a short period during installation or removal. If materials are used which have low thermal diffusivity (such as stainless steel), the thermal transient time during which installation or removal must take place is of the order of 1 to 2 minutes. This is felt to be practical. With materials of higher diffusivity, however, this time reduces to the order of 10 seconds, which is marginal. Aside from the material and installation time requirements, the thermal shrink method introduces the practical disadvantage of requiring an auxiliary external heater or heating elements in the IMU block. Also, the uniformity of interference is affected by the tolerance on the IMU block dimensions. For example, if a shell having 1/4 inch thick walls is used to hold the cylinder, the tolerance on wall thickness is 0.001 inches. Although this is certainly feasible, it requires precision machining of a surface other than the mating ones.

The use of hydraulic pressure to produce an effective interference between the cylinder and hole was also found to be basically feasible for this application. Loading pressures are reasonable and stresses are not high. The same requirement on wall thickness or elastic symmetry holds, however, as for the thermal fit. Thus, precision machining is required throughout the deflecting structure. The hydraulic loading method also requires pressure regulation against the effects of ambient temperature variations. This could be provided by loading the oil volume with a spring-loaded piston. Finally, the hydraulic method is subject to potential catastrophic failure if an oil leak develops.

Analysis of the split clamp concept shows that its geometry introduces symmetry tolerances which are more stringent than the continuous interfering cylindrical geometry. Friction forces occurring during installation introduce uncertainty for both two-piece and one-piece split clamp geometries. The two-piece clamp requires plane-on-plane locating surfaces in addition to the cylindrical surfaces, and the installation force must be maintained uniform. The various disadvantages of the split-clamp systems are not offset by any obvious advantages over alternative methods. Thus, this concept was not considered further.

Those cylinder-in-hole concepts of Table XVI which were not analyzed in Appendix G were considered from a design standpoint. The threaded cylinder concept, illustrated in Figure B-8 of Appendix B, was originally conceived as a method for overcoming the effects of dirt. In this concept, a self-tapping cylindrical fixture is screwed into a slightly undersized hole; the resultant

wiping action and small thread crest contact area provide a practically dirt-insensitive clamping action. This concept is not felt to be promising due to possible misalignment that can be produced by nonuniform friction forces and plastic deformation.

A common feature of clamps involving tapered cylinders and holes, collets, and expanding plugs (such as those shown in Figure B-7, B-9, and B-10 of Appendix B), is that they require precision tapered surfaces. Unfortunately, machining a taper is an order of magnitude less accurate than machining a hole or a cylinder. In general, the Total Indicator Runout (TIR) of these surfaces cannot be controlled to better than $50 \mu \text{ in}^2$. Consequently, the position of the centerline of the cylinder will have an uncertainty of this order, which is intolerable. A further disadvantage of clamping concepts involving tapered surfaces is that nonuniform friction effects can produce cocking and misalignment of the tapered member. Contact pressures will depend on frictional effects and are therefore unpredictable. Consequently, the tapered cylinder in a tapered hole, together with collet-type clamps, and expanding plug clamps have not been considered further.

Cylinder in V-block clamp.- The cylinder in V-block geometry was analyzed from the standpoint of the Hertz stresses and deformation at the line contacts between the cylinder and V-block planes as described in Appendix E. This analysis shows that, for a typical configuration, the stresses can be maintained below critical levels and misalignment due to nonuniform clamping load can likely be kept within the specified design goal. Its main disadvantage compared with the other clamp geometries is the need to produce three highly precision locating surfaces, the cylinder and the two planes forming the V-block. The plane-on-plane clamp and the cylinder-in-hole clamp, on the other hand, require only two such surfaces. Since there do not seem to be any offsetting advantages, the cylinder in V-block was not considered further.

Sensor mounted on centers.- Another basic method for locating the sensor axis is to mount it on centers. If the centers are formed by the apparent centers produced by relatively large tapered clamp areas, the concept falls into the tapered cylinder method of clamping for the cylinder-in-hole concept. If small contact points are used, the problem becomes similar to the three-point contact problem discussed in Appendix E. Although mating geometries can be used which minimize Hertz contact stresses, perfect fits cannot be produced and it is not likely that the stresses produced under realistic clamping and dynamic loads can be kept below critical levels.

Quasi-verification.- As discussed under "Concept Generation", quasi-verification was envisioned as including the following two basic methods of embodying a partial verification of alignment during installation:

- (a) provision of a simple measurement of the repeatability rather than the actual value for the degree of alignment; and
- (b) provision of a mounting jig, previously set up and verified in the laboratory, which is capable of locating the sensor while a bonding matrix is formed between the locating interfaces.

As noted in previous discussion, the use of a bonding matrix is not now considered promising as a clamping method. Moreover, it is not possible to make a jig less sensitive to dirt than a simple plane-on-plane clamp because of the extremely small critical size for hard dirt particles. Thus, this method of quasi-verification was not considered further.

The repeatability measurement, however, remains a potentially useful means of quasi-verification in the field. Alternative methods envisioned include a small portable autocollimator as shown schematically in Figure B-16 of Appendix B, or an optical flat mounting flange as shown in Figure B-17.

At the present time, it is felt that quasi-verification in the field should be regarded as an undesirable expedient, the necessity for which should be established experimentally before its adoption.

The most critical potential misaligning factor for the plane-on-plane clamp is the presence of dirt and foreign particles. Methods for overcoming this factor, as discussed under "Interface Considerations", include installation with a wiping action and the use of a soft dirt-absorbent film. If by further experimentation these methods are found inadequate for ensuring alignment in the presence of dirt, then quasi-verification in the field should be considered.

Summary and Conclusions

Of the various orienting geometries considered, the plane-on-plane, the cylinder-in-hole, and the cylinder in V-block concepts were found to be feasible from the standpoint of maintaining axis alignment under the influence of the operating loads which have the expected degree of asymmetry. The cylinder in V-block offered no advantages over the other two concepts and required more precise surfaces. Thus, it was dropped from further consideration.

The cylinder-in-hole class of clamps has two major disadvantages in comparison with the plane-on-plane concepts:

- (a) A survey of the state-of-the-art in precision machining indicates that the degree to which the hole can initially

be produced relative to the reference axis is of the order of 2 to 4 times less accurate than for a plane. Thus, a large portion of the error budget for the system could be used up by machining error.

- (b) Clamping, although feasible with a thermal shrink fit or hydraulic loading, is inherently more complex than the simple spring-loaded retainer possible with the plane-on-plane clamp. It introduces the necessity for accurately machined surfaces other than the locating surfaces. Moreover, interference fits complicate installation.

The major offsetting advantage of the cylinder-in-hole clamp is its relative insensitivity to misalignment from thermal effects in a vacuum. These effects, which are mainly due to thermal contact resistance variations, can be mitigated in the plane-on-plane concepts by the use of a fluid film at the interfaces or by a thermal shunt path. This, of course, introduces a sealing problem for vacuum operation, while it is likely that the cylinder-in-hole concept would not require such a measure.

The most promising methods for dealing with the dirt problem are the use of a light wiping action during installation, or the depositing of a thin dirt-absorbent coating on the locating surfaces. Although these methods are theoretically possible for either concept, practical difficulties arise with the cylinder-in-hole clamps. The most promising method for providing the requisite interference for the cylinder-in-hole clamp is a thermal shrink fit. This results in a limited thermal transient time, during which the interference force is building up between the members. For effective wiping action, the installation process would require careful timing in order to wipe with the desired light loading and not damage the surfaces as the loading increased. In order to achieve the necessary control of coating thickness, the dirt-absorbent coating must be vacuum-deposited on the locating surfaces. The plane locating surface is likely to be more favorable for achieving accurate thickness control with this process than the cylindrical surface.

Thus, on balance, it is concluded that the most promising fixed clamp geometry is the plane-on-plane class of concepts. The locating surface of the sensor should be a continuous plane or be formed by discrete flat mounting pads rather than being defined by three-point geometry such as three spherical feet.

The most promising method for providing the clamping force is by means of a spring-regulated force. This can be easily implemented by using Belleville washer springs in conjunction with bolts, or a bayonet-type retainer, or a cam surface.

PRELIMINARY DESIGN OF THE ADJUSTABLE CLAMP

As discussed under "Description of the System", an adjustable clamp is required as the internal clamp between the sensor and its interface piece. The preliminary design tasks for the adjustable clamp are described in the following sections.

The design of the adjustable clamp encompasses the problems associated with the basic influences tending to misalign the system with those of obtaining the requisite range and resolution of adjustment. While machining accuracy is not as critical as that for the fixed clamp since the adjustable clamp will not be installed in an open-loop manner without verification and adjustment, material instabilities, thermal distortion, and applied loads can all contribute to subsequent misalignment.

The general method of attack was the same as that described for the fixed clamp, except that the bulk of the effort was concentrated on the mechanical design problem of obtaining the desired adjustment rather than on the various fundamental problems already treated in the process of evaluating the fixed clamp concepts. An initial concept generation process was followed by preliminary design evaluation to screen out the least promising concepts before conducting a more detailed design analysis. As in the case of the fixed clamp, an effort was made to classify concepts in a manner which would optimize the evaluation process.

The end result of these studies was the selection of the three most promising adjustable clamp concepts to be combined with the two promising fixed clamps for later experimental investigation.

Concept Generation

As with the fixed clamp concept generation, a wide range of clamp concepts was obtained by means of "brainstorming" sessions involving a number of engineers. The emphasis in this brainstorming process was placed on the means of adjustment.

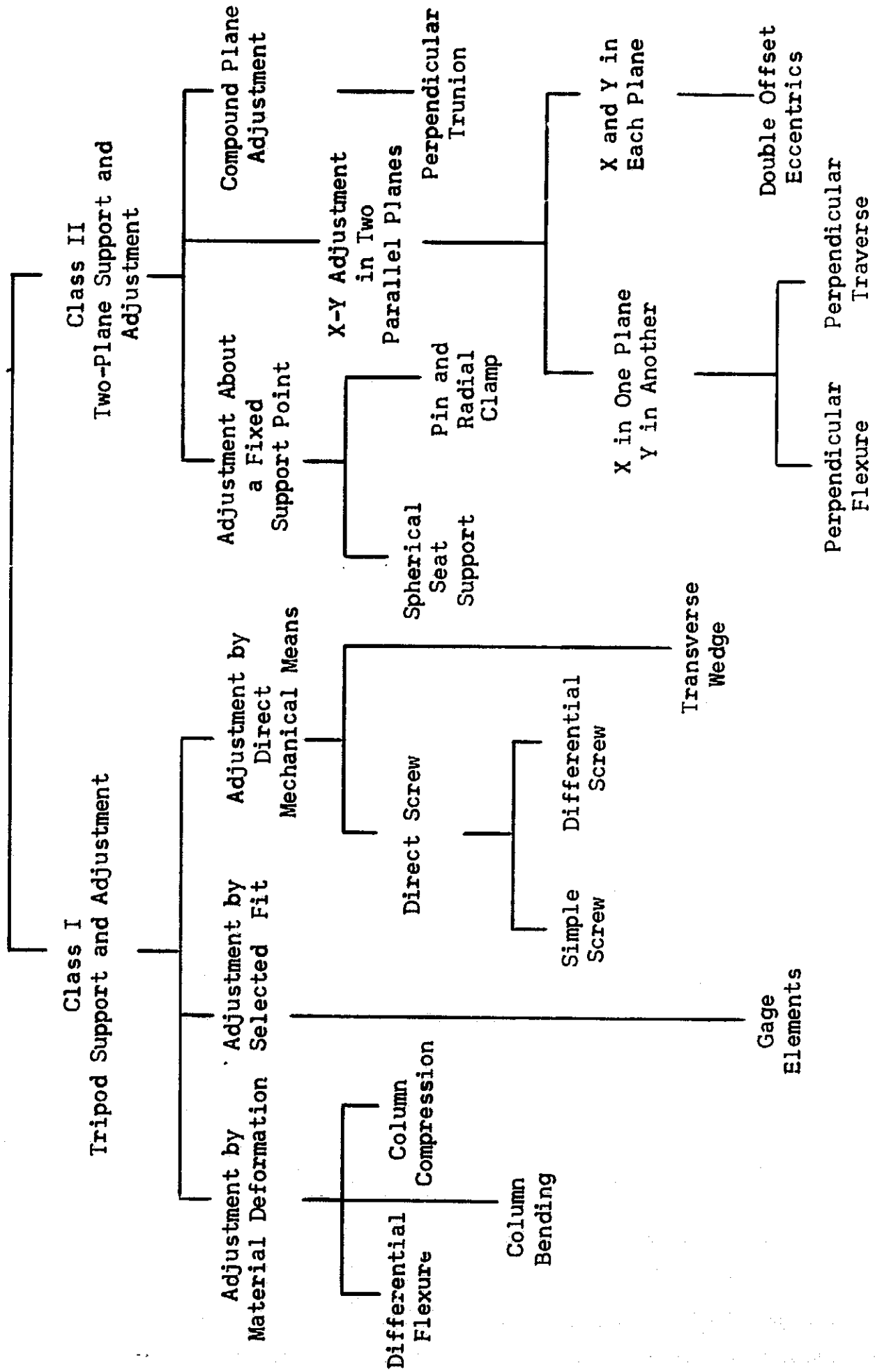
The range of concepts generated is shown in Table XVI after classification, combination of similar ideas, and elimination of obviously unpromising concepts. For the interested reader, a schematic diagram of each tabulated concept is provided in Appendix I to this report.

Two overall classes of concept were identified and are described briefly as follows.

Tripod support and adjustment.- These concepts provide three adjustable connecting elements as shown in the general configuration

Table XVI

Classification of Adjustable Clamp Concepts



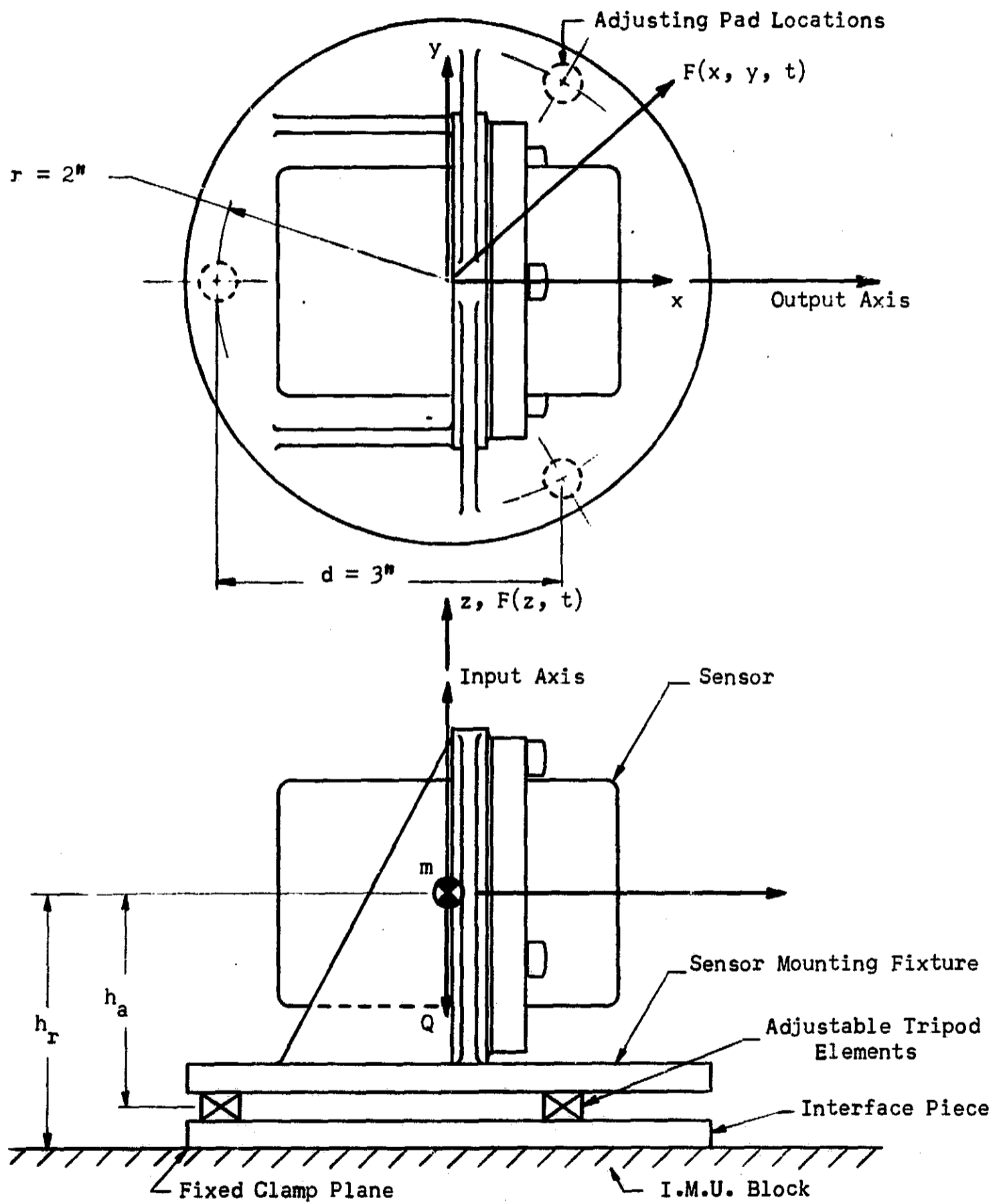


Figure 15. Schematic Diagram of the Assumed Clamp Configuration Illustrating the Major Overall Dimensions used for Concept Evaluation

of Figure 15 between the sensor and the interface piece. Both support and adjustment are accomplished at the same point on these elements, the support point on the interface piece for all three elements being coplanar. Three main types of adjustment were identified:

- (a) Material Deformation Adjustment - where the length of the element between the sensor and the interface piece is varied by elastic deformation of the structure.
- (b) Selected Fit Adjustment - where the length is varied by interchangeable spacer elements.
- (c) Direct Mechanical Adjustment - where the length is varied by mechanical elements which move the sensor relative to the interface piece.

These types of adjustment are illustrated in Figures I-1 through I-3 of Appendix I.

Two-plane support and adjustment.- This class includes several categories of clamps, as illustrated in Figures I-9 through I-14 of Appendix I, all either providing support and adjustment at two different planes on the assembly or providing support and adjustment at separate points. For example, the Perpendicular Trunion Concept of Figure I-14 uses two parallel orthogonal wedge-flexure assemblies to achieve adjustment of the axis in two perpendicular planes, the support being provided to the sensor in a single plane. The Perpendicular Flexure and Traverse concepts provide similar orthogonal axis adjustment but provide support at separated planes along the sensor.

The Double Offset Eccentric Concept shown in Figure I-13, on the other hand, does not provide orthogonal axis motion since the angular orientation of the axis is a complex function of the differential or coupled motion between the two adjustment eccentrics. Another method of adjustment conceptually similar to the offset eccentric method but acting at only a single support plane uses mating swash plates. This concept was eliminated as unpromising due to difficulties: (a) in holding sensor during swash plate adjustment without changing the output axis alignment; and (b) in obtaining the required swash plate rotation mechanically.

The concepts where adjustment is made about a fixed support as shown in Figures I-9 and I-10 form the final category. The support in this case allows axis motion in any plane. Adjustment is accomplished at a separate plane on the sensor and can be orthogonal or not, depending upon the details of the adjustment procedure.

Concept Evaluation

Evaluation of the adjustable clamp concepts of Table XVI involved a preliminary overall comparison of the two major classes on a qualitative basis, followed by a more detailed design analysis of the specific concepts in the more promising Class I. Design criteria based upon the specified goals for the prototype clamp system were formulated for this latter stage of evaluation. These studies are summarized in the following sections.

Comparison of the two major classes.- Review of the schematic diagrams in Appendix I of the various adjustable clamp concepts shows that, in general, the Class II concepts require dimensionally larger structures than the Class I. This is due to the fact that the means of adjustment and support are at separate locations on the sensor. Also, because of the extremely stringent stiffness requirements introduced by the required insensitivity to accelerations and vibration, a much more massive structure results for the Class II concepts than the Class I. In addition to the obvious weight penalty, a characteristic which is subject to a stringent specification on its own, the size and weight of the support structure also magnify the misaligning effects of thermal gradients and produce higher dynamic loads at critical support points under inertial loading.

The adjustment elements for the Class II concepts are also, in general, more intricate than their Class I counterparts. Specifically, they incorporate more mechanical parts of greater complexity. This results in increased cost and the inability to take advantage of the most accurate available machining methods. The most direct result of the latter is a reduction in adjustment resolution due to the accumulation of mechanical tolerances. In addition, the large uncertainty and variation in thermal resistances at interfaces between the mating parts is expected to introduce a greater probability of angular instability due to asymmetrical thermal expansion. Parts with complex shapes are also more susceptible to configurational dimensional instability.

In view of these disadvantages and the fact that no outstanding relative advantages were identified for the Class II concepts, the preliminary conclusion was reached that Class I concepts are more promising than Class II concepts. Subsequent sizing and evaluation was confined to the various Class I concepts as summarized in the following sections.

Formulation of design criteria.- For subsequent more detailed analysis of the various concepts in Class I, it was necessary to formulate a set of quantitative design criteria. These were based upon a number of assumptions as well as the system goals outlined in Appendix J as follows.

- (a) Adjustment Range.- The total adjustment range must be capable of accommodating the sum of misalignment errors arising from the error between the sensor input axis and its mounting surface and reference pin or notch, and the tolerance build-up from the sensor mount to the IMU reference surface. The former was estimated from sensor vendor catalogs to total up to 21 arc-minutes, while the latter could likely be held to 3 or 4 arc-minutes with good machining practice. Thus, the total required range is assumed to be 25 arc-minutes.
- (b) Adjustment Resolution.- This is specified in Appendix J as 1 arc-second, based upon the half cone angle of the input axis.
- (c) Stability.- The total required adjustment accuracy was taken conservatively for design purposes as 3 arc-seconds. The total stability requirement is 2 arc-seconds obtained by subtracting the resolution, 1 arc-second, from the total adjustment accuracy. Assuming that a plane-on-plane fixed clamp is used, this stability requirement is tentatively budgeted as follows:
- | | |
|---|--------------|
| 1. Installation errors at the fixed clamp interface | 0.5 arc-sec. |
| 2. Dimensional instabilities | 0.5 arc-sec. |
| 3. Thermal instabilities | 0.5 arc-sec. |
| 4. Distortion under dynamic load | 0.5 arc-sec. |
- (d) Configuration.- For purposes of analysis the general overall dimensions of the assembly are needed. These were assumed as shown in Figure 15. This tentative configuration, with mounting supports as shown, was selected to provide maximum adjustment resolution and stability under dynamic load within the general size imposed by typical sensors. It is seen that the center portion is left open for possible inclusion of a thermal shunt path as discussed under "Preliminary Design of the Fixed Clamp."
- (e) Weight Proportions.- The weight goal for the total clamp assembly, including those portions of the IMU which are part of the clamping system, is 2-1/2 times the sensor weight. The latter is typically 1 lb. Thus, the total supported weight at the adjustable clamp supports is 1.75 lbs.
- (f) Preload.- The preload was set assuming that the load at a support point must not reach zero under the

maximum 50-g acceleration. Assuming the geometry of Figure 15, the supported static weight of (e) above, and maximum acceleration in the worst direction, this preload becomes 52 lbs.

- (g) Stiffness - The structure stiffness must be capable of withstanding either 15-g steady acceleration or the vibrational accelerations of Appendix J without exceeding the budgeted angular distortion of (c) above. The most stringent criterion is imposed by the 15-g's in a sidewise direction, requiring a minimum total stiffness of 3.5×10^6 lbs/in. The vibrational requirement imposes a minimum stiffness requirement of 1.5×10^6 lbs/in.
- (h) Maximum Stress - It has been assumed that the maximum steady stress in the structure should not exceed 10,000 psi which is a typical value for 1/2 the micro-yield stress for the materials of interest. Transient stresses under shock loading will be allowed to reach 20,000 psi.

Evaluation and selection of the Class I concepts.-

Preliminary design consideration of the three types of clamp concepts included in Class I of Table XVI did not indicate one which is obviously superior to the others.

The material deformation concepts inherently involve the highest operating stresses although these can be maintained below the criterion of the previous section. They are simple in concept and design, provide good symmetry, and involve methods giving ease of adjustment. Their relative cost is felt to be low compared with the other types. They also have the advantage of being capable inherently of minimizing the number of discontinuous interfaces between sensor and fixed clamp, providing a minimum of one while the other types require at least two. This has the benefit of minimizing the effects of thermal asymmetry due to thermal contact resistance variations. It also minimizes the locations where surface effects such as dirt and wear can influence the alignment process.

The selected fit concept is inherently a trial and error method which will likely require several iterations to achieve alignment, depending on the accuracy of the verification system output. It is basically a low-stress concept requiring only the preload specified in the previous section. It is also simple in design, provides good force symmetry, and is expected to be competitive in cost once set up on a production basis. The main relative disadvantage is the inherently greater number of contact interfaces which result in a greater susceptibility to thermal asymmetry, dirt, and wear.

The mechanical adjustment concepts fundamentally involve sliding contact at interfaces under load. Thus, they are

relatively the most susceptible to wear and stick-slip function effects. The stresses can be kept low at the required preload values, however, and these concepts provide the largest inherent range of adjustment. Although relatively complex in terms of number of parts, the parts are simple to produce. The number of contact interfaces between sensor and IMU cannot be reduced below two.

The above qualitative consideration of the three concept types of Class I did not reveal any basis for a priori selection or elimination of one concept type relative to the others. Since it is desired to select the three most promising adjustable clamp concepts, it was decided to select the best concept from each of these three basic types. This has the feature of providing the full range of potential concepts with their attendant relative advantages and disadvantages for later experimental evaluation.

Thus, the further analysis of the adjustable clamps was devoted to preliminary sizing and to determining the best particular design to use for each of the three basic types. For this purpose a number of design analyses were performed for the clamps shown in Figures I-1 through I-8 of Appendix I. In general, these analyses were stress-deflection analyses of the various component parts to size the elements to meet the various criteria of the previous section, and to determine the limits of adjustment resolution. The analyses were all based upon available solutions in the literature, conservative idealizing models being formulated for the elements where necessary.

Of the Material Deformation type of concepts, the column bending concept was found least promising on the basis of providing a very small adjustment range for reasonable column lengths within the stress and stiffness criteria. The Differential Flexure and Column Compression concepts were found comparable in this respect giving a fine adjustment range of 15 arc-secs. Thus coarse adjustment must be used. The method selected was gage blocks, requiring 100 sizes in increments of 0.0001 inch \pm 0.000050. For each case the angular offset caused by possible differences in length from one mounting pad to another requires that a spherical seat be used to provide good distribution of contact stresses without overstressing the tripod elements. This can be integrated with the coarse adjustment element in order to minimize contact interfaces. The means of verification must be capable of providing accuracy of measurement within \pm 5 arc-seconds for selection of correct coarse adjustment elements in addition to providing a null indication within 1 arc-sec. Since both of these concepts were feasible and comparable in performance, the Column Compression Concept was selected as the best material deformation type of concept in view of its relative simplicity of structural elements.

The Selected Fit Concept reduces mainly to a compromise choice of the coarse and fine spacer elements to achieve the required range and resolution. The best preliminary selection is 33 sizes of coarse elements in increments of $0.0003 \pm .0001$ in and 27 sizes of fine elements in increments of $15 \pm 7.5 \mu$ in. The verification accuracy must be good enough to choose the correct fine element, i.e., of the order of 7.5 in which is equivalent to 1.5 arc-seconds. A spherical seat, which can be integrated with the coarse element is required as for the Column Compression Concept.

The simplest Direct Mechanical Adjustment Concept is the Direct Screw. On the basis of analytical study, the Direct Screw was not felt to be feasible due to poor resolution with practical thread pitches. This is compounded by thread errors which can cause high local stresses with plastic deformation and long-term dimensional instability. This concept is felt to be particularly susceptible to external loading and vibration after adjustment since misalignment can be produced directly through the relatively coarse thread pitch. Also, like the Differential Screw discussed below, two spherical joints are necessary to eliminate bending, requiring locking which can introduce misalignment.

The Differential Screw overcomes the resolution problem by supplying a motion which is the resultant difference between the action of two threads having a small difference in pitch. Attainment of the required resolution is feasible with 80 to 100 pitch threads. The major problems with the Differential Screw Concept are associated with producing thread accuracies such that the mating elements are uniformly stressed and mate perfectly without axial clearances or plastic deformation. Any error in the screw threads acts directly to affect the angular alignment and not through the differential screw multiplication factor. This is in contrast with the other concepts which use screw threads to load a column through a relatively compliant spring element, or to position a wedge with a very small incline angle. The differential screw also has the disadvantage of requiring two spherical joints in order to eliminate undesirable bending of the screw. These joints, unlike the single spherical seats for the other concepts, will require locking which may introduce misalignment. The minimum number of contact interfaces is four, thereby increasing the sensitivity of the concept to thermal contact resistance variations.

The Transverse Wedge Concept can give a fine adjustment range of 75 arc-seconds, requiring 20 sizes of coarse gage elements in increments of $.0005 \pm .00025$ inches to span the entire 25 arc-minute adjustment range. Thus, this concept requires the minimum verification readout accuracy for proper selection of coarse elements. Mechanically, it offers the fine resolution possible with the differential screw but employs relatively simple geometry with minimum chance for errors due to machining inaccuracies, poor fits, and locally stressed sections. The minimum number of thermal contact interfaces is reduced to three.

Summary and Conclusions

Of the various adjustable clamp concepts generated during this study, the Tripod Support and Adjustment Class, which provides the simplest means of support and adjustment at one plane between the sensor and interface piece, was selected as the most promising for further development.

Within this class, the most promising means of adjustment from the three different Class I types of Table XVI were selected. These are:

- (a) Column Compression Concept
- (b) Selected Fit Concept
- (c) Transverse Wedge Concept

These concepts are illustrated schematically in Figures I-4, I-5, and I-8, respectively, of Appendix I.

Each of these concepts requires a spherical contact seat to avoid the effects of angular offset within the range of adjustment. Each requires a varying mixture of coarse and fine adjustment to span the 25 arc-min range with resolution to 1 arc-sec. The concepts are listed above in order of increasing range of fine adjustment. As the range of fine adjustment increases, the required number of coarse gage spacer elements decreases.

The means of verification measurement used in the laboratory must be capable of resolving alignment of the input axis to within 1 arc-second. The readout, however, must also be accurate enough to make proper selection of gage elements. The Selected Fit Concept is the most stringent in this respect, requiring readout accuracy of the order of 1.5 arc-seconds. This is followed by the Column Compression Concept with readout to 5 arc-seconds and the Transverse Wedge with 37 arc-seconds.

It is concluded that these three concepts give the best range of adjustable clamp concepts for further development. They also provide a wide range of basic characteristics for subsequent experimental evaluation.

CONFIGURATIONAL DESIGN

The previous sections of this report cover the preliminary design tasks, both for the fixed and adjustable clamp assemblies. Effort has been devoted in these studies mainly to evaluating the performance feasibility of each concept, sizing the elements to meet the various design criteria, and selecting those concepts having the best compromise characteristics for further development.

In general, it should be recognized and kept in mind, that the design goals for adjustment accuracy, stability, and interchangeability represent a substantial advance over the present state-of-the-art. The analysis of fundamental factors and the design analyses of clamp concepts indicate that although feasible, the achievement of these goals in the presence of the many disturbances engendered by the environmental conditions and the characteristics of actual materials will be marginal.

Thus, before further more detailed design is performed, it is appropriate to consider the overall configuration in an attempt to obtain the benefits of any gains that can be effected by optimizing the configuration. Study of this problem indicated two main areas where optimization is feasible: (1) reduction of misaligning moments at support and adjustment points; and (2) the provision of maximum overall mechanical and thermal symmetry.

Zero-Moment Configuration

For purposes of this discussion, the general configuration which was shown in Figure 15 of the previous section is assumed to identify the major elements of the clamp assembly. The z-direction is assumed to be coincident with the sensor I.A., the x- and y-directions lying in a plane parallel to that of the mounting pads.

The static clamping force, F_z , does not necessarily result in asymmetric reaction moments at the adjustment and support planes. Axisymmetric moments about the I.A. can be absorbed by local angular deflection rather than by misalignment of the I.A. In fact, provision of the requisite mounting pad and clamping force symmetry to ensure that no reaction moments resulted was a prime consideration in the preliminary design of the clamps. The above discussion also applied to the component of inertial forces in the z-direction.

Inertial forces in the x- and y-directions, however, do result in an unbalancing moment for the general configuration, the magnitude being proportional to the height, h , of the sensor assembly center of mass above the plane in question.

Although this dynamic moment was taken into account in the design analysis, it is desirable to minimize or eliminate it by making the adjustment and fixed clamp interfaces coplanar with the center of mass. A clamp configuration of this type is shown in Figure 16. The price for this configuration is a larger, more complex structure.

The analysis of the proper trade-off between these factors rightfully belongs further along in the design process. For the time being, there is considerable virtue in providing the smallest monolithic interface structure possible. However, no further separation between the plane of the center of mass and the mounting and adjustment planes should be made beyond that required for the above condition. A possible compromise configuration is shown schematically in Figure 17. It can be seen that this configuration requires a sensor mounting flange in a plane perpendicular to that usually provided.

Symmetry Considerations

Symmetry can be either functional or configurational, the latter being the usual type. In either case, the purpose of symmetry in the clamp system design is to accept displacements due to mechanical or thermal loadings without causing an angle change of the sensor input axis.

An example of functional without configurational symmetry is a load placed off center on a truss, the stiffnesses of the structure being adjusted to compensate for the difference in reaction loads at either end. Similar types of functional symmetry can be imagined for thermal expansion. Functional symmetry is sometimes useful but its design into a system is more complex than that for configurational symmetry, requiring a greater ability to predict the behavior of the system. Thus, it was not considered further at this time.

Configurational symmetry about an axis parallel to the I.A. and passing through the center of mass and the heat source is sufficient to minimize angular errors due to axial force, F_z , and to the heat flow from the sensor to the mounting block. This axi-symmetry should include geometry, elastic moduli or stiffnesses, and thermal moduli or resistances plus any thermal contact resistance. Although a surface or body of rotation is one form of such axi-symmetry, there are other forms as illustrated schematically in Figure 18.

A combination of axi-symmetry about the I.A. and symmetry about the x-y plane containing the center of mass is ideal since angular distortions due to F_y , as well as those due to F_z and heat flow, are eliminated. Mechanical symmetry about the x-y plane containing the center of mass was discussed in the previous section. Since the adjustment and fixed-clamp action occurs in a single plane, this plane must be made to coincide with the x-y

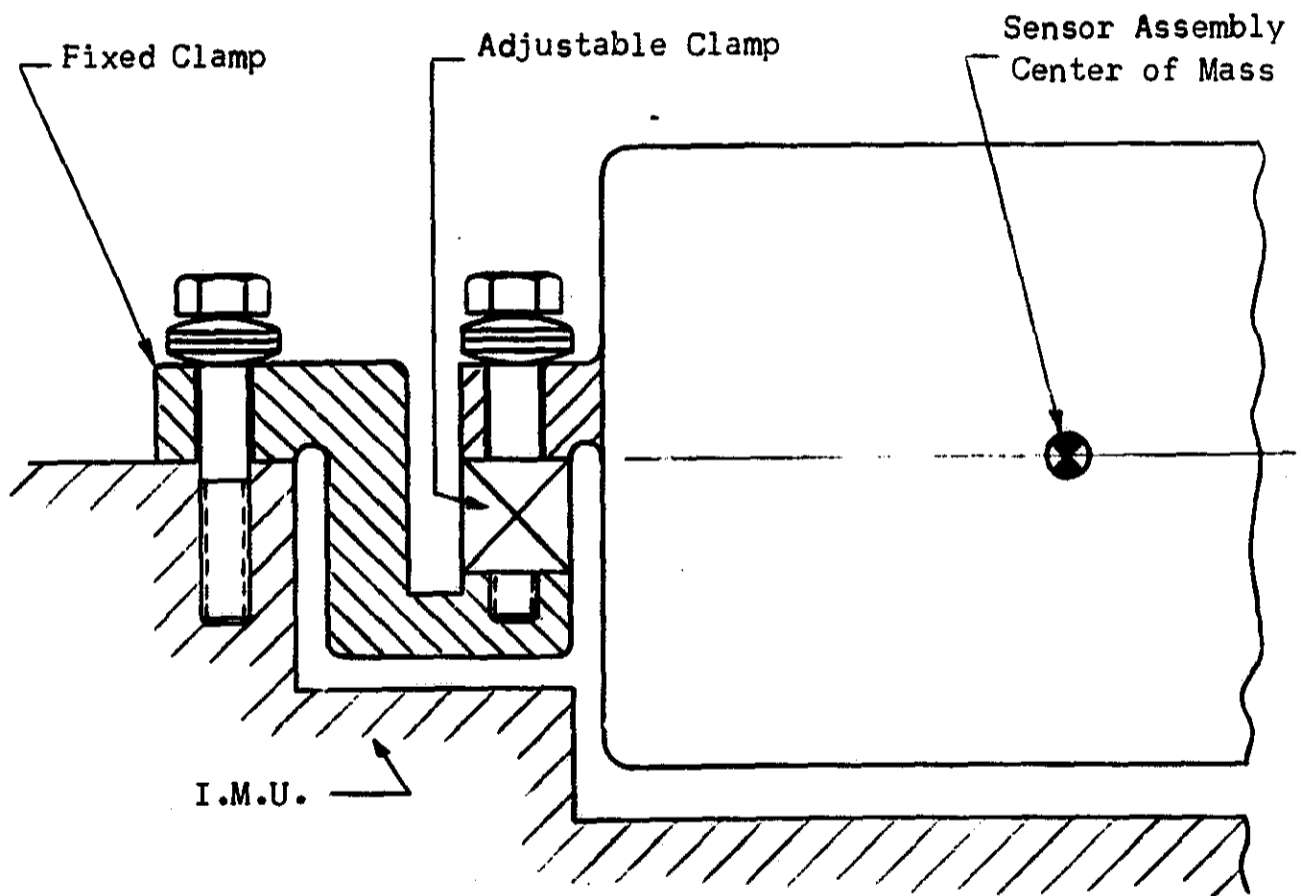


Figure 16. Zero-Moment Clamp Configuration

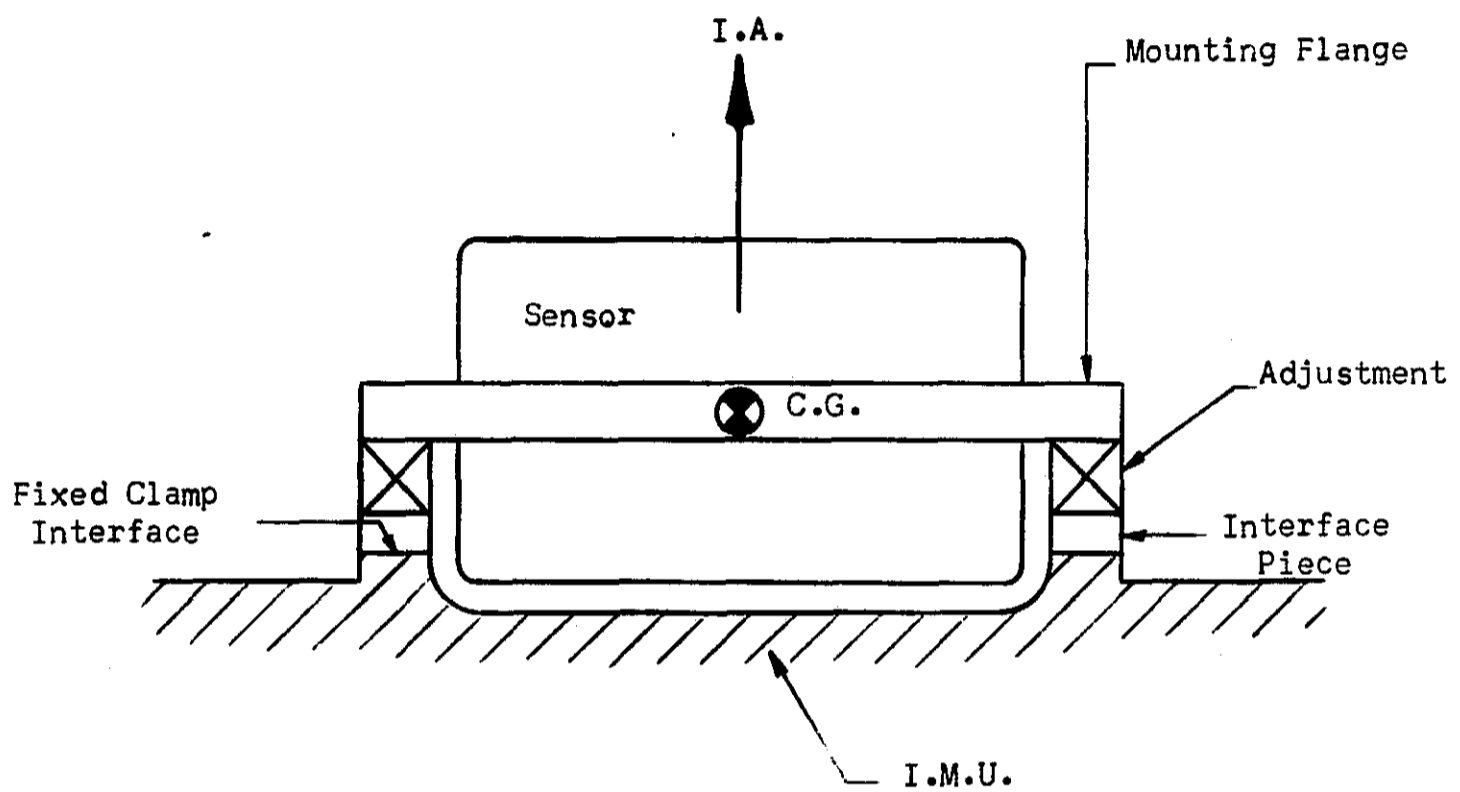
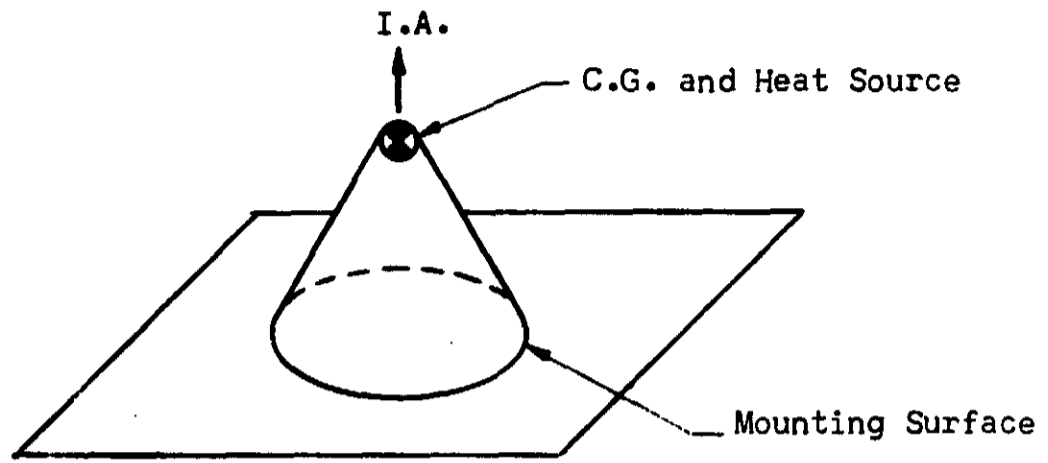
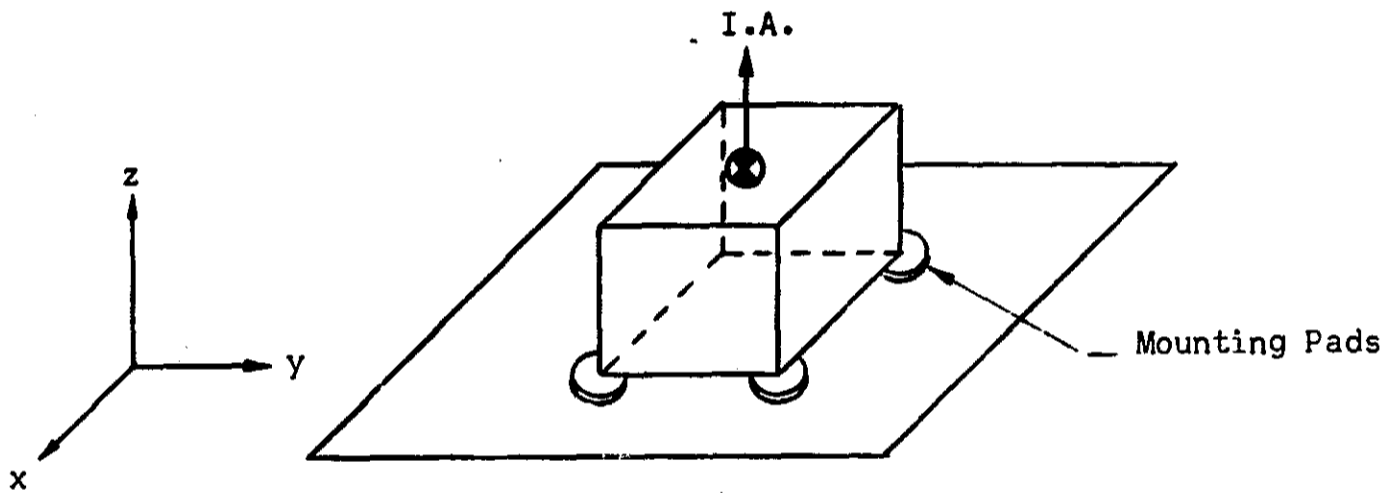


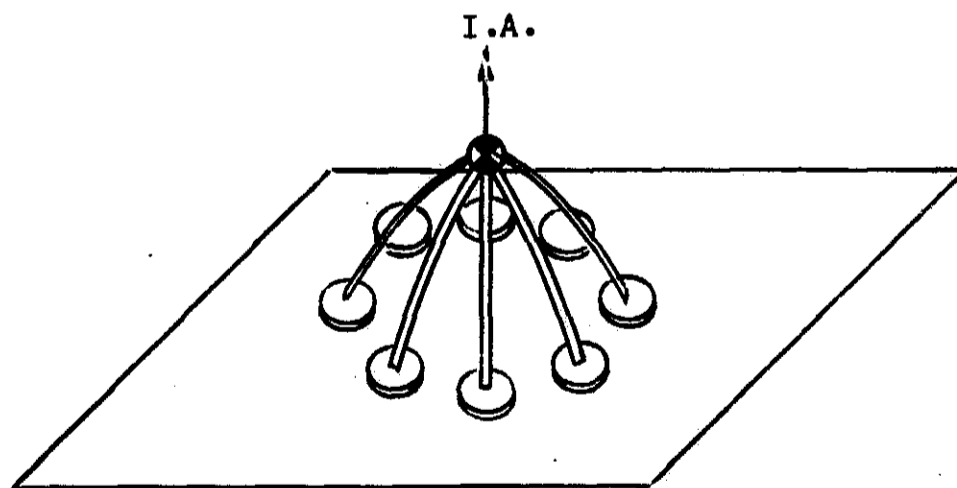
Figure 17. Optimum Moment Configuration with
Minimum Interface Piece Size



(a) Rotational Axi-Symmetry



(b) Cubic Axi-Symmetry



(c) Spider-Leg Axi-Symmetry

Figure 18. Various Configurational Symmetries About the I. A.

plane which includes the center of mass in order to achieve the desired symmetry.

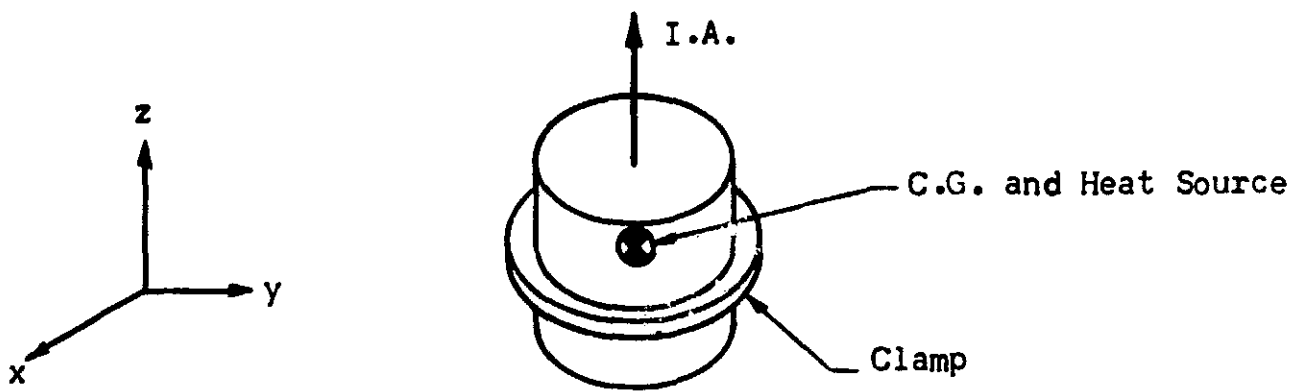
Figure 19 shows schematically various configurations with the combined symmetry. This type of configuration is insensitive to the heat load from the sensor so long as the heat flow into the structure or interface piece occurs along the sensor input axis, in either direction.

Symmetry between the sensor and its mounting flange is also important. Both sensor and flange are typically symmetric about the output axis which is perpendicular to the plane of the flange. If this type of sensor mounting is to be used, configurational symmetry can only be achieved by placing the center of mass at the center of the flange plane where the output and input axes intersect. In this case, any heat source is allowable as long as it is symmetric about the output axis.

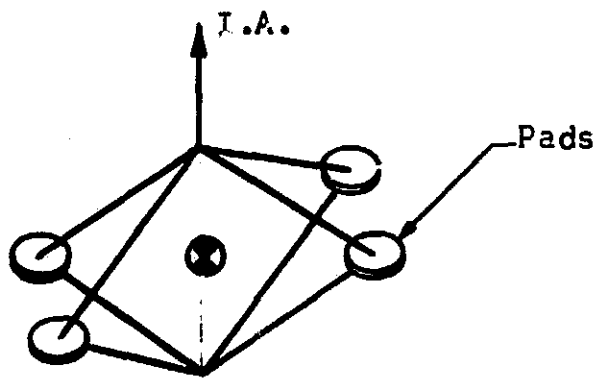
Thus, the general rules for optimum configurational symmetry are:

- (a) Maintain axi-symmetry about both input and output axes for all elements except the sensor.
- (b) Place the center of mass in the plane of the sensor mounting flange.
- (c) Maintain the sensor axi-symmetric about the output axis, including all of its heat sources.

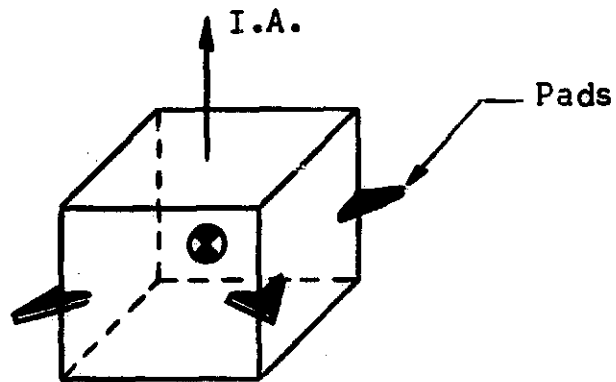
Two configurations of this type are illustrated schematically in Figure 20.



(a) Cylindrical Configuration

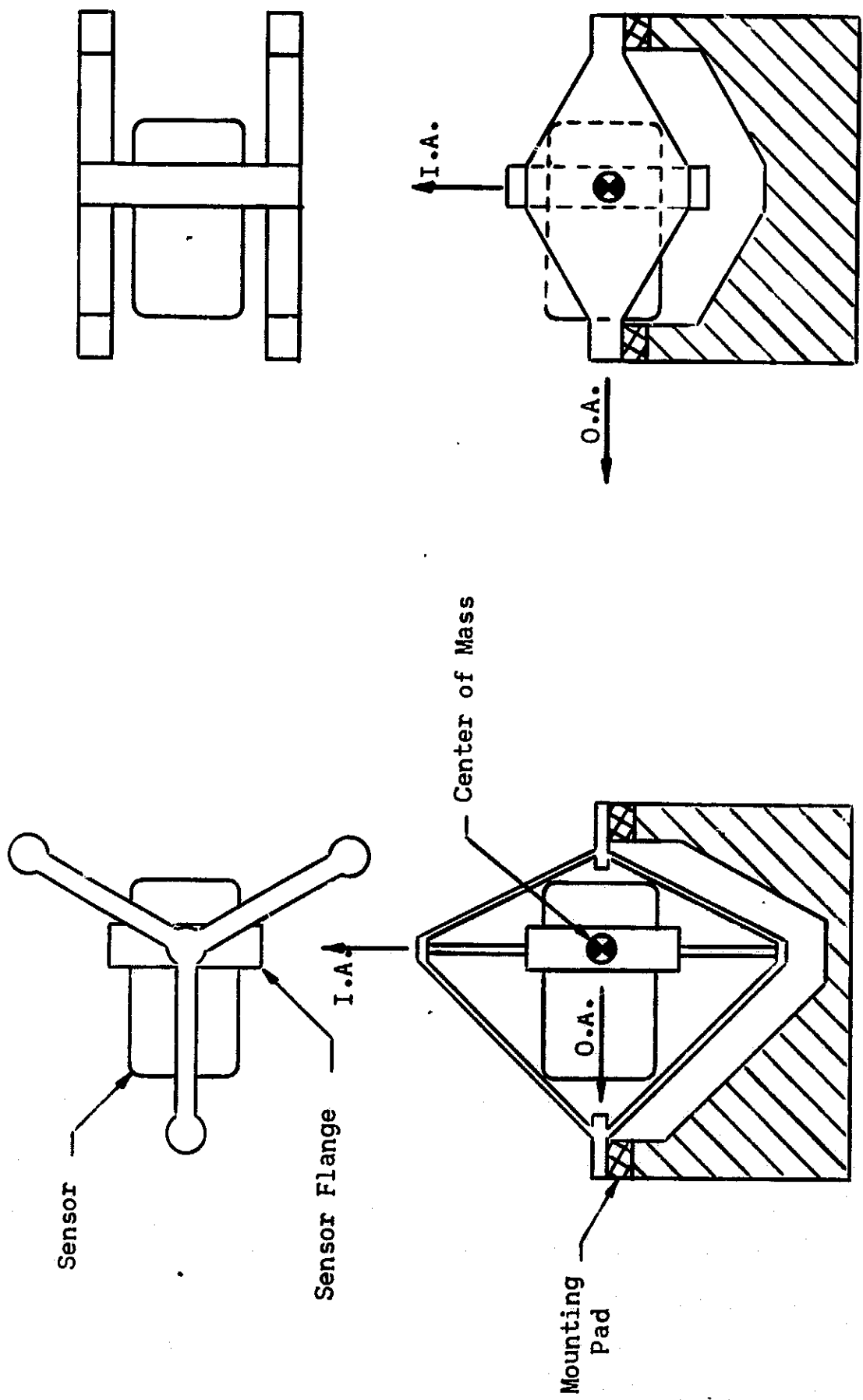


(b) Spider Configuration



(c) Cubic Configuration

Figure 19. Various Configurations Providing I.A. Axi-Symmetry and Symmetry about the x-y Plane Containing the Center of Mass



(a) Tripod Mounting Configuration

(b) Four-Pad Mounting Configuration

Figure 20. Schematic Diagram of Configurationally Symmetric Designs

CONCLUSIONS

The overall objective of this study has been to investigate the factors affecting the feasibility of a strap-down inertial navigation system with field-replaceable sensors, and to develop methods for establishing and maintaining sensor alignment. An early conclusion in the study was that the optimum clamping system for this purpose consists of an adjustable internal clamp between the sensor and an interface piece, and a fixed mutual clamp between the interface piece and the Inertial Measuring Unit. This allows field replacement of a prealigned assembly, hopefully without field verification of alignment.

Investigation of the feasibility of this clamping system led to the study of a number of fundamental factors including the state-of-the-art in pertinent areas, material considerations, and interface problems. Preliminary design tasks, including concept generation and evaluation, were then carried out to identify the most promising fixed and adjustable clamp concepts for further development. The salient conclusions drawn from these studies are outlined in the following paragraphs.

State-of-the-Art

The review of the state-of-art in pertinent areas identified the following important factors:

- (a) Transfer of gyro sensors to a mounting fixture presently results in an angular error which is much larger than the design goal. Thus, an adjustable internal clamp is required for alignment of a gyro relative to the nominal axis on the clamp assembly.
- (b) Present methods of measuring the deviation of the actual sensor input axis from its expected location use up a substantial portion of the error budget allowable within the design goals. Thus, these methods will require improvement in order to take full advantage of an improved clamping system.
- (c) The present state-of-the-art in ultra precision machining appears sufficiently advanced so that it will not be the limiting factor in achieving the desired clamp accuracies, provided simple locating geometries are used, such as plane-on-plane or cylinder-in-hole types.
- (d) It appears that the art of angular measurement is about an order of magnitude more advanced than the art of precision machining. Thus, the former should not provide any inherent limitation on the accuracy to which the adjustable clamp may be set.

- (e) The state-of-the-art in clean room technology is such that the probability of misalignment due to dirt particles can only be reduced rather than made insignificant. Thus, a design goal for the clamps, especially the fixed clamp, should be the ability to handle the dirt in the normal atmosphere.

Material Considerations

The state-of-the-art on the stability characteristics of materials both under stress and in the free state is still in its infancy. Considerable work needs to be done before an optimum material can be picked to provide maximum dimensional stability. It appears that some understanding is available of the possible metallurgical phase changes inducing instability in metals, and of desirable heat treatments to minimize these changes.

Successful hardening and heat-treating processes have been developed for hardenable steels used for precision gauge block materials to provide ultrastability. However these materials are heavy and may prove to be undesirable for aerospace applications. Also microyield strength (MYS) and microcreep data on these materials are not available.

Limited data on microcreep characteristics of the lighter-weight, lower-strength alloys is available. But corresponding data on dimensional stability is lacking. The early work of Lement and Averbach (9) is the only source of data on types of heat treatment to provide maximum dimensional stability.

Residual machining stresses have been shown to have a considerable effect on dimensional stability. Very little, however, is known about the stress level resulting from different types of machining operations on various materials.

Microcreep values obtained for the lower-strength alloys tested indicate that the MYS appears to be a useful indication of the stress value where significant dimensional changes will occur with time.

Ceramics, in particular beryllia, appear quite attractive from a dimensional stability point of view, having both good mechanical and thermal properties as well as a high dimensional stability.

On the basis of the information summarized in the preceding paragraphs, the following general conclusions may be drawn:

- (1) A metal or ceramic material should be selected which is known to be metallurgically stable, on the basis of past data.

- (2) A symmetrical configuration should be used wherever possible relative to the critical axes. Mechanical loading and thermal symmetry should also be provided.
- (3) Machining, chemical etching, and heat-treatment techniques should be chosen to minimize residual stresses. The sequence of heat-treatment operations should be one which has proven in the past to provide good dimensional stability for the chosen material. Fabrication by forging should be avoided.
- (4) Operating stresses in all critical elements of the clamp should be kept below 50% of the MYS.
- (5) The fabrication process should include a number of cycles of the expected thermal operating history before the final finishing operations in order to "shake out" dimensional changes due to thermal cycling.

Interface Considerations

Phenomena occurring at the various contacting interfaces in the clamping system can have a critical effect in determining the alignment capability of the system. In summary, the major conclusions which have been drawn from studies of these phenomena are as follows:

- (a) Although adhesive wear does not appear to be sufficient to cause significant misalignment provided soft materials are not used, the formation of relatively large wear particles may be critical for a sliding type of fixed clamp. This will likely require the use of special combinations of surface materials or film lubrication during installation.
- (b) If fluid films are present on the locating surfaces of a fixed clamp, either unavoidably or intentionally to provide lubrication or thermal conductance, the film will likely have ample time to relax between installation and operation. However, after installation, it is advisable to wait several minutes before proceeding with verification of alignment if required.
- (c) Excessive misalignment of a fixed clamp can be caused by soft particles of the order of 100 microns in diameter and larger, and by hard particles of the order of 5 microns and larger. The critical hard particles are small enough so that they can lodge in the peaks of the surface roughness to cause excessive misalignment under clamping load.
- (d) Although, particles in the above size ranges may be largely excluded for the clean-room assembly of an adjustable clamp,

it is not practical to eliminate them for the field assembly of fixed clamps. Two means for overcoming their misaligning effects seem promising at this time:

1. the assembly of the clamp interfaces with a light wiping or sliding motion to sweep any particles present on the peaks of the surface roughness into the valleys.
 2. the use of a vacuum-deposited, dirt-absorbent coating on the interface.
- (e) Thermal contact resistance in a vacuum has been found to vary by an order of magnitude for similar tests, while a 10% variation from one locating pad to another appears critical from an alignment point of view. Although various steps may be taken to minimize such variation, the only reliable one appears to be the removal of the contact points from the main heat flow path between the sensor and the mounting block. This may be done by providing a fluid film at the interface or by the use of a separate thermal shunt path for heat flow.

Preliminary Design of the Fixed Clamp

Of the various locating geometries considered, the plane-on-plane, the cylinder-in-hole and the cylinder-in-V-block geometries were found to be feasible from the standpoint of maintaining axis alignment under the influence of the operating loads with their expected asymmetries. The cylinder in V-block offered no advantages over the other concepts but required three extremely precise surfaces instead of two. Thus, it was dropped from further consideration.

The cylinder-in-hole class of clamps has two major disadvantages in comparison with the plane-on-plane concepts:

- (a) A survey of the state-of-the-art in precision machining indicates that the degree of accuracy to which the hole can initially be produced relative to the reference axis is of the order of 2 to 4 times less than that of a plane. Thus, a large portion of the error budget for the system would be used up by machining error.
- (b) Clamping, although feasible with a thermal shrink fit or hydraulic loading, is inherently more complex than the simple spring-loaded retainer possible with the plane-on-plane clamp. Moreover, clamping the cylinder requires precision machining of more than the mating surfaces, e.g., the outside of the shrunk shell. Finally, shrink fits introduce installation difficulty.

The major offsetting advantage for the cylinder-in-hole clamp is its relative insensitivity to misalignment due to thermal effects in a vacuum. These effects, which are mainly due to thermal contact resistance variations, can be mitigated in the plane-on-plane concepts by the use of a fluid film at the interfaces or some form of thermal shunt path. This, of course, introduces a sealing problem for vacuum operation, while it is likely that the cylinder-in-hole concept would not require such a measure.

The most promising methods for dealing with the dirt problem are to use a light wiping action during installation or to deposit a thin dirt-absorbent coating on the locating surfaces. Although these methods are possible in principle with either class of concepts, practical difficulties arise with the cylinder-in-hole clamps. The most promising method for providing the requisite interference for the cylinder-in-hole clamp is a thermal shrink fit. This results in a limited thermal transient time, during which the interference force is building up between the members. For effective wiping action, the installation process would require careful timing in order to wipe with the desired light loading and not damage the surfaces as the loading increased.

To achieve the necessary control of coating thickness, the dirt-absorbent coating must be vacuum deposited on the locating surfaces. The plane locating surface is likely to be more favorable for achieving accurate thickness control with this process than the cylindrical surface.

Thus, on balance, it is concluded that the most promising fixed-clamp geometry is the plane-on-plane class of concepts. The plane locating surfaces should be formed by a continuous plane or by discrete flat mounting pads, rather than by three-point geometry, such as spherical contacts.

Promising methods for supplying the clamping force include the spring-regulated force from a cap screw, bayonet-type retainer, or a cam surface, all using Belleville washer springs.

Preliminary Design of the Adjustable Clamp

Of the various adjustable clamp concepts generated during this study, the Tripod Support and Adjustment class was selected as the most promising for further development. This provides the simplest means of support and adjustment at one plane between the sensor and interface piece.

Within this class, the most promising means of adjustment for each of three different types was selected. These types of adjustment are:

- (a) Column Compression concept
- (b) Selected Fit concept
- (c) Transverse Wedge concept

Each of these concepts requires a spherical seat to avoid the effects of angular offset within the range of adjustment. Each requires a varying mixture of coarse and fine adjustment to span the 25 arc-min range with resolution to 1 arc-sec. The above types of adjustment are listed in order of increasing range of fine adjustment, and corresponding decreasing numbers of required gage block spacer elements for coarse adjustment.

The means of verification used in the laboratory must be capable of resolving alignment of the axis to within 1 arc-sec. The readout, however, must also be accurate enough to make proper selection of gage elements. The Selected Fit concept is the most stringent in this respect, requiring readout accuracy of the order of 1.5 arc-secs. This is followed by the Column Compression concept with readout to 5 arc-secs and the Transverse Wedge with 37 arc-secs.

It is concluded that these three give the best range of adjustable clamp concepts for further development, providing a wide range of basic characteristics for subsequent experimental evaluation.

Configurational Design

A brief study was devoted to identifying methods by which proper choice of the overall system configuration might optimize performance.

The provision of maximum configurational symmetry was identified as the most important factor in order to minimize or eliminate the misaligning effects of mechanical and thermal loads. The rules for optimum configurational symmetry were found to be:

- (a) Maintain axi-symmetry about both input and output axes for all elements except the sensor.
- (b) Place the center of mass of the sensor assembly in the plane of the sensor mounting flange.
- (c) Maintain the sensor axi-symmetric about the output axis, including all of its heat sources.

Mechanical symmetry about the transverse plane containing the center of mass can eliminate misalignment due to lateral inertial forces. The limit to which this can be carried is making the adjustment and fixed clamp planes co-planar with this transverse plane.

All of these optimizing configurations carry the price of a larger, more complex structure. Although the decision between increased complexity versus improved performance must be made during the design process, it is felt that it should be postponed until after the initial experimental stages of development. This type of optimization is not critical to the basic operation of the clamp system, and the simplest embodiment of each concept should be tested in the next phase to determine its basic performance capabilities.

RECOMMENDATIONS

Based upon the results of the studies to date, it is recommended that the two most promising fixed clamp concepts and the three adjustable clamp concepts be implemented with test prototype hardware, and tested to determine their basic performance capabilities.

This program would require initial design tasks to translate the various clamp concepts into specific detailed test prototype designs. These prototype designs should then be fabricated for testing.

The test program should be designed to determine the degree to which the clamps meet the design goals which are summarized in Appendix J. Specific tests should be made to:

- (a) determine the accuracy to which the adjustable clamps can prealign a sensor.
- (b) determine the repeatability of alignment possible for a number of installation and removal cycles with the fixed clamp concepts.
- (c) establish the sensitivity of the clamps to shock, vibrational, and steady inertial loading.
- (d) determine the misaligning influences of thermal cycling and induced temperature gradients.
- (e) measure the operating characteristics in a vacuum consistent with the ultimate application.
- (f) test the stability of the clamp over a long period of time under constant conditions.

REFERENCES

1. Holden, F. C., A Review of Dimensional Instability in Metals, Defense Metals Information Center, Battelle Memorial Institute, Columbus, Ohio DMIC Memorandum 189, March, 1964
2. Maringer, R. E., A Review of Dimensional Instability in Metals, Defense Metals Information Center, Battelle Memorial Institute, Columbus, Ohio DMIC Memorandum 213, June 23, 1966
3. Maringer, R. E., et al, Stability of Structural Materials for Spacecraft Application, First Topical Report submitted to Goddard Space Flight Center, Greenbelt, Maryland, Battelle Memorial Institute, Ohio, December, 1966
4. Maringer, R. E., et al, Stability of Structural Materials for Spacecraft Application, Second Topical Report submitted to Goddard Space Flight Center, September, 1967
5. Maringer, R. E., et al, Stability of Structural Materials for Spacecraft Application, Third Topical Report submitted to Goddard Space Flight Center, November, 1967
6. Maringer, R. E. et al, Study of Microplastic Properties and Dimensional Stability of Materials, Technical Report AFML-TR-67-232, May 1967, submitted to Air Force Materials Laboratory, Wright-Patterson Air Force Base, Ohio
7. Weihrauch, P. F., and Hordon, M. J., The Dimensional Stability of Selected Alloy Systems, Alloyd General Corporation, Cambridge, Mass. Final Report August, 1964 Prepared under Contract No. N140(131)-75098B
8. Meyerson, R. M. et al, "Gage Blocks of Superior Stability III: The Attainment of Ultrastability", ASM Transactions Quarterly, Vol: 57, No. 1 March, 1964
9. Lement, B. S. and Averbach, B. L., Measurement and Control of the Dimensional Behavior of Metals, Report R-95, Massachusetts Institute of Technology, December, 1955
10. Mikus, E. B., Hughel, T. J., Gerty, J. M. and Knudsen, A. C., "The Dimensional Stability of a Precision Ball Bearing Material", Trans ASM, Vol. 52, p 307-315 (1960)
11. Jennings, C. G., Shankman, A. D. and Colteryahn, L. E., "Processing and Testing Guidance System Material for Maximum Dimensional Stability", paper presented at Western Metals Congress, Los Angeles, California, February 22-25, 1965

12. Hughel, T. J., An Investigation of the Precision Mechanical Properties of Several Types of Beryllium, General Motors Research Staff Report MR-120 (April 3, 1960)
13. Rockower, B. and Hall, E., Investigation of Physical Properties of Beryllium Oxide as a Material for Integrating Gyros, Massachusetts Institute of Technology, Instrumentation Laboratory, Report No. R-560, September, 1966
14. Bonfield, W., Sartell, J. A., and Li, C. H., "The Effect of Surface Condition on the Microstrain of Beryllium", Trans AIME, Vol. 227 p 669-673, 1963
15. Jennings, C. G., Maslow, C., Colteryahn, L. E., Precision Mechanical Properties of Some Ceramics, Metallurgical Laboratory Report No. TR-63-527, Autonetics, Inc., California, November, 1963
16. Gross, A. G., Jr., Metallurgical Evaluation of Beryllium Gyro Components Manufactured by Various Processes, Autonetics, California, Project Report No. PR-63-103, November, 1963
17. Maringer, R. E., et al, Study of Microplastic Properties and Dimensional Stability of Materials, Fifth Quarterly Progress Report to Air Force Systems Command, Wright-Patterson Air Force Base, Ohio, December 15, 1967
18. Rabinowicz, E., Friction and Wear of Materials, John Wiley and Sons, New York, N. Y., 1965
19. Gross, A. G., Jr., Gas Film Lubrication, John Wiley and Sons, New York, N. Y., 1962
20. Hill, R., The Mathematical Theory of Plasticity, Oxford University Press, London, 1950
21. McClintock, F. A., and Argon, A., Mechanical Behavior of Materials, Addison-Wesley Publishing Company, Reading, Massachusetts, 1966
22. Bloom, M. F., Thermal Contact Conductance in a Vacuum Environment, Douglas Report SM47700, NASA CR-75148, 1964
23. Clausing, A. M., An Experimental and Theoretical Investigation of the Thermal Contact Resistance, University of Illinois, Final Report for NASA Contract Ns G 242, 1966
24. Blum, H. A., Heat Transfer Across Surfaces in Contact: Practical Effects of Transient Temperature and Pressure Environments, NASA Report Numbers CR 69696 and CR 76878, 1965 - 1966
25. Clausing, A. M., Some Influences of Macroscopic Construction on the Thermal Contact Resistance, NASA Report Number CR 74622, 1965

26. Proceedings of the Conference on Thermal Joint Conductance, NASA Report No. TMX-56300 (N37806-37810), Washington, D. C., February 19, 1964
27. Mikic, B. B., and Rohsenow, W. M., Thermal Contact Resistance, NASA Report Number CR 78319, 1966
28. Muskhelishvili, Some Basic Problems of the Mathematical Theory of Elasticity, P. Noordhoff Ltd., Groningen, Holland, 1953
29. Timoshenko, S., Theory of Elasticity, (2nd Edition), McGraw-Hill Book Company, New York, N. Y., 1951
30. Shaw and Macks, Analysis and Lubrication of Bearings, McGraw-Hill Book Company, New York, N. Y., 1949
31. DenHartog, J. P., Strength of Materials, McGraw-Hill Book Company, Inc., New York, N. Y., 1949
32. Schneider, P., Thermal Response Charts, J. Wiley and Sons, Inc., New York, N. Y., 1963
33. Timoshenko, S., Strength of Materials, Part II, (2nd Edition), D. Van Nostrand Company, Inc., New York, N. Y., 1941
34. Den Hartog, J. P., Advanced Strength of Materials, McGraw-Hill Book Company, New York, N. Y., 1952
35. Marks, L. S., Mechanical Engineers Handbook, McGraw-Hill Book Company, New York, N. Y., 1941
36. Instrument Specialties Company, Catalog 13-B Precision Springs, Little Falls, New Jersey
37. Wallace Barnes Company, Catalog of Belleville Spring Washers, Bristol, Connecticut

APPENDIX A

FEASIBILITY OF A DIRT-ABSORBENT COATING ON

THE FIXED CLAMP INTERFACE

Introduction

A number of fixed clamp concepts have been proposed as a means of establishing and maintaining the input axes of a set of strapdown gyros. Most of these concepts involve maintaining two planes parallel to each other by keeping them in contact with clamping forces. It is expected that the inevitable presence of foreign particles between the two surfaces will cause a deviation of the relative orientation of the surfaces from the desired parallelism. One concept that has been proposed to minimize this misalignment due to trapped foreign particles is to use a thin coating on one of the mating surfaces that will absorb the foreign particles without allowing misalignment of the planes. It is necessary for the coating to be stiff enough not to deflect significantly due to unbalanced clamping forces and acceleration forces. It is also important that the coating either have a dimensional stability that is comparable to that of the gyro fixture and mounting block, or that it be sufficiently thin so that its stability is not important.

The object of this study is to determine the feasibility of the thin coating concept. In particular, the tradeoff between the ability of the coating to absorb particles without creating a misalignment and the ability of the coating to resist angular distortion has been investigated.

Description of the Problem and its Idealization

The geometry and applied loads of the system to be analyzed are shown in Figure A-1. The two parallel mating planes are the contact surfaces of a gyro fixture block and a mounting block. The clamping force holding the fixture block in contact with the mounting block is temporarily assumed to be a uniform pressure loading. An absorbent coating is placed on the contact surface of the fixture block. Random sized dirt particles are assumed to be trapped between the two surfaces. It is desired to determine what clamping loads are required to absorb the dirt particles without causing plastic deformation of the other parts of the system.

In order to idealize the problem, the following assumptions are made:

(1) $E_3, E_1 \gg E_2$

$Y_3, Y_1 \gg Y_2$

(E is the elastic modulus)

(Y is the yielding stress)

(2) Elastic distortions are negligibly small compared with plastic deformations.

(3) The dirt particles are much harder than the soft coating.

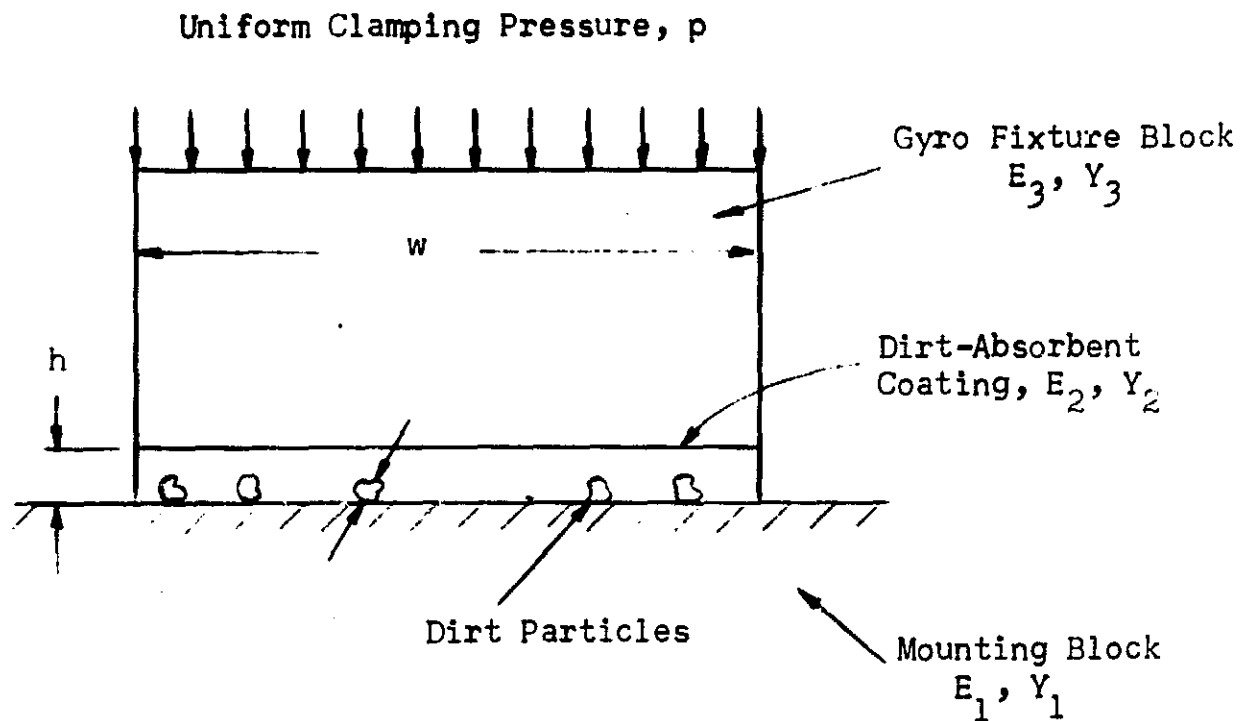


Figure A-1. Geometry for the Analysis of a Dirt-Absorbent Coating

In order for the concept to be useful, the following design criteria must be satisfied:

- (1) The clamping load should be large enough to absorb all of the foreign particles but not so large as to cause yielding of the gyro fixture, mounting block, and parts of the coating that do not absorb dirt.
- (2) The thickness of the soft film has to be large enough to absorb all of the particles when the clamping load is applied.

Determination of the Allowable Limits of the Clamping Load

According to the first design criterion of the previous section, the clamping load must be within the following limits:

$$\sum_{i=1}^N L_d(i) < L_g < [L_f, (Y_1, 3 A)] \quad (A-1)$$

where L_g = clamping load applied to the gyro fixture block
 $L_d(i)$ = the load to completely indent the i th dirt particle into the soft coating

N = number of dirt particles

L_f = yielding load of the soft coating

Equation (A-1) can also be expressed in terms of pressure by dividing by the nominal contact area, A so that

$$\frac{1}{A} \int_{A_d} \bar{p}_d(i) dA_d < \bar{p}_g < [\bar{p}_f, Y_1, Y_3] \quad (A-2)$$

where A = nominal contact area

A_d = projected area of the dirt

\bar{p}_d = average pressure necessary to be exerted by the dirt in order to become completely embedded in the coating

\bar{p}_g = L_g/A

\bar{p}_f = L_f/A

Thus, if the clamping load satisfies Equation (A-2), all of the particles will be absorbed into the coating without plastically deforming it.

Calculation of the Coating Yielding Point Load

The problem of determining \bar{p}_f , the load necessary to cause plastic yielding of a material sandwiched between two slabs, has been treated in the literature and several different results for \bar{p}_f are listed below:

$$\frac{\bar{p}_f}{2K} = 3/4 + \frac{w}{4h} \quad (\text{Reference (20) assuming rough contacting surfaces}) \quad (A-3a)$$

$$\frac{\bar{p}_f}{2K} = 1 + \frac{\mu w}{2h} \quad (\text{Reference (20) assuming friction coefficient, } \mu) \quad (A-3b)$$

$$\frac{\bar{p}_f}{2K} = 1 + \frac{w}{4h} \quad (\text{Reference (21) using a limit load analysis}) \quad (A-3c)$$

where $2K = Y$ for the Tresca yield criterion

$2K = \frac{2}{\sqrt{3}} Y$ for the Von Mises yield criterion

The above results are compared in Figure 10.19 of Reference (21). For the present analysis, Equation (A-3c) is suitable. Therefore, \bar{p}_f , the yielding point load of the soft coating is given by

$$p_f \cong \frac{2}{\sqrt{3}} Y_2 \left(1 + \frac{w}{4h} \right) \quad (A-4)$$

The Load Required for Indentation of a Dirt Particle into the Cavity

The load, \bar{p}_d , required to cause local yielding of the coating so that it absorbs the particles will now be calculated. The geometry is shown in Figure A-2. If the coating material does not strain harden, an estimate for \bar{p}_d can be obtained from the Prandtl solution of a blunt knife edge being pressed into a plane of infinite thickness. From Equation (13.18) of Reference (21)

$$\bar{p}_d \cong 3 Y_2$$

where Y_2 is the uniaxial yield stress of the infinitely thick plane material which in the present case is taken to be the coating. The effect of the finite thickness of the coating is discussed in the next section.

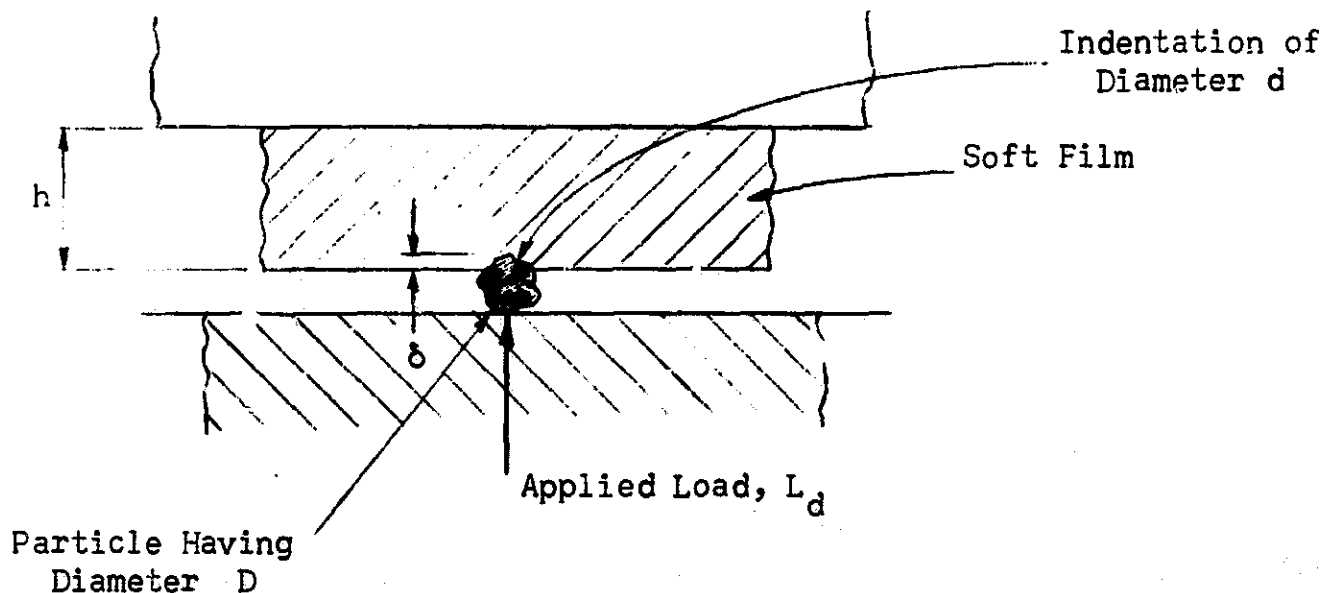


Figure A-2. Indentation of a Particle into the Coating

For a linearly strain-hardening material, Equation (13.25) of Reference (21) gives the following relationship between Brinell hardness, B and the uniaxial flow stress

$$B = 3.2 (\text{uniaxial flow stress}) \text{ at } \epsilon = 0.2 \frac{d}{D} \quad (\text{A-5})$$

where d = diameter of indentation

D = diameter of indenter

Since by definition, \bar{p}_d is identical to B evaluated at $d = D$, \bar{p}_d is as follows

$$\bar{p}_d = 3.2 (Y_2)_{\epsilon=0.2}$$

where $(Y_2)_{\epsilon=0.2}$ is the uniaxial flow stress evaluated at $\epsilon = 0.2$

Thus, for design purposes, it can be approximated that

$$\bar{p}_d \approx 3 (Y_2)_{0.2} \quad (\text{A-6})$$

It should be noticed that the \bar{p}_d values are independent of the size of the particle. The overall load to absorb all of the particles is given by

$$L_d = \int_{A_d} \bar{p}_d dA_d = 3(Y_2)_{0.2} A_d \quad (\text{A-7})$$

where A_d is the projected area of the particles

Thickness of the Coating

The thickness of the coating affects the yielding point load exerted by the dirt particles. This effect is treated in Reference (20) where the geometry shown in Figure A-3 is analyzed.

If there is no friction, as h/d is decreased from a large value down to one half, the indentation pressure decreases approximately by a factor of two. However, friction produces a constraint which will tend to offset this decrease in indentation pressure. Therefore the indentation pressure previously calculated for an infinitely thick plane can be used as a design criterion.

In order to prevent a particle from being able to touch both the mounting block and the fixture block, the coating thickness must be made larger than the maximum expected particle dimension. It is undesirable to make the coating too thick or else the rigidity of the structure will be decreased.

Therefore it is necessary to make a compromise that is based upon the reliability of the information on expected particle sizes.

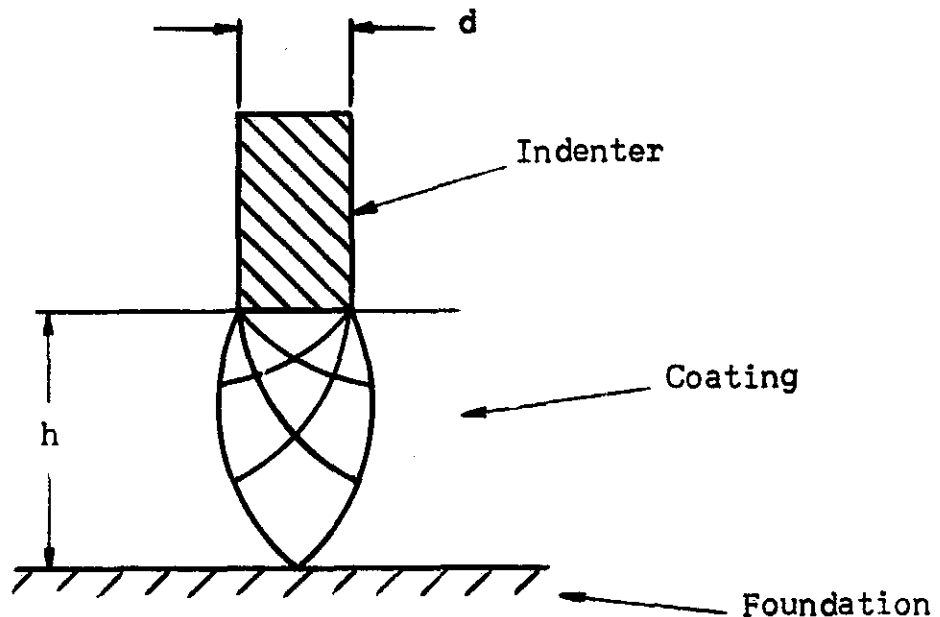


Figure A-3. Indentation into a Medium of Finite Thickness

Evaluation of Clamping Load Limits

The final equations are obtained by substituting Equations (A-4) and (A-7) into Equation (A-2). The clamping load limits finally become

$$3(Y_2)_{0.2} \gamma_A < \bar{p}_g < \left[\frac{2}{\sqrt{3}} Y_2 \left(1 + \frac{w}{4h} \right), Y_1, Y_3 \right] \quad (A-8)$$

where $\gamma_A = \frac{A_d}{A}$

Angular Misalignment Due to Nonuniform Distortion of the Thin Coating

In order to conservatively estimate the effective angular stiffness of the thin coating, the geometry shown in Figure A-4 has been analyzed. A thin coating having thickness, h , is placed between mounting pads on the rigid gyro fixture block, which is held to the rigid mounting block by clamping forces, F_{C_1} and F_{C_2} . For simplicity, it will be assumed that the load is

less than the coating yielding load and that embedded particles do not significantly influence the coating deformation. The vertical deflections of pads 1 and 2 are given by the following relationships:

$$\delta h_1 = \frac{F_1 h}{aE} \quad (A-9)$$

$$\delta h_2 = \frac{F_2 h}{aE}$$

where F_1 and F_2 are the vertical loads supported by pads 1 and 2

The resulting angular misalignment can be calculated as follows:

$$\delta h_1 - \delta h_2 \equiv \Delta \delta h = \frac{(F_1 - F_2) h}{aE} \quad (A-10)$$

$$\Delta \theta = \frac{\Delta \delta h}{2l} = \frac{(F_1 - F_2) h}{aE} \frac{1}{2l} \quad (A-11)$$

If the load unbalance is assumed to be due to lateral acceleration, shown in Figure A-4, the unbalance between F_1 and F_2 is equal to

$$(F_1 - F_2) = (F_{C_1} - F_{C_2}) + \frac{F_a t}{2l} \quad (A-12)$$

where $F_a = \text{acceleration force} = M \ddot{x}$

Numerical Evaluation

In order to help determine whether the soft coating concept is feasible, the following typical application is evaluated numerically. It is assumed that the gyro fixture and the mounting block are made of stainless steel, and the coating is made of lead. Thus,

$$Y_1 = Y_3 \approx 40 \times 10^3 \text{ psi}$$

$$Y_2 = 1.6 \times 10^3 \text{ psi}$$

$$E_2 = 2 \times 10^6 \text{ psi}$$

The width of the fixture block will be taken as one inch. The following parameter values for the dirt will be assumed:

$$\gamma_A = A_d/A = 1/3$$

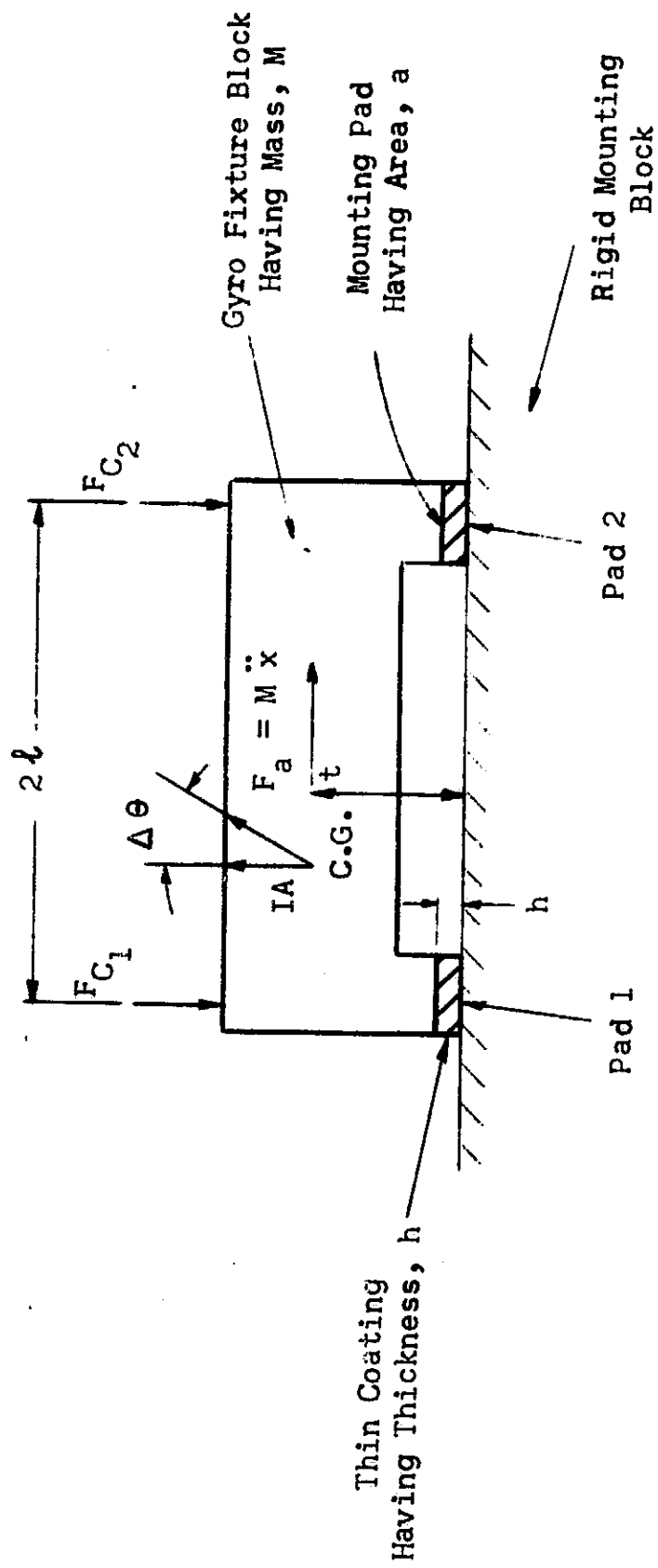


Figure A-4. Simplified Analysis of Thin Coating Deflection in the Presence of Nonuniform Clamping Forces and Accelerations

$$d_{\max} = 0.5 \times 10^{-3} \text{ in}$$

and the thickness of the coating, h , is taken to be 10^{-3} inches.

From Equation (A-6),

$$\bar{p}_d = 3 \gamma_A (\gamma_2)_{0.2} = (3) \times (1/3) \times (1.6 \times 10^3) = 1.6 \times 10^3 \text{ psi}$$

From Equation (A-4),

$$\bar{p}_f = \frac{2}{\sqrt{3}} 1.6 \times 10^3 \left(1 + \frac{1}{4 \times 10^{-3}} \right) = 0.46 \times 10^6 \text{ psi}$$

Substituting the above values into Equation (A-8), the clamping load is limited to the following range

$$1.6 \times 10^3 \text{ psi} < \bar{p}_g < 40 \times 10^3 \text{ psi}$$

It can be seen that there should be little difficulty in keeping the clamping force within allowable limits. In order to estimate possible misalignments due to nonuniform deformation of the coating, the following numerical values have been assumed:

$$t = 1 \text{ inch}$$

$$l = 1 \text{ inch}$$

$$a = 1 \text{ in}^2$$

$$F_{C_1} - F_{C_2} = 100 \text{ lbs}$$

$$M = \frac{2 \text{ lb}}{g}$$

$$F_a = 100 \text{ lbs}$$

$$F_{C_1} = 300 \text{ lbs (so that the coating does not yield)}$$

From Equations (A-11) and (A-12), the angular deformation of the coating for the above situation is

$$\Delta\theta = \frac{(150 \text{ lb}) 10^{-3} \text{ in}}{1 \text{ in}^2 \cdot 2 \times 10^6 \frac{\text{lb}}{\text{in}^2} \cdot 2 \text{ in}} \approx 0.04 \mu\text{in/in}$$

Thus, the small thickness of the coating compensates for its lower elastic modulus so that the overall angular stiffness of the clamp is not significantly reduced.

APPENDIX B

FIXED CLAMP CONCEPTS

As a result of the concept generation studies, several fixed clamp concepts were identified. As defined in the main body of this report, these concepts included clamps with no verification as well as clamps embodying methods of quasi-verification.

In this appendix several fixed clamp concepts using the basic plane-on-plane and cylinder-in-hole locating geometries are described for the interested reader.

Clamps Without Verification

Clamps utilizing plane-on-plane geometry. - Conceptually, the simplest way to establish the orientation of the input axis is to make it perpendicular to a plane on the sensor element. Prior to the installation, the sensor would be adjusted in a fixture so that its input axis is perpendicular to the interface surface of the fixture. This surface would then be clamped to the surface of the IMU block. If the two surfaces were kept exactly parallel to each other, then the input axis would be perpendicular to the surface of the IMU block. The most straightforward arrangement of sensors would be to have three such sensor fixtures clamped to three mutually perpendicular faces of an ultraprecise cube. The major sources of misalignment in such an arrangement would probably be nonuniform clamping forces, uneven temperature distribution, and foreign particles trapped between the sensor fixture and the cube.

As discussed under "Interface Considerations" in the main body of this report, it may be possible to solve the dirt problem by wringing the sensor fixture to the cube in the same manner as a machinist wrings gage blocks together. Gage blocks can be wrung together with a repeatability in their combined length of several microinches without using a clean room. Moreover, this combined length does not change more than 1 or 2 μ in over long periods of time, i.e., the "film" thickness does not change drastically. If particles do get trapped between the two surfaces, then they cannot be wrung together. Thus it appears that a good wringing technique eliminates the particles that might cause misalignment.

Another method for solving the dirt problem is to apply to one of the mating surfaces a coating that is soft enough to absorb the particles; stiff enough not to deform and destroy the alignment; thick enough to absorb the largest particle likely to be encountered; and thin enough so that asymmetries in its dimensional stability will not significantly affect the overall alignment. The two surfaces would have to be held together by a symmetrical arrangement of forces which did not cause misalignment. This method is described under "Interface Considerations" and analyzed in Appendix A of this report.

If the two parallel surfaces touch only at point contacts, and there are voids where foreign particles can lodge, then dirt effects can be minimized.

An example of this technique is the use of precision balls as shown in Figure B-1. If a large number of balls is used, then the load will be distributed to minimize creep and other deformations.

An alternative might be to prepare the surfaces independently by etching or scraping in order to create "hills and valleys" to accommodate foreign particles.

Any of the clamping forces listed in Table XV could be used to hold the two planes parallel to each other. Figure B-2 shows a possible configuration using hydraulic pressure that is especially well suited to produce a uniform clamping load. A fixed deflection is applied to the bellows which causes a known pressure to be applied. The flexible membrane prevents any vertical bellows force from being transferred to the sensor.

If a symmetrical arrangement of bolts is used to hold the sensor to the IMU, uniformity of the applied force can be obtained by use of the spacer technique that is shown in Figure B-3. The spacer ensures that the spring is deflected a fixed amount, thereby causing a fixed force to be applied to the sensor. Alternatives to the coil spring are a Belleville washer or a hydraulic spring consisting of a sealed, slightly-flexible compressed volume of oil. Other possible sources of uniformly distributed forces are precision wedges and permanent magnets.

Dowel potting can also be used to hold the sensor fixture to the mounting block as shown in Figure B-4. The fixture can be removed by applying solvent to holes that are left in the "dowels" when they cure. The alignment is determined by mating surfaces that are not in contact with the potting compound. Hence dimensional stability and material uniformity requirements of the potting compound are not critical except insofar as they cause asymmetry of the clamping load.

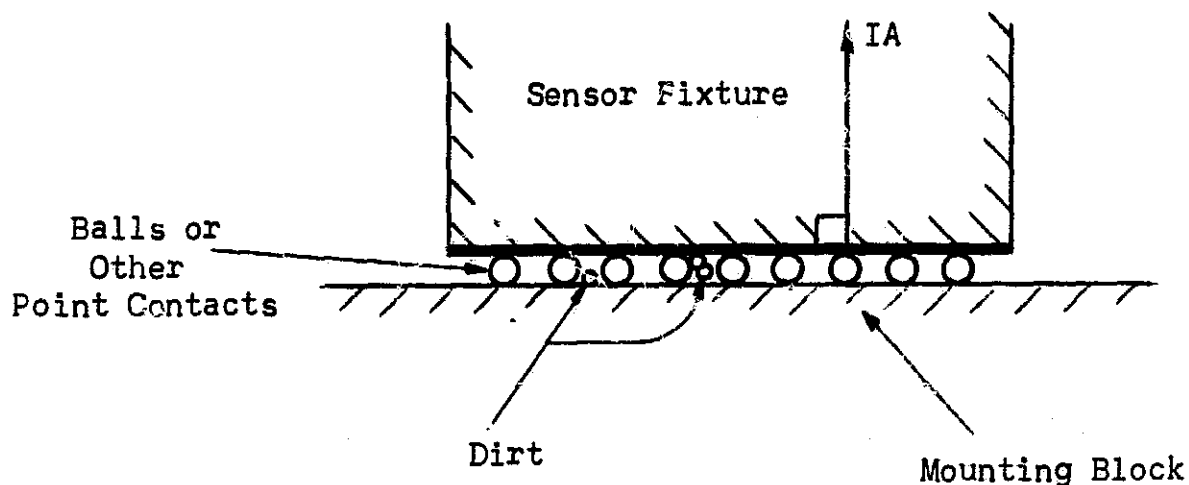


Figure B-1. Series of Point Contacts Maintaining Alignment in the Presence of Dirt

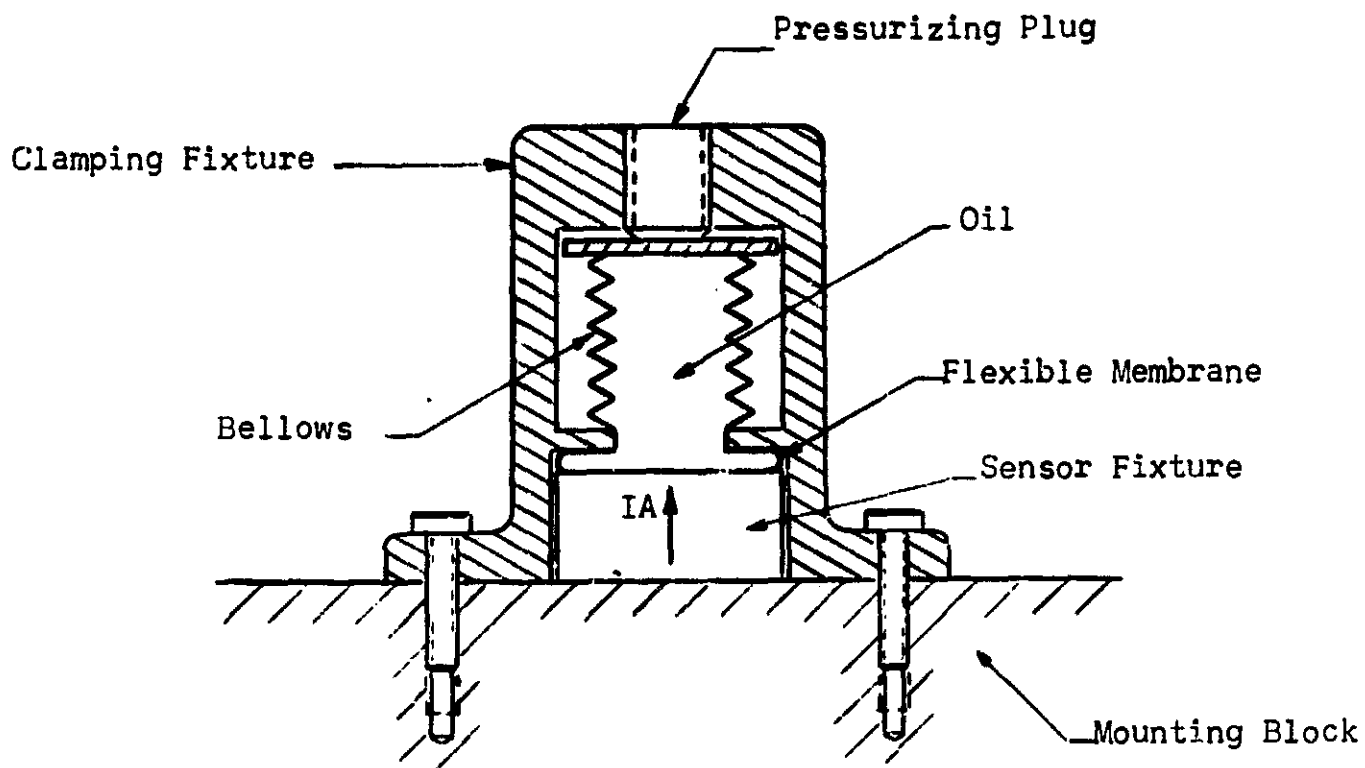


Figure B-2. Clamping the Sensor with Hydraulic Pressure

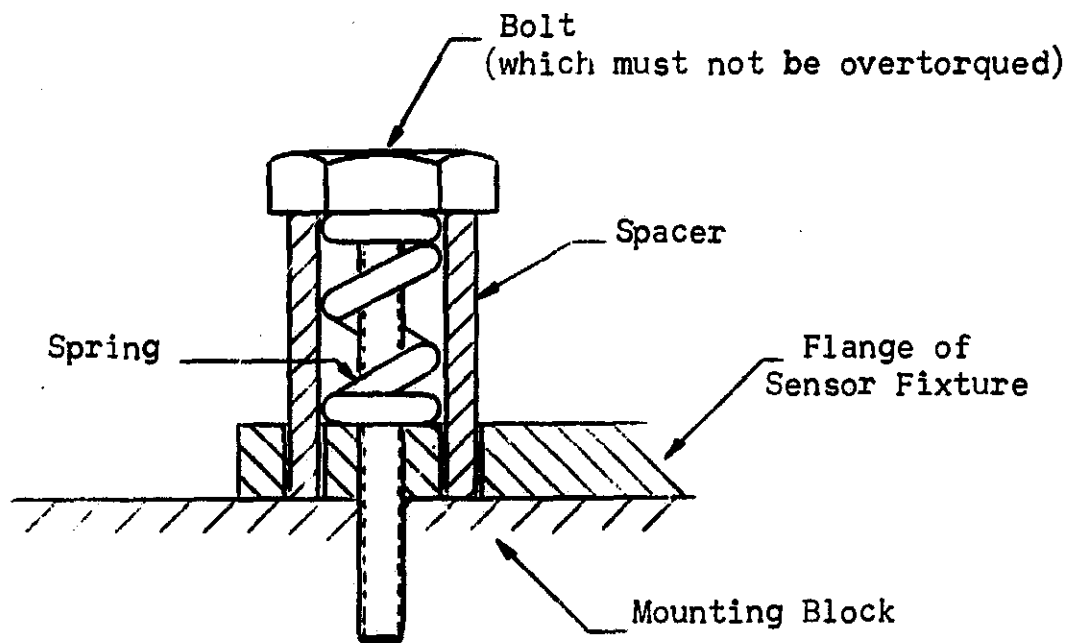


Figure B-3. Controlled Force Clamp

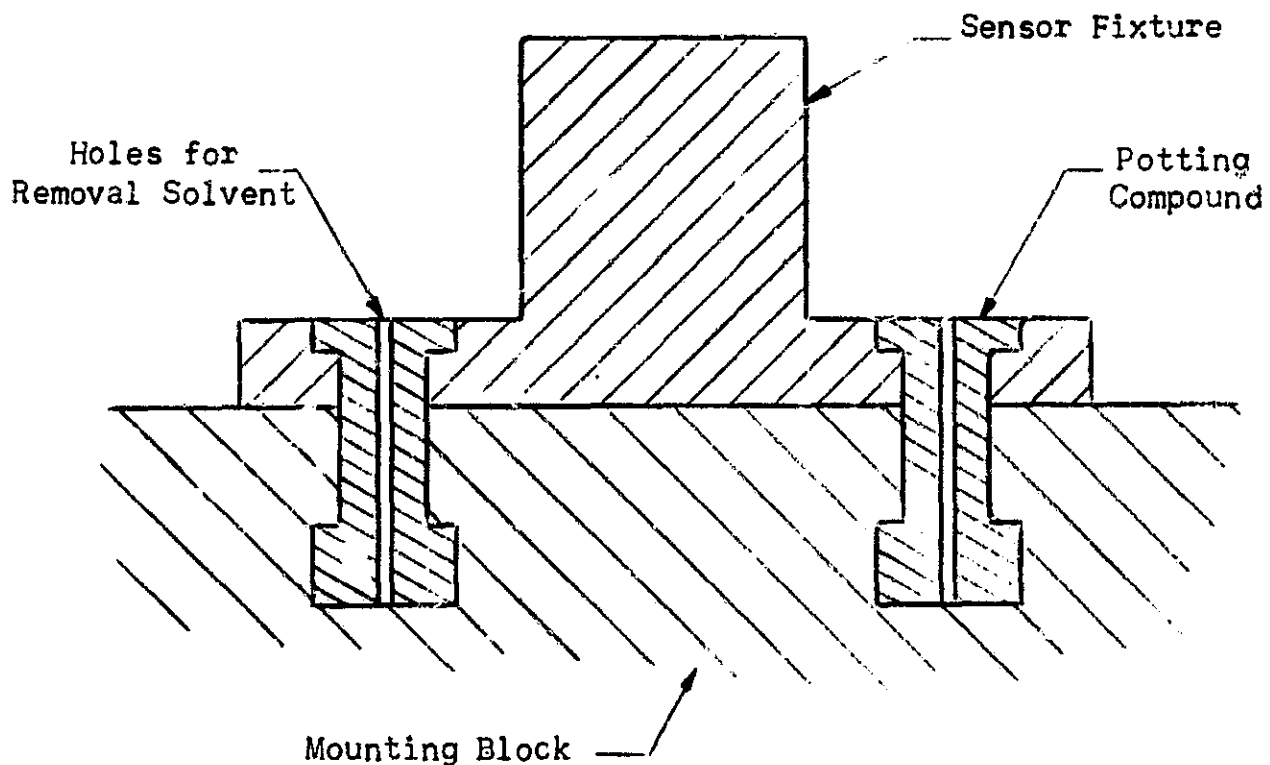


Figure B-4. Clamping the Sensor Fixture Using Dowel Potting Techniques

Clamps utilizing the cylinder-in-hole geometry. - The second major method for establishing the alignment of the sensor utilizes the cylinder-in-hole locating geometry. The input axis is made parallel to the axis of a cylindrical sensor fixture which is then inserted into a hole whose centerline is parallel to the reference axis.

Two conflicting requirements with this type of clamp are:

- (1) the need to insert and remove the sensor from the hole; and
- (2) the need to have no clearance between the sensor fixture and the hole.

One way to achieve this is to use heating elements in the mounting block to cause thermal expansion of the hole when a sensor is to be removed or inserted. At the normal operating temperature of the sensor, an interference fit would exist between the hole and the cylinder. The sensor and the hole walls could have different coefficients of thermal expansion to facilitate removal of the sensor fixture when heat is applied. (An alternative would be for the sensor fixture to have a cooling jacket which would be activated when it is to be removed.) The danger of plastic deformation of the sensor fixture and hole wall would be minimized by carefully controlling the interference fit and the

amount of heat that is applied. It might be preferable to have the hole with peripheral heaters in a fixture that is attached to a cube rather than put these elements in the cube itself. The dirt problem could be minimized by using a fluted hole together with a clean lubricant as shown in Figure B-5. The lubricant and dirt would tend to flow into the space provided by the flutes. Applying a soft coating to the sensor fixture surface would also help in this respect.

A different method for varying the clearance between the cylinder and the hole walls would be to use hydraulic pressure to cause elastic deformation of the mounting block hole. A typical configuration is shown in Figure B-6. This technique would require that the deformable walls have a very uniform thickness around the periphery.

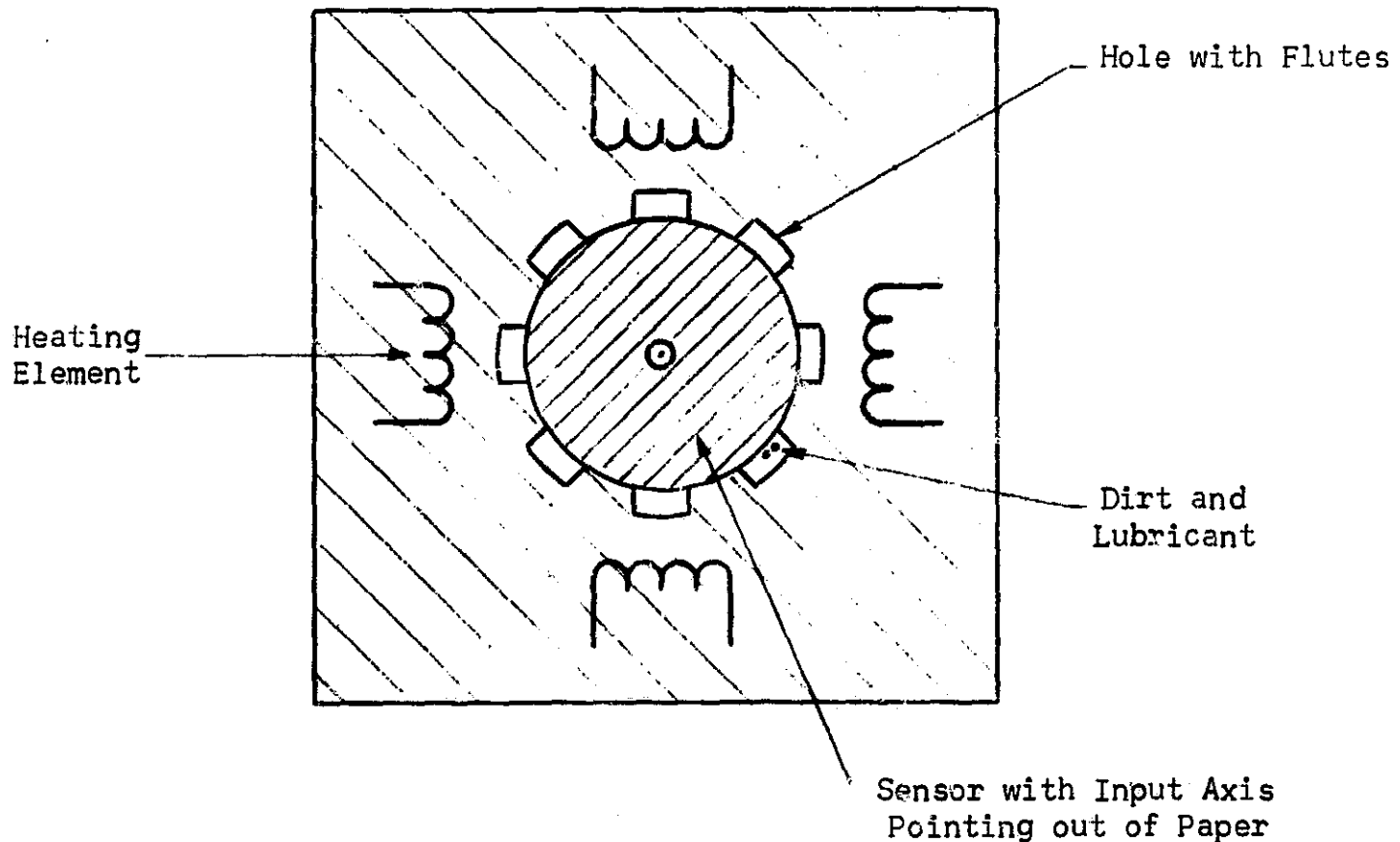


Figure B-5. Cylinder Placed in Fluted Hole
(Looking Down onto Mounting Block)

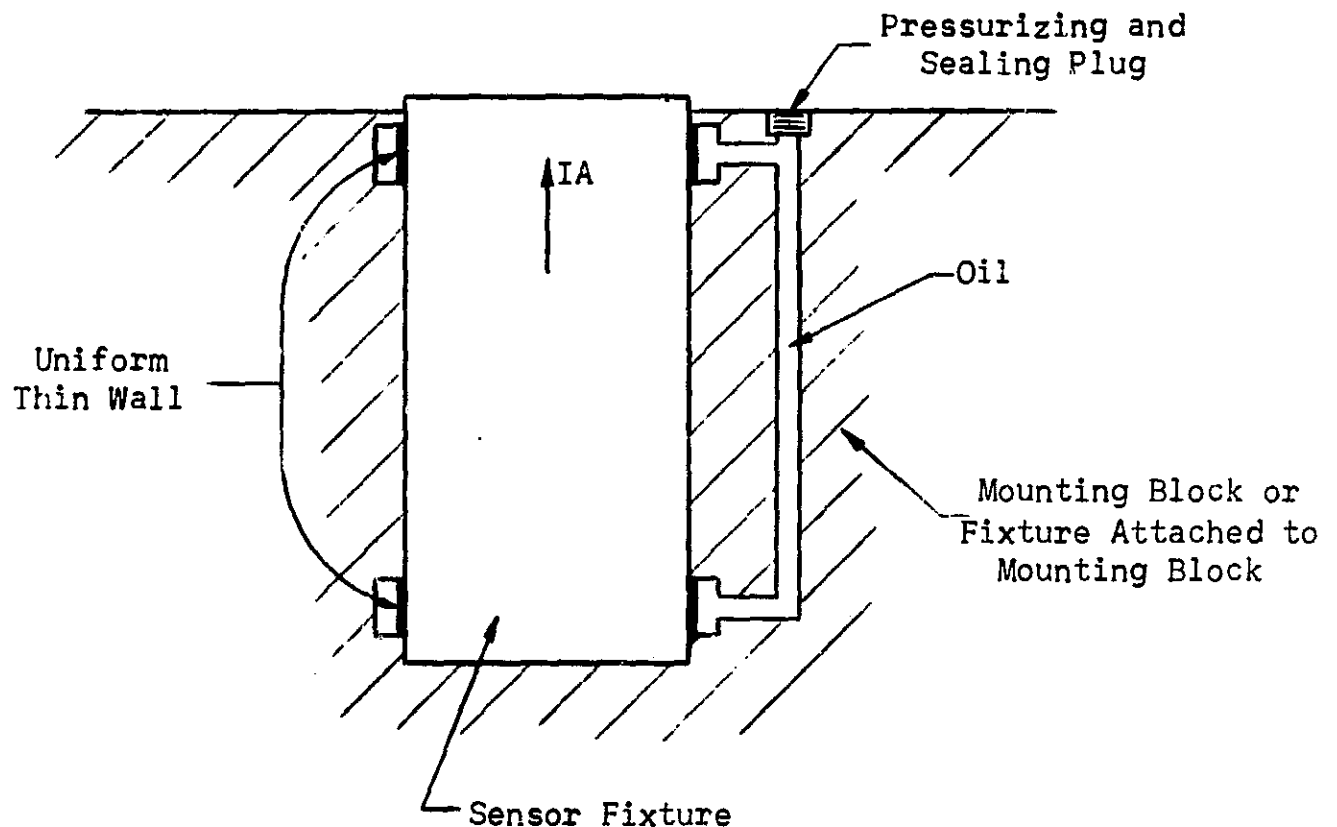


Figure B-6. Clamping the Sensor by Means of Hydraulic Cylindrical Contraction

A cylindrical analogy to wringing gage blocks could be used to hold the cylinder in the hole. A thin film of ultraclean oil would tend to support the cylinder in the hole due to surface tension effects. The cylinder and the hole could have a very slight taper as shown in Figure B-7.

Instead of maintaining a clearance between the sensor and the hole during installation, an alternate approach is for the cylinder to be defined by the thread crest of a hardened, fluted sensor sleeve which literally taps its way into the relatively softer hole as shown in Figure B-8. This crest would provide a very light interference fit with the hole. The resulting helical line contact would tend to push aside foreign particles which could escape to the flutes. The accuracy of this type of orientation is enhanced by the averaging effect of the long helical line contact. Subsequent installations are made by starting a new thread each time.

After this tapping process has been completed, the sensor could be further secured by applying adhesive through the flutes, or by using expansion-plug type clamps such as shown in Figure B-9. Another possibility is to use precision, collet-type clamps as shown in Figure B-10.

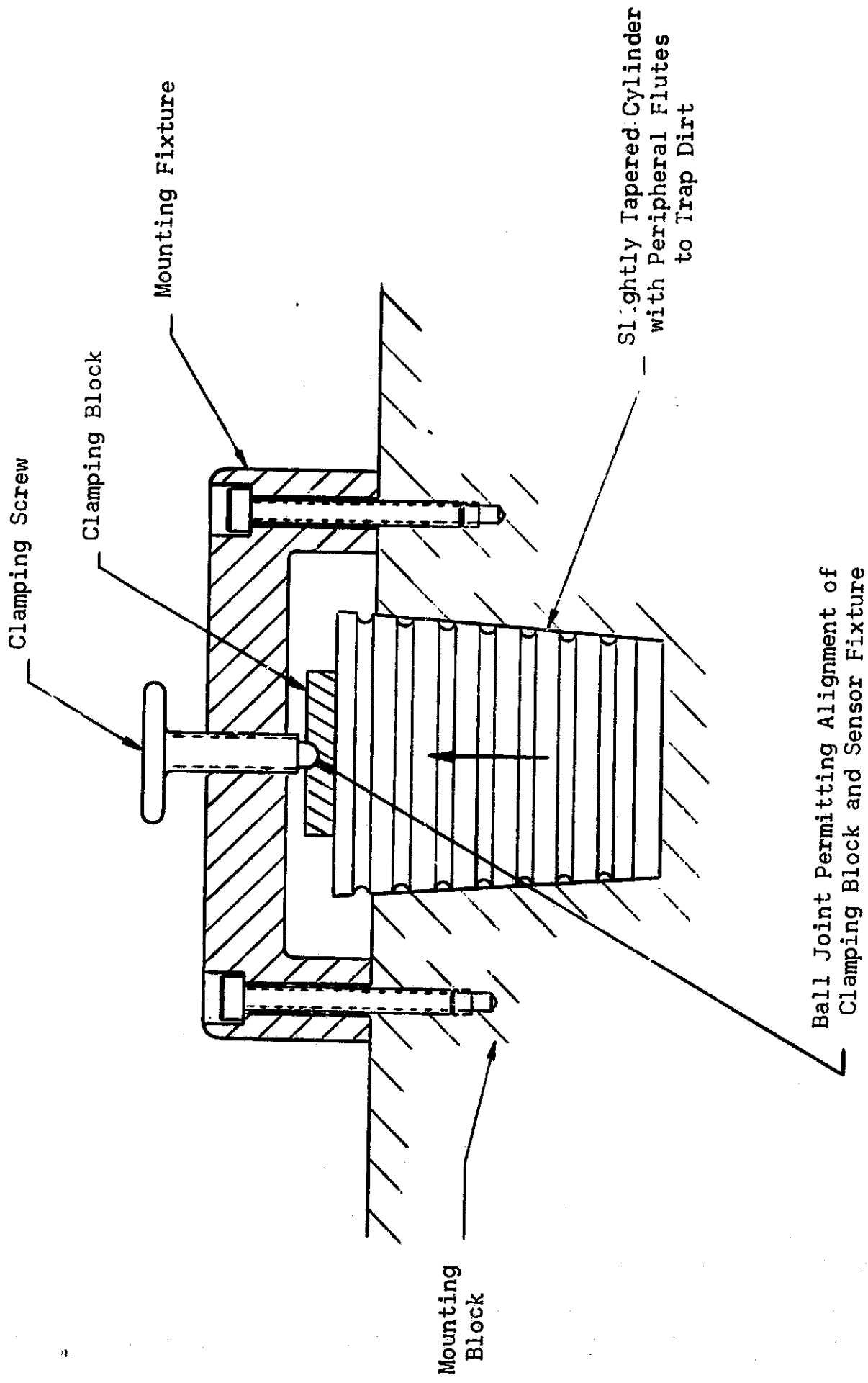


Figure B-7. Fixed Clamp Using Cone-in-Tapered Hole Geometry

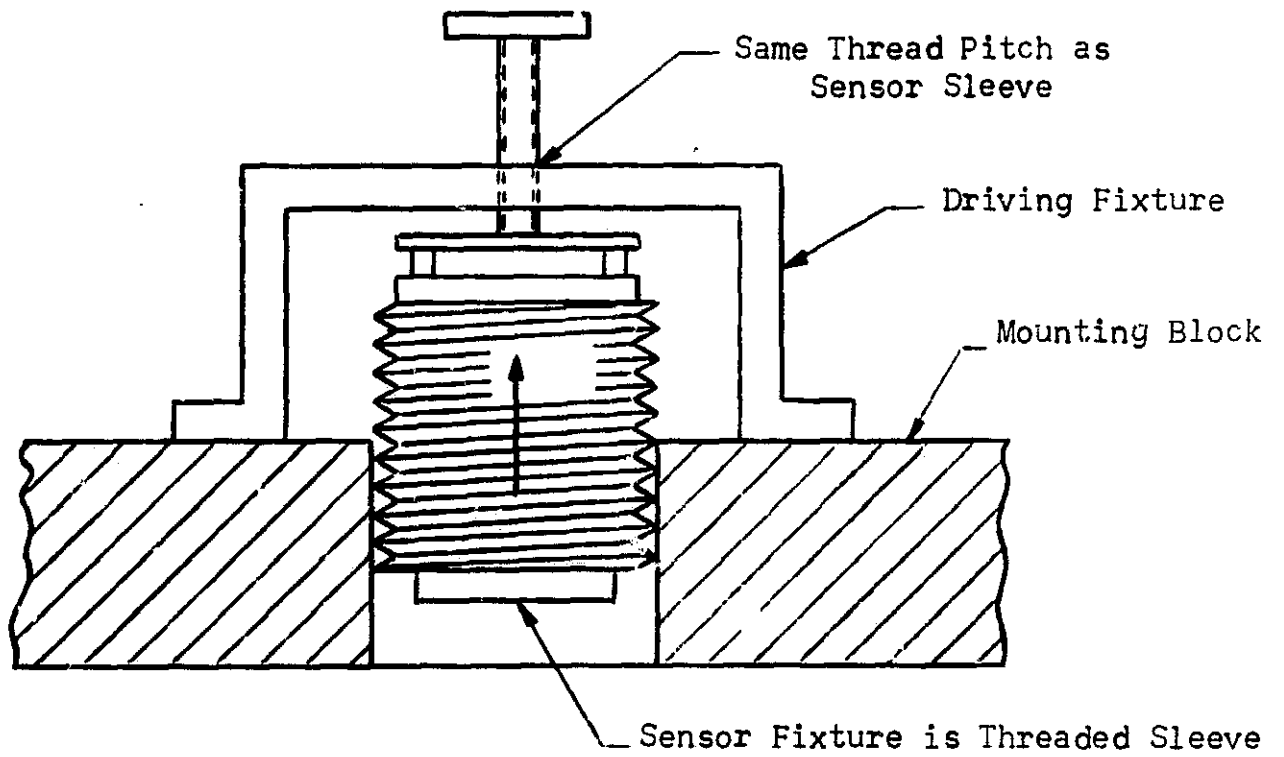


Figure B-8. Self-Tapping Sensor Fixture

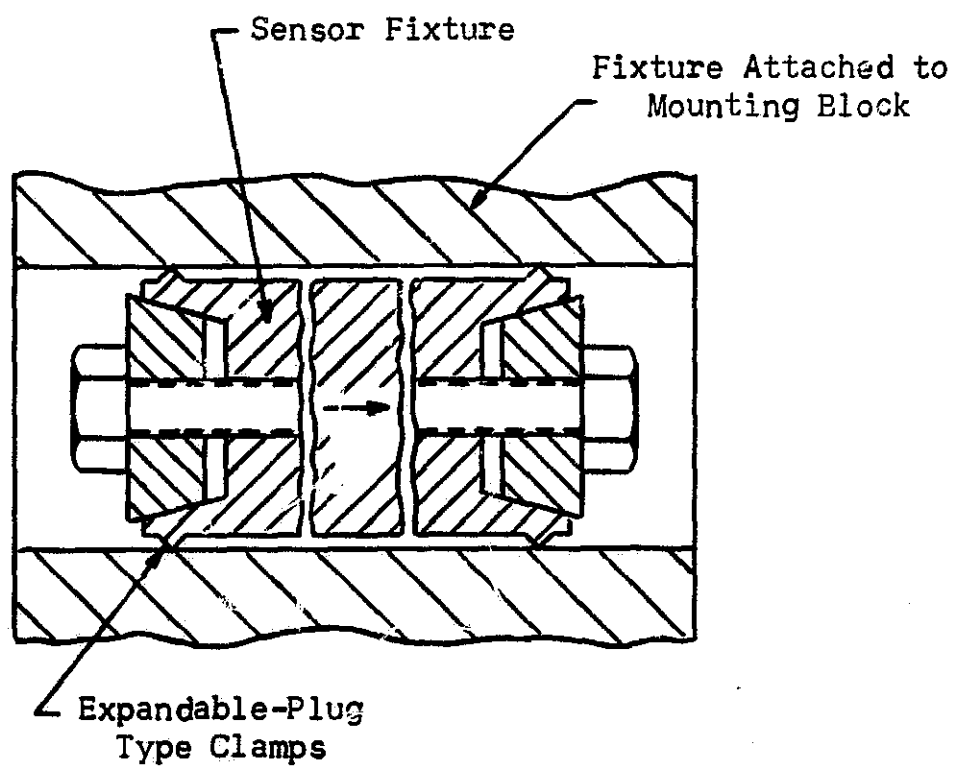


Figure B-9. Clamping the Sensor with Expandable Plugs

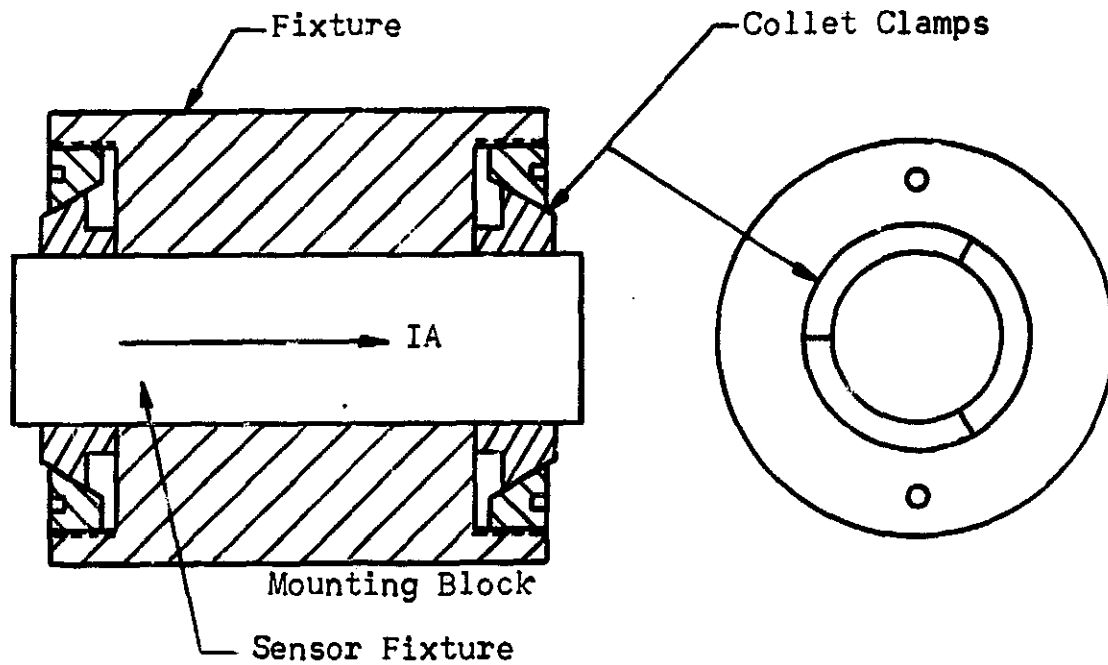


Figure B-10. Clamping the Sensor with Collet-Type Clamps

The use of a split cylinder is another approach to using cylindrical symmetry to orient the sensor axis. Figure B-11 shows a typical configuration. A soft coating on the sensor could be used to embed trapped particles. If half of this clamp were made extremely rigid, satisfactory accuracy might be obtained with this method. A gas journal bearing could also be used to hold the sensor. If the clearance were larger than any particles, they could escape with the air. The great disadvantage of this method is that it would require an air pressure supply.

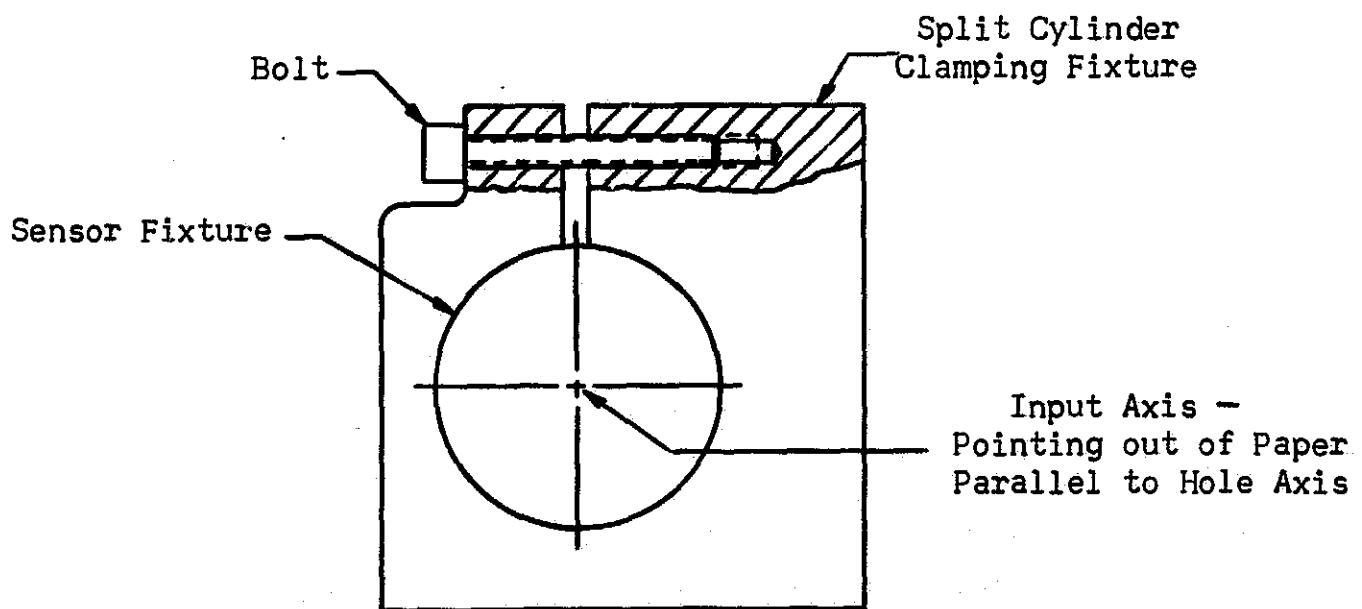
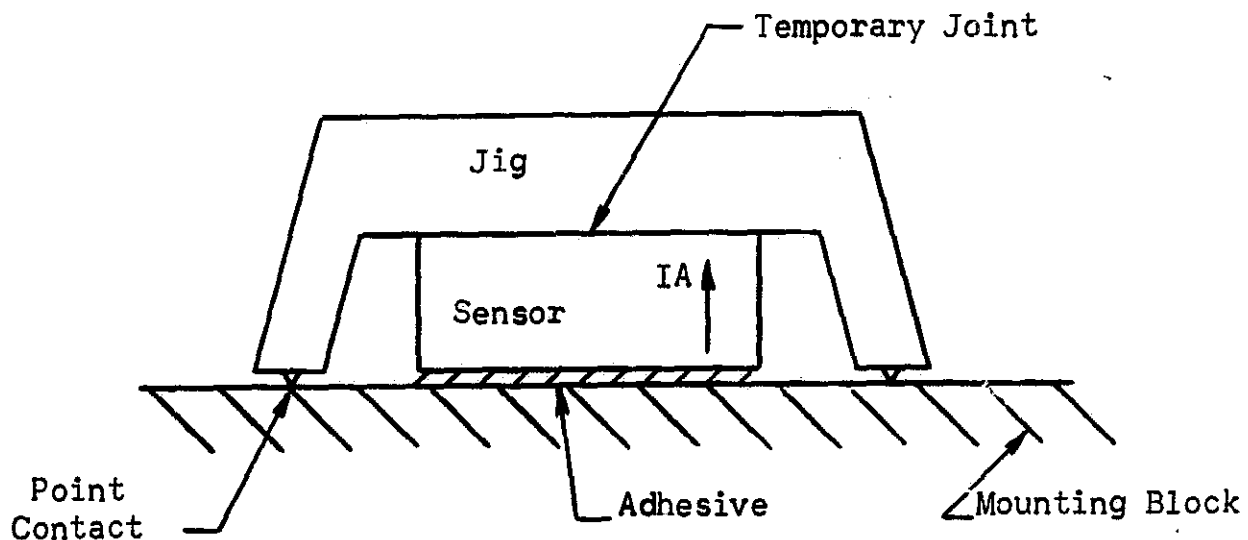


Figure B-11. Split Cylindrical Clamp

Clamps With Quasi-Verification

Clamps utilizing a precision jig. - This class of clamping technique utilizes a conveniently located clean facility and/or verification means that do not have to be in the vehicle, while still enabling sensors to be replaced on location. The basic feature of the method is that the sensor is attached to a jig which establishes the proper alignment of the sensor and the mounting block. The jig alignment relative to the mounting block is not affected by dirt. The sensor alignment relative to the jig is either verified or it is performed in a clean facility where dirt can not influence it.

A typical technique would be to temporarily attach the sensor to a jig which had three extremely small point contacts as shown in Figure B-12. The input axis of the sensor would be perpendicular to a surface of the sensor. Optical flats would be used to verify that this surface is parallel to the plane formed by the three point contacts. A clean facility could be used for this verification but would probably not be necessary since dust particles do not affect the use of optical flats. The jig would be placed on the mounting block and a small clearance would exist between the sensor and the mounting block. The three point contacts would be insensitive to dust due to their small area. Creep would not be important due to the short time involved and the low one "g" loading. The sensor would then be attached to the block with adhesive or solder. Heating elements in the mounting block could be used to destroy the joint during removal and replacement of units. If necessary, these elements could be supplemented with lifting cams. When the joint was solid, the jig could then be detached from the sensor. One possible problem area would be loading put on the jig when the joint solidifies. This might cause undesirable surface penetration by the point contacts. However, only asymmetries would affect the alignment.



Sensor Input Axis is Normal to Sensor Flange which is
Made Parallel to the Plane of the Point Contacts

Figure B-12. Precision Jig Maintaining Alignment During
Solidification of Joint

A different type of jig, using the concept of mounting on centers, is illustrated in Figure B-13. Adhesive is used to hold the sensor in the position that is determined by the centers. Heating elements soften the adhesive so that the sensor can be removed. A variation of this is shown in Figure B-14. The sensor and jig are preassembled in a clean room. Adhesive bonds the cylinder to a slightly oversized hole. Three point contacts on the jig ensure alignment while solidification takes place. Another variation is illustrated in Figure B-15 where a gas journal bearing maintains the cylinder alignment while the anchoring medium solidifies. This medium could either be an adhesive, or solder with a low melting point.

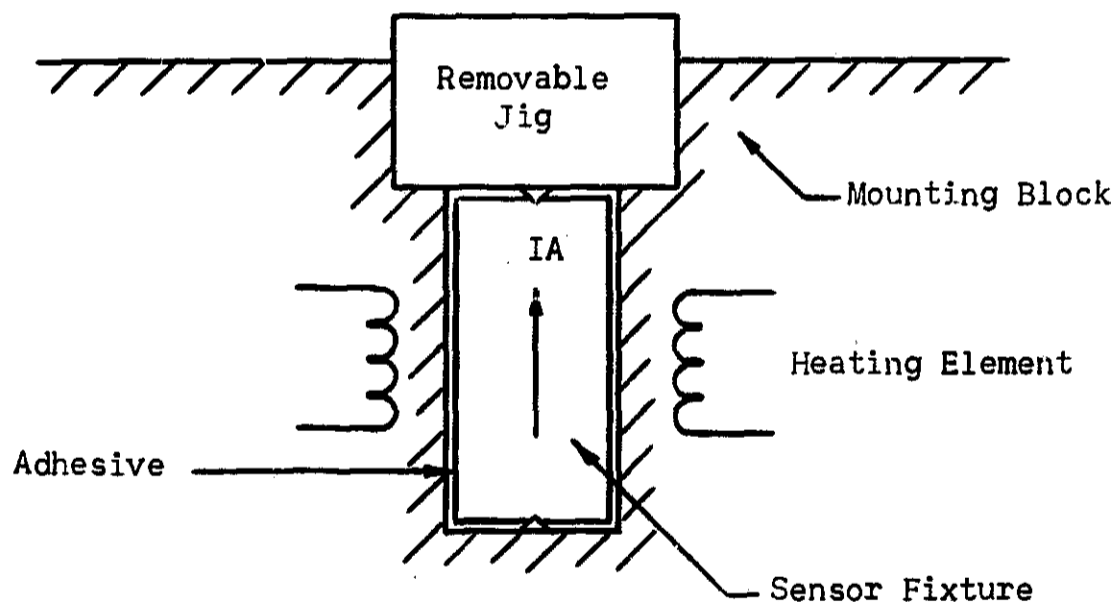


Figure B-13. Center Mounting Jig for Aligning Input Axis Parallel to Hole Axis

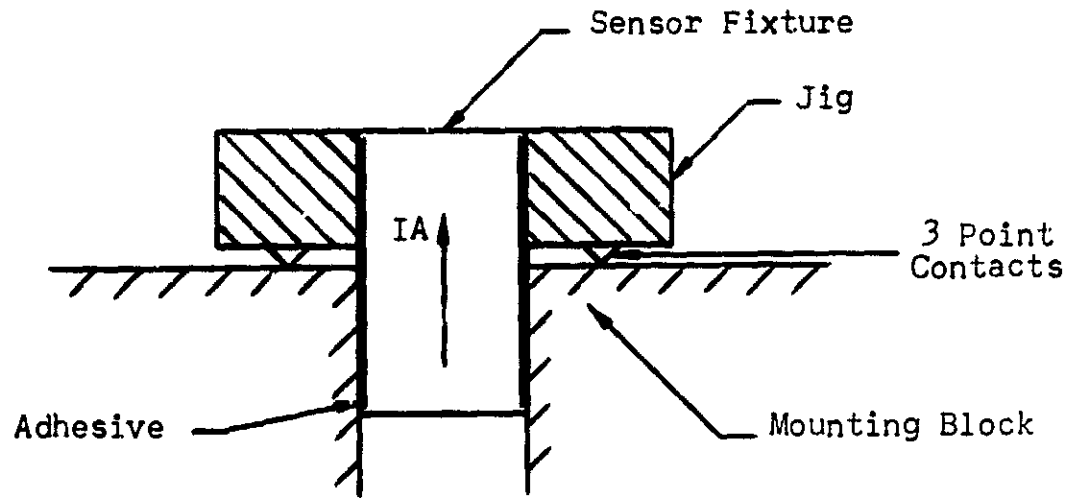


Figure B-14. Cylindrical Jig for Aligning
Input Axis Parallel to Hole Axis

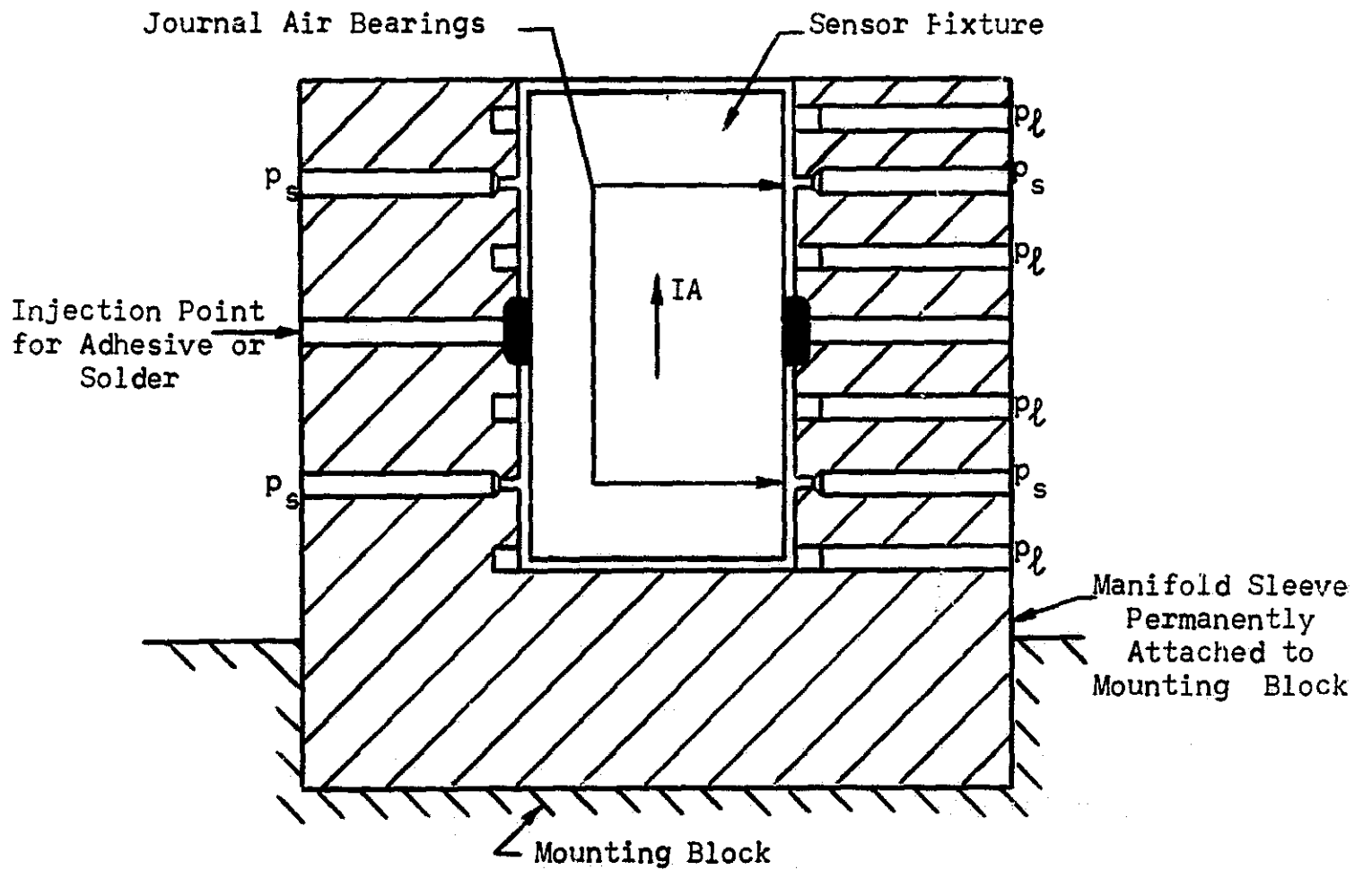


Figure B-15. Air Bearing Jig for Aligning
Input Axis Parallel to Hole Axis

Clamping techniques utilizing repeatability verification. - It is far simpler to determine the repeatability of the clamping process than to determine the exact alignment of the sensor and the mounting block. Monitoring the repeatability of successive clamping operations can eliminate the random type of misalignment errors that foreign particles would cause. The operator would know that dirt effects had been eliminated when successive clamping operations repeated themselves.

A typical configuration using this verification technique is shown in Figure B-16. Here the sensor fixture is wrung to the mounting block, and miniature autocollimators are used to monitor repeatability. Such autocollimators are commercially available with adequate sensitivity, and are only two or three cubic inches in size. They do not have to be accurately aligned to the mounting block or sensor fixture since they are merely used as null sensors.

A variation of this technique is shown in Figure B-17. The sensor input axis is parallel to the axis of the cylindrical sensor fixture which is placed through a hole which is perpendicular to the face of the transparent optical flat. The flat is then wrung to the surface of the mounting block until examination of the fringe pattern shows that the two are acceptably parallel. For greater symmetry to meet thermal requirements, the flat should serve as a "belly band" around the middle of the sensor fixture. This technique could be made "adjustable" by providing a thin, deformable shim between the flat and block at the clamping points.

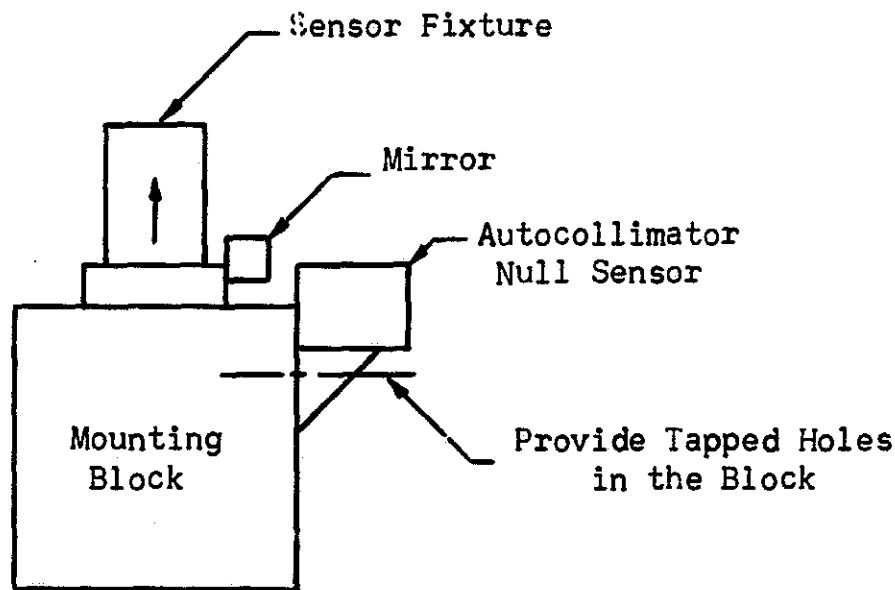


Figure B-16. Repeatability Verification Using
Miniature Autocollimators

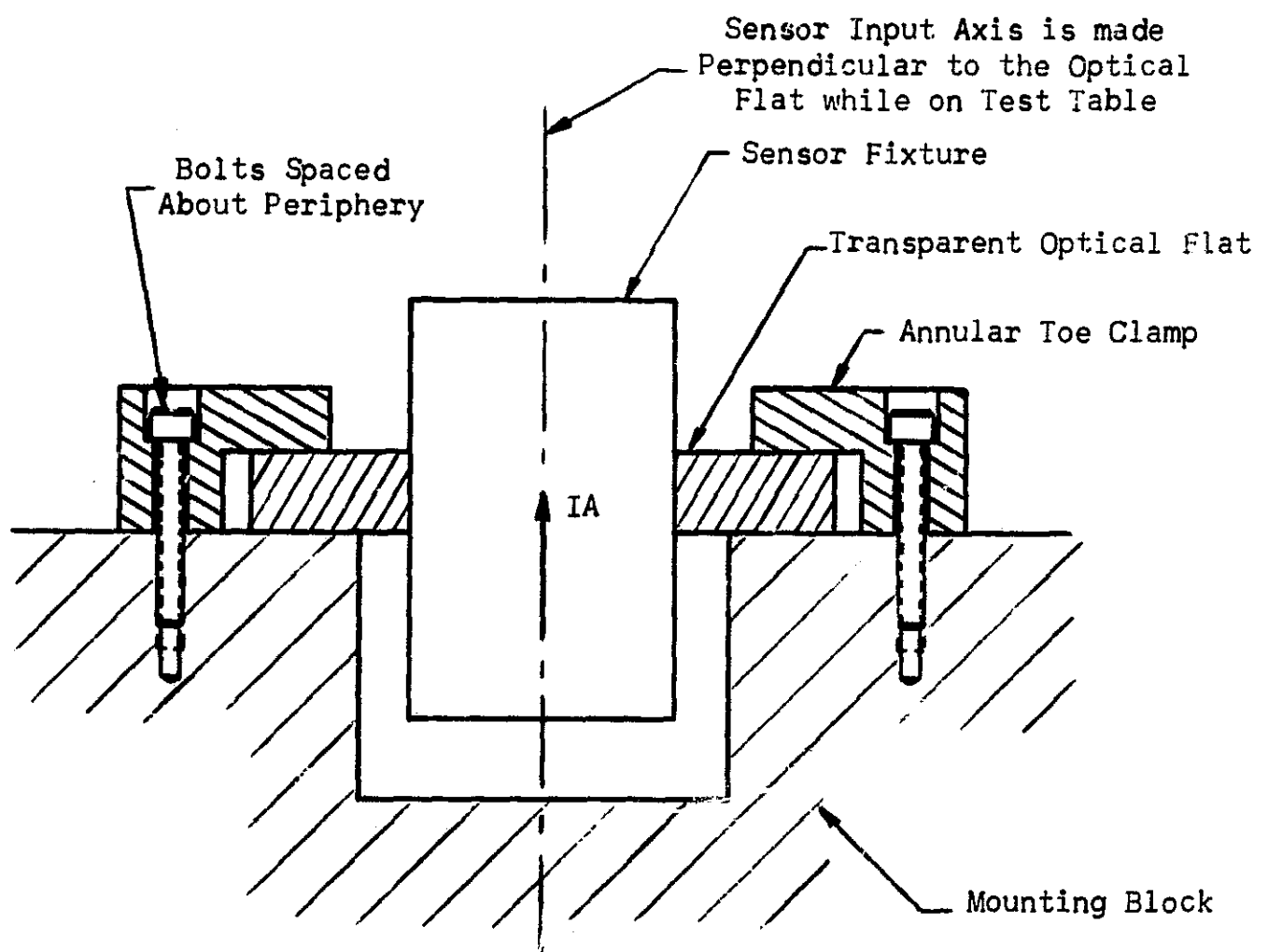


Figure B-17. Optical Flat Belly Band Clamping and Verification Technique

APPENDIX C

DISTRIBUTED PARAMETER LOAD-DEFLECTION ANALYSIS OF

THE PLANE-ON-PLANE CLAMP GEOMETRY

A number of fixed clamp concepts have been proposed as a means of establishing and maintaining the input axes of a set of strapdown sensors. These concepts can be classified into several different geometries, one of which involves placing two planes in contact with each other and maintaining parallelism between them. The sensor input axis is assumed to have been aligned perpendicular to one of the planes, and the desired input axis orientation is perpendicular to the other plane. In practice, the former plane is a surface of the sensor fixture while the latter plane is a surface of some form of mounting block.

Two factors which will disturb the parallelism between the two planes are:

- (1) asymmetry of the forces holding the two planes together; and
- (2) acceleration loadings that will occur after the vehicle is launched.

In addition, the system must be able to survive the large accelerations that may be present when the vehicle is launched without permanent damage (i.e., negligible plastic deflection).

This appendix contains an approximate analysis of the angular distortions of the sensor fixture and the mounting block when the above-mentioned loads are present. The results of the analysis specify the clamping force levels that are required and the allowable asymmetries in clamping force as a function of geometry, acceleration level, and permissible angular distortion. This information will be subsequently used to evaluate specific clamps that utilize the same basic plane-on-plane-geometry.

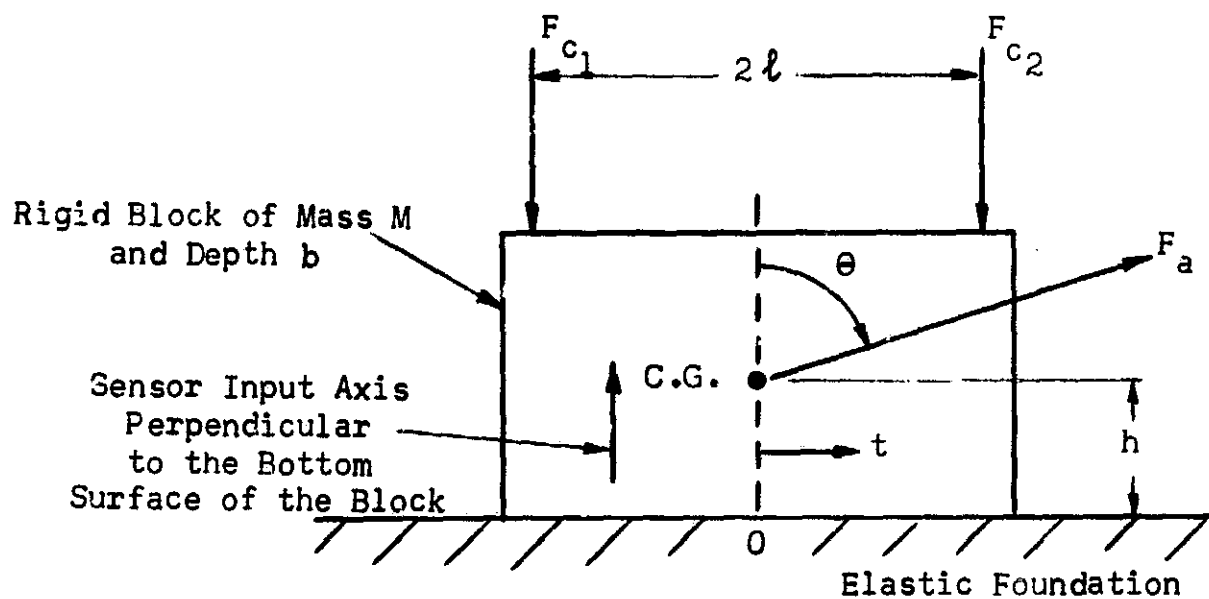
The following idealized models will be employed:

- (1) A rigid block on a semi-infinite elastic foundation (2-dimensional model). This model will show the displacement of the foundation when the sensor fixture is very stiff.
- (2) An elastic sensor fixture on a rigid foundation. This model will show the effect of a sensor fixture having finite stiffness.

A conservative estimate of input axis misalignment can be obtained by taking the sum of the misalignments resulting from the above two models.

Deflections of an Elastic Foundation in Contact with a Rigid Block

The first model to be analyzed shows the effect of the finite stiffness of the mounting block. Figure C-1 shows the geometry of the model and the applied loads. A rigid block is held to an elastic plane by two line contact clamping forces, F_{c_1} and F_{c_2} . Due to an acceleration force, F_a , which is determined by the mass of the rigid block and the acceleration of the system, and due to F_{c_1} being unequal to F_{c_2} , the block will tend to deform the foundation creating a misalignment of the sensor input axis, as shown in Figure C-2.



F_{c_1} , F_{c_2} concentrated line force clamping loads per unit length (into the page).

$$F_a = \left(\frac{M}{b}\right) \cdot (\text{acceleration}) \text{ the inertial force per unit length.}$$

Figure C-1. Rigid Block Clamped to an Elastic Foundation

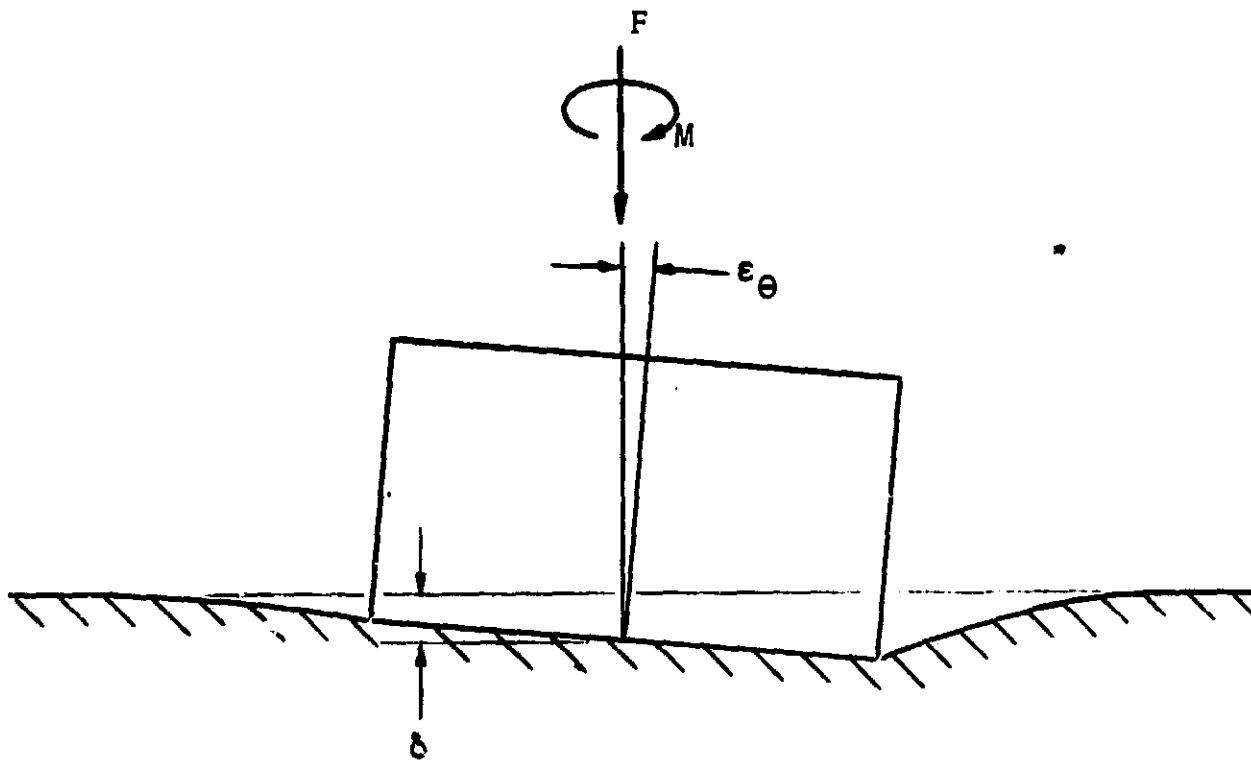


Figure C-2. Elastic Foundation Deflections

Let ΔF be defined as

$$\Delta F \equiv F_{c_2} - F_{c_1} \quad (C-1)$$

The resultant loads on the rigid block are

vertical component

$$F = F_{c_1} + F_{c_2} - F_a \cos \theta \quad (C-2)$$

horizontal component

$$Q = F_a \sin \theta \quad (C-3)$$

resultant moment

$$M = \frac{(F_{c_2} - F_{c_1})}{2} \cdot (2l) + h \cdot F_a \sin \theta \quad (C-4)$$

It will be assumed that the shear force at the contact surface has a negligible effect on the angular distortion. Then, from Muskhelishvili (28), ϵ_{θ} , the angular distortion, is given by

$$\epsilon_{\theta} = (M - 2 \alpha \ell F) \frac{4 (1 - \nu)}{2 \pi G (1 - 4 \alpha^2) \ell^2} \quad (C-5)$$

where $\alpha = \frac{1}{\pi} \tan^{-1} \left[f \frac{(1 - 2 \nu)}{2 (1 - \nu)} \right]$

f = friction coefficient

ν = Poisson's ratio

Also, from relations given by Reference (28), it can be shown that Equation (C-5) is valid for the following load conditions:

$$(2 \alpha - 1) < \frac{M}{(F \frac{\ell}{2})} < (2 \alpha + 1) \quad (C-6)$$

This equation expresses the conditions that are necessary for the block and plane to remain in contact with each other over the length 2ℓ .

The contact pressure is given by (28)

$$p(t) = \frac{\cos \pi \alpha}{4 \pi (1 - \nu)} \left[\frac{F \cdot 4(1 - \nu) - (8 \pi G \alpha \cdot \ell + 4 \pi G t) \epsilon_{\theta}}{(\ell + t)^{1/2} + \alpha (\ell - t)^{1/2} - \alpha} \right] \quad (C-7)$$

The infinite values of p at $t = \pm \ell$ result from the assumed rigidity of the block. For simplicity, a conservative result will be obtained by setting the friction coefficient to zero. With $\alpha = 0$, Equations (C-5), (C-6) and (C-7) become

$$\epsilon_{\theta} = \frac{4 (1 - \nu)}{2 \pi G \ell^2} M \quad (C-8a)$$

$$\left| \frac{M}{F} \right| < \frac{\ell}{2} \quad (C-8b)$$

$$p(t) = \frac{1}{4 \pi (1 - \nu)} \left[\frac{4(1 - \nu)F - 4 \pi G t \epsilon_{\theta}}{\sqrt{(\ell + t)(\ell - t)}} \right] \quad (C-8c)$$

Since

$$G = \frac{E}{2(1 + \nu)}$$

Equation (C-8a) can be expressed as

$$E \epsilon_{\theta} = \frac{4(1 - \nu^2)}{\pi \ell^2} M \quad (C-8d)$$

and Equation (C-8c) as

$$p(t) = \frac{1}{\sqrt{1 - \frac{t^2}{\ell^2}}} \left[\frac{F}{\pi \ell} - \frac{E t \epsilon_{\theta}}{2\ell (1 - \nu^2)} \right] \quad (C-8e)$$

In order to get the worst inertia force conditions, θ will be set equal to $\pi/2$. Then, from Equations (C-2) and (C-4)

$$F = F_{c_1} + F_{c_2}, \Delta F = F_{c_2} - F_{c_1} \quad (C-9a)$$

$$M = \left(\frac{\Delta F}{2}\right) \cdot 2\ell + h \cdot F_a \quad (C-9b)$$

and Equation (C-8d) becomes

$$\epsilon_{\theta} = \frac{8(1 - \nu^2)}{\pi} \cdot \left[\frac{\Delta F}{2E\ell} + \left(\frac{h}{\ell}\right) \left(\frac{F_a}{2E\ell}\right) \right] \quad (C-9c)$$

$$\text{or } \frac{\Delta F}{2\ell E} = \frac{\pi \epsilon_{\theta}}{8(1 - \nu^2)} - \left(\frac{h}{\ell}\right) \left(\frac{F_a}{2\ell E}\right)$$

Let ΔF^* and F_a^* be the resultant loads on a block of width b , so that

$$\Delta F^* = b \Delta F \quad (C-9d)$$

$$F_a^* = b F_a$$

The nondimensionalized allowable unbalanced clamping force can finally be written as

$$\frac{\Delta F^*}{2\ell b E} = \frac{\pi \epsilon_{\theta}}{8(1 - \nu^2)} - \left(\frac{h}{\ell}\right) \left(\frac{F_a^*}{2\ell b E}\right) \quad (C-10)$$

By combining Equations (C-8e), (C-9b), and (C-9d), it is possible to express the resultant clamping load as

$$\frac{F^*}{2\ell b} > 2 \left[\frac{\Delta F^*}{2\ell b} + \left(\frac{h}{\ell}\right) \left(\frac{F_a^*}{2\ell b}\right) \right] \quad (C-11)$$

Equations (C-10) and (C-11) are the desired results of this analysis. They express the required clamping force and the allowable unbalance in clamping force as functions of acceleration, angular distortion and geometry.

Deflections of an Elastic Sensor Fixture Block that is Clamped to a Rigid Plane

The second model to be analyzed shows the effect of the finite stiffness of the sensor fixture block. The geometry and applied loads are shown in Figure C-3. Two line contact clamping forces, F_{c1} and F_{c2} , clamp an elastic mounting block to a rigid foundation in the presence of an acceleration load F_a .

According to Reference (29), the stress at the bottom of the block due to the concentrated loads F_{c1} goes to zero at $x/d \approx 1.35$. This means that only a small area in the fixture is affected by the concentrated clamping forces.

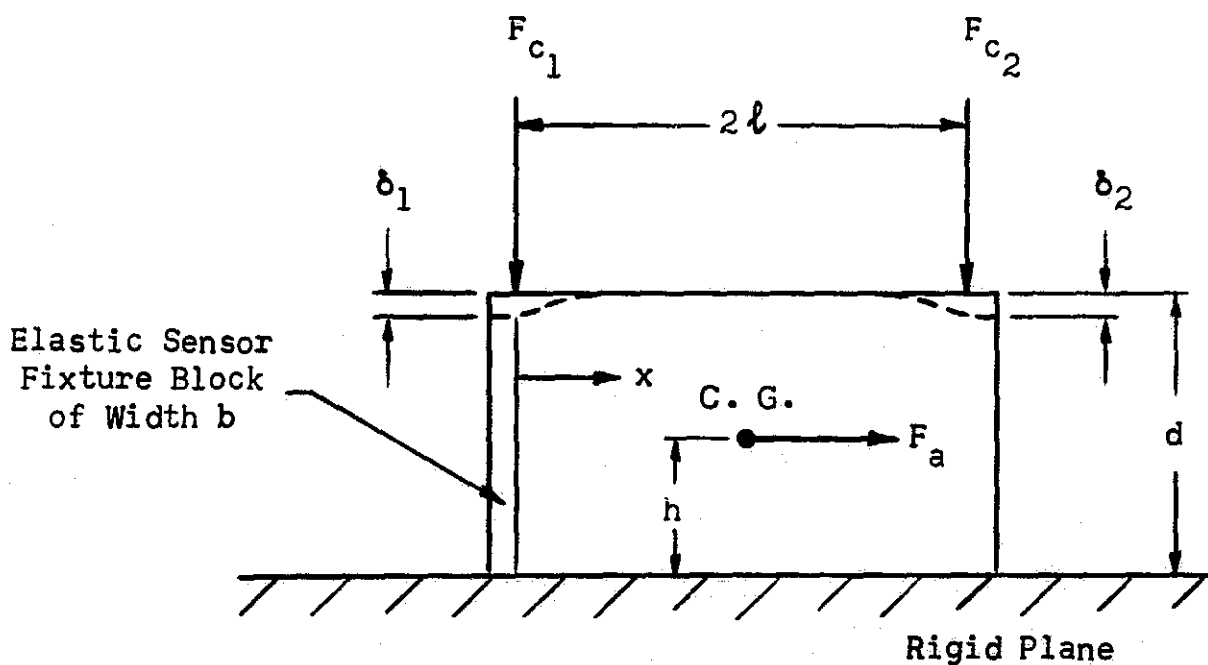


Figure C-3. Elastic Block Clamped to a Rigid Foundation

From the stress distribution at the contact surface, we may assume that this effective area is approximately

$$A \approx (0.5d) \times b \times 2 = bd$$

Thus, the deflection difference due to an unbalanced clamping load will be

$$\Delta b = \delta_2 - \delta_1 = \Delta F^*/Eb \quad (C-12)$$

The maximum angular distortion may be conservatively approximated by assuming that the block undergoes a rigid body rotation by an angle, ϵ_θ , given by

$$\epsilon_\theta = \frac{\Delta b}{2l} = \frac{\Delta F^*}{2Ebl} \quad (C-13)$$

If an acceleration force is present, the additional increment of the unbalancing load can be expressed as

$$l \cdot \Delta F^* = F_a^* h$$

or

$$\Delta F^* = \frac{h}{l} F_a^* \quad (C-14)$$

Therefore, the resultant angular deflection due to nonuniform clamping and acceleration forces will be

$$\epsilon_\theta = \frac{\Delta F^*}{2Ebl} + \frac{h}{l} \frac{F_a^*}{2Ebl} \quad (C-15)$$

Equation (C-15) expresses the angular misalignment of the input axis as a function of unbalance of clamping force and acceleration force.

Total Misalignment of Sensor Input Axis

The angular misalignments resulting from deflections of the foundation and the mounting block will now be combined in order to give a conservative estimate of the sensor input axis misalignment due to accelerations and unbalanced clamping forces. Using Equations (C-9c), (C-9d) and C-15), the total misalignment can be written as

$$\epsilon_\theta = 1 + \frac{8(1-v^2)}{\pi} \left[\frac{\Delta F^*}{2Ebl} + \frac{h}{l} \frac{F_a^*}{2Ebl} \right] \quad (C-16)$$

Thus, the maximum allowable unbalanced clamping load is given by

$$\frac{\Delta F^*}{2Ebl} = \frac{\pi \epsilon_\theta}{\pi + 8(1-v^2)} - \frac{h}{l} \left(\frac{F_a^*}{2Ebl} \right) \quad (C-17)$$

It is interesting to note from Equation (C-16) that deflection of the foundation is about three times more important than deflections of the mounting block. The required clamping force is given by the condition that

$$F^* > 2 \Delta F + \frac{h}{l} F_a^*$$

The possibility that the system may experience plastic deformation can be evaluated by using Equation (C-8e) to see if the contact pressure exceeds the yield stress of the material in any region except at the edge where the model is a poor representation of the actual situation. Equation (C-17) will be evaluated for the following parameters

$$e_\theta = 10\mu \text{ radian}$$

$$\nu = 0.3$$

$$\frac{\Delta F^*}{2Elb} < 3 \times 10^{-6} - \frac{h}{l} \frac{F_a^*}{2Elb} \quad (\text{C-18})$$

Figure C-4 shows a family of design curves that were drawn using Equation (C-18).

Numerical Example

To take a typical numerical example, assume

$$2l = 4 \text{ inches, } h = 1 \text{ inch}$$

$$b = 2 \text{ inches}$$

$$\text{weight} = 2 \text{ lbs}$$

$$\text{acceleration level} = 50g$$

$$E = 10 \times 10^6 \text{ psi}$$

then, the dimensionless acceleration force is

$$\frac{F_a^*}{2Elb} = \frac{2 \times 50}{(2)(10 \times 10^6)(2)(2)} = 1.26 \times 10^{-6}$$

$$h/l = 0.5$$

From Figure C-4, the allowable dimensionless unbalanced load is

$$\frac{\Delta F^*}{2Elb} < 2.35 \times 10^{-6}$$

Thus,

$$\Delta F^* < 185.0 \text{ lbs}$$

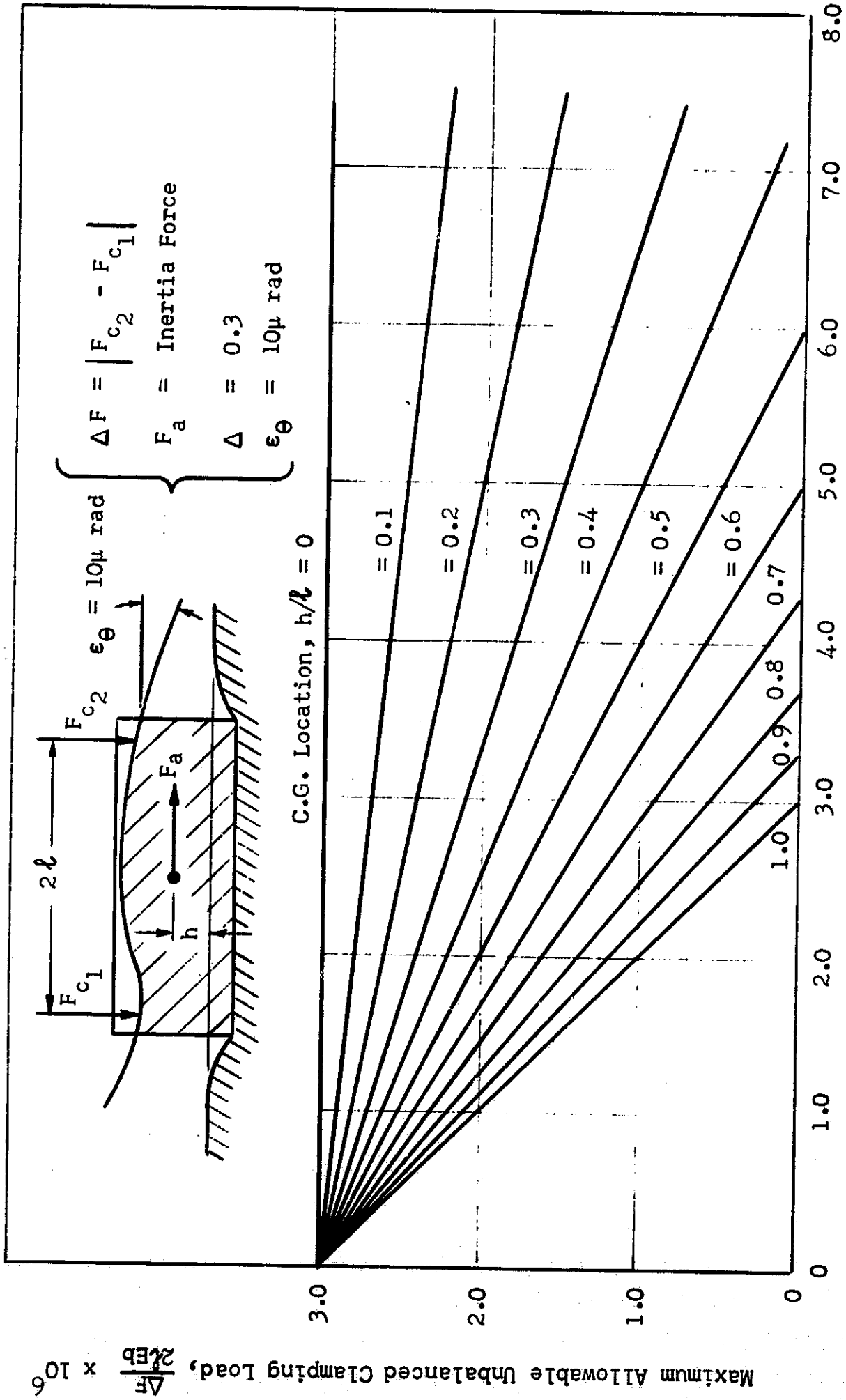


Figure C-4. Dimensionless Acceleration Force, $\frac{F_a}{2lEb} \times 10^6$

Limiting Unbalanced Clamping Load versus Acceleration

From Equation (C-11), the clamping force may be

$$F^* > 2 \left[(185) + \left(\frac{1}{2}\right) \left(\frac{100}{(4)(2)}\right) \right] = 382 \text{ lbs}, F = \frac{382}{2} = 191 \text{ lbs}$$

From Equation (C-8e) the contact pressures at two locations are

$$p(0) = \left(\frac{192}{\pi}\right) = 60 \text{ psi}$$

$$p(0.95l) = (3.15) \left[\frac{192}{\pi} + \frac{0.95 (10 \times 10^6) (2 \times 10^{-6})}{2(0.9)} \right]$$
$$= 3.15 (60 + 10) = 220 \text{ psi}$$

Thus, no plastic deformation would occur with normal materials.

The large allowable clamping force unbalance indicates that bolts and Belleville washers would form a clamp that would provide satisfactory force uniformity.

APPENDIX D

LOAD-DEFLECTION ANALYSIS OF THE PLANE-ON-PLANE

CLAMP GEOMETRY WITH DISCRETE MOUNTING PADS

An important method for implementing the plane-on-plane fixed clamp concept, which recurs in a number of the design concepts generated in this study, is the use of several discrete mounting pads on the sensor element. Although not substantially different from the continuous plane-on-plane geometry treated in Appendix C (provided the length of the mounting pads is not large) a lumped parameter analysis was formulated to treat the discrete pad case. The results of this analysis provide relations for subsequent design work and serve as a check on the conclusions of the distributed parameter model.

For purposes of analysis, the idealized, two-dimensional model of Figure D-1 was used to represent the system. A rigid block is pushed against a rigid plane by two clamping forces, F_1 , and F_2 . The block is separated from the plane by two springs, K_1 and K_2 , that are in line with the clamping forces. The free lengths of both springs are equal. The length of the block is 2ℓ , the height is d , and its depth is b .

Governing Relations

The spring deflections, δ_1 , and δ_2 , are given by

$$\delta_1 = \frac{F_1}{K_1} \quad (D-1)$$

$$\delta_2 = \frac{F_2}{K_2} \quad (D-2)$$

Since the block is rigid, the angle $\Delta\theta$ that it makes with respect to the plane is given by

$$\Delta\theta = \frac{\delta_1 - \delta_2}{2\ell} \quad (D-3)$$

or

$$\Delta\theta = \frac{\frac{F_1}{K_1} - \frac{F_2}{K_2}}{2\ell} \quad (D-4)$$

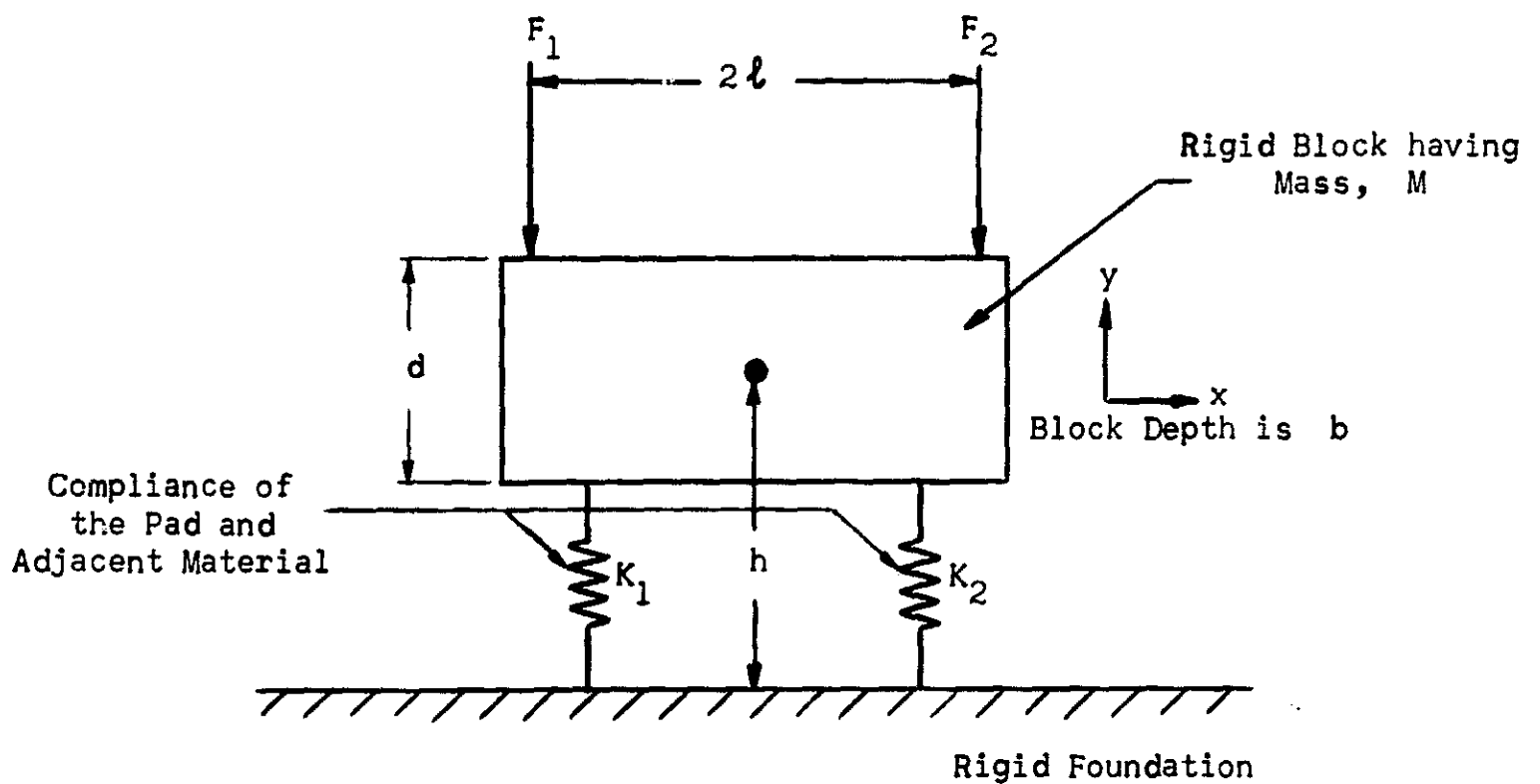


Figure D-1. Lumped Parameter Idealization of the Plane-on-Plane Geometry with Mounting Pads

Of interest are the angular distortions produced by asymmetries in both force and in spring rate. If the two spring rates K_1 and K_2 are equal, then

$$\Delta\theta = \frac{\Delta F}{2lK} \quad (D-5)$$

where

$$\Delta F = F_1 - F_2$$

$$K = K_1 = K_2$$

If the two clamping forces are equal, then

$$\Delta\theta = \frac{F}{2l} \left(\frac{1}{K_1} - \frac{1}{K_2} \right) = \left(\frac{F}{2lK_1} \right) \frac{\Delta K}{K_2} \quad (D-6)$$

where

$$\Delta K = K_2 - K_1$$

$$F = F_1 = F_2$$

$$K = \left(\frac{K_1 + K_2}{2} \right)$$

$$\delta = \frac{F}{K}$$

The effective spring constant K is given by

$$K = \frac{AE}{L} \quad (D-7)$$

where

A = the effective pad area

L = the length of the stressed material

E = Young's Modulus

It is assumed that the sensor fixture block and the mounting block have the same Young's Modulus. If the sensor fixture block has four mounting pads, each with area a_p , then $A = 4 a_p$. The distance L is taken to be the height of the sensor fixture block plus an equal depth, d , into the mounting block. Thus, K is given by the following expression

$$K = \frac{AE}{L} = \frac{4 a_p E}{d} \quad \text{for four mounting pads} \quad (D-8)$$

If the vehicle accelerates, an inertial force acting at the center of gravity of the sensor fixture block will cause additional misalignment. The unbalance moment, M_a , is given by

$$M_a = (M \ddot{x}) h \quad (D-9)$$

where

\ddot{x} is the vehicle acceleration parallel to the mating surfaces

M is the mass of the sensor fixture block

h is the distance between the center of gravity of the fixture block and the mating plane

This unbalance moment is supported by a difference in the deflections of the springs. Thus

$$(\delta_2 - \delta_1) K \cdot l = M_a \quad (D-10)$$

The misalignment, $\Delta \theta$, is

$$\Delta \theta = \left(\frac{M \ddot{x}}{K l} \right) \left(\frac{h}{2l} \right) \quad (D-11)$$

This misalignment must be added to the misalignment produced by unbalanced clamping forces.

The minimum clamping force is determined by the requirement that the block does not lift off the plane when the maximum acceleration \ddot{x} or \ddot{y} is present. This may be written as

$$F > \frac{M \ddot{y}}{2}, \frac{M \ddot{x}}{2} \left(\frac{h}{l}\right) \quad (D-12)$$

The stress level should always be well below the yield stress of the fixture and the mounting block material so that plastic deformation does not occur during large vehicle accelerations. When the maximum load is present, the average stress in the clamp, σ , is equal to

$$\left. \begin{aligned} \sigma &= \frac{F + \frac{M \ddot{x}}{2} \frac{h}{l}}{A} \\ \text{or} \quad \sigma &= \frac{F + \frac{M \ddot{y}}{2}}{A} \end{aligned} \right\} \quad (D-13)$$

where $A = 2 a_p$

For a given set of loads, the area A should be chosen so that

$$\sigma < \sigma_{\max} \quad (D-14)$$

where σ_{\max} is the maximum working stress for the clamp material

Numerical Example

A numerical example will be given in order to determine the magnitudes of the various quantities. The following values are assumed:

$$l = 2 \text{ in}$$

$$b = 2 \text{ in}$$

$$d = 2 \text{ in}$$

$$h = 1 \text{ in}$$

$$M = \frac{2}{g} \text{ lb}$$

$$\ddot{x} = 50g$$

$$\ddot{y} = 50g$$

$$E = 10 \times 10^6 \text{ psi}$$

From Equation (D-12), the minimum clamping load is

$$F > \left(\frac{2}{g}\right) \left(\frac{50g}{2}\right) = 50 \text{ lb}$$

Thus, it may be assumed conservatively that a 200 lb clamping force is used.

If a conservative microyield stress of 2000 psi is assumed as the maximum working stress, then Equation (D-13) may be written as

$$\sigma = \frac{200 + \left(\frac{2}{g}\right) (50g)}{2 a_p} < 2000 \text{ psi} \quad (\text{D-15})$$

Thus, the pad area becomes

$$a_p = \frac{250}{(2000)(2)} = 0.0625 \text{ in}^2$$

From Equation (D-8), the stiffness, K, is

$$K = \frac{(0.0625 \text{ in}^2) (10 \times 10^6 \text{ psi})}{(2 \text{ in})} = 0.31 \times 10^6 \frac{\text{lb}}{\text{in}}$$

In order that $\Delta \theta$ not exceed two arc seconds or 10×10^{-6} in/in, the allowable ΔF is calculated from Equation (D-5) as

$$\Delta F = (10 \times 10^{-6} \text{ in/in})(2)(2 \text{ in})(0.3 \times 10^6 \frac{\text{lb}}{\text{in}}) = 12 \text{ lb}$$

Thus, the allowable percentage force unbalance is

$$\frac{\Delta F}{F} = 6\%$$

A 50 g acceleration will cause an additional transient misalignment which from Equation (D-11) is

$$\Delta \theta = \frac{\left(\frac{2 \text{ lb}}{g}\right) (50 \text{ g}) \left(\frac{1 \text{ in}}{2 \text{ in}}\right)}{\left(0.3 \times 10^6 \frac{\text{lb}}{\text{in}}\right) (2 \text{ in})(2)} = 41.5 \mu \text{ in/in} \approx 8 \text{ arc secs}$$

For the case where the clamping force is symmetric and $\Delta \theta$ is limited to two arc seconds, the allowable percentage difference in spring constants is calculated from Equation (D-6) as

$$\frac{\Delta K}{K} = \frac{(4 \text{ in}) \left(0.3 \times 10^6 \frac{\text{lb}}{\text{in}}\right) (10 \times 10^{-6})}{(200 \text{ lb})} = 6\%$$

APPENDIX E

ANALYSIS OF POINT AND LINE CONTACT

FIXED CLAMP GEOMETRIES

A number of the fixed clamp concepts proposed in the main body of this report involve the use of point or line contact locating geometry. These include plane-on-plane concepts where the plane is defined by three point contacts, rather than by flat contact pads, as a means for reducing the probability of misalignment due to dirt particles. Another example is the concept of mounting the sensor element on centers which also requires small point contacts for the same reason. The final concept of this type is the cylinder in V-block concept where the force holding the locating elements together acts along the line contact between the cylinder and the V-block planes.

Although the influence of dirt may be minimized for these types of clamps, the small contact area can result in relatively high stress levels, causing misalignment due to creep and plastic deformation.

This appendix presents analysis aimed at determining the importance of these effects.

Three Point Contact Geometry

Figure E-1 shows a typical configuration for this type of clamping geometry in which a sensor fixture with three spherical contacts is held by force W against a mounting plane. If it is assumed that W is equally divided between the three point contacts, then the following expressions from the Hertz elastic solution can be written (30):

$$\delta = 1.55 \left(\frac{P^2}{d E^2} \right)^{1/3} \quad (E-1)$$

$$\sigma_{\text{mean}} = 0.410 \left(\frac{PE^2}{d^2} \right)^{1/3} \quad (E-2)$$

$$a = 0.88 \left(\frac{P d}{E} \right)^{1/3} \quad (E-3)$$

$$\frac{\sigma_{\text{max}}}{\sigma_{\text{mean}}} = \frac{0.616}{0.410} = 1.5 \quad (E-4)$$

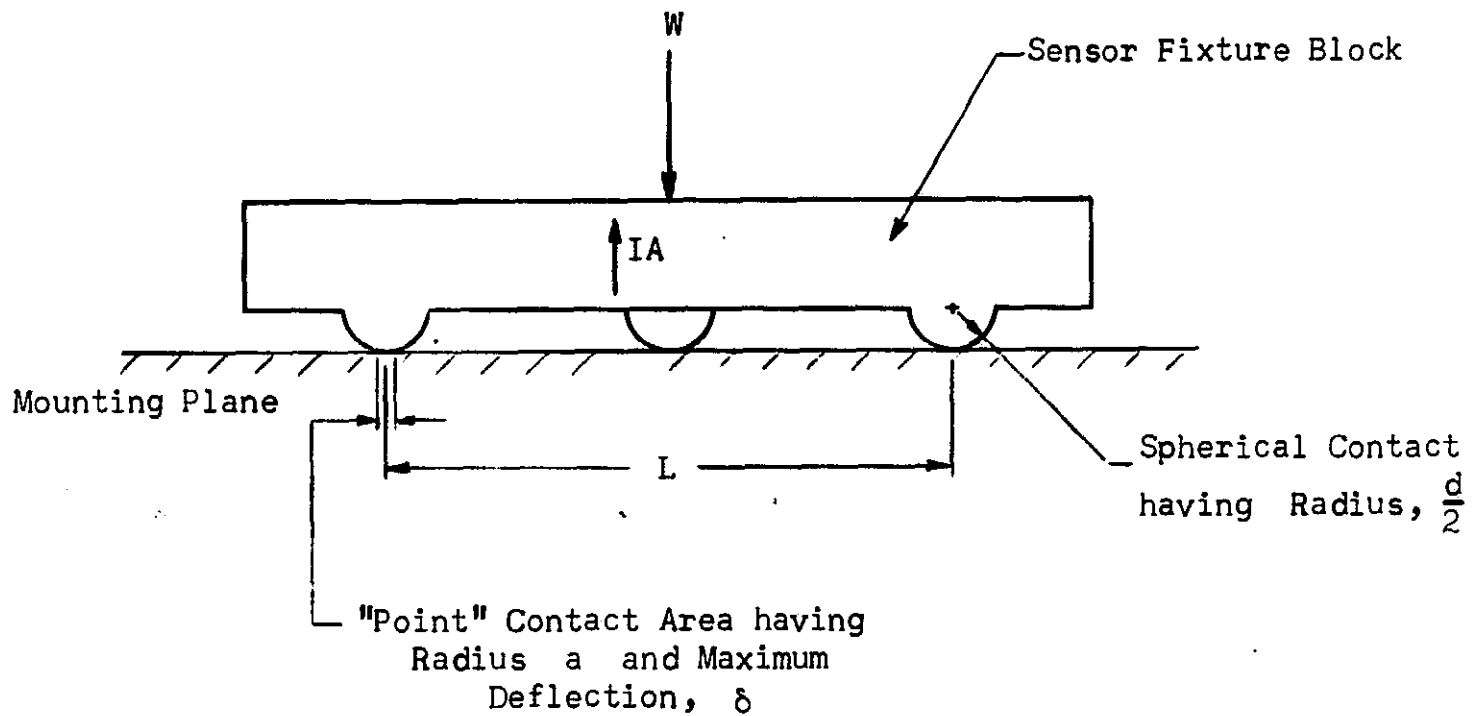


Figure E-1. Three Point Contact Clamping Geometry

- where
- δ = maximum deflection of the mounting plane
 - P = applied contact point load = $W/3$
 - d = diameter of spherical contact
 - E = Young's Modulus
 - a = radius of contact area
 - σ_{mean} = average stress = $P/\pi a^2$
 - σ_{max} = maximum stress in the contact area

A Poisson's ratio equal to 0.3 has been assumed for these expressions.

Since the deflection varies as the $2/3$ power of P ,

$$\frac{\Delta\delta}{\delta} = \frac{2}{3} \frac{\Delta P}{P} \quad (\text{E-5})$$

where Δ is an incremental change

If W is not evenly divided between the three contacts, a misalignment $\Delta \theta$ will result which can be approximated as

$$\Delta \theta = \frac{2}{3} \left(\frac{d}{L} \right) \left(\frac{\Delta P}{P} \right) \quad (\text{E-6})$$

where ΔP is the variation in load from the nominal value

The following typical application will be considered

$$\begin{aligned} L &= 3 \text{ inches} \\ d &= 1 \text{ inch} \\ W &= 180 \text{ lb} \\ E &= 30 \times 10^6 \text{ psi} \end{aligned}$$

From Equations (E-1), (E-2) and (E-3),

$$\delta = 1.55 \left[\frac{(60 \text{ lb})^2}{(1 \text{ in}) (30 \times 10^6 \text{ psi})^2} \right]^{1/3} = 250 \mu \text{ in}$$

$$\sigma_{\text{mean}} = 0.410 \left[\frac{(60 \text{ lb}) (30 \times 10^6 \text{ psi})^2}{(1 \text{ in})^2} \right]^{1/3} = 160,000 \text{ psi}$$

$$a = 0.88 \left[\frac{(60 \text{ lb}) (1 \text{ in})}{(30 \times 10^6 \text{ psi})} \right]^{1/3} = 0.011 \text{ in}$$

If $\frac{\Delta P}{P}$ is 10%, then the misalignment is

$$\Delta \theta = \left(\frac{2}{3} \right) \left(\frac{250 \mu \text{ in}}{3 \text{ in}} \right) (0.1) = 5.5 \mu / \text{in/in} \approx 1 \text{ arc second}$$

The above example clearly shows that even if a relatively large diameter "point" contact is used, the stress level is high enough to cause creep and plastic deformation. If there were perfect symmetry during this deformation, no misalignment would occur. However, since a finite amount of asymmetry will always be present, there is increased probability that significant misalignment will occur if the overall level of deformation is large.

Thus, it appears that the three-point contact geometry is unsatisfactory in comparison with flat mounting pads for the ultraprecision alignment of sensor elements due to the high stresses involved.

Sensor Unit Mounted on Centers

A proposed alternative locating geometry to the plane-on-plane concept was the mounting of the sensor unit on centers. This concept could be implemented by creating apparent centers by means of relatively large tapered clamp areas. This is discussed separately as a method of clamping for the cylinder-in-hole concept. If, however, relatively small contact points are used as the mounting centers in order to minimize the effects of dirt, the problem becomes similar to that discussed in the previous section. Although mating geometries could be provided to minimize Hertz contact stresses, perfect fits are not possible. Thus, it is not likely that the stresses induced under realistic clamping and dynamic loads can be kept low enough to avoid the extremely small creep or plastic deformations consistent with angular misalignment greater than 1 arc-second.

Cylinder in V-Block Geometry

The cylinder in V-block geometry consists of a V-block which holds a cylinder having its axis parallel to the sensor input axis. The orientation of the cylinder is determined by the two "line" contacts that exist between the cylinder circumference and the two intersecting planes of the V-block. The "line" contacts provide the advantage of a small contact area which reduces the probability of misalignment due to dirt. However, the small contact area will result in high stress levels which may cause misalignment due to creep and plastic deformation.

Figure E-2 shows a cylinder having length L and radius R that is held in a V-block having length L with included angle ϕ . If the clamping load, W , is assumed to be equally divided between the two line contacts, and if frictional effects are neglected, then the following expressions can be written (10):

$$\delta = \frac{1.33 P}{L E} (7.4 - \log_{10} \frac{P}{4LR}) \quad (E-7)$$

$$\sigma_{\text{mean}} = 0.465 \sqrt{\frac{P E}{2LR}} \quad (E-8)$$

$$a = 1.075 \sqrt{\frac{P 2 R}{E}} \quad (E-9)$$

$$\frac{\sigma_{\text{max}}}{\sigma_{\text{mean}}} = \frac{(0.591)}{(0.465)} = 1.27 \quad (E-10)$$

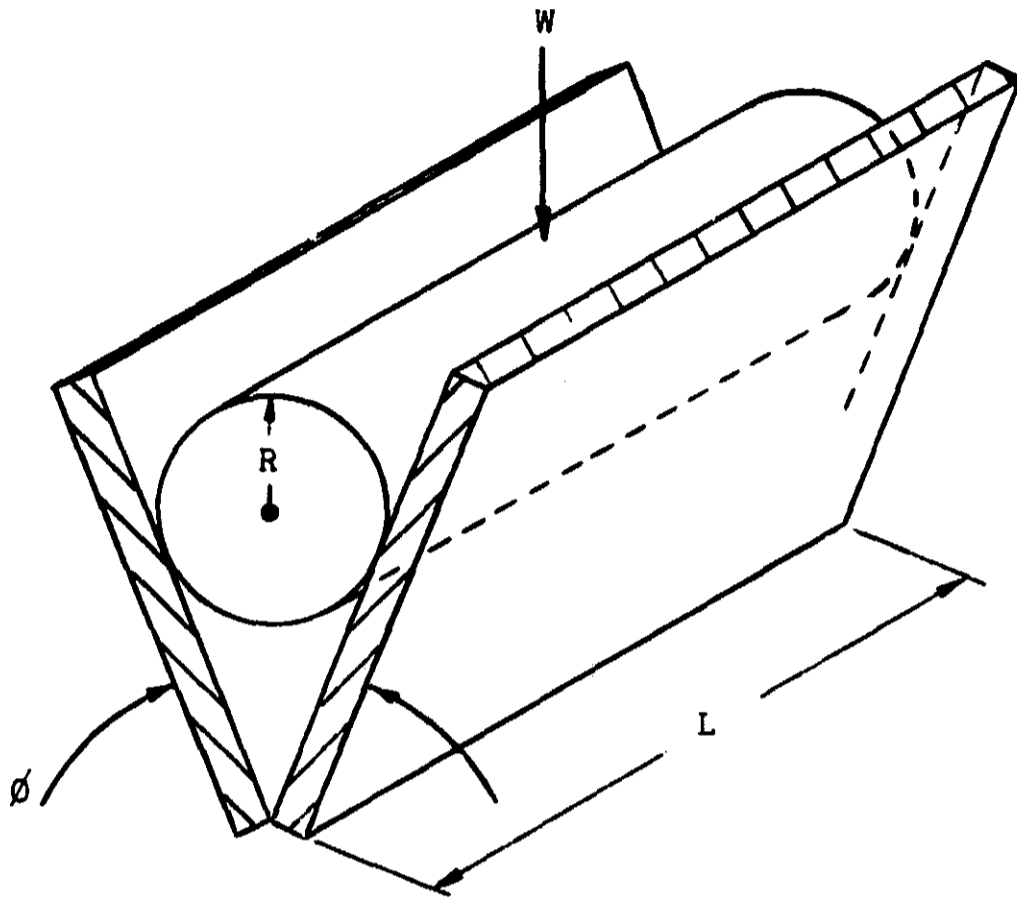


Figure E-2. Cylinder in a V-Block Locating Geometry

- where
- δ = deflection of the plane surface
 - P = load applied at each line contact = $\frac{W}{2 \sin (\phi/2)}$
 - E = Young's Modulus
 - a = half width of rectangular contact area of length L
 - σ_{mean} = average stress = $\frac{P}{2aL}$
 - σ_{max} = maximum stress occurring in the contact area

A Poisson's ratio of 0.3 has been assumed in the above relations.

The angular misalignment, $\Delta\theta$, of the cylinder may be approximated by

$$\Delta\theta = \frac{\Delta\delta}{L} \quad (\text{E-11})$$

where $\Delta\delta$ is the variation in deflection at the line contacts from one end of the V-block to the other.

The following values were taken as a typical numerical example:

$$\begin{aligned}L &= 2 \text{ inches} \\R &= 2 \text{ inches} \\W &= 200 \text{ lbs} \\E &= 30 \times 10^6 \text{ psi} \\\phi &= 90^\circ\end{aligned}$$

Substitution into Equations (E-7) through (E-9) gives the following results:

$$\begin{aligned}\delta &= 17 \text{ } \mu\text{inches} \\\sigma_{\text{mean}} &= 10,300 \text{ psi} \\a &= 0.0045 \text{ inches}\end{aligned}$$

The worst possible misalignment can be computed from Equation (E-11) assuming the above deflection, δ , at one end of the cylinder varying to zero deflection at the other. Thus,

$$\Delta\delta = \delta$$

and

$$\begin{aligned}\Delta\theta &= \frac{17 \text{ } \mu\text{inches}}{2 \text{ inches}} = 8.5 \times 10^{-6} \frac{\text{in}}{\text{in}} \\&\approx 1.7 \text{ arc-seconds}\end{aligned}$$

Since this worst case would not be expected to occur if care is taken to maintain the clamping load uniform, a much lower angular deflection is likely. For example, a 10% unbalance in load would lead to angular deflection in the range of 0.17 arc-seconds which is well within the error budget available for the fixed clamp.

The calculated σ_{mean} of 10,300 psi also shows that the contact stress can probably be maintained below the MYS for the typical materials which are likely to be used for the clamp. Thus, on the basis of deformation under load, the cylinder in V-block appears feasible. The main disadvantage that it suffers in comparison with the plane-on-plane concepts is the need to machine a precise cylinder as well as two planes. There is no clear advantage to offset this disadvantage.

APPENDIX F

LOAD-DEFLECTION ANALYSIS OF THE CYLINDER-IN-HOLE

FIXED CLAMP CONCEPT

A number of the fixed clamp concepts generated use the cylinder-in-hole locating geometry. For these concepts, a cylinder is mated with a hole to align the axes associated with the two elements. The cylindrical element could be on either the sensor fixture or the mounting block.

Proper alignment between the two elements cannot be ensured without an interference fit. In addition, clamping action between the two elements may be achieved with sufficient interference.

This appendix presents an idealized model to predict the limiting values of misalignment expected as a result of asymmetry in the interference between the cylinder and the hole.

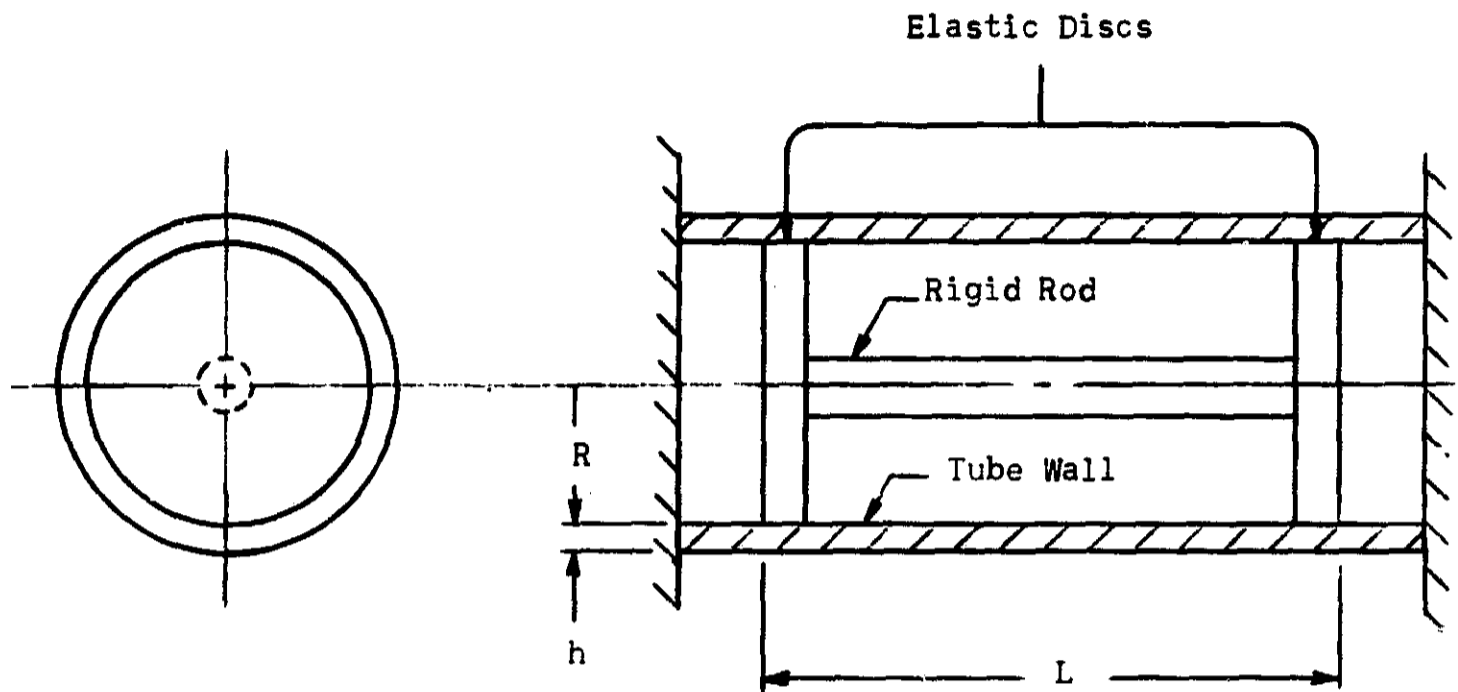
Description of the Model

To provide a limit analysis of the effects of machining asymmetry on the alignment of a cylinder-in-hole clamp without resorting to complex analysis requiring computer solution, the idealized model described in Figure F-1 was used. In this model the elastic cylinder of length, L , and radius, R , is in an elastic tube and is first represented by two elastic discs of radii, R , separated by a rigid rod as shown in Figure F-1(a). The disc model, is, in turn, represented by the lumped parameter model shown in Figure F-1(b) for one end of the structure. Each disc is divided into two parts for which the elastic properties are modeled by equivalent springs, K_{1c} and K_{2c} . The tube walls are likewise divided into two parts and represented by springs, K_{1s} and K_{2s} . The deflection, Δ , is the deflection of the centerline of the disc. When Δ is zero, the freely extended lengths of K_{1s} and K_{1c} interfere by an amount δ_1 , and the freely extended lengths of K_{2s} and K_{2c} interfere by an amount δ_2 . When all of the pieces are forced to fit together, Δ will move from its middle position if there is any asymmetry or difference between δ_1 and δ_2 . The complete expression for Δ is

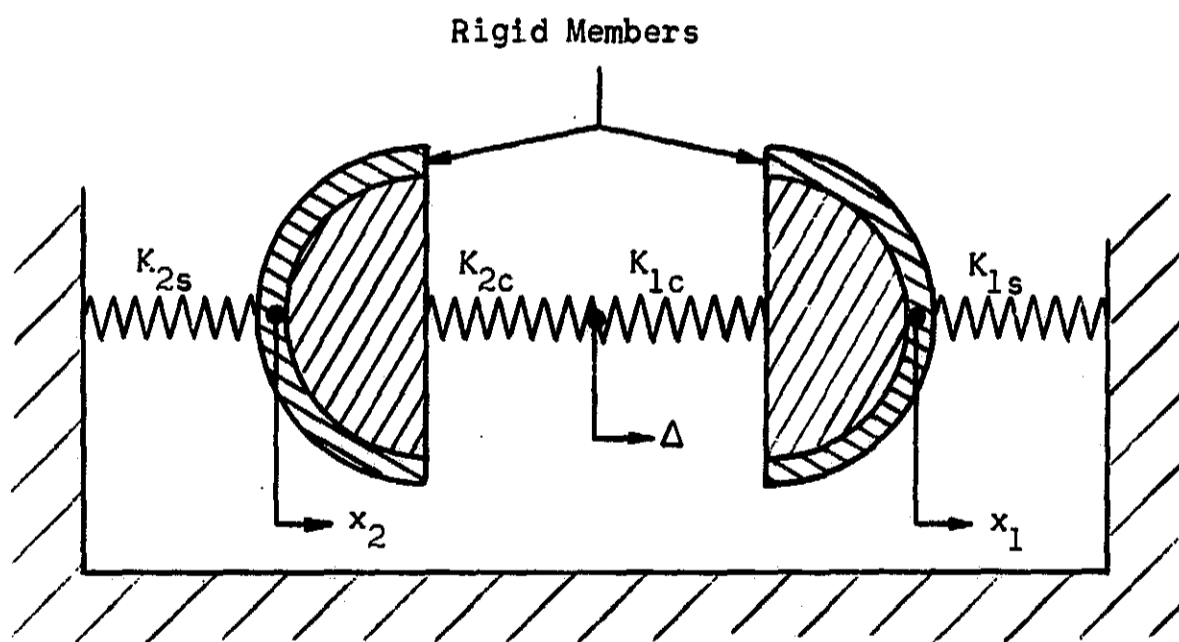
$$\Delta = \frac{\delta_2 - (1 + \epsilon) \delta_1}{1 + (1 + \epsilon)} \quad (F-1)$$

where

$$\epsilon = \left[\begin{array}{cc} \left(\frac{K_{1s}}{K_{2s}} \right) & \left(\frac{K_{1c}}{K_{2c}} \right) \\ \left(\frac{K_{2s} + K_{2c}}{K_{1s} + K_{1c}} \right) \end{array} \right] - 1 \quad (F-2)$$



(a) Disc Model for Cylinder



(b) Lumped Parameter Model for the Disc and Walls at One End of the Structure

Figure F-1. Schematic Diagram Showing the Lumped Parameter Model for the Cylinder-in-Hole

If all of the K's are symmetrical, this reduces to

$$\Delta = \frac{\delta_2 - \delta_1}{2} \quad (F-3)$$

If δ_1 is equal to δ_2 , and ϵ is small, then Equation (F-1) becomes

$$\Delta \approx \frac{\delta}{2} \epsilon \quad (F-4)$$

If the tube walls are assumed to be infinitely stiff compared to the disc, then

$$e = \frac{K_{1c}}{K_{2c}} - 1 \approx \frac{\Delta K_c}{K_c} \quad (F-5)$$

where

$$\Delta K_c = K_{1c} - K_{2c}$$

$$K_c = \frac{K_{1c} + K_{2c}}{2}$$

If the disc is assumed to be infinitely stiff compared to the tube walls, then

$$e = \frac{K_{1s}}{K_{2s}} - 1 \approx \frac{\Delta K_s}{K_s} \quad (F-6)$$

where

$$\Delta K_s = K_{1s} - K_{2s}$$

$$K_s = \frac{K_{1s} + K_{2s}}{2}$$

The maximum angular misalignment between the cylinder axis and the hole axis can be found by assuming that both ends of the cylinder are deflected by an amount Δ in opposite directions. This worst case would cause a cocking angle, $\Delta \theta$, equal to

$$\Delta \theta = \frac{2\Delta}{L} \quad (F-7)$$

The misalignment, $\Delta \theta$, can be approximated conservatively by separately adding all of the above effects together so that $\Delta \theta$ becomes

$$\Delta \theta = \left(\frac{\delta_2 - \delta_1}{L} \right) + \frac{\delta}{L} \left(\frac{\Delta K_c}{K_c} + \frac{\Delta K_s}{K_s} \right) \quad (\text{F-8})$$

The relationship between $\frac{\Delta K}{K}$ and asymmetries of the cylinder, hole, or tube wall thickness, will depend on the type of stresses associated with the deformation that accommodates the asymmetry. For example, the bending stiffness of a structural member such as the tube wall varies inversely with the cube of depth, h . Thus,

$$\left(\frac{\Delta K}{K} \right)_{\text{bending}} \approx -3 \left(\frac{\Delta h}{h} \right) \quad (\text{F-9})$$

The stiffness of a member in compression or tension varies as inversely with depth, h . Thus,

$$\left(\frac{\Delta K}{K} \right)_{\text{compression or tension}} \approx - \left(\frac{\Delta h}{h} \right) \quad (\text{F-10})$$

Considering the case where $L = 2$ inches and the asymmetry in stiffness, $\frac{\Delta K}{K}$, is the same for the cylinder and tube walls, Equation (F-8) may be used to determine the allowable asymmetry in radial interference and stiffness for a given nominal interference. Figure F-2 gives these values assuming that the maximum allowable angular misalignment, $\Delta \theta$, is 2 arc seconds or 10 $\mu\text{in/in}$.

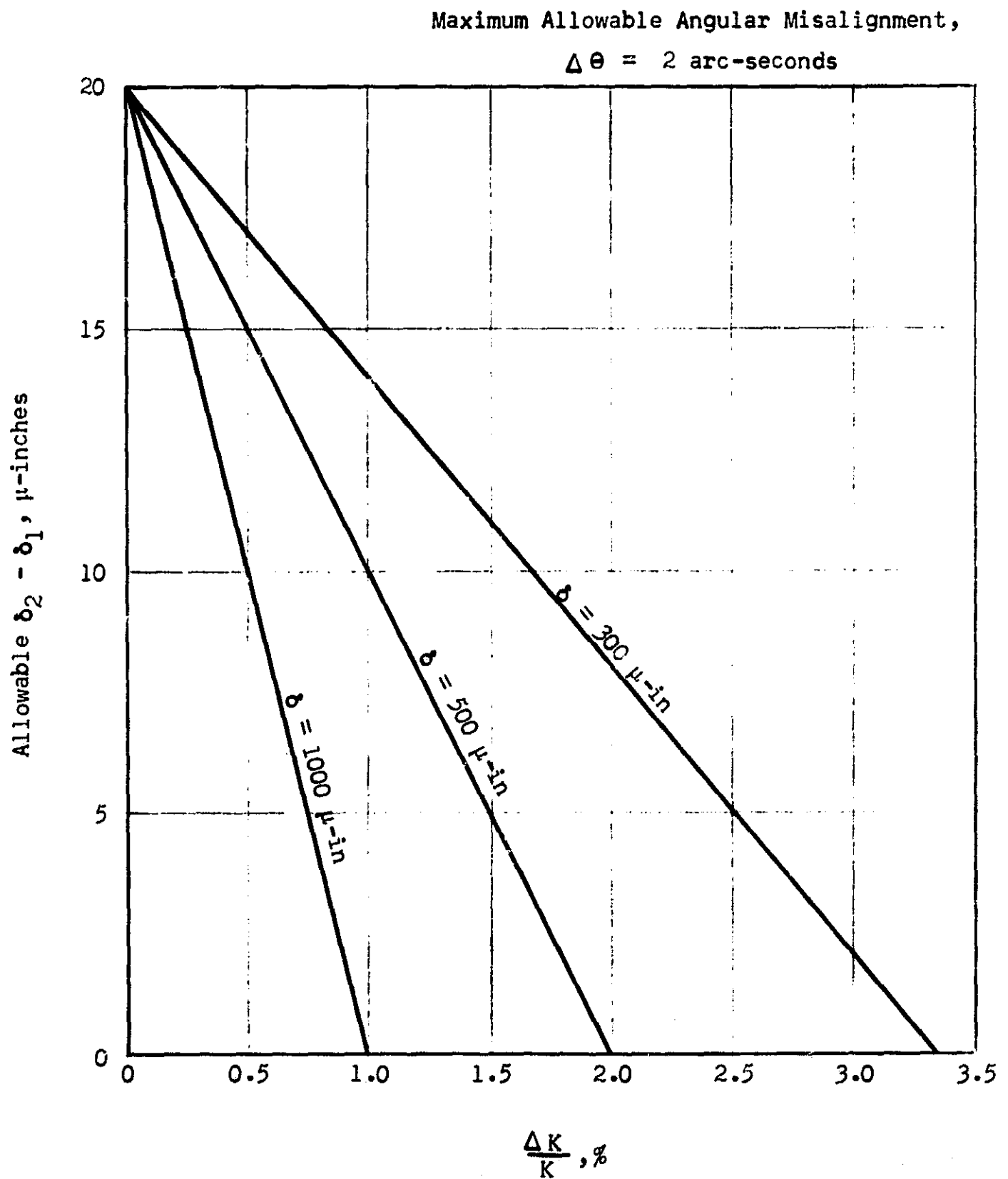


Figure F-2. Allowable Asymmetry in Interference versus Asymmetry in Structure Stiffness for Various Values of Nominal Interference

APPENDIX G

ANALYSIS OF CYLINDER-IN-HOLE CLAMPING TECHNIQUES

The interference fit required for the cylinder-in-hole clamping concept may be supplied in one of several ways:

- (1) thermal shrink fit;
- (2) hydraulic pressure; and
- (3) use of a split clamp.

In Appendix F, it was seen that the allowable asymmetry in interference due to machining errors is likely within the state-of-the-art for typical conditions, provided the asymmetry in the effective spring rate of the structure can be controlled closely enough. Further, the amount of nominal radial interference required also has a strong influence on the allowable asymmetry. These factors are analyzed in this appendix for the various clamping techniques.

Determination of Required Radial Interference

It is desirable, especially if repeated installation of sensors with a given assembly is contemplated, to avoid plastic deformation of the cylinder and hole walls. This puts an upper limit on the radial interference.

From the theory of thick shells (31), the relationship between the maximum shear stress, τ , and the nominal interference, δ , is expressed as

$$\tau = \frac{E}{2} \frac{\delta}{R_i} \quad (G-1)$$

where E = Young's Modulus

R_i = radius of the hole

Thus, plastic deformation can be avoided if $\frac{\delta}{R_i}$ is less than $(\frac{\delta}{R_i})_{\max}$

$$(\frac{\delta}{R_i})_{\max} = \frac{2 \tau_{\max}}{E} \quad (G-2)$$

where τ_{\max} is the shear stress at the yielding condition for the material

One possible criterion for the minimum interference is that it be capable of holding the cylinder in the hole under the influences of inertial loadings. This can be expressed by

$$p > \frac{M \ddot{x}}{a \mu} \quad (G-3)$$

where p = the contact pressure between the cylinder and wall
 M = the mass of the sensor fixture block
 \ddot{x} = the largest expected axial acceleration
 a = the contact area between the cylinder and the hole walls
 μ = the coefficient of friction between the cylinder and the hole walls

The interference that is necessary to establish a given contact pressure, p , is (31)

$$\frac{\delta}{R_i} = \left(\frac{2p}{E}\right) \frac{r_o^2}{R_o^2 - R_i^2} \quad (G-4)$$

where R_o = the outer radius of the tube

Equations (G-3) and (G-4) can be combined to determine $\left(\frac{\delta}{R_i}\right)_{\min}$, the minimum value of $\frac{\delta}{R_i}$, as

$$\left(\frac{\delta}{R_i}\right)_{\min} = \left(\frac{2}{E}\right) \left(\frac{1}{1 - \frac{R_i^2}{R_o^2}}\right) \frac{M \ddot{x}}{a \mu} \quad (G-5)$$

Thus, an interference fit can be used to clamp the gyro in the presence of inertial forces, without incurring plastic deformation, provided that the following inequality can be satisfied:

$$\left(\frac{2}{E\mu}\right) \left(\frac{1}{1 - \frac{R_i^2}{R_o^2}}\right) \left(\frac{M \ddot{x}}{a}\right) R_i < \delta < \left(\frac{2 \tau_{\max}}{E}\right) R_i \quad (G-6)$$

The following conservative numerical example illustrates the magnitude of the various quantities. Assume the following values:

$$\begin{aligned} \tau_{\max} &= 4000 \text{ psi} \\ E &= 10 \times 10^6 \text{ psi} \\ \mu &= 0.1 \\ M &= \frac{2}{9} \text{ lb} \end{aligned}$$

$$\bar{x} = 50 \text{ g}$$

$$R_i = 2 \text{ inches}$$

$$a = 3 \text{ in}^2$$

$$R_o = 2.5 \text{ inches}$$

Equation (G-6) then gives

$$0.00037 < \delta < 0.0016 \text{ inches} \quad (\text{G-7})$$

An interference within this range can be readily achieved with precision machining.

The Use of a Thermal Shrink Fit as a Means of Providing Clamping Force

One way of controlling the interference so that the cylinder can be inserted and removed from the hole is to utilize thermal expansions. The cylinder and the hole walls can either be made from materials having different thermal expansion coefficients, or they can be heated to different temperatures.

In order to insert or remove the cylinder from the hole, the following condition concerning the average temperatures of the cylinder and hole walls must be satisfied

$$\alpha_w (T_w - T_o) - \alpha_c (T_c - T_o) = \frac{\delta}{R} \quad (\text{G-8})$$

where α_w = thermal expansion coefficient of the hole wall

α_c = thermal expansion coefficient of the cylinder

T_w = average temperature of the hole wall

T_c = average temperature of the cylinder

T_o = initial temperature of the cylinder and the hole walls

δ = radial interference when the cylinder and the hole walls have temperature T_o

R = hole radius

If the cylinder and hole walls are made from the same material, then

$$\alpha_c = \alpha_w = \alpha$$

and

$$(T_w - T_c) = \left(\frac{\delta}{R}\right) \frac{1}{\alpha} \quad (G-9)$$

The cylinder can easily be inserted into the hole if heat is applied only to the hole walls. It is merely necessary to raise temperature, T_w , high enough for Equation (G-9) to be satisfied. The problem of removing the cylinder from the hole is complicated by the practical difficulty of raising the temperature of the hole walls without also raising the temperature of the cylinder. One way to solve this is to use a thin walled shell to hold the cylinder. A controlled heat rate is applied to the outer surface of the shell and during the ensuing thermal transient, Equation (G-9) can be satisfied for a time that is long enough to remove the cylinder. A disadvantage of this technique is that the outer surface of the shell must be raised by a temperature, $(T_e - T_o)$, that is considerably larger than the value of $(T_w - T_c)$ that is given in Equation (G-9). Another possible difficulty is that the thermal transient may take place too rapidly for the withdrawal operation to be carefully performed.

The temperature rise, $(T_e - T_o)$, and the time available for extracting the cylinder, τ , will be estimated in the following analysis. The problem will be idealized by making two conservative assumptions:

- (1) The cylinder and shell combination is equivalent to a solid cylinder of radius R_o .
- (2) There is no thermal contact resistance between the cylinder and the shell.

The ideal interface between the cylinder and the shell occurs at radius ratio, R_i/R_o . The temperature, T_w , is the temperature at R_w , the effective average wall radius. The temperature, T_c , is the temperature at R_c , the effective average cylinder radius.

If the temperature of the outer surface of the cylinder is suddenly raised from T_o to T_e , then the time history of $T_w - T_c$ can be determined from the thermal response chart that is shown in Figure G-1 (32). The temperature, T_x , at radius ratio R_x , is related to the nondimensionalized ordinate T'_x of Figure G-1 as follows:

$$T_x = T'_x T_e + (1 - T'_x) T_o \quad (G-10)$$

Thus,

$$T_w - T_c = \left[T'_w T_o + (1 - T'_w) T_e \right] - \left[T'_c T_o + (1 - T'_c) T_e \right] \quad (G-11)$$

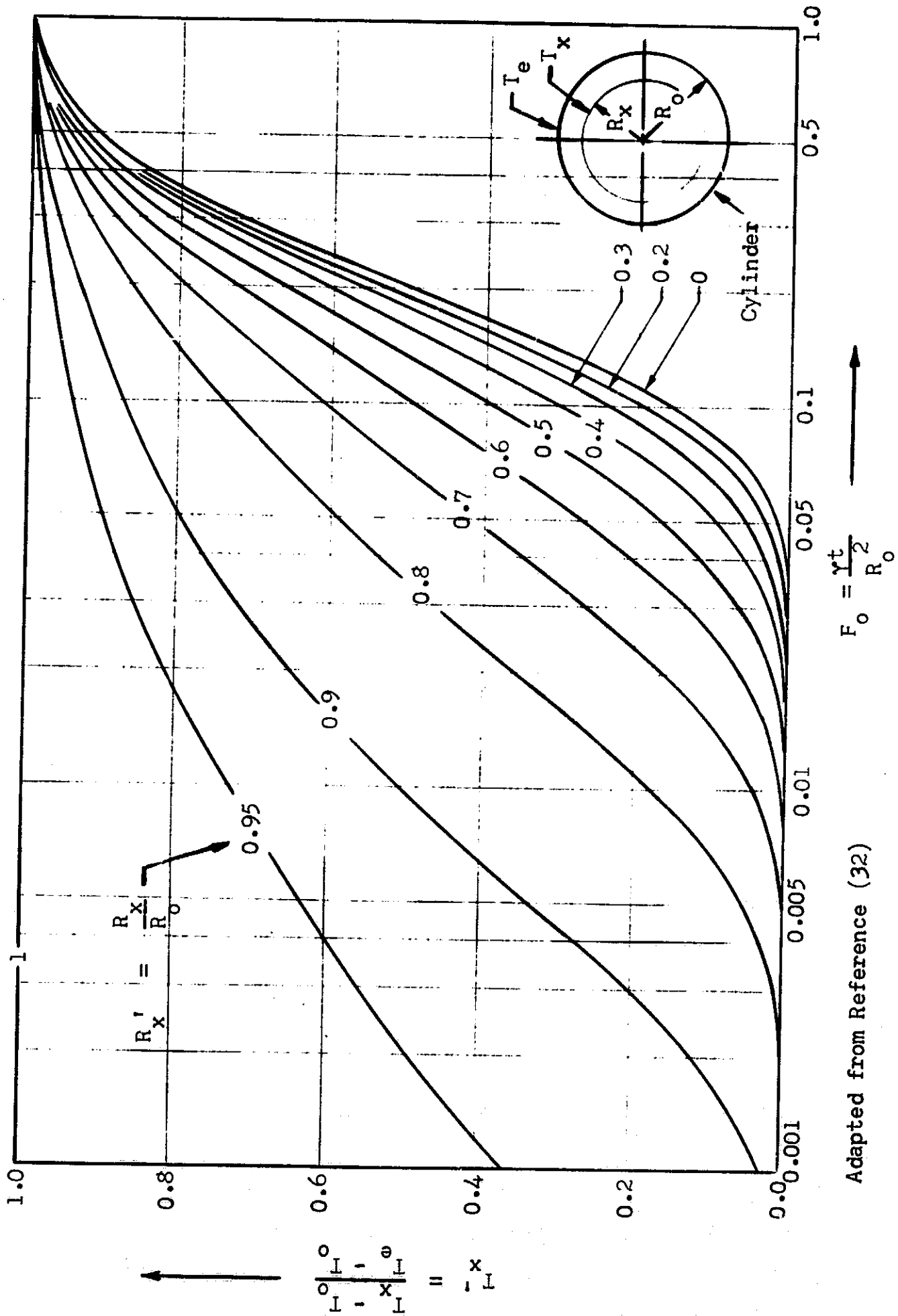


Figure G-1. Transient Temperature Response of a Cylinder, Initially at T_0 , After Being Subjected to a Step Change in External Surface Temperature.

$$\text{or, } T_w - T_c = (T_w' - T_c') (T_e - T_o) \quad (\text{G-12})$$

The withdrawal time, τ , is the time during which $(T_w - T_c)$ exceeds the value given in Equation (G-9). Since $(T_e - T_o)$ is fixed, τ is the time during which $(T_w' - T_c')$ exceeds the value

$$(T_w' - T_c') = \frac{(T_w - T_c)}{(T_e - T_o)} \quad (\text{G-13})$$

The time, t , and the nondimensionalized abscissa, F_o , are related as follows:

$$t = F_o \frac{R_o^2}{\gamma} \quad (\text{G-14})$$

where γ is thermal diffusivity in ft^2/in

Thus, the withdrawal time, τ , is given by

$$\tau = \frac{R_o^2}{\gamma} [F_{o_2} - F_{o_1}] \equiv \frac{R_o^2}{\gamma} \Delta F_o \quad (\text{G-15})$$

where F_{o_2} = the largest value of F_o for which $(T_w' - T_c')$ is greater than the value in Equation (G-13)

F_{o_1} = the smallest value of F_o for which $(T_w' - T_c')$ is greater than the value in Equation (G-13)

$$\Delta F_o = F_{o_2} - F_{o_1}$$

For a given geometry and material, τ can be increased only if ΔF_o is increased. From Figure G-1, $T_w' - T_c'$ must be decreased in order to increase ΔF_o . Since $(T_w - T_c)$ is fixed by Equation (G-9), Equation (G-13) shows that $(T_e - T_o)$ must be increased in order to decrease $T_w' - T_c'$. Thus, larger values of $(T_e - T_o)$ result in longer withdrawal times.

The withdrawal time is also influenced by the thermal diffusivity of the clamp material. The thermal diffusivities of aluminum and stainless steel are

$$\gamma_{\text{alum}} = 3.6 \text{ ft}^2/\text{hr} = 8.8 \text{ in}^2/\text{min}$$

$$\gamma_{S.S.} = 0.17 \text{ ft}^2/\text{hr} = 0.4 \text{ in}^2/\text{min}$$

The thermal diffusivities of other possible clamp materials such as Beryllium, Beryllia, Magnesium, and Titanium lie between these limits.

The withdrawal time for a typical application is calculated assuming the following parameters:

$$R_o = 2 \text{ inches}$$

$$\frac{R_i}{R_o} = 0.8$$

$$\gamma = 8.8 \text{ in}^2/\text{min}$$

Since $\frac{R_i}{R_o} = 0.8$, estimated values for R_w and R_c are

$$R_w = 0.9 R_o$$

$$R_c = 0.6 R_o$$

Examination of the thermal response curves of Figure G-1 at R_w and R_o yields the following results

$T_w' - T_c'$	ΔF_o
0.5	0.04
0.33	0.15
0.1	0.3

If $(T_w' - T_c') = 0.33$ is used, then

$$(T_e - T_o) = \frac{T_w - T_c}{0.33} = 3 (T_w - T_c) \quad (G-16)$$

The withdrawal times for aluminum, and for stainless steel, τ_{alum} , and $\tau_{S.S.}$, respectively may be computed using Equation (G-15) as

$$\tau_{\text{alum}} = \frac{(0.15) (2 \text{ in})^2}{(8.8 \text{ in}^2/\text{min})} = 0.07 \text{ min} \approx 11 \text{ seconds}$$

(G-17)

$$\tau_{S.S.} = \frac{(0.15) (2 \text{ in})^2}{(0.04 \text{ in}^2/\text{min})} = 1.5 \text{ min} = 90 \text{ seconds}$$

It is seen that the feasibility of the transient thermal withdrawal method depends on the size and materials of the clamp. It probably could be used with stainless steel parts, but its use with aluminum is marginal. It is possible that the removal of the cylinder in 10 seconds would damage it.

Thermal stresses will be induced in the shell when its surface temperature is raised to T_e . These stresses will occur wherever the shell is held to the mounting block since the thermal expansion will be restricted at this point. In the limiting case in which thermal expansions are restrained to be zero, the thermal stress, σ_T , will be

$$\sigma_T = \left[\frac{(E \alpha)}{1 - \nu} \right] (T_e - T_o) \quad (G-18)$$

where ν is Poisson's ratio

Combining Equation (G-18) with Equation (G-9) and the minimum interference requirement of Equation (G-5) leads to the following relation

$$\sigma_T = \left(\frac{2 M X}{a} \right) \left(\frac{1}{1 - \frac{R_i^2}{R_o^2}} \right) \left(\frac{1}{1 - \nu} \right) \left(\frac{1}{T_w - T_c} \right) \frac{1}{\mu} \quad (G-19)$$

If the interference is made larger than the minimum value required by Equation (G-5), then σ_T will be correspondingly larger.

As an example, the numerical values from the previous typical application are used giving the result,

$$\sigma_T = \frac{(2) \left(\frac{2}{g} \text{ lb} \right) (50g)}{(3 \text{ in}^2)} \left(\frac{1}{0.36} \right) \left(\frac{1}{0.7} \right) \left(\frac{1}{0.33} \right) = 6000 \text{ psi}$$

where $\nu = 0.3$ has been assumed for Poisson's ratio

If the interference is made equal to twice the minimum amount as a safety factor, then σ_T will be 15,000 psi.

The above example shows that the temporary thermal stresses that occur during withdrawal of the cylinder are reasonable for most of the potential clamp materials, especially in view of the fact that they will not exist long enough to result in long-term dimensional change through creep.

The applied temperature, $(T_e - T_o)$ can be reduced if the shell is made out of a material which has a larger coefficient of thermal expansion than the cylinder material. From Equation (G-8), it is seen that the value of $(T_w - T_c)$ that is necessary in order to withdraw the cylinder is

$$(T_w - T_c) = \left(\frac{\delta}{R}\right) \frac{1}{\alpha_w} - \left(\frac{\alpha_w - \alpha_c}{\alpha_w}\right) (T_c - T_o) \quad (G-20)$$

Comparison with Equation (G-9) shows that the second term on the right hand side of Equation (G-20) is the reduction in $(T_w - T_c)$ that is achieved due to the use of materials having different thermal expansion coefficients.

A possible drawback to the technique of using different thermal expansion coefficients is that the contact stresses will be a function of the ambient temperature. If the sensors and heaters are turned off while the vehicle is in outer space, the ambient temperature, T_a , could change by several hundred degrees. This will result in an additional effective interference δ_a , which is given by Equation (G-8) evaluated with T_w and T_c equal to T_a . Thus,

$$\frac{\delta_a}{R} = (\alpha_w - \alpha_c) (T_o - T_a) \quad (G-21)$$

From Equation (G-1), the additional maximum shear stress, τ_a , due to δ_a is equal to

$$\tau_a = \frac{E}{2} (\alpha_w - \alpha_c) (T_o - T_a) \quad (G-22)$$

As an example, it will be assumed that

$$T_o - T_a = 300^\circ\text{F}$$

$$\alpha_w - \alpha_c = 2 \times 10^{-6} \text{ (degrees)}^{-1}$$

$$E = 10 \times 10^6 \text{ psi}$$

From Equation (G-22)

$$\tau_a = \left(\frac{10 \times 10^6 \text{ psi}}{2}\right) (2 \times 10^{-6} \text{ degrees}^{-1}) (300 \text{ degrees}) = 3000 \text{ psi}$$

Since this stress must be added on to the shear stress resulting from the nominal interference, plastic deformation might occur. If a smaller difference in thermal expansion coefficients is used, this possibility will be reduced, but a larger $(T_o - T_a)$ will be needed to withdraw the cylinder.

In Appendix F, it was shown that the effective spring constant of the hole walls must not vary typically by more than 1%. If a shell is used to hold the cylinder, the shell thickness must be held constant to within

approximately 1/3%. If this thickness is nominally 1/4 inch, then the thickness tolerance is approximately 0.001 inches, which can be maintained with precision machining.

In conclusion, if state-of-the-art machining of cylinders and holes is used, the thermal shrink fit appears to be a feasible method of providing acceptable sensor alignment accuracy. However, this method introduces the following practical disadvantages:

- (1) an external heater is necessary for installation and removal of the cylinder;
- (2) withdrawal of the cylinder must be performed within a short time interval;
- (3) precision machining is required at surfaces other than the mating surfaces, i.e., uniform wall thickness; and
- (4) the technique can only be used with materials having a low thermal diffusivity unless the cylinder and the shell are made from dissimilar materials.

The Use of Hydraulic Pressure as a Clamping Force

Hydraulic pressure can be used to control the interference between the cylinder and the hole wall. This is illustrated in Figure B-6 of Appendix B. For this technique, the cylinder radius is smaller than the hole radius, R_i , by an amount c . After the cylinder is inserted, the outer wall of the tube is pressurized so that the inner wall contracts, and contacts the cylinder. When the cylinder is in place, an effective interference, δ , is established.

$$\delta = u - c \quad (G-23)$$

where u is the deflection of the tube under pressure, p_e , with no cylinder present and is given by (33)

$$\frac{u}{r_i} = \left(\frac{2}{1 - \frac{R_i^2}{R_o^2}} \right) \frac{p_e}{E} \quad (G-24)$$

Equation (G-4) gives the interference in terms of p , the contact pressure between the cylinder and the hole, as

$$\frac{\delta}{R_i} = \frac{2p}{E} \left(\frac{1}{1 - \frac{R_i^2}{R_o^2}} \right) \quad (G-4)$$

The relation between external pressure p_e , contact pressure p , and initial clearance c , is obtained by combining Equations (G-23), (G-24), and (G-4).

$$p_e = p + \left(\frac{E}{2}\right) \left(1 - \frac{R_i^2}{R_o^2}\right) \frac{c}{R_i}$$

or

$$p_e = p + \frac{E}{2} \left(\frac{R_o + R_i}{R_o}\right) \left(\frac{h}{r_o}\right) \frac{c}{R_i} \quad (G-25)$$

where $h = R_o - R_i =$ wall thickness

The minimum acceptable clamping pressure is given by Equation (G-3). As a typical example, the following parameters will be assumed:

$$\begin{aligned} R_i &= 2 \text{ inches} \\ R_o &= 2 \frac{1}{4} \text{ inches} \\ E &= 10 \times 10^6 \text{ psi} \\ c &= 0.0005 \text{ inches} \\ M \ddot{x} &= 100 \text{ lb} \\ a &= 12 \text{ in}^2 \\ \mu &= 0.1 \end{aligned}$$

From Equation (G-3), the minimum contact pressure is

$$p = \frac{(100 \text{ lb})}{(12 \text{ in}^2) (0.1)} = 83 \text{ psi}$$

A conservative contact pressure $p = 250$ psi will be assumed. The external pressure, p_e , from Equation (G-25) is then

$$\begin{aligned} p_e &= 250 + \frac{(10 \times 10^6)}{(2)} \frac{(4.25 \text{ in})}{(2.25 \text{ in})} \frac{(0.25 \text{ in})}{(2.25 \text{ in})} \frac{(5 \times 10^{-4} \text{ in})}{(2 \text{ in})} \text{ psi} \\ &= 520 \text{ psi} \end{aligned}$$

This small pressure will not produce plastic deformations in the cylinder or in the shell. In order that the effective spring constant of the clamp be uniform to within 1%, the wall thickness h , and all end effects associated with it must be machined to within 1/3% accuracy, as noted in Appendix F. For the preceding example in which h is equal to 1/4 inch, this implies machining the wall thickness to an accuracy of 0.001 inches.

It is important that the hydraulic clamping walls have sufficient bending stiffness to resist accelerations perpendicular to the cylinder axis without allowing plastic deformation. Approximate analysis using plate theory (34) shows that the 1/4 inch tube walls of the preceding case will not deflect significantly under the contact pressure caused by a cylinder undergoing a sidewise acceleration of 50 g's.

In order to generate the external pressure, p_e , that is used to contract the cylinder walls, a closed volume of oil is compressed by some form of pressurizing plug. This plug must have seals that prevent oil leakage from allowing the pressure to decrease. However, if the volume is maintained perfectly constant, then moderate changes in ambient temperature will cause large changes in oil pressure.

If a change in temperature, ΔT , is applied to a volume of oil that is allowed to expand freely, then the fractional volume change is given by

$$\frac{\Delta V}{V} = \alpha \Delta T \quad (G-26)$$

where

α is the thermal expansion coefficient of the oil

V is the volume of oil

If a fixed amount of oil undergoes a fractional volume change, $\Delta V/V$, then its pressure, p , will increase an amount, Δp , that is

$$\Delta p = - \beta \left(\frac{\Delta V}{V} \right) \quad (G-27)$$

where β is the bulk modulus of the oil

If the oil is held in a rigid container, then an increase in temperature, in effect, causes a negative fractional volume change that results in a pressure increase that is given by

$$\Delta p = \alpha \beta \Delta T \quad (G-28)$$

For a typical hydraulic oil,

$$\alpha = 0.5 \times 10^{-3} \frac{\text{in}^3 \text{ } ^\circ\text{F}}{\text{in}^3}$$

$$\beta = 2 \times 10^5 \text{ psi}$$

From Equation (G-28),

$$\Delta p = 100 \Delta T \text{ psi} = 5000 \text{ psi}$$

for a $\Delta T = 50^\circ\text{F}$

Large increases in pressure due to temperature changes can be avoided by letting the volume contract and expand. The pressure can be established by

a spring loading mechanism. A properly sized Belleville washer will produce a reasonably constant force for a large range of deflections. In the above example, if a total temperature range of 400°F is expected, then the spring will have to accommodate a volume change which, from Equation (G-26), is

$$\frac{\Delta V}{V} = \frac{(0.5 \times 10^{-3})}{^{\circ}\text{F}} (400^{\circ}\text{F}) = 20\%$$

In conclusion, if state-of-the-art of machining cylinders and holes is used, the hydraulic cylinder-in-hole clamping technique appears to be a feasible method of providing acceptable alignment accuracy. However, it has the following practical disadvantages:

- (1) It is prone to failure if there is oil leakage.
- (2) It is relatively complicated, requiring a sealed pressurizing plug and a spring-loaded oil volume.
- (3) Precision machining is required at surfaces other than the mating surfaces, e.g., uniform wall thickness, etc.

The Use of a Split Cylinder Clamp

The interference between the cylinder and the hole can be controlled by a split clamp such as the one illustrated in Figure G-2(a). The cylinder and hole radii are R_i , and R_o , respectively. A clamping force is generated by an interference fit that results because R_i exceeds R_o by an amount δ . Each half of the clamp will make contact with the cylinder when its center of curvature is a distance, s , from the center of the cylinder. It can be shown that

$$s = \sqrt{2 \delta r_o} \quad (\text{G-29})$$

If the corners of the clamps are relieved so that initial contact is made at angle ψ , as shown in Figure G-2(b), then the distance, s , is given by

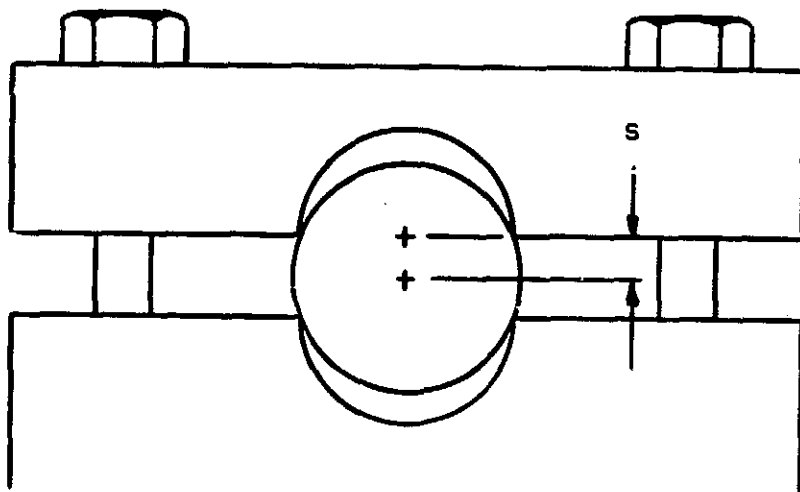
$$\frac{s}{R_i} = \sqrt{\sin^2 \psi + \frac{2\delta}{R_i}} - \sqrt{\sin^2 \psi} \quad (\text{G-30})$$

This can be approximated as follows

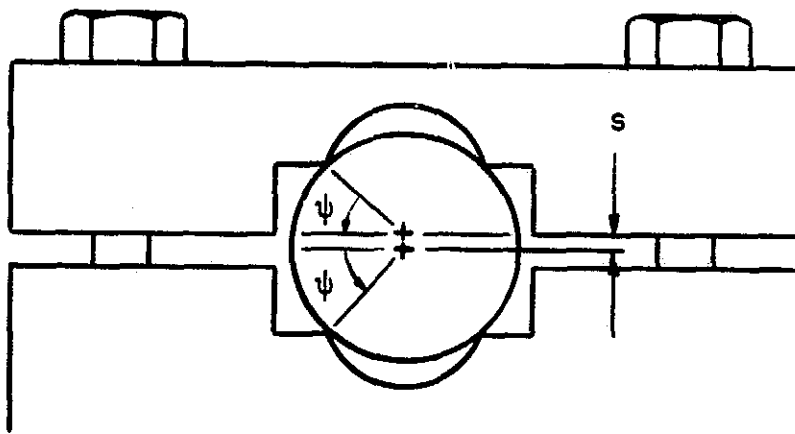
$$s \approx \frac{\delta}{\sin \psi} \quad (\text{G-31})$$

provided that

$$\psi^2 \gg \frac{2\delta}{R_i}$$



(a)



(b)

Figure G-2. Two Piece Split Clamp

The following example illustrates the effect of relieving the corners.
Let

$$\delta = 0.0001 \text{ in}$$

$$r_o = 2 \text{ inches}$$

If there is no relief, from Equation (G-29)

$$s = \sqrt{2 (100 \mu\text{in}) (2 \text{ in})} = 0.020 \text{ inch}$$

If a relief of $\psi = 10^\circ$ is used, then from Equation (G-31)

$$s = \frac{(100 \mu\text{in})}{0.17} = 0.0006 \text{ inch}$$

Initially the cylinder and each clamp contact each other at two points. When the two clamping members are pulled together, the contact zone spreads around the circumference of the clamp as the cylinder and the clamps deform. This deformation, and the resulting contact pressure is influenced by local frictional effects which are not readily predicted. If the top clamp deforms more than the bottom clamp, or the left half deforms more than the right half, the cylinder center line will shift causing an alignment error. In the worst possible case in which the top half deforms and the bottom half is rigid, the cylinder center will shift by a distance s . By this reasoning, in Equations (F-1) through (F-4) of Appendix F, the quantity δ should be replaced by s . Thus, the split cylinder clamp has symmetry tolerances that are $(1/\sin \psi)$ more stringent than other cylindrical clamps in which the interference is controlled uniformly around the periphery.

If the relief angle, ψ , is increased in order to make s approach δ , the split cylinder clamp becomes similar to two block-on-plane clamps which have slightly curved mating surfaces. The split cylinder clamp requires external forces to bring the two clamps together. Consequently, there is a force uniformity problem similar to the block-on-plane clamp. The mating surfaces of the two clamps must have the same flatness as the block-on-plane mating surfaces and the distance between the curved clamping surfaces, and the mating planes is also subject to a fine tolerance.

An alternative type of split cylinder clamp is shown in Figure B-11 of Appendix B. Once again, unpredictable friction effects will influence the deformation and contact pressure since the interference mechanism is essentially the same as has previously been described. This configuration has the additional disadvantage that the asymmetry caused by the single slit is likely to enable residual machining stresses to cause irregularities in the hole radius.

In conclusion, the split type of cylinder clamp is not a particularly satisfactory way to obtain ultra precision alignment. Although the method is theoretically possible if state-of-the-art machining is used, the performance is subject to undesirable uncertainties. Moreover it is necessary to satisfy both flatness and cylindrical machining tolerances.

APPENDIX H

ANALYSIS OF MISALIGNMENT DUE TO THERMAL EXPANSION

Asymmetric thermal gradients can lead to thermal expansions that cause distortion of the clamp. These distortions can cause unacceptable sensor misalignment errors. The most important sources of asymmetry are nonuniform thermal contact resistances, and variations in the heat output of the sensor. These effects have been analyzed so that the required tolerances on symmetry can be established. In addition, a method for greatly reducing misalignment due to variations in contact resistance has been evaluated.

Lumped parameter analyses have been performed for typical plane-on-plane, and cylinder-in-hole fixed clamp concepts. The assumptions of the analyses and the results for two specific examples are presented in this appendix.

Plane-on-Plane Clamp

A thermal analysis was performed for the typical plane-on-plane clamp that is shown in Figure H-1. The clamp consists of a cradle type of fixture holding a cylindrical sensor. The cradle has four legs that contact the mounting block at four mounting pads. Heat flows out of the sensor, down the four cradle legs, and into the mounting block. Some of the heat is radiated and convected away from the sensor surface. An optional shunt thermal path having a high conductivity is also indicated.

The shunt conductive path can be designed to have a very low contact resistance between the clamp and the mounting block. If this path carries most of the heat away from the sensor, variations in the contact resistance of the four mounting pads will not materially affect the temperature distribution.

The above-described thermal system will be idealized as follows:

- (a) Heat flow from the sensor will be considered to come from a single heat source, q_T .
- (b) Unless special measures are employed, such as a surrounding boiling 2-phase medium, surface radiation and convection heat transfer can be shown to be negligible in comparison with conduction through the structure to the mounting block. Thus, convection and radiation are ignored in the analysis.
- (c) All heat leaving the source q_T is assumed to flow through five parallel thermal paths consisting of lumped thermal resistance, R_{ij}

$$\text{where } R_{ij} = \frac{\Delta T_{ij}}{q_{ij}} \quad \left[\begin{array}{l} i = 1-4 \\ j = 1-4, s \end{array} \right] \quad (\text{H-1})$$

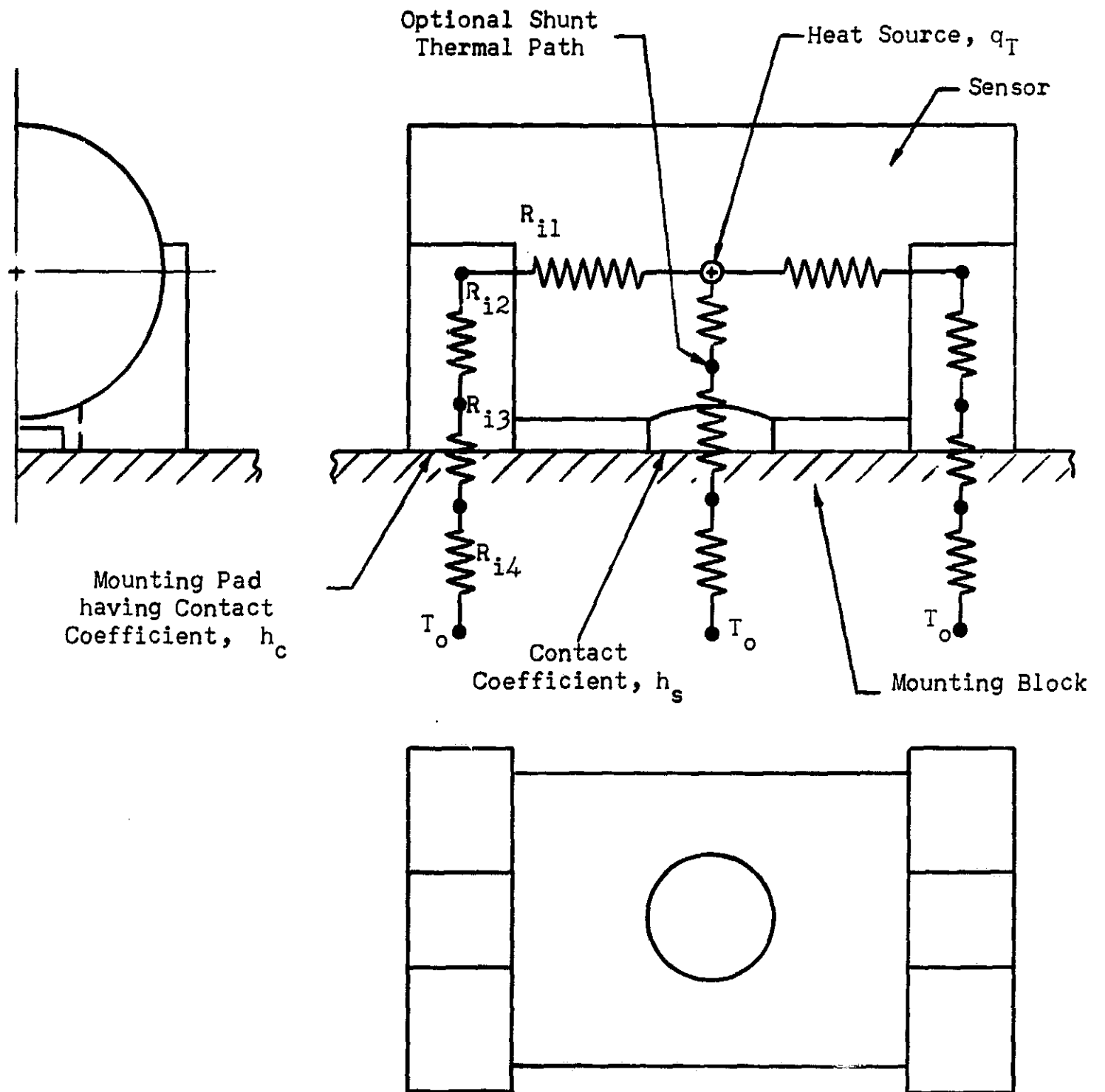


Figure H-1. Plane-on-Plane Fixed Clamp and Lumped-Parameter Thermal Resistances

where ΔT_{ij} is the temperature drop across R_{ij}

q_{ij} is the heat flow through R_{ij}

(d) Each thermal path, R_i , consists of the series combination of the following resistances R_{ij} , where

(1) R_{i1} is the resistance to heat flow through the sensor;

(2) R_{i2} is the resistance to heat flow through a leg of the cradle;

(3) R_{i3} is the contact resistance to heat flow through the interface between the mounting pad and the mounting block;

(4) R_{i4} is the resistance to heat flow through the mounting block.

(e) The mounting block is an infinite slab which has a constant temperature, T_0 , at a distance infinitely far away from the mounting pad.

(f) The system is at steady-state.

The above assumptions enable the thermal system shown in Figure H-1 to be reduced to the linear thermal resistance network shown in Figure H-2. This network can be solved by straightforward application of Kirchoff's Laws and the temperature versus heat flow relationships for each element. The network solution yields the temperatures at discrete points in the system as functions of the sensor heat source and the thermal resistances.

Sensor misalignment will result from unequal thermal expansions of the cradle legs. These expansions can be calculated by integrating the thermal strain over the length of the leg. The thermal strain is obtained by assuming that the temperature in the leg varies linearly between the temperature levels at the ends of the leg. Since these levels are known from the network solution, it is possible to relate the thermal expansions of the legs to the heat flow and the various thermal resistances. Asymmetries in the thermal path will cause the four legs to have different amounts of thermal expansion. The resulting angular misalignment can be expressed in terms of the deviations of the various parameters from their nominal values. The most important deviations are due to the contact heat transfer coefficient in a vacuum References (22) through (27). Unless very large contact pressures are used, this coefficient is strongly dependent on the properties of the individual contacting surfaces. Moreover, the scatter of data is considerably larger than 10%. Thus in a vacuum, it is extremely difficult to avoid significant differences in the contact resistances. Also, if the heat source is not symmetrically located, changes in heat output will produce asymmetrical temperature distributions.

The general expressions that have been derived for the various temperature differences and the resulting misalignment are evaluated for the geometry shown in Figure H-3. The clamp and the mounting block are assumed

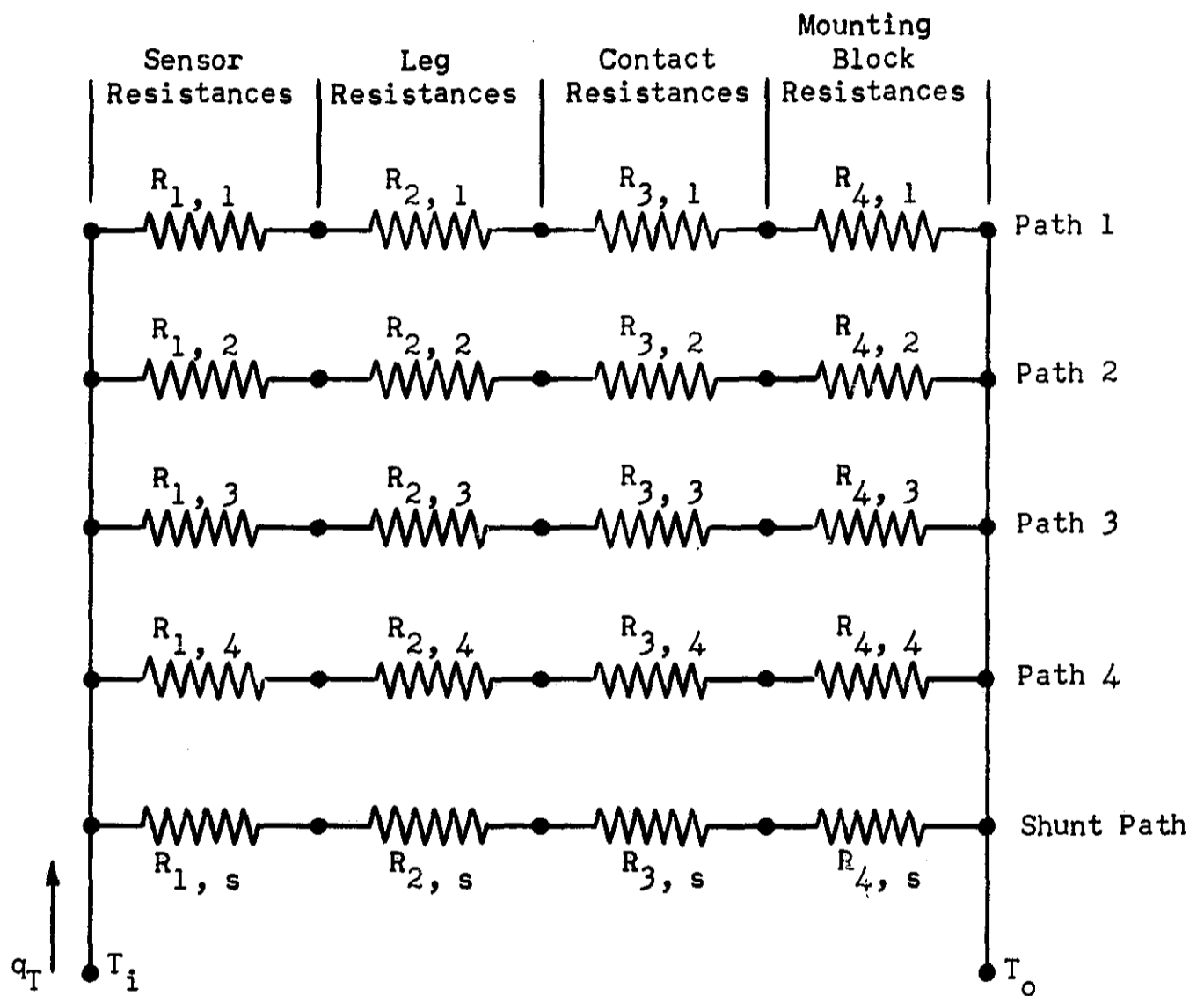


Figure H-2. Lumped-Parameter Thermal Network Representing Plane-on-Plane Clamp

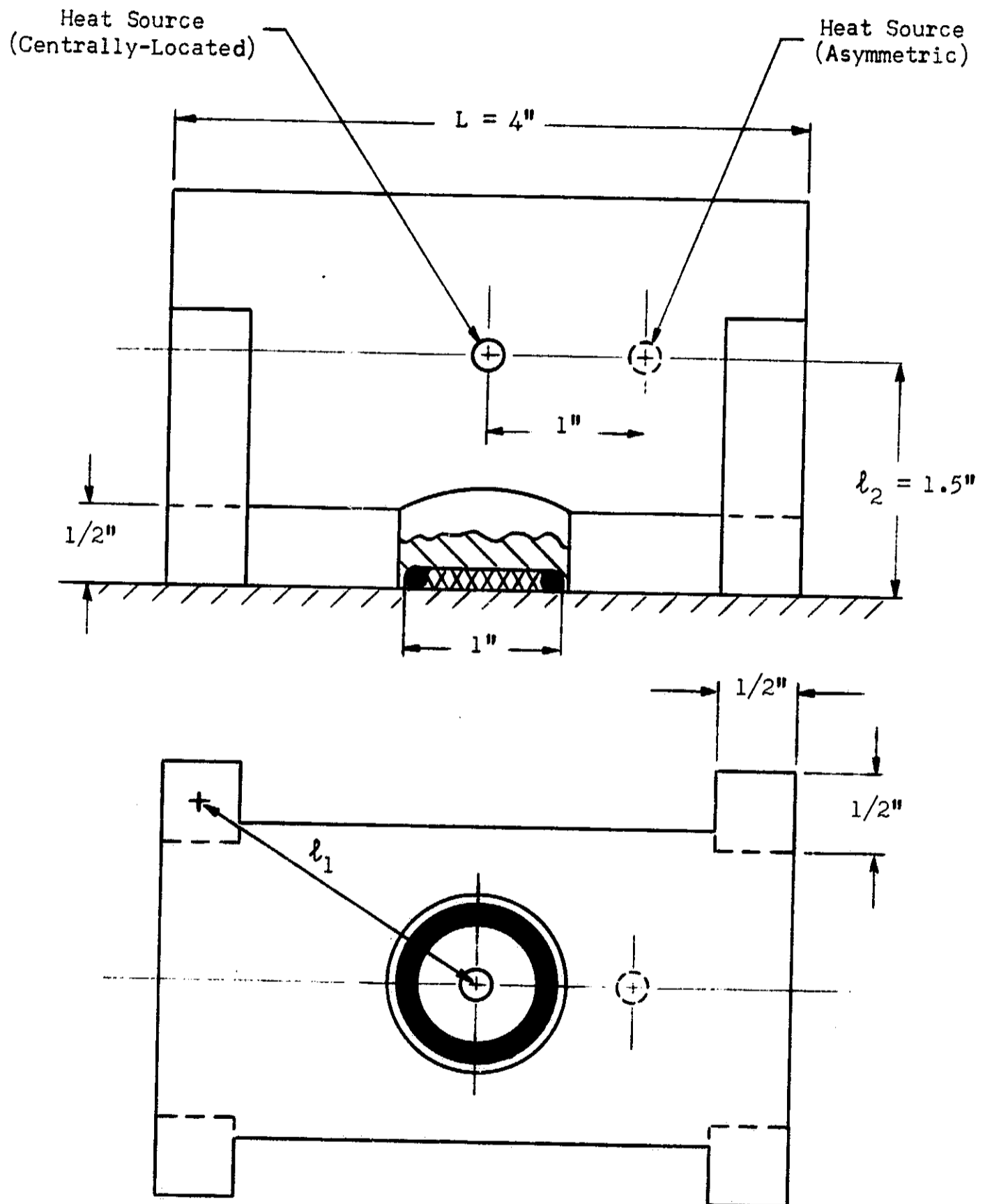


Figure H-3. Dimensions of Plane-on-Plane Clamp Selected for Thermal Calculations

to be made of stainless steel. The heat source has a nominal value of 10 watts. The variations from the nominal values of the contact resistances of the left-hand and right-hand mounting pads are optimistically assumed to be +10% and -10%, respectively.

The calculated misalignment error of this configuration is shown in Figure H-4 as a function of the nominal contact resistance heat transfer coefficient, h_c . The error is plotted for two cases, with and without a thermal shunt path. The shunt path is assumed to have a contact heat transfer coefficient h_s of 10^4 BTU/hr ft² °F. This large value can be obtained if a highly-conductive thin film of oil is used at this interface. The oil would have to be sealed into the clamp if the unit were used in a vacuum environment.

It is clearly seen that if a suitable shunt thermal path is employed, variations in the mounting pad contact resistance do not cause appreciable misalignment error. In the absence of a shunt path, however, low values of h_c lead to unacceptable errors. In order to avoid these low values of h_c in a vacuum environment, it is necessary to use large contact pressures that will adversely affect the long-term dimensional stability of the clamp. The above conflicting requirements on the mounting pad contact pressures can be avoided if the shunt thermal path is used.

Sensors generally do not have their heat source located at the geometrical center. Consequently, fluctuations in the heat source output will cause an angular misalignment. The curves of Figure H-4 can also be used to predict this misalignment error for the geometry of Figure H-3 for the case where heat source, q_T , is located halfway between the center and the edge of the sensor, (shown by the dashed circle in Figure H-3) and deviates by 20% from its nominal value. The contact resistances are assumed to remain at their nominal values for this case. Since heat source fluctuations are normally considerably less than 20%, this source of error is less important than nonuniformities in contact resistance.

In conclusion, for the configuration that was analyzed, small variations in thermal contact resistance can cause unacceptable misalignment errors. However, if a shunt thermal path having a low-contact resistance is used, the error can be reduced to an acceptable level. Variations in sensor heat output produce less serious misalignment.

Cylinder-in-Hole Clamp

A thermal analysis was performed for the cylinder-in-hole fixed clamp that is shown in Figure H-5. The sensor has an attached cylinder that is inserted into a hole in the mounting structure. Heat flows out of the sensor, down the cylinder and into the mounting block.

This thermal system can be idealized as follows:

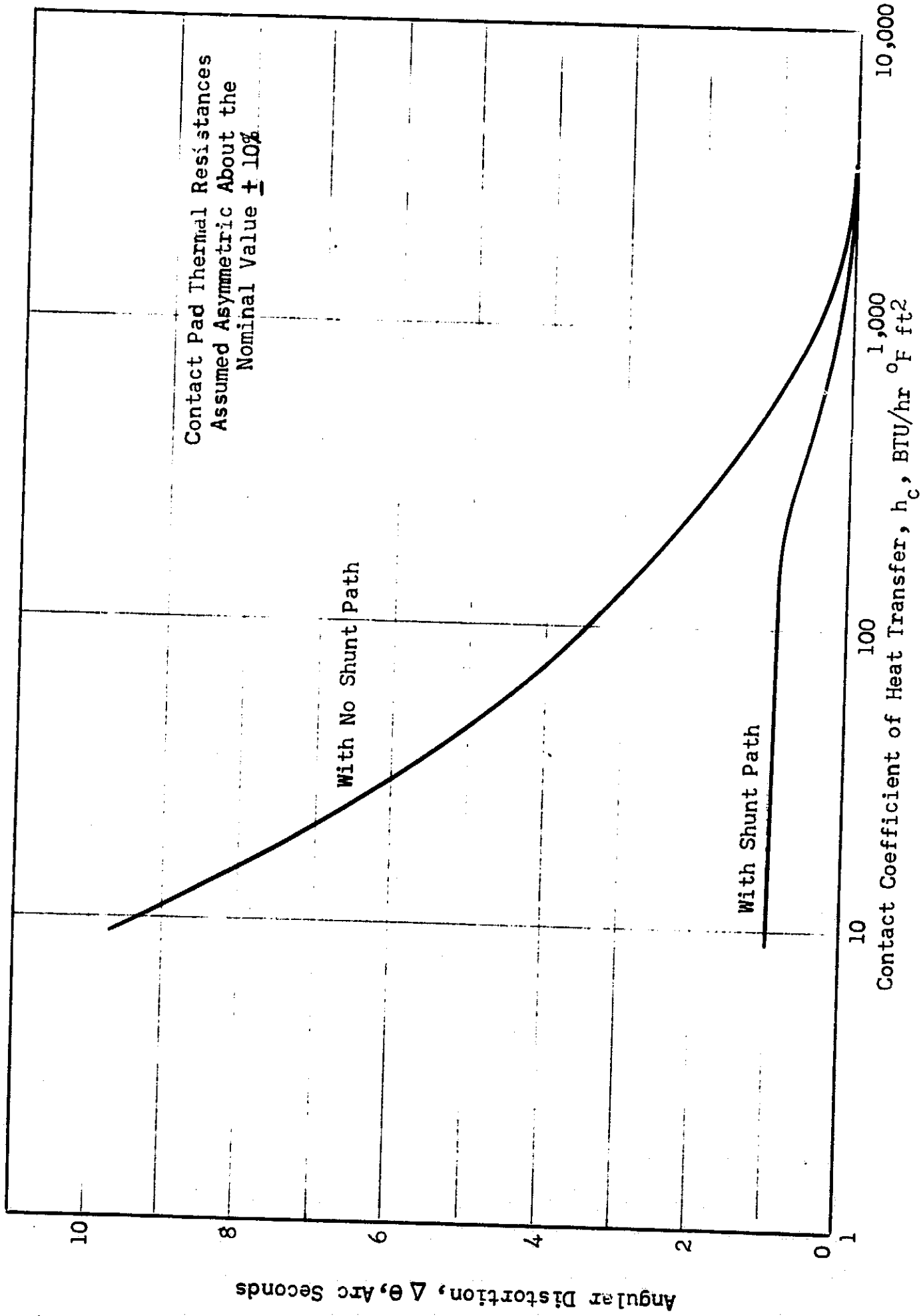


Figure H-4. Angular Distortion of the Plane-on-Plane Clamp Due to Asymmetric Thermal Contact Resistances

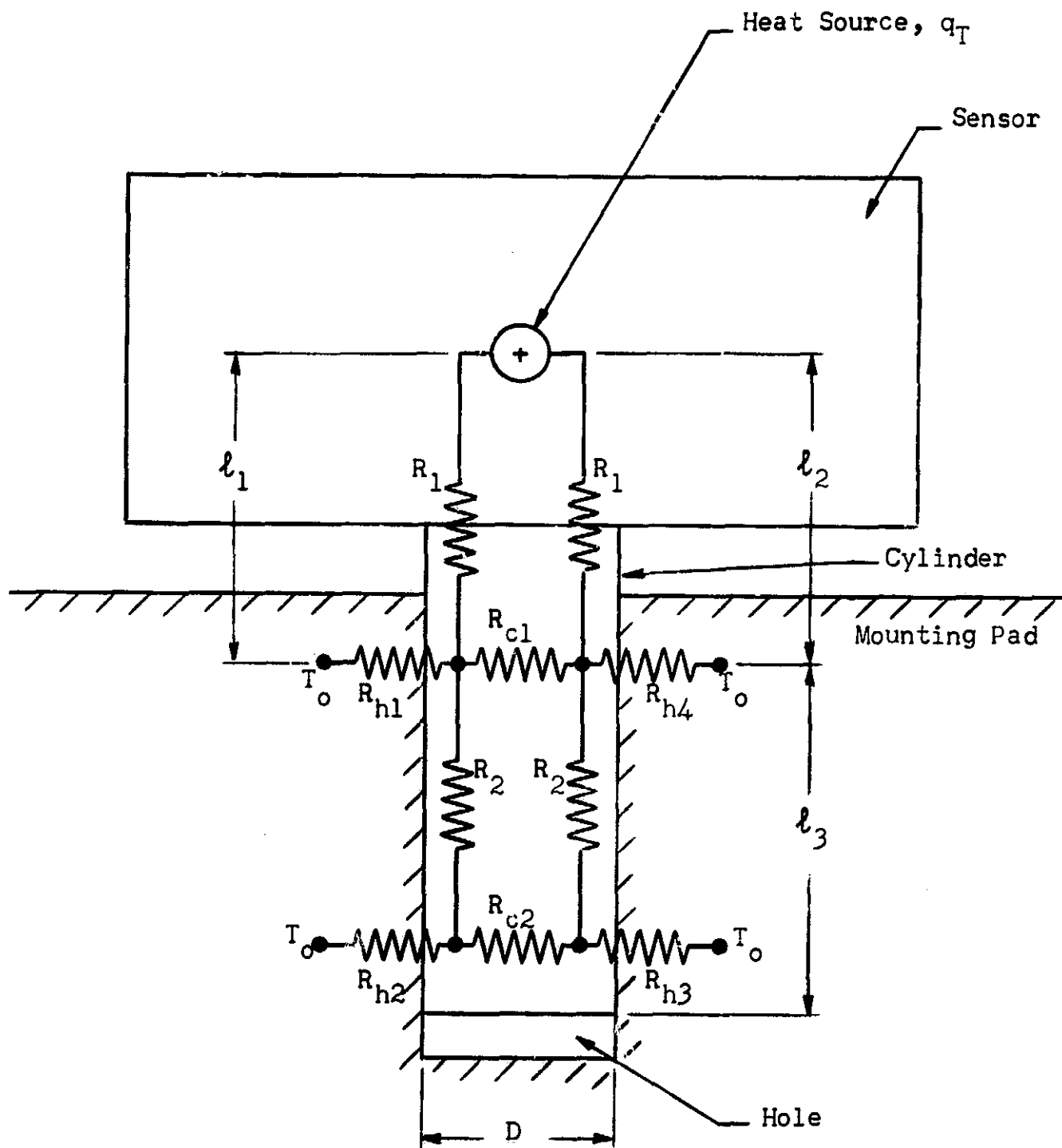


Figure H-5. Cylinder-in-Hole Fixed Clamp, and Lumped-Parameter Thermal Network

- (a) Heat flow from the sensor will be considered to come from a single heat source, q_T .
- (b) Convection and radiation heat flow are negligibly small compared with conduction heat flow.
- (c) The cylindrical supporting leg is replaced by one of square cross section to idealize it as a two-dimensional model.
- (d) All heat leaving the source, q_T , flows through two parallel resistances R_1 having the lengths l_1, l_2 that are indicated in Figure H-5.
- (e) Heat flows out of the cylinder into the mounting block through four contact resistances, R_{h1}, R_{h2}, R_{h3} and R_{h4} .
- (f) Heat flow within the cylinder takes place through four resistances, R_{c1}, R_{c2} , and two R_2 .
- (g) The mounting block is an infinite slab which has a constant temperature, T_0 , at a distance infinitely far away from the cylinder.
- (h) The system is at a steady-state condition.

The lumped-resistance thermal network that results from the above assumptions is also shown in Figure H-5. The various resistances are superimposed on the actual parts of the system that they represent. The analysis of this network is similar in principle to the previously described analysis for the plane-on-plane clamp.

A misalignment error will occur if there is asymmetry in the system. The primary source of asymmetry is deviation of the contact resistances from their nominal values. This will cause unequal temperature drops across the two resistances, R_1 . Thus, a misalignment error will occur due to unequal thermal expansions of the two portions of the cylinder and sensor that are indicated by lengths l_1 and l_2 in Figure H-5. The misalignment error, $\Delta\theta$, is given approximately by

$$\Delta\theta = \frac{l_1 - l_2}{D} \quad (H-2)$$

It is assumed that the cylinder (of diameter D) is rigidly clamped to the hole wall over the rest of its length, l_3 .

The misalignment error was calculated for the specific configuration shown in Figure H-6. The materials were assumed to be stainless steel, and the heat source output is ten watts. The error is plotted in Figure H-7 as a function of the nominal thermal contact heat transfer coefficient, h_c .

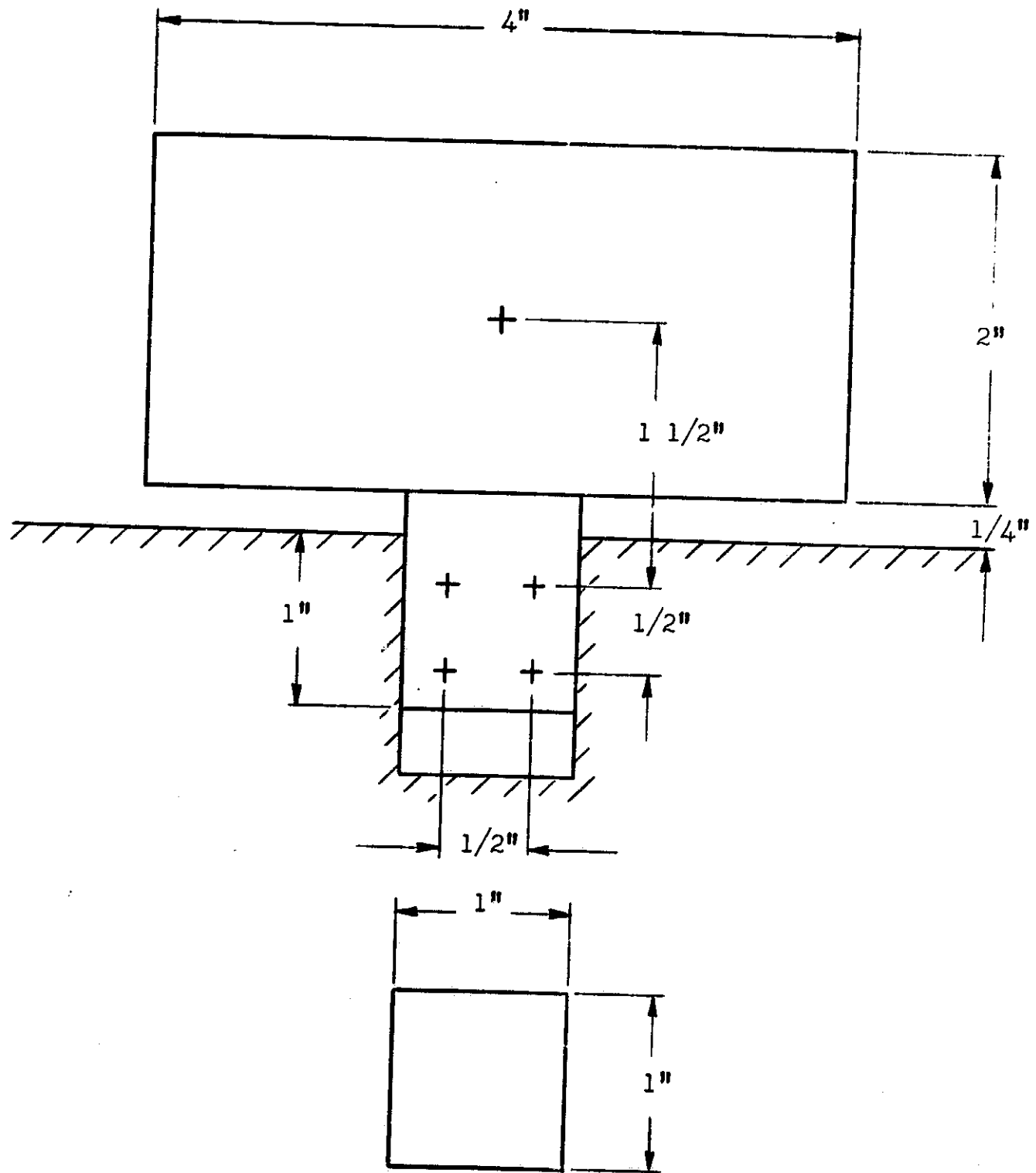


Figure H-6. Dimensions of Idealized
Cylinder-in-Hole Configuration

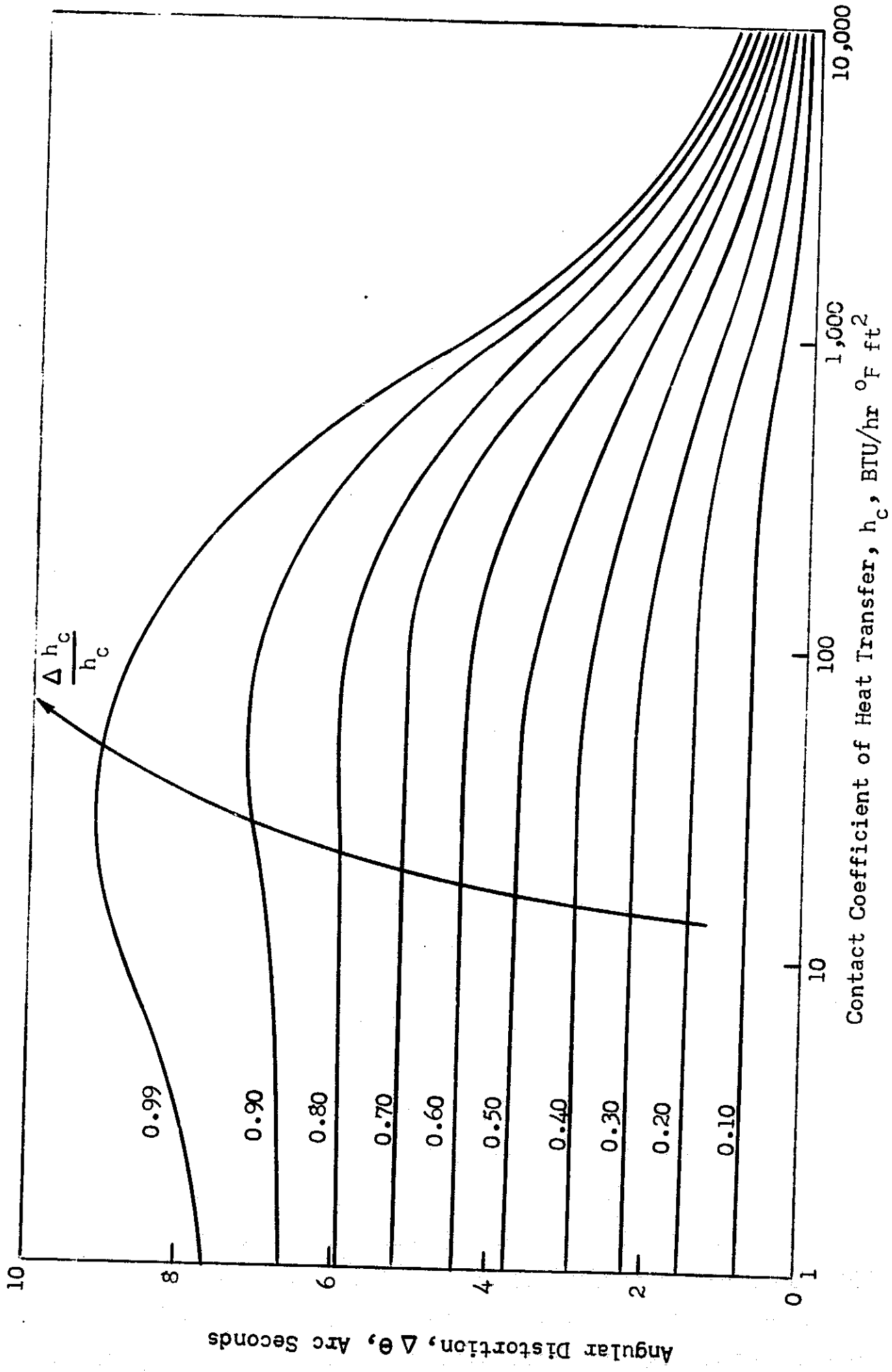


Figure H-7. Angular Distortion of Cylinder-in-Hole Clamp Due to Asymmetric Thermal Gradients

The parameter is the percent deviation of the contact heat transfer coefficient from its nominal value. It was assumed that R_{h1} and R_{h2} were smaller than their nominal values, and that R_{h3} and R_{h4} were larger than their nominal values.

The curves in Figure H-7 indicate that serious misalignment errors can result unless large values of contact coefficient are achieved. It can be seen that a 10% variation in contact resistance causes considerably less misalignment for the cylinder-in-hole clamp than for the plane-on-plane clamp. This effect results from heat flow through the resistances R_{c1} and R_{c2} , which reduces asymmetry about the vertical centerline of the system.

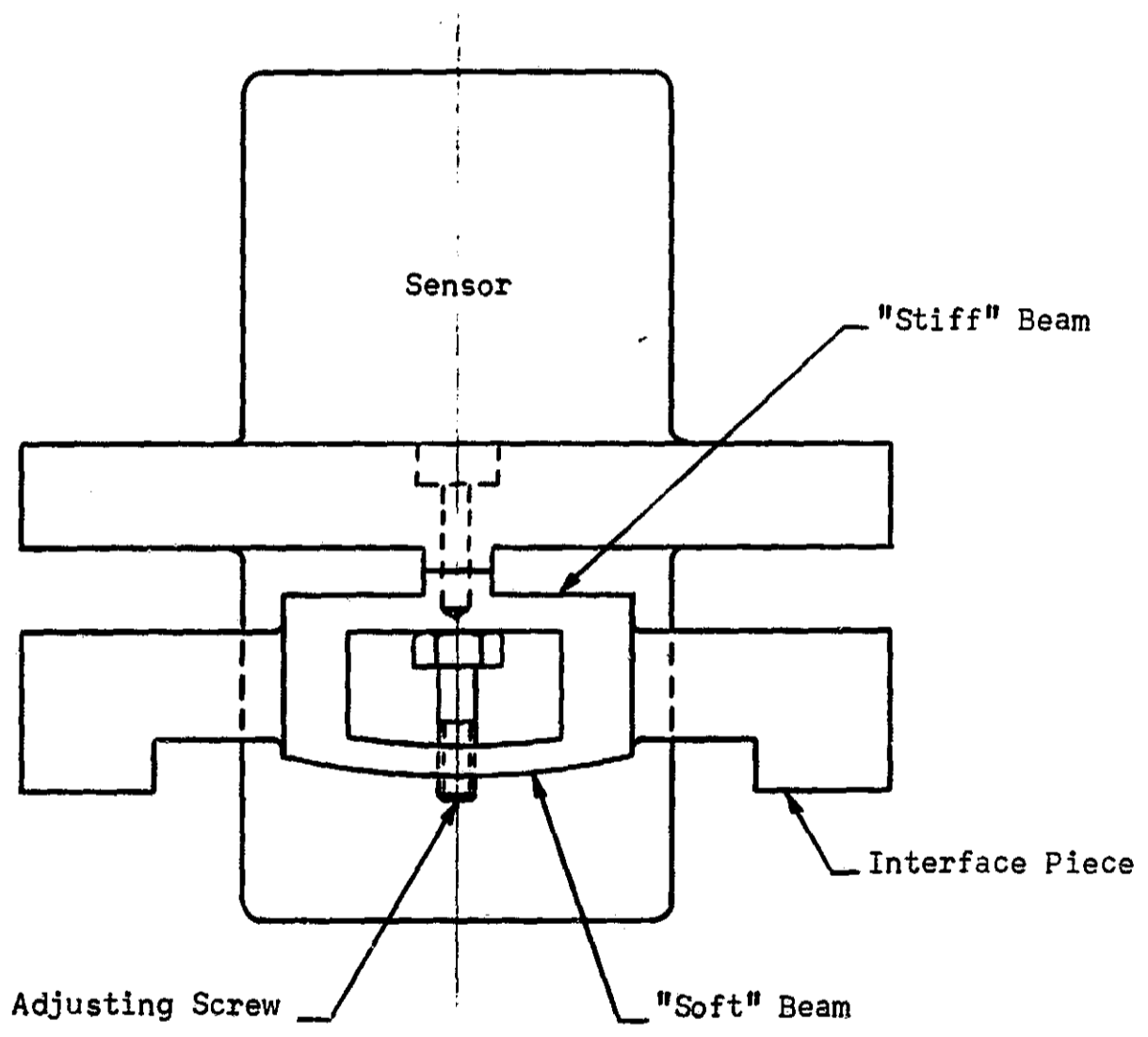
A symmetric, highly-conductive shunt thermal path between the sensor and the mounting block could be provided. The resulting reduction of the misalignment error will be similar to that which was analyzed for the plane-on-plane clamp.

In conclusion, serious misalignment can also occur in the cylinder-in-hole fixed clamp if large percentage variations in thermal contact resistance occur around the cylinder. When no highly-conducting thermal shunt path is used, however, the cylinder-in-hole concept is not as sensitive to these contact resistance variations as the plane-on-plane. The physical reason for this reduced sensitivity is the cross-conduction effects from one side of the cylinder to the other.

APPENDIX I

SCHEMATIC DIAGRAMS OF ADJUSTABLE CLAMP CONCEPTS

This appendix presents schematic diagrams of the various adjustable clamp concepts retained for evaluation after initial concept generation. In each case, the essential adjustment and support elements are illustrated. Discussion of the concepts and their distinguishing features is included in the main body of the report.



Note: Typical Configuration for Each of 3 Legs

Figure I-1. Adjustable Internal Clamp
 Three-Point Sensor Support
 Differential Beam Adjustment Concept

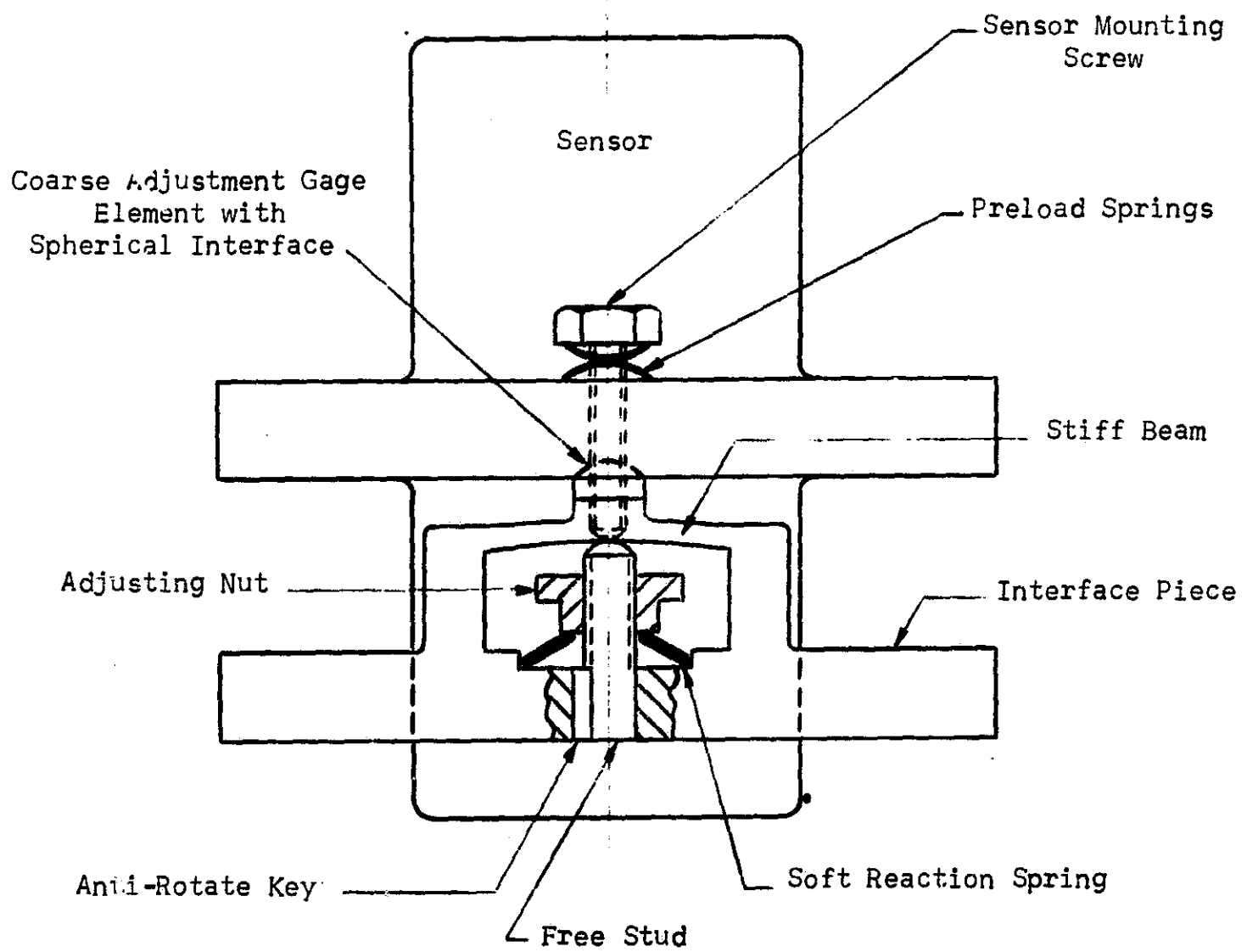


Figure I-2. Adjustable Internal Clamp
 Three-Point Sensor Support
 Differential Beam and Spring Adjustment Concept

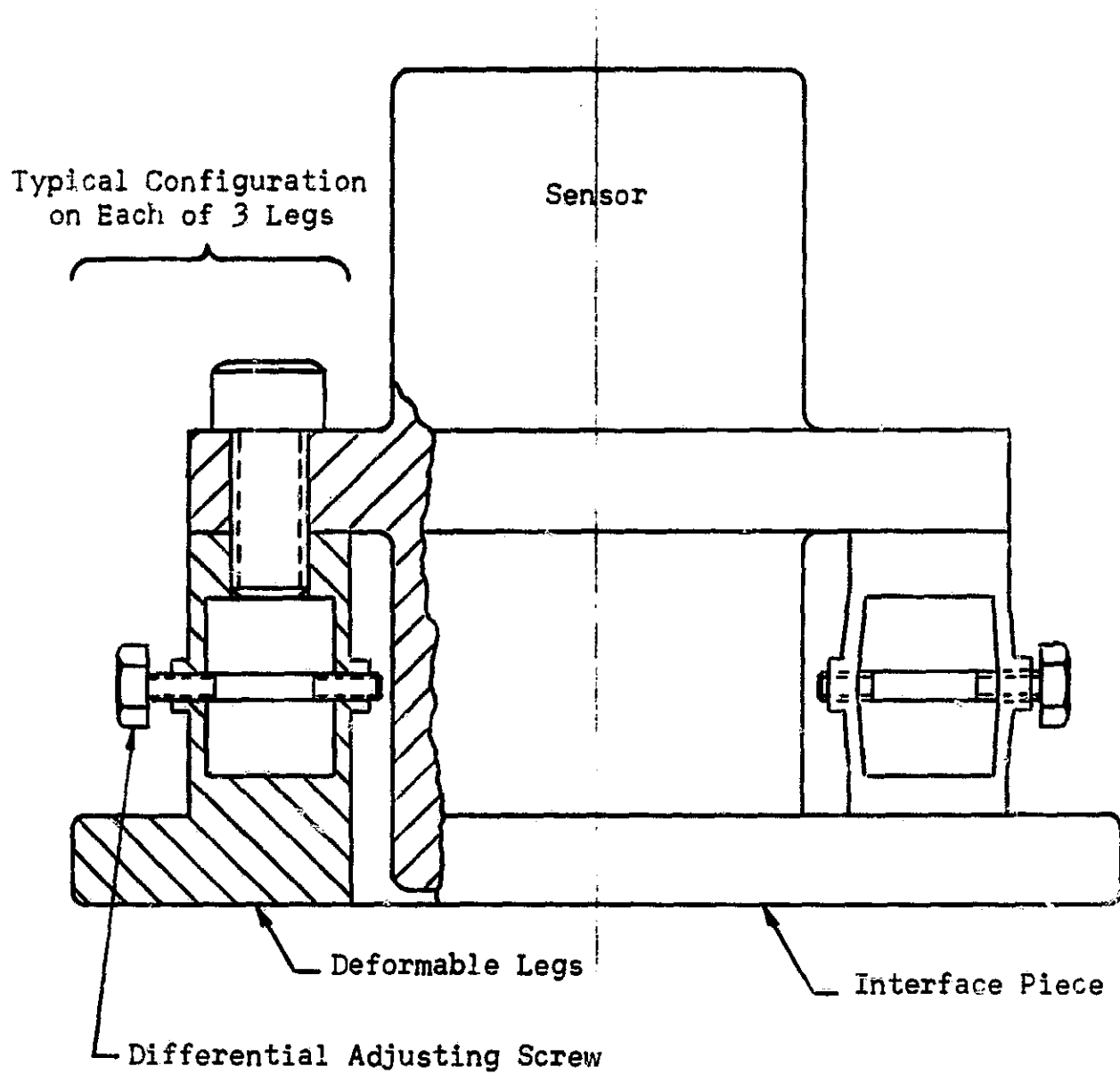


Figure I-3. Adjustable Internal Clamp
 Three-Point Sensor Support
 Catenary Action Adjustment Concept

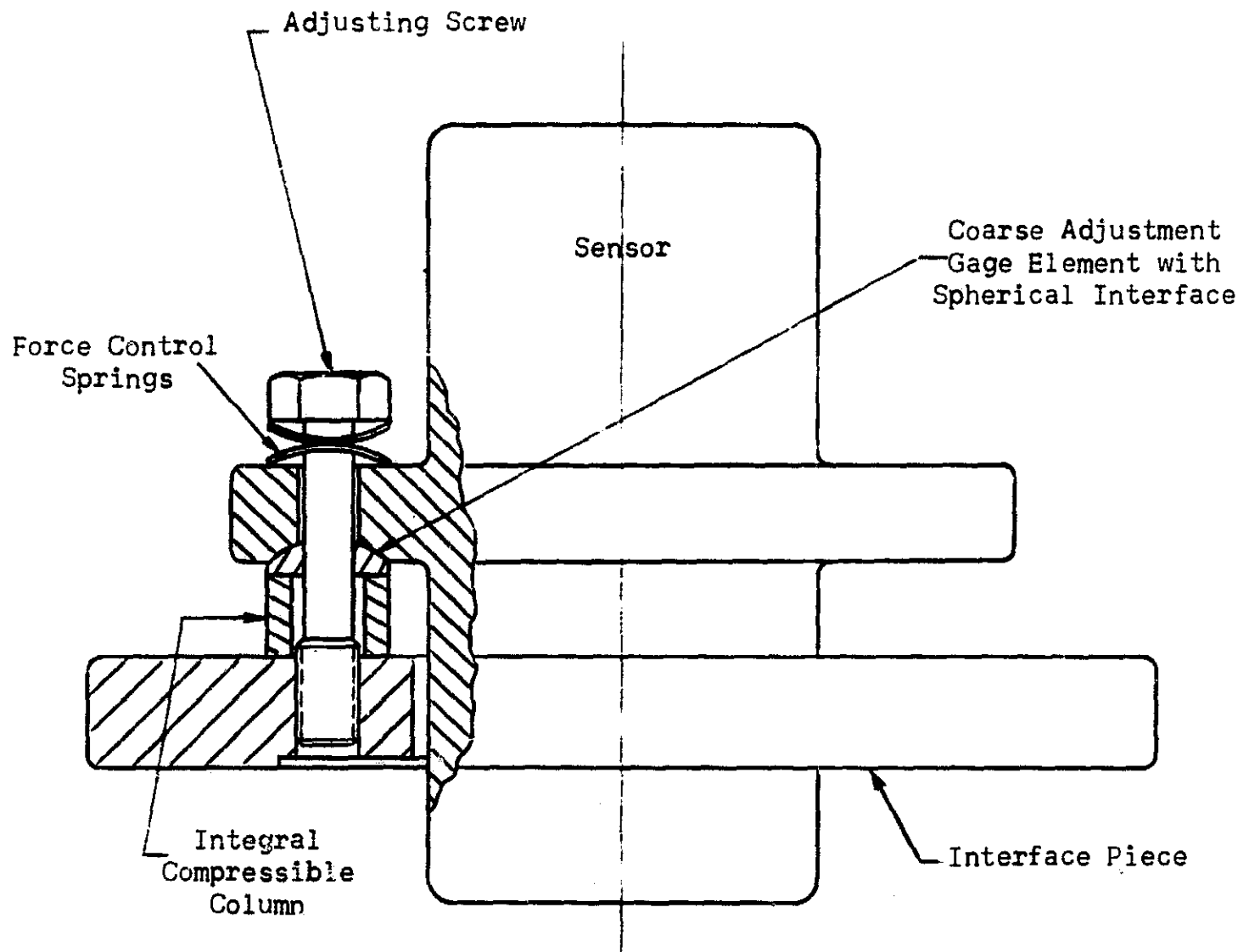


Figure I-4. Adjustable Internal Clamp
 Three-Point Sensor Support
 Interchangeable, Compressible Column Concept

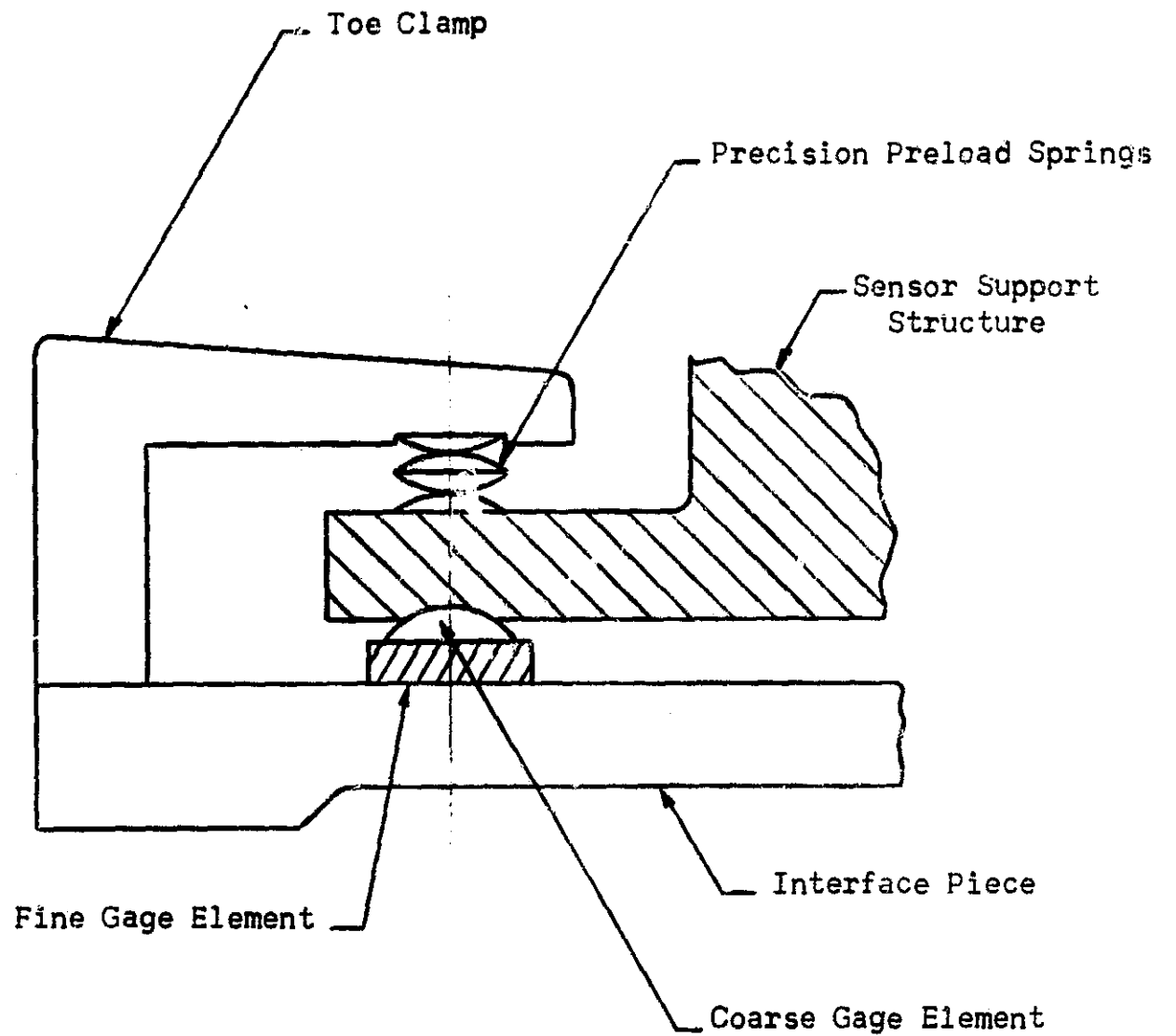


Figure I-5. Adjustable Internal Clamp
Three-Point Sensor Support
Selected Fit Adjustment Using Precision Gage Elements

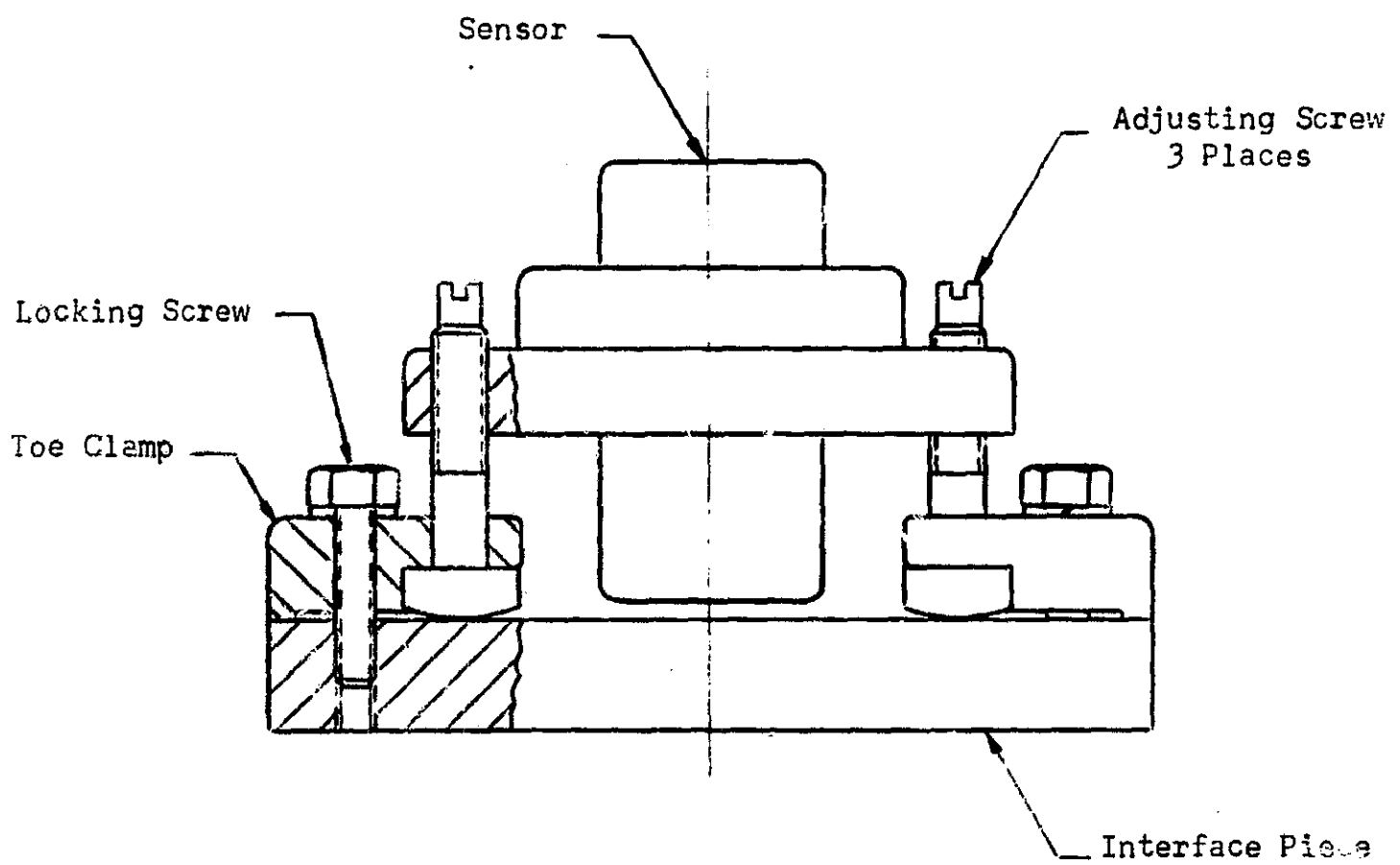


Figure I-6. Adjustable Internal Clamp
Three-Point Sensor Support
Direct Screw Adjustment Concept

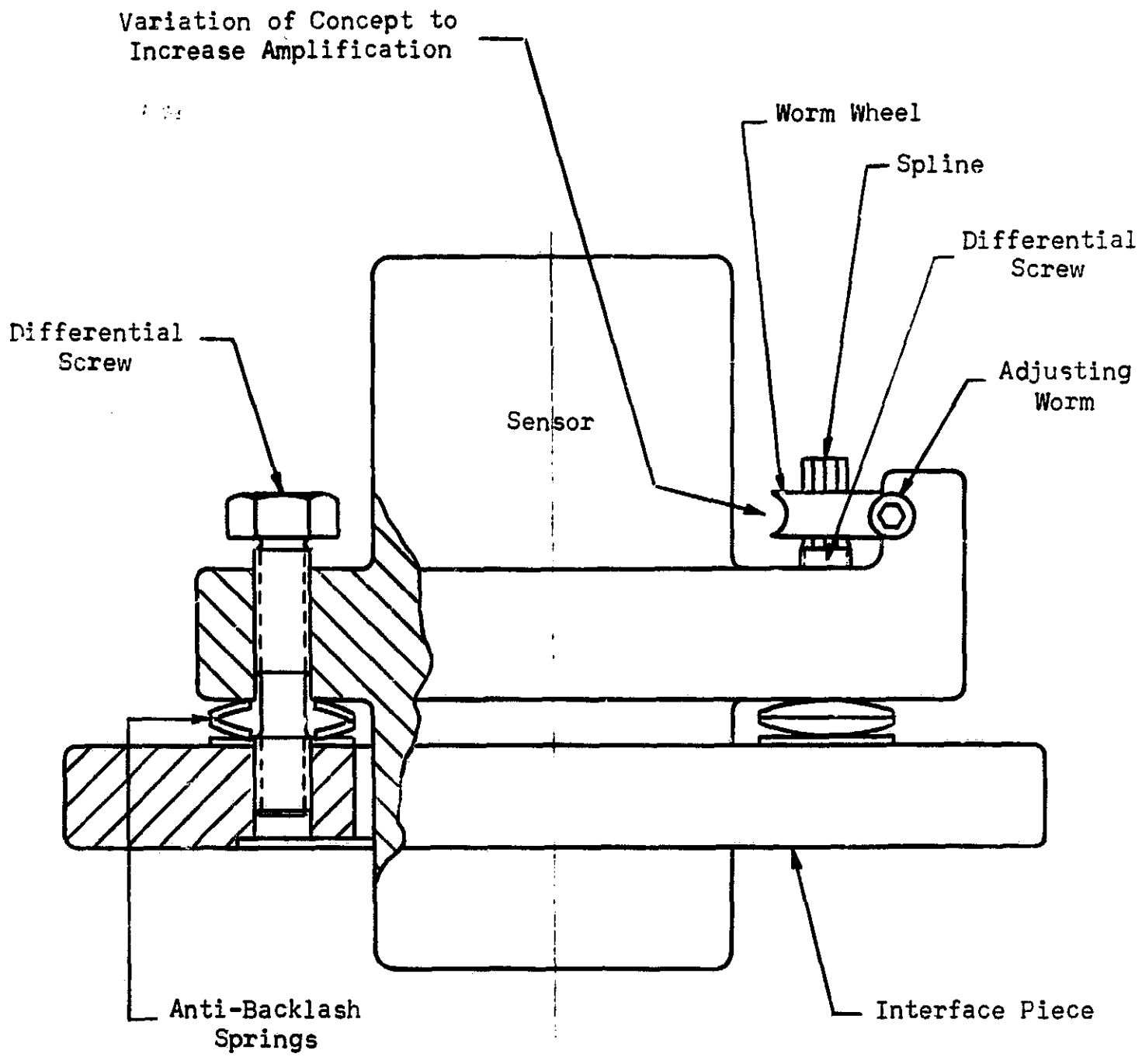


Figure I-7. Adjustable Internal Clamp
 Three-Point Sensor Support
 Direct Differential Screw Adjustment Concept

4

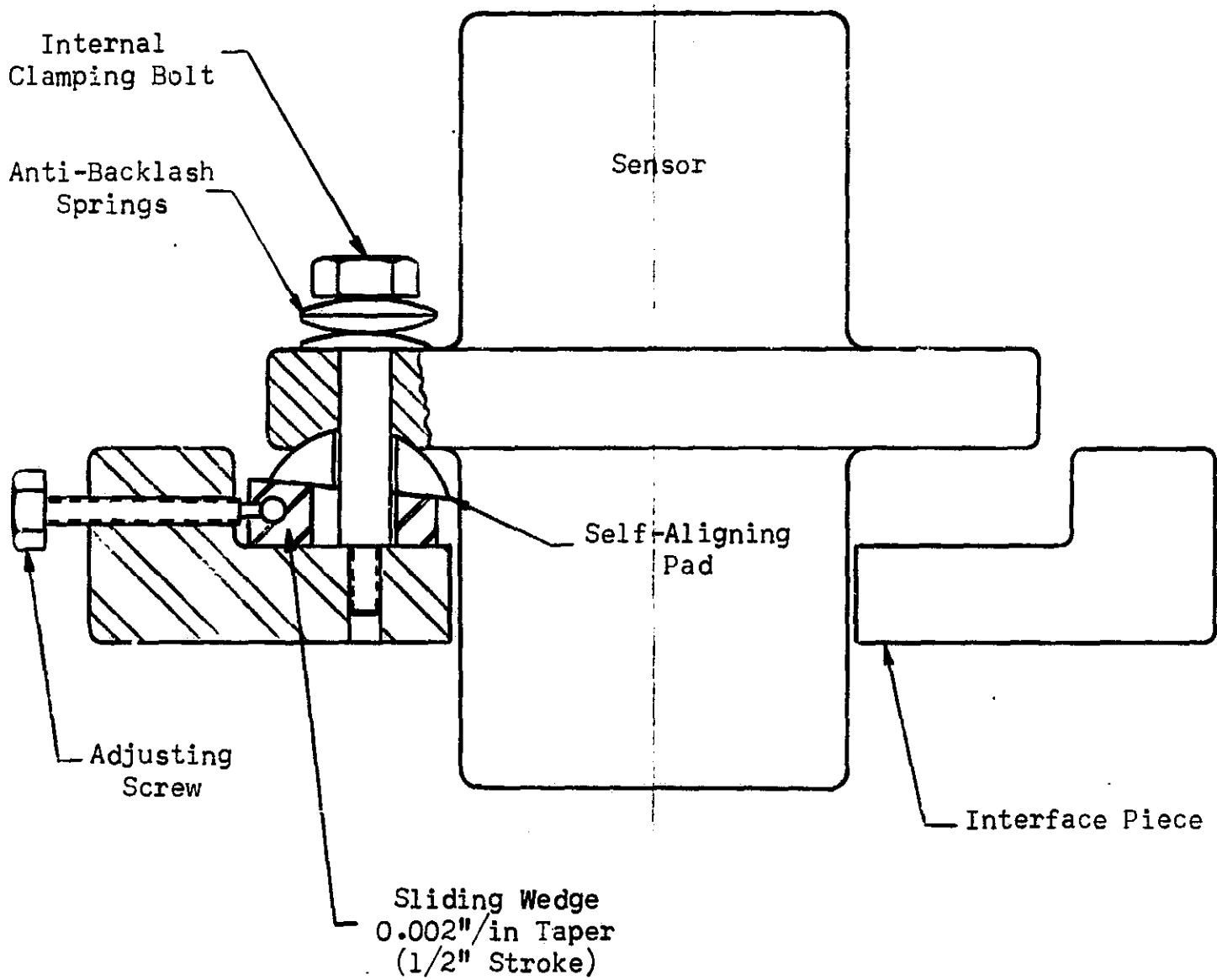


Figure I-8. Adjustable Internal Clamp
 Three-Point Sensor Support
 Transverse Wedge Adjustment Concept

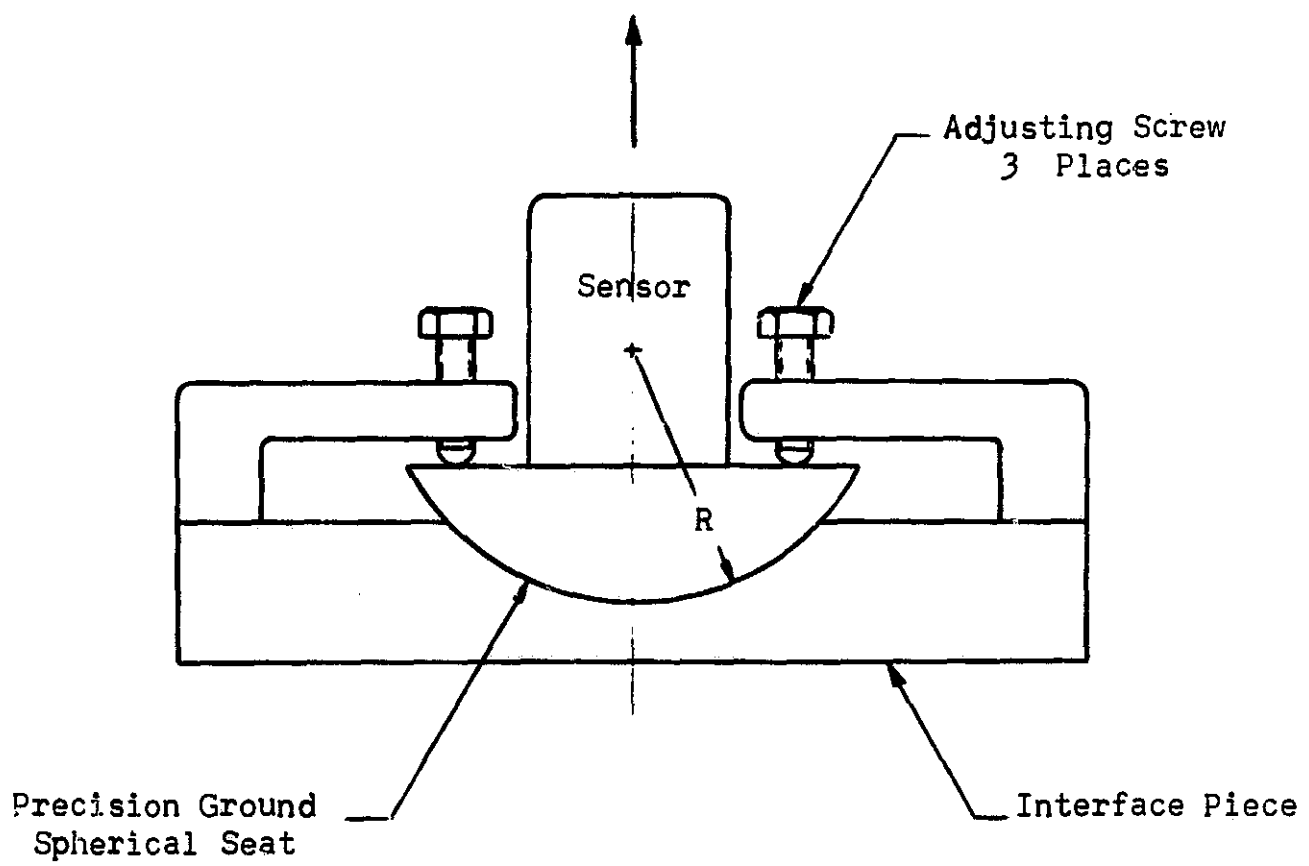


Figure I-9. Adjustable Internal Clamp
Spherical Seat Sensor Support
Combination Adjusting and Locking Screws Concept

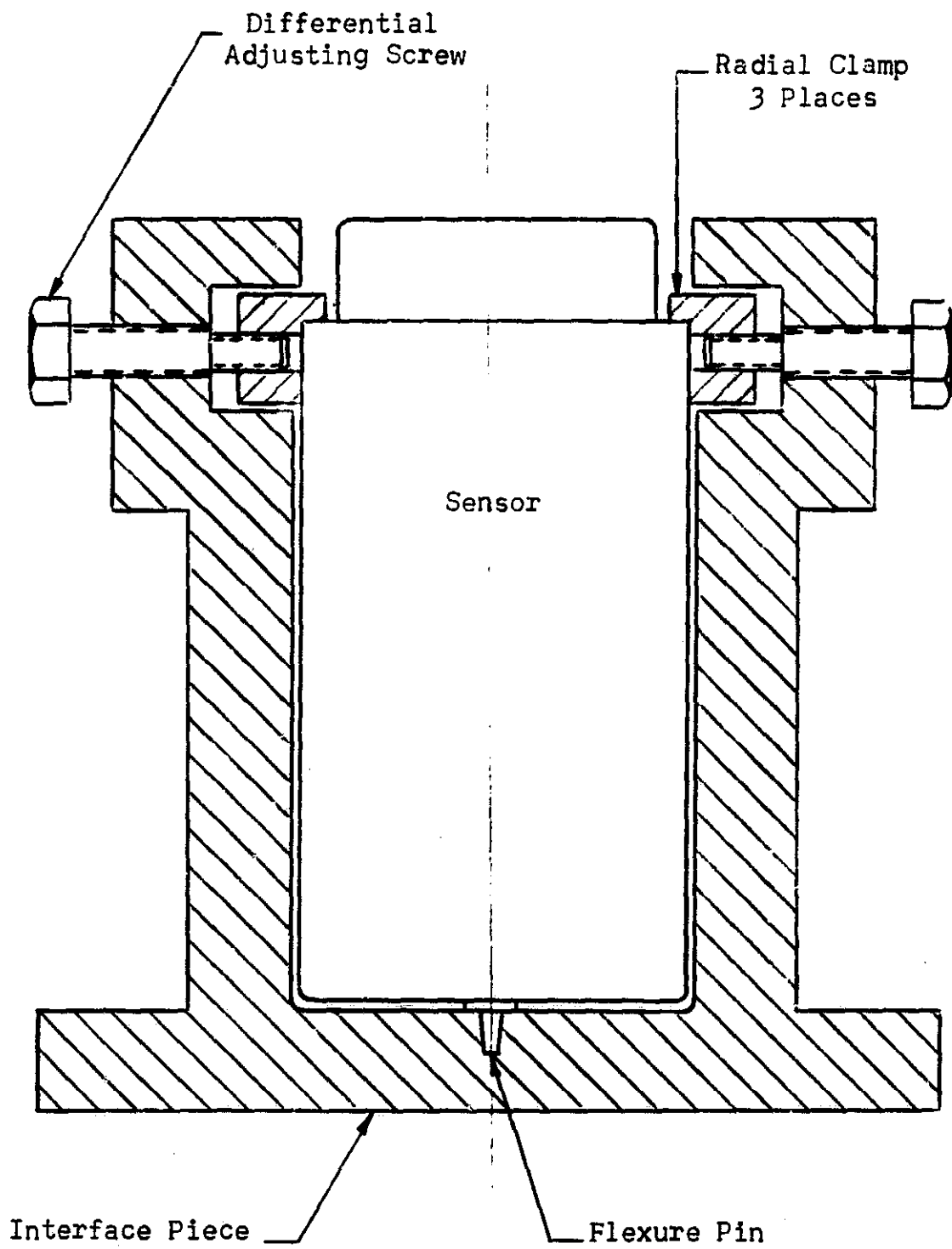


Figure I-10. Adjustable Internal Clamp
Pin and Radial Clamp Adjusting Concept

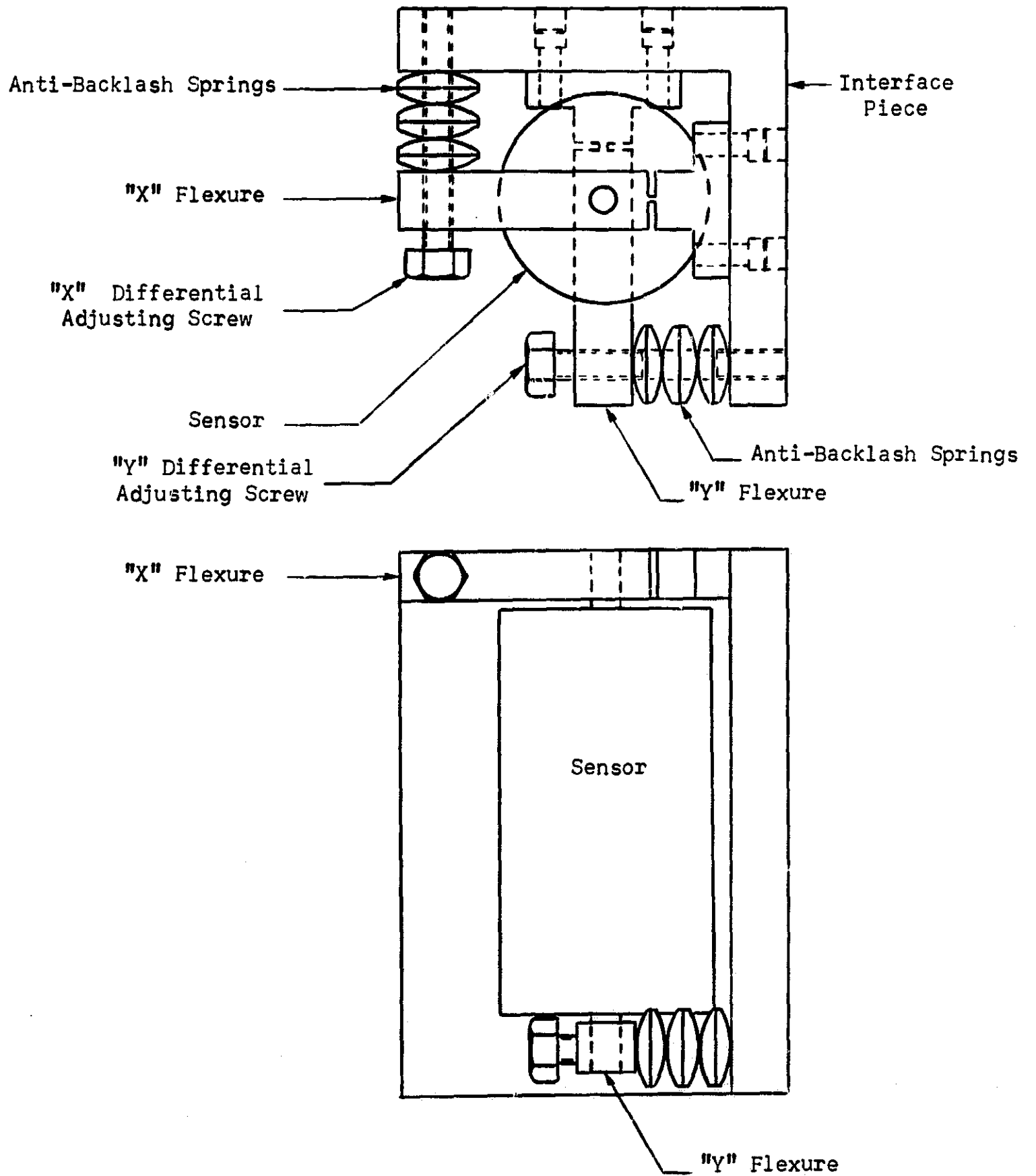


Figure I-11. Adjustable Internal Clamp Perpendicular Flexure Adjustment Concept

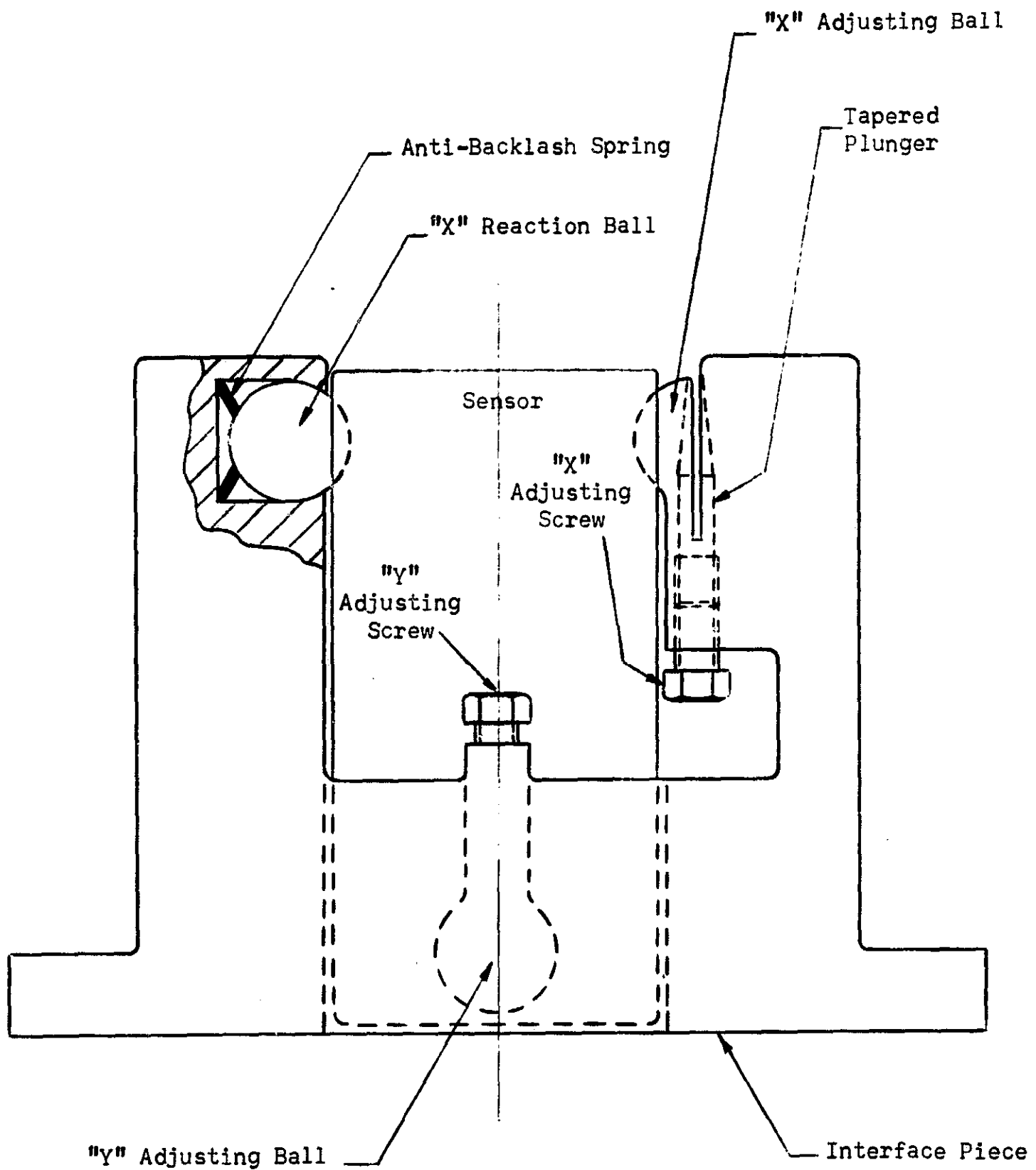


Figure I-12. Adjustable Internal Clamp
 Four-Point Spherical Sensor Support
 Perpendicular Traverse Adjustment Concept

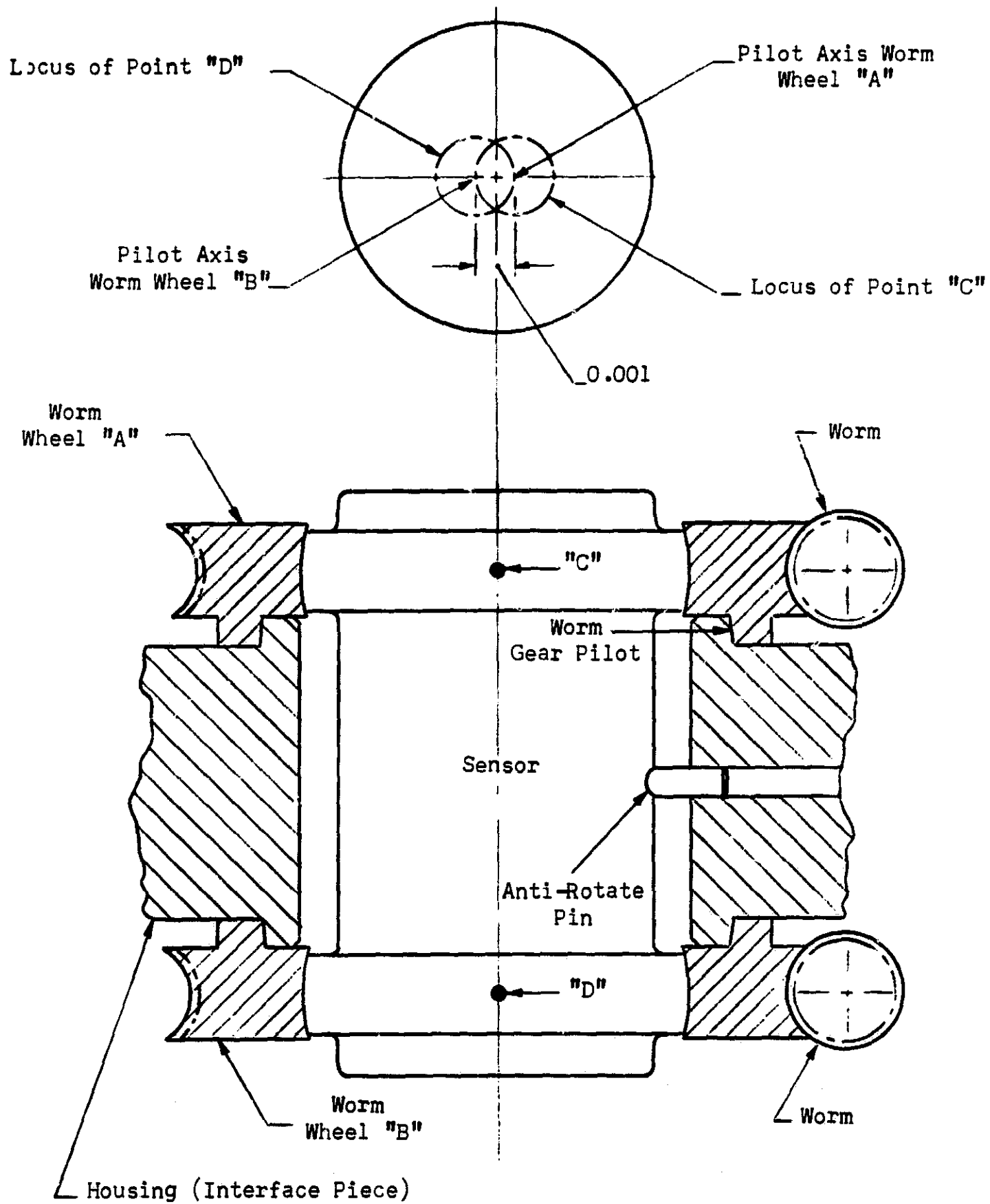


Figure I-13. Adjustable Internal Clamp
 Ring End Sensor Support
 Double Offset Eccentric Adjustment Concept

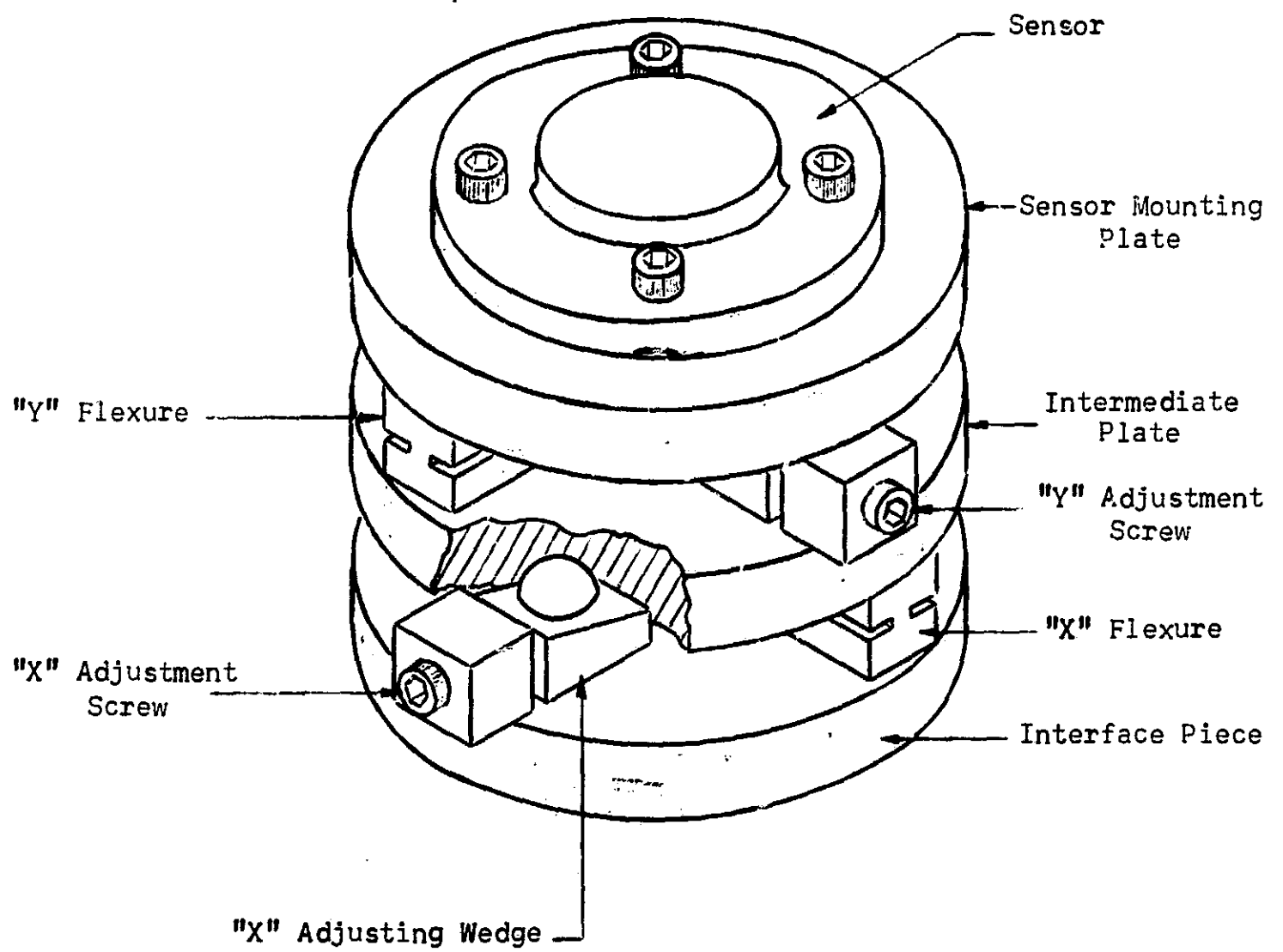


Figure I-14. Adjustable Internal Clamp
Perpendicular Trunion Adjustment Concept

APPENDIX J

DESIGN GOALS FOR THE CLAMP SYSTEM

The following design goals were established by NASA during the present study for subsequent test clamp assemblies. These goals were used as a basis for defining some of the design criteria for sizing and evaluating adjustable clamp concepts in this study.

(1) Alignment Accuracy of the Input and Output Axes

The goal will be to locate the Input Axis within a cone with a half-angle of 3.0 sec about a specified nominal axis. The Output Axis shall be located within a cone having a half-angle of 60 sec about a specified nominal axis.

(2) Prealignment

The Input and Output Axis prealignment capability must conform to (1) above with Input Axis position adjustment resolution of 1 sec.

(3) Repeatability

Different prealigned clamp assemblies must be inserted, clamped, tested for alignment, and removed 4 times within a period of 12 hours on the same I.M.U. prototype.

(4) Acceleration

- (a) Shock 50 g's for 10 msec
- (b) Steady Centrifugal 15 g's for 15 sec
- (c) Steady Centrifugal 3 g's for 24 hrs

The goal will be to maintain alignment after condition (a) and during (b) and (c). Tests will be confined to measurements following the acceleration conditions.

(5) Vibration

The assembly will be designed to withstand the following vibration conditions while providing alignment. Alignment will be checked following each test condition.

- | | | | |
|----------------|--------|----------|-----|
| (1) Sinusoidal | 0.5 in | 5-17 | cps |
| | 7.0 g | 17-22 | cps |
| | 5.0 g | 22-400 | cps |
| | 7.5 g | 400-3000 | cps |

- (b) Random 0.05 g²/cps 20- 400 cps
 0.12 g²/cps 400-2000 cps

(6) Acoustic Excitation

The assembly will be designed to provide alignment in the presence of the following acoustic excitation:

<u>Frequency, cps</u>	<u>Sound Pressure Level, decibels, re 0.0002 dynes/cm²</u>
Overall	154
37.5-75	128
75-150	132
150-300	146
300-600	146
600-1200	147
1200-2400	148
2400-4800	148
4800-9600	148

(7) Thermal Conditions

The assembly shall be designed to provide alignment under the following thermal conditions:

- (a) Ambient temperature cycling between 40^oF and 180^oF.
 (b) With temperature gradients in critical elements of the assembly of 1^oF/inch for short periods (e.g. 10 sec) and 1/4^oF/inch for long periods.

(8) Insertion and Removal

The assembly shall be designed so that the sensor can be inserted or removed in a time period of 1 hour or less with normal dexterity, and with the assistance of manually portable equipment if necessary.

(9) Physical Characteristics

- (a) The design goal for the weight of the assembly will be that it not exceed 2.5 times the dummy sensor weight.
 (b) The goal for volume will be that the assembly not occupy more than 4 times the volume of the dummy sensor.

These goals do not include portions of the simulated I.M.U. which are peculiar only to the test system.

(10) Pressure

The assembly shall be designed to maintain alignment in an environment where the ambient pressure is 10^{-5} Tor.

APPENDIX K

DEFORMATION OF THE CYLINDRICAL SHELL ELEMENT OF A CYLINDER-IN-HOLE CLAMP

Introduction

One general method for implementing the cylinder-in-hole clamp is to mate a cylindrical shell element with a solid cylindrical post as illustrated in Figure K-1. The clamping action could be achieved by a thermal shrink or hydraulic loading as analyzed in Appendix G.

A potential source of misalignment for this type of clamp is a local irregularity or bump on one of the mating surfaces as shown in Figure K-1. The deformations produced in the cylindrical shell could result in an angular error, ψ , between the sensor and the axis of the locating cylindrical post.

This appendix describes an analysis of the deformations of the shell element, assuming a rigid cylindrical post with a small local bump. The objective is to determine the magnitude of possible axial deflections of the shell leading to angular misalignment of the sensor.

The stiffness of the cylindrical shell is due to both circumferential resistance and bending of the shell elements in the axial direction. To simplify the analysis, a ring problem in the plane of the bump is studied to see how much of the ring is deformed. Then, the axial region of disturbance is estimated using energy methods. Finally, these results are combined to estimate cylinder end deformations.

Ring Problem

Consider a ring fitting perfectly on a rigid cylinder with no stresses anywhere. A point load $2P$ is applied to the top of the ring as shown in Figure K-2(a), causing a small deflection, δ_y . The ring will deform as shown in the figure, not touching the cylinder over an angle θ . For small deflections and for rings which are not extremely thin, the load will be carried by bending and shear forces with negligible contribution from circumferential tension. However, certain deformations must be compatible; and for these, all forces including circumferential tension must be considered.

In Figure K-2(b), the relevant free-body diagram is shown with forces P and F and moment M_0 . The ring undergoes bending from the top to point A where it touches the cylinder. From point A to the bottom of the cylinder, the ring is in tension only and stretches slightly. For the bending of the top portion, the ring segment is considered to be "fixed" at point A; i. e., with radial deflection, slope and curvature matching the cylinder at that point. Point A will have a slight circumferential displacement due to the previously mentioned circumferential stretching of the ring on the bottom. At the top of the ring, there will be x and y deflections as well as a

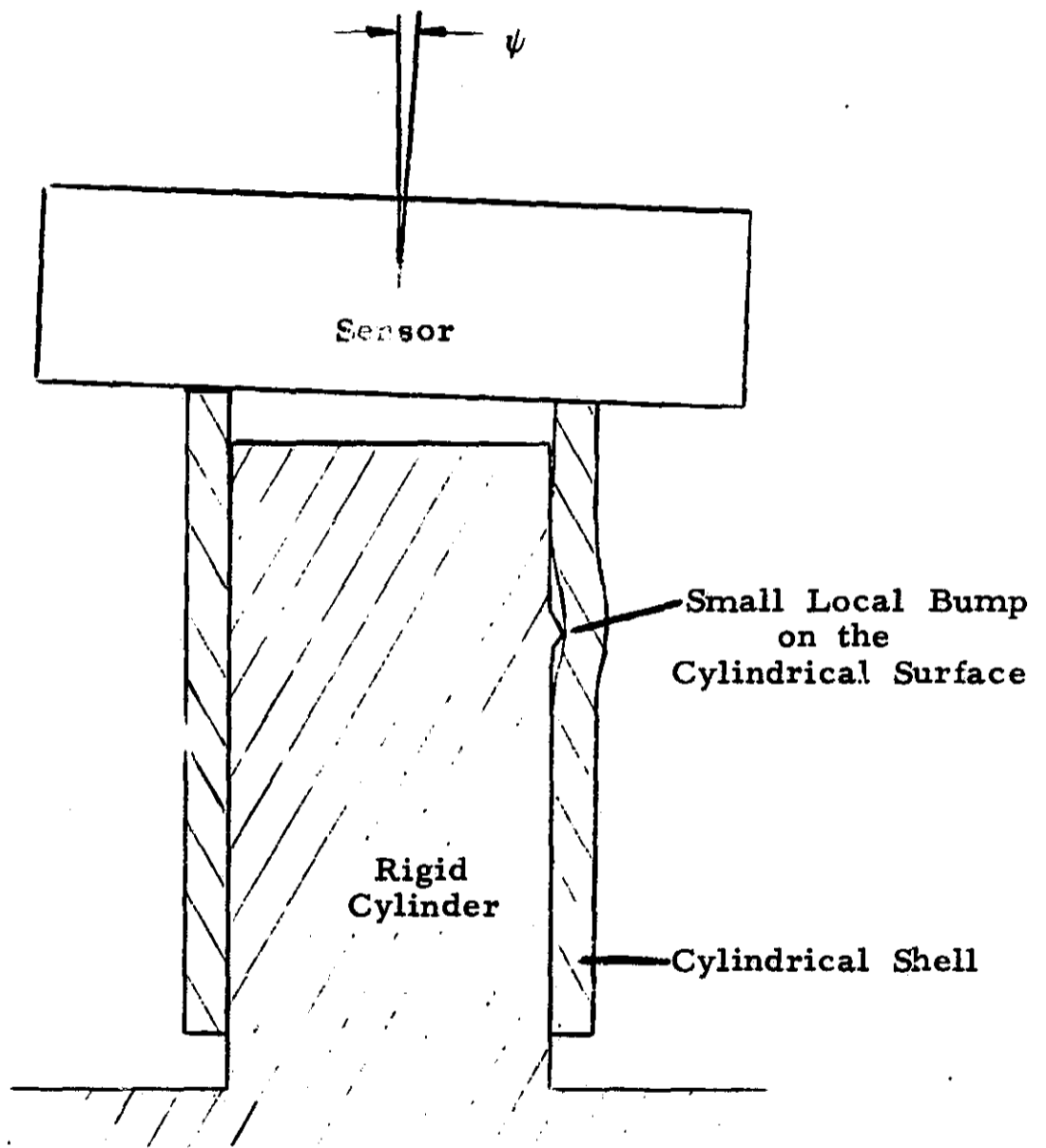


Figure K-1. Misaligning Influence of a Local Bump on a Cylinder-In-Hole Clamp.

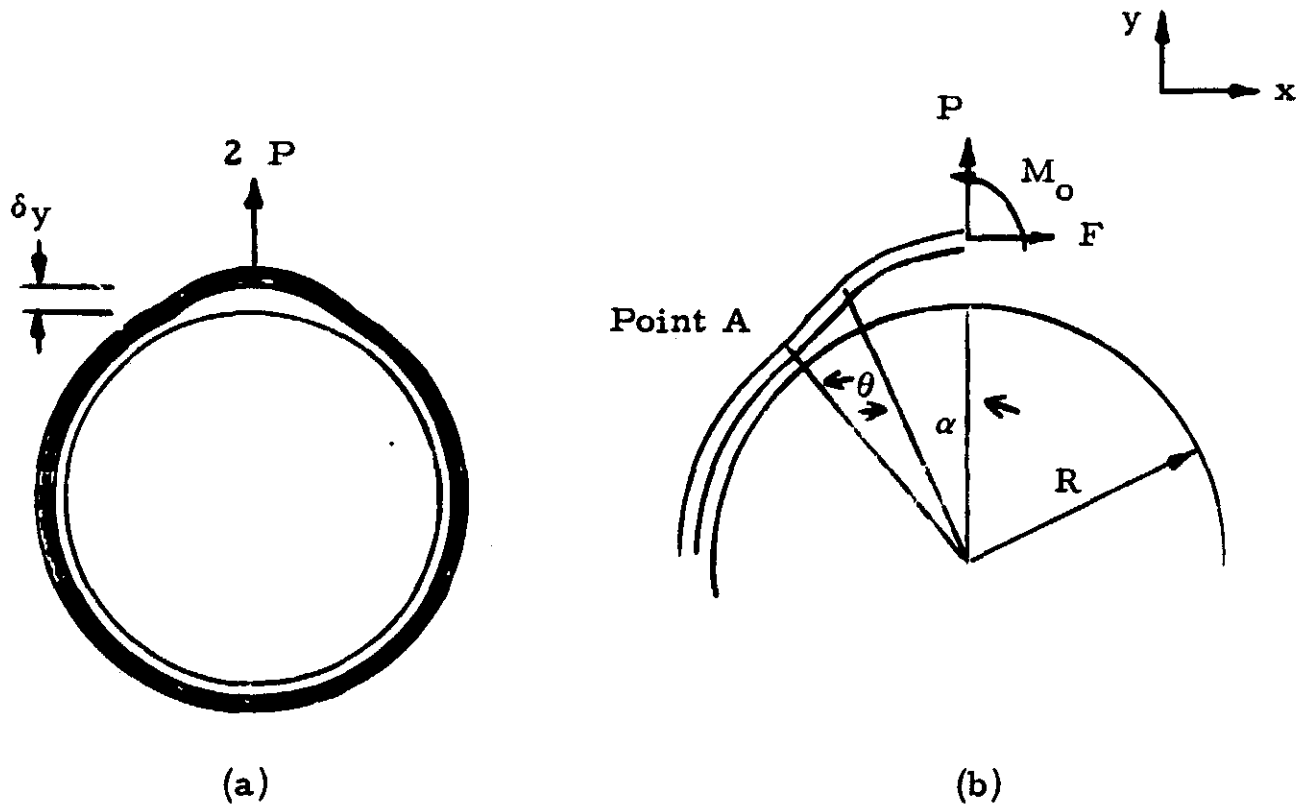


Figure K-2. Schematic Diagram of an Element of the Cylindrical Shell Considered as a Ring.

slope, indicated by δ_x , δ_y and φ due to the loads P , F and M_0 .

The conditions to be satisfied are that

- (1) φ should be zero which can be accomplished for any P and F by properly choosing M_0 .
- (2) The net x -deflection should be zero. The deflection δ_x due to P , F and M_0 will be exactly balanced by the circumferential stretching around the entire cylinder.
- (3) The bending moment (and, thus, the change in curvature) at point A should be zero so that the ring remains in contact with the cylinder.

Conditions (2) and (3) are met by adjusting and solving for the value of F and θ .

Bending Analysis

The strain energy due to bending in the top part of the ring is given for thin rings by

$$U = \int \frac{M^2}{2EI} ds = \int_0^\theta \frac{M^2}{2EI} R d\alpha \quad (K-1)$$

where the local bending moment M is

$$M = M_o + PR \sin \alpha - FR (1 - \cos \alpha). \quad (K-2)$$

The deflections at the top of the ring are given by

$$\left. \begin{aligned} \delta_x &= \frac{\partial U}{\partial F} \\ \delta_y &= \frac{\partial U}{\partial P} \\ \varphi &= \frac{\partial U}{\partial M_o} \end{aligned} \right\} (K-3)$$

which worked out are

$$\begin{aligned} \frac{EI}{R^3} \delta_x &= -\frac{M_o}{R} \left[\theta - \sin \theta \right] + P \left[(1 - \cos \theta) - \frac{\sin^2 \theta}{2} \right] \\ &\quad - \frac{F}{2} \left[3\theta - \sin \theta (4 - \cos \theta) \right] \end{aligned} \quad (K-4)$$

$$\begin{aligned} \frac{EI}{R^3} \delta_y &= \frac{M_o}{R} \left[1 - \cos \theta \right] + \frac{P}{2} \left[\theta - \sin \theta \right] \\ &\quad - F \left[(1 - \cos \theta) - \frac{\sin^2 \theta}{2} \right] \end{aligned} \quad (K-5)$$

$$\frac{EI}{R^2} \varphi = \frac{M_o}{R} \theta + P (1 - \cos \theta) - F (\theta - \sin \theta) \quad (K-6)$$

Setting $\varphi = 0$ in Equation (K-6) yields $\frac{M_o}{R}$ in terms of P and F as

$$\frac{M_o}{PR} = - \left[\frac{1 - \cos \theta}{\theta} - \frac{F}{P} \left(1 - \frac{\sin \theta}{\theta} \right) \right] \quad (K-7)$$

The bending moment at point A, M_1 (see Figure K-3), is determined by static considerations as

$$\frac{M_1}{R} = \frac{M_o}{R} + P \sin \theta - F (1 - \cos \theta) \quad (K-8)$$

Combining Equations (K-7) and (K-8) gives

$$\frac{M_1}{R} = P \left[\sin \theta - \frac{1 - \cos \theta}{\theta} \right] + F \left[\cos \theta - \frac{\sin \theta}{\theta} \right] \quad (\text{K-9})$$

Setting $M_1 = 0$ yields an equation for the ratio $\frac{F}{P}$ in terms of θ as

$$\frac{F}{P} = - \frac{\sin \theta - \frac{1 - \cos \theta}{\theta}}{\cos \theta - \frac{\sin \theta}{\theta}} \quad (\text{K-10})$$

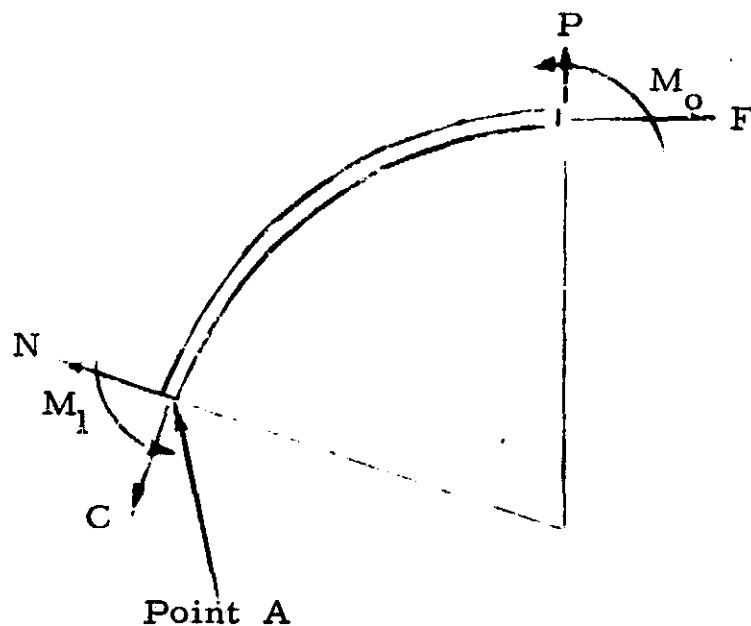


Figure K-3. Free-Body Diagram of the Ring Segment.

If C is defined as the component force in the ring along the cylinder at point A , as shown in Figure K-3, it is given by

$$C = P \sin \theta + \frac{F}{P} \cos \theta \quad (\text{K-11})$$

If $\frac{F}{P}$ is eliminated from Equation (K-11) using Equation (K-10), then $\frac{C}{P}$ is a function of θ only.

For a given θ , the x and y deflections at the top due to bending are now completely known in the form

$$\frac{EI\delta_x}{PR^3} = -\frac{M_o}{PR} \left[\theta - \sin \theta \right] + \left[(1 - \cos \theta) - \frac{\sin^2 \theta}{2} \right] - \frac{F}{2P} \left[3\theta - \sin \theta (4 - \cos \theta) \right] \equiv f_1(\theta) \quad (K-12)$$

$$\frac{EI\delta_y}{PR^3} = \frac{M_o}{PR} (1 - \cos \theta) + \frac{1}{2} (\theta - \sin \theta \cos \theta) - \frac{F}{P} \left[(1 - \cos \theta) - \frac{\sin^2 \theta}{2} \right] \equiv f_2(\theta) \quad (K-13)$$

where $\frac{M_o}{PR}$ and $\frac{F}{P}$ are given in terms of θ by Equations (K-10) and (K-7).

The net deflection in the x-direction must be zero. The circumferential deflection from point A to the bottom is given by the first part of the right-hand side of Equation (K-14) and the circumferential stretching which occurs in the portion undergoing bending is given by the integral in Equation (K-14).

$$\delta_T = C (\pi - \theta) \frac{R}{AE} + \int_0^\theta (P \sin \alpha + F \cos \alpha) \frac{R}{AE} d\alpha \quad (K-14)$$

Equation (K-14) may be written as

$$\frac{AE\delta_T}{PR} = \frac{C}{P} (\pi - \theta) + \int_0^\theta (\sin \alpha + \frac{F}{P} \cos \alpha) d\alpha \quad (K-15)$$

Carrying out the integration gives

$$\frac{AE\delta_T}{PR} = \frac{C}{P} (\pi - \theta) + (1 - \cos \theta) + \frac{F}{P} \sin \theta \equiv f_c(\theta) \quad (K-16)$$

which is purely a function of θ . Equating $\delta_T + \delta_x$ to zero for no net horizontal deflection at the top at the point of loading yields

$$\delta_x = -\delta_T = \frac{PR^3}{EI} f_1(\theta) = -\frac{PR}{AE} f_3(\theta) \quad (K-17)$$

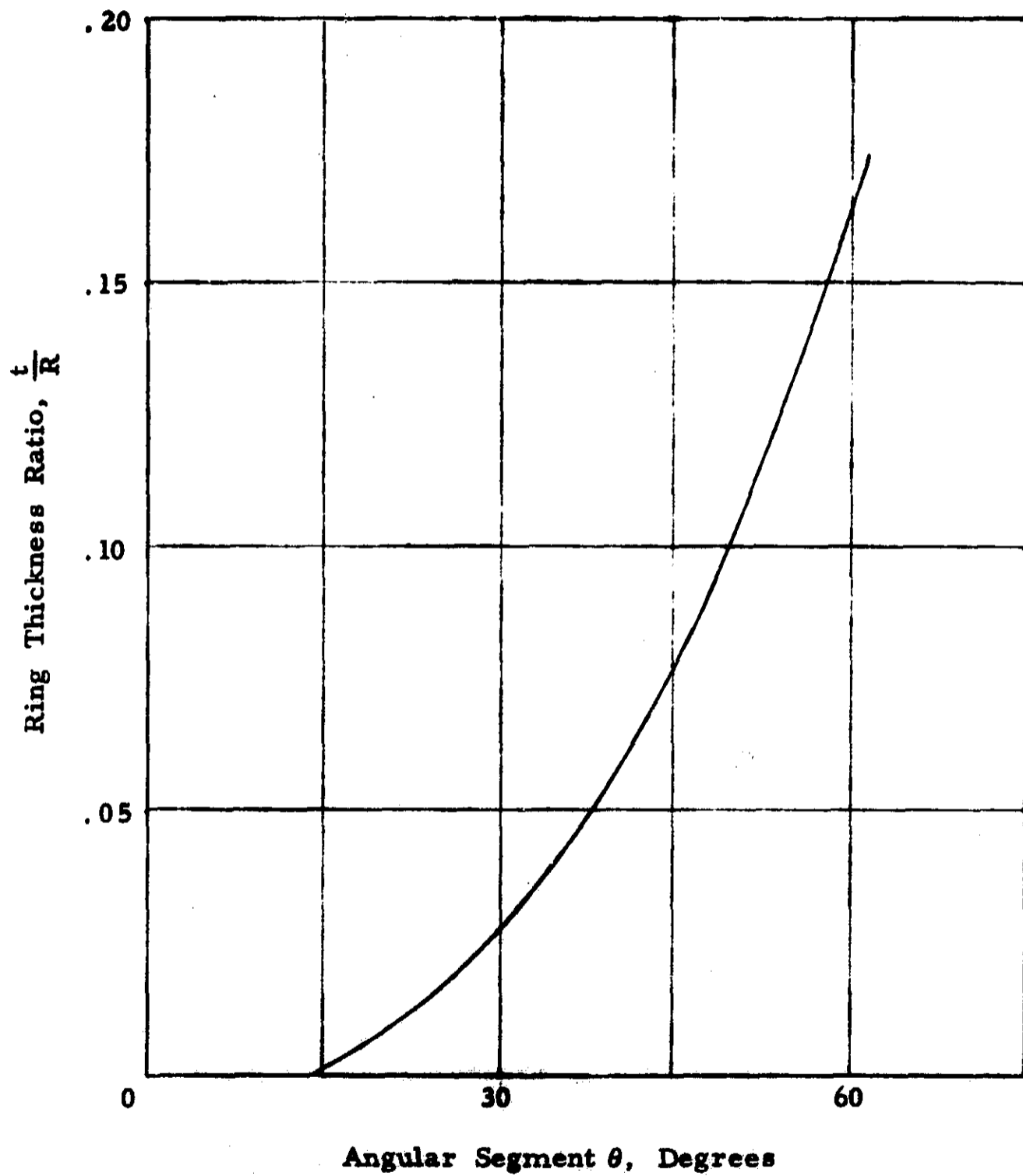


Figure K-4. Relation Between the Ring Thickness Ratio and the Portion of the Ring Subjected to Bending.

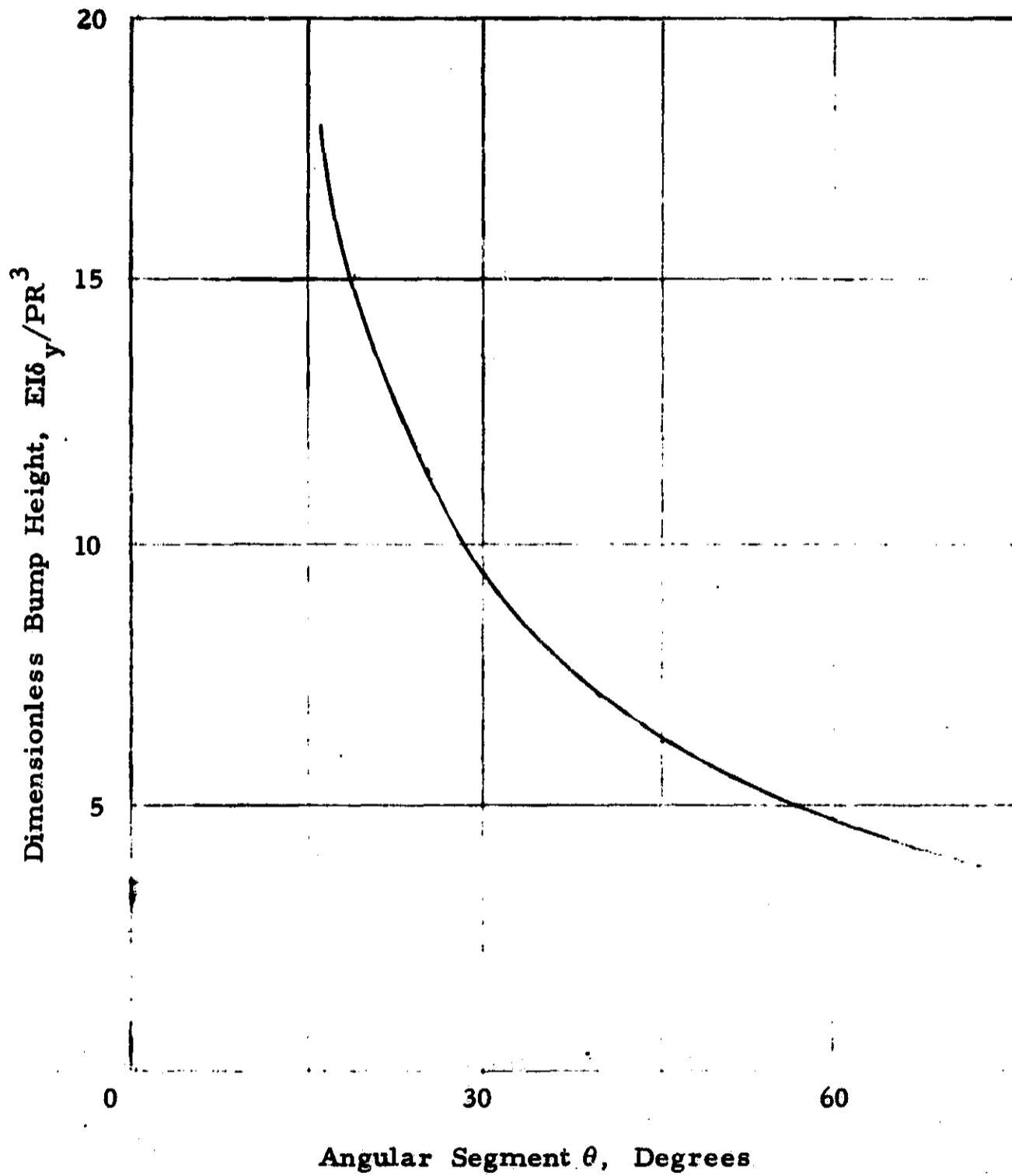


Figure K-5. Relation Between the Dimensionless Bump Height and the Portion of the Ring Subjected to Bending.

Assuming a rectangular ring cross-section with area, $A = \delta t$, and moment of inertia, $I = \frac{1}{12} b t^3$, Equation (K-17) reduces to

$$\left(\frac{t}{R}\right)^2 = 12 \frac{f_1(\theta)}{f_3(\theta)}. \quad (K-18)$$

Equation (K-18) is plotted in Figure K-4 showing the relationship between the thickness-radius ratio and θ , the portion of the ring subjected to bending.

In Figure K-5, the relation between the bump height, δ_y , the load P , and the angle θ as given in Equation (K-13) is plotted.

Deformation in the Axial Direction

The deformation study of the ring can now be extended in order to estimate the axial distance, L , required for the radial displacement, u , to drop from δ_y to zero, as shown in Figure K-6. It is assumed that bending resistance is most significant for variations in the z -direction. The strain energy for the relevant portion of cylindrical shell near the bump or load is given by the expression

$$U = \iint \left[u_{zz}^2 + u_{vv}^2 + 2\mu u_{zz} u_{vv} + 2(1-\mu) u_{zv}^2 \right] \frac{D}{2} dz dv = \iint f \frac{D}{2} dz dv \quad (K-19)$$

where u is the displacement as a function of axial distance z and circumferential distance v .

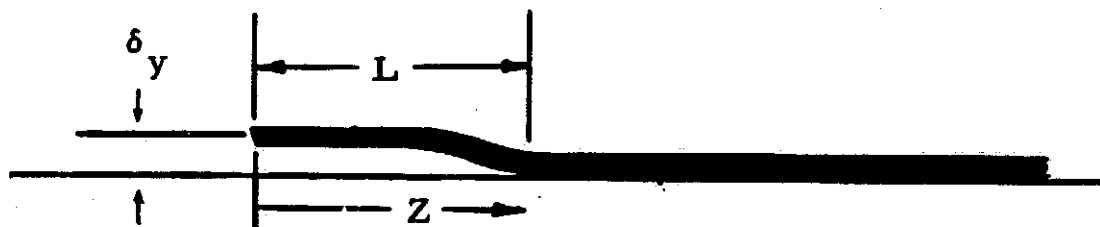


Figure K-6. Schematic Diagram of the Deformation of the Cylinder Along the Axial Direction.

A form of the displacement u is chosen as

$$u = \frac{u_0}{4} \left[1 + \cos \left(\frac{n\nu}{R} \right) \right] \left[1 + \cos \left(\frac{\pi z}{L} \right) \right] \quad (\text{K-20})$$

The value of n is determined from the previous ring study. The value of L is as yet undetermined. An estimate of L can be obtained by minimizing the potential energy of the system. Since the only external load, P , is at the origin where the displacement is fixed, no change in external potential energy is involved in varying L and, consequently, only the strain energy, U , has to be minimized with respect to L .

Substituting Equation (K-20) into Equation (K-19) and integrating yields

$$U = \int_0^L \int_0^{\frac{\pi R}{n}} + \frac{D}{2} dv dz = \frac{u_0^2}{64} \pi D \left[\frac{3\pi^4 R^3}{2nL^3} + \frac{3n^3 L}{2R^3} + \frac{n\pi^2}{RL} \right] \quad (\text{K-21})$$

Minimizing U with respect to L yields

$$\frac{\partial U}{\partial L} = 0 = -\frac{9\pi^4 R^3}{2nL^4} + \frac{3n^3}{2R^3} - \frac{n\pi^2}{RL^2} \quad (\text{K-22})$$

or
$$\frac{9}{2} \frac{\pi^4}{n} \left(\frac{R}{L} \right)^4 + n\pi^2 \left(\frac{R}{L} \right)^2 - \frac{3n^3}{2} = 0 \quad (\text{K-23})$$

Letting $r = \frac{\pi R}{L}$ changes Equation (K-23) to

$$r^4 + \frac{2}{9} n^2 r^2 - \frac{1}{3} n^4 = 0 \quad (\text{K-24})$$

Solving Equation (K-24) for r gives

$$r = \frac{n}{3} \left[\sqrt{28} - 1 \right]^{\frac{1}{2}} \quad (\text{K-25})$$

or
$$L = 1.44 \frac{R}{n} \quad (\text{K-26})$$

A typical numerical example of the results is obtained by assuming the following values,

$$t = .1 \text{ inch}, \quad R = 1.0 \text{ inches}$$

$$\frac{t}{R} = .1$$

From Figure K-4,

$$\theta = 50^\circ = .87 \text{ radians} = n$$

and $L = 1.65 R.$ (K-27)

Axial Deformation of Shell Ends

The shortening effect, Δ , of putting a small bump in an originally straight line of length, L , can be calculated from

$$\Delta = \int_0^L (1 + u_z^2)^{\frac{1}{2}} dz - L. \quad (\text{K-28})$$

With $u = \frac{u_0}{2} (1 + \cos \frac{\pi z}{L})$ and $u_0 \ll L$, Equation (K-28) becomes

$$\Delta = \int_0^L (1 + \frac{1}{2} u_z^2) dz - L = \frac{1}{2} \int_0^L u_z^2 dz$$

and $\frac{\Delta}{L} = \frac{\pi^2}{16} \left(\frac{u_0}{L}\right)^2.$ (K-29)

With $L = 1.65 R$ from the illustrative example, Equation (K-29) becomes

$$\frac{\Delta}{R} = 0.373 \left(\frac{u_0}{R}\right)^2. \quad (\text{K-30})$$

For a bump of $u_0 = 0.001$ inch on a 1.0 inch radius cylinder

$$\Delta = 0.4 \times 10^{-6} \text{ inches (shorter).}$$

Furthermore, this shortening is calculated assuming no axial stretching in the z -direction which would reduce the absolute value of Δ to even a smaller value.

The circumferential force, C , causes an axial contraction due to Poisson's ratio. However, the force C is approximately constant around the ring and, therefore, all angular positions of the ring contract about the same amount. Variations in C are necessary to affect the plane of the end of the ring. Adjacent ring sections not subject to a surface bump would tend to smooth any variations resulting from a local variation in C .

The above shortening would bring about an angular error, ψ , as shown in Figure K-1 of 0.4×10^{-6} radians or approximately 1 arc-sec. Since it is likely that the cylindrical elements could be controlled to avoid anomalies as large as 0.001 inch, misalignment from this source is not likely to be a problem.